Dissertation zur Erlangung des Doktorgrades
der Fakultät für Chemie und Pharmazie
der Ludwig-Maximilians-Universität München

Structural and functional characterization of the INO80 chromatin remodelling complex

Kevin René Schall
aus
Schorndorf, Deutschland
2022

Erklärung

Diese Dissertation wurde im Sinne von § 7 der Promotionsordnung vom 28. November 2011 von Herrn Prof. Dr. Karl-Peter Hopfner betreut.

Eidesstattliche Versicherung

Diese Dissertation wurde eigenständig und ohne unerlaubte Hilfe erarbeitet.

München, den 08.06.2022

_____

Kevin René Schall

Dissertation eingereicht am: 09.06.2022

1. Gutachter: Prof. Dr. Karl-Peter Hopfner

2. Gutachter: PD Dr. Philipp Korber

Mündliche Prüfung am: 20.12.2022

This thesis was prepared from July 2015 to April 2020 in the laboratory of Prof. Dr. Karl-Peter Hopfner at the Gene Center of the Ludwig-Maximilians Universität.

This is a cumulative thesis based on the following publications:

Schwarz, M., Schall, K., Kallis, E., Eustermann, S., Guariento, M., Moldt, M., Hopfner, K.P. and Michaelis, J., 2018. Single-molecule nucleosome remodeling by INO80 and effects of histone tails. *FEBS letters*, *592*(3), pp.318-331.

Eustermann, S.*, Schall, K.*, Kostrewa, D., Lakomek, K., Strauss, M., Moldt, M. and Hopfner, K.P., 2018. Structural basis for ATP-dependent chromatin remodelling by the INO80 complex. *Nature*, *556*(7701), pp.386-390.

Knoll, K.R.*, Eustermann, S.*, Niebauer, V., Oberbeckmann, E., Stoehr, G., Schall, K., Tosi, A., Schwarz, M., Buchfellner, A., Korber, P. and Hopfner, K.P., 2018. The nuclear actin-containing Arp8 module is a linker DNA sensor driving INO80 chromatin remodeling. *Nature structural and molecular biology*, *25*(9), pp.823-832.

*These authors contributed equally

Parts of this have been presented at international conferences:

Poster presentation at the 5th Munich Chromatin Symposium: Chromatin Dynamics – October 2019 in Munich, Germany.

Poster presentation and short talk at the FASEB Science Research Conference: Machines On Genes – June 2018 in Base Villiage Snowmass, CO, USA.

Table of contents

1 Summary

DNA is the carrier of the genetic information in all kingdoms of life. Cells face the challenge to pack DNA and ensure its integrity on the one hand while enabling access to the genetic code on the other hand. This holds in particular true for eukaryotes, whose genomes are typically larger than those of prokaryotes and organized in multiple linear DNA molecules, termed chromosomes, within the nuclear envelope. Their genetic information is stored as a nucleoprotein complex referred to as chromatin, in which DNA is associated with histone proteins. It compacts DNA and at the same time provides an elaborate platform to regulate access to the genetic code. Various fundamental cellular processes depend on this access and thus are regulated by the organization of chromatin, such as transcription, cell division, cell differentiation and DNA repair. The fundamental unit of chromatin is the nucleosome core particle, in which 147 bp of DNA are wrapped around an octamer of the four core histone proteins (H2A, H2B, H3 and H4) or variants thereof, giving rise to a disk-shaped particle. The nucleosome core particle originated from archaea. These possess one or two histone proteins, which are orthologous to eukaryotic histones and assemble with DNA in an overall similar fashion.

Being the fundamental unit of chromatin, the formation, disassembly, localization and composition of the individual nucleosome core particles directly impacts the chromatin landscape and therefore gene regulation. These actions are carried out by chromatin remodelling complexes ('remodellers'). The catalytic core of all remodellers is a Snf2-type ATPase, which converts the energy of ATP hydrolysis in DNA translocation. Based on flanking domains and additional subunits, remodellers can be grouped into four families: ISWI, CHD, SWI/SNF and INO80. While ISWI and CHD carry out their function as small complexes or even as single subunits, remodellers of the SWI/SNF and INO80 families form multi-subunit complexes in the megadalton range. In the past twenty years, several hallmark studies characterized the biological functions of these multi-subunit complexes and analyzed their composition and architecture. However, insights on a detailed structural level into how the individual subunits cooperate remained elusive, mainly due to technical limitations. These could partly be overcome in the past years, especially by the advent of high-resolution cryogenic electron microscopy.

This thesis analyzes the INO80 chromatin remodelling complex (INO80), the founding member of the INO80 family, from a structural and functional perspective with an emphasis on its action on the nucleosome core particle. INO80 translocates DNA around the nucleosome core particle and spaces nucleosomes to form genic arrays. The presented results reveal, how the evolutionarily conserved subunits of INO80 interact with the nucleosome and catalyze DNA translocation in a coordinated fashion. A cryo-EM structure of the core module of INO80 bound to the nucleosome core particle demonstrates that the ATPase domain and the actin fold of Arp5 bind nucleosomal DNA at SHL -6 and SHL -2, respectively, while the insert domain of Arp5 contacts the acidic patch. The Rvb1/2 heterohexamer connects these subunits without forming major nucleosome contacts. This arrangement provides valuable information about the mechano-chemical catalysis cycle of INO80, in which the ATPase domain acts as a motor, Arp5 as a counter grip and the Rvb1/2 ring as a stator element. The ATPase pumps DNA inside the nucleosome core particle against Arp5, which leads to a DNA strain. Once sufficient force is generated, the counter grip is released and DNA translocation occurs. Thus, these results explain the biochemically and biophysically observed step size of 10 – 20 bp of DNA translocation catalyzed by INO80. The X-ray structure of the Arp8 module in combination with biochemical data shows that the module binds outside the nucleosome core particle to

extranucleosomal DNA. Arp8, actin and Arp4 organize the HSA domain of Ino80 in a way that a number of conserved and positively charged lysine and arginine residues interact with entry DNA ahead of the ATPase domain. This interaction is crucial for the catalysis of DNA translocation by INO80. The combination of these structures leads to a composite model of the evolutionarily conserved subunits of INO80, which is supported by a more recent cryo-EM structure. It suggests that the Arp8 module prevents DNA residing in a transition state between the ATPase and Arp5 from slipping back. Moreover, the Arp8 module could also act as a molecular ruler as its footprint matches the distance between two nucleosome core particles in genic arrays formed by INO80. Small molecule analysis reveals that histone tails regulate nucleosome invasion by INO80. They constitute a regulatory barrier and constrain conformations of nucleosome-bound INO80.

2 Introduction

2.1 Chromatin organization in eukaryotes

Walther Flemming introduced the term "Chromatin" in the late 19th century describing easily stained material, which he extracted from nuclei[1]. In the subsequent decades, extensive research characterized it as a nucleoprotein complex through which the genomic information of eukaryotes is stored in their nucleus[2,3]. Its organization is fundamental to all processes depending on genomic DNA and consequently for maintenance, replication and translation of the genetic code.

2.1.1 The nucleosome is the basic unit of chromatin

In the 1970's, several hallmark publications showed that the nucleosome is the basic unit of chromatin. In a first step, it was demonstrated that the histone proteins H2A, H2B, H3 and H4 appear in equimolar amounts in the eukaryotic nucleus and that they form an octamer comprised of two copies of each histone[4]. Taken together with the fact that endonucleolytic digest of eukaryotic DNA results in fragments of 200 bp or multiples thereof[5], a chromatin organization in repeating units of one histone octamer associated with about 200 bp of DNA could be proposed[6]. Later, the existence of a "core particle" which comprises about 140 bp of DNA only was demonstrated[7]. The number of base pairs of DNA contained in one core particle could be specified to be close to 146 bp shortly afterwards[8]. Further evidence for this view on chromatin organization came from the visualization of chromatin by electron microscopy[9]. Micrographs on which chromatin from different species was stained, showed an array of spherical particles connected by thin filaments[9]. These particles constitute the basic unit of chromatin and were initially referred to as ν bodies[9], but were later termed nucleosomes[10]. A first low-resolution crystal structure of the nucleosome core particle (NCP) revealed that DNA is wrapped around the outside of the histone octamer giving rise to a disk-shaped particle with dimensions of 57 Å x 110 Å x 110 Å[11]. The discovery of chromatin being organized in distinct particles formed by a globular histone octamer around which DNA is coiled, revolutionized the understanding of genome organization[12].

2.1.1.1 Three-dimensional structure of the nucleosome core particle

After this breakthrough, a series of structural, biochemical and biophysical studies examined the three-dimensional arrangement of the NCP, among them a 7 Å structure of the NCP[13] and a 3.1 Å structure of the histone octamer[14]. However, it was not until 1997 that the first high-resolution structure revealed the atomic details of the NCP[15] described in the following paragraph.

The four core histones are small basic proteins, which are highly conserved in their primary sequence among eukaryotes[16,17]. They all share a central histone fold comprising 80-90 amino acids, in which three α-helices are connected by two loops[14]. This is specified as α1-L1-α2-L2-α3 arrangement (Fig. 1a, b)[14]. While H2A and H2B possess additional residues at their N- and C-termini, H3 and H4 are extended from their histone fold at the N-terminus only (Fig. 1a)[14]. Complementary histone folds specifically interact with each other to form heterodimers in a handshake motif; H2A pairs with H2B, while H3 pairs with H4 (Fig. 1b)[4,14]. In this motif, the shorter helices α1 and α3 fold back onto the central α2 helix, while L1 interacts with L2 of the complementary histone (Fig. 1b)[14]. The histone octamer is formed by two H2A-H2B dimers and one H3-H4 tetramer (Fig. 1c)[4]. The assembly of the H3-H4 tetramer is mediated by a four-helix bundle motif formed between the two adjacent H3 chains (Fig. 1c)[15]. In this motif, the C-terminal part of α2, L2 and α3 interact in a head-to-head arrangement[14,18]. Two H2A-H2B

dimers associate with this tetramer on opposing sides[14]. A four-helix bundle between H2B and H4 is the main mediator of this interaction, again formed by the C-terminal portions of the two histone folds (Fig. 1c)[14,15]. Additionally, the C-terminus of H2A (also termed "docking domain"[19]) interacts with the H3-H4 tetramer[15]. Furthermore, the C-terminal α-helix of H2B loops back to stabilize the H2A-H2B handshake motif from the top, and a small interface between the two H2A-H2B dimers is formed between the L1 loops of the H2A chains[15].

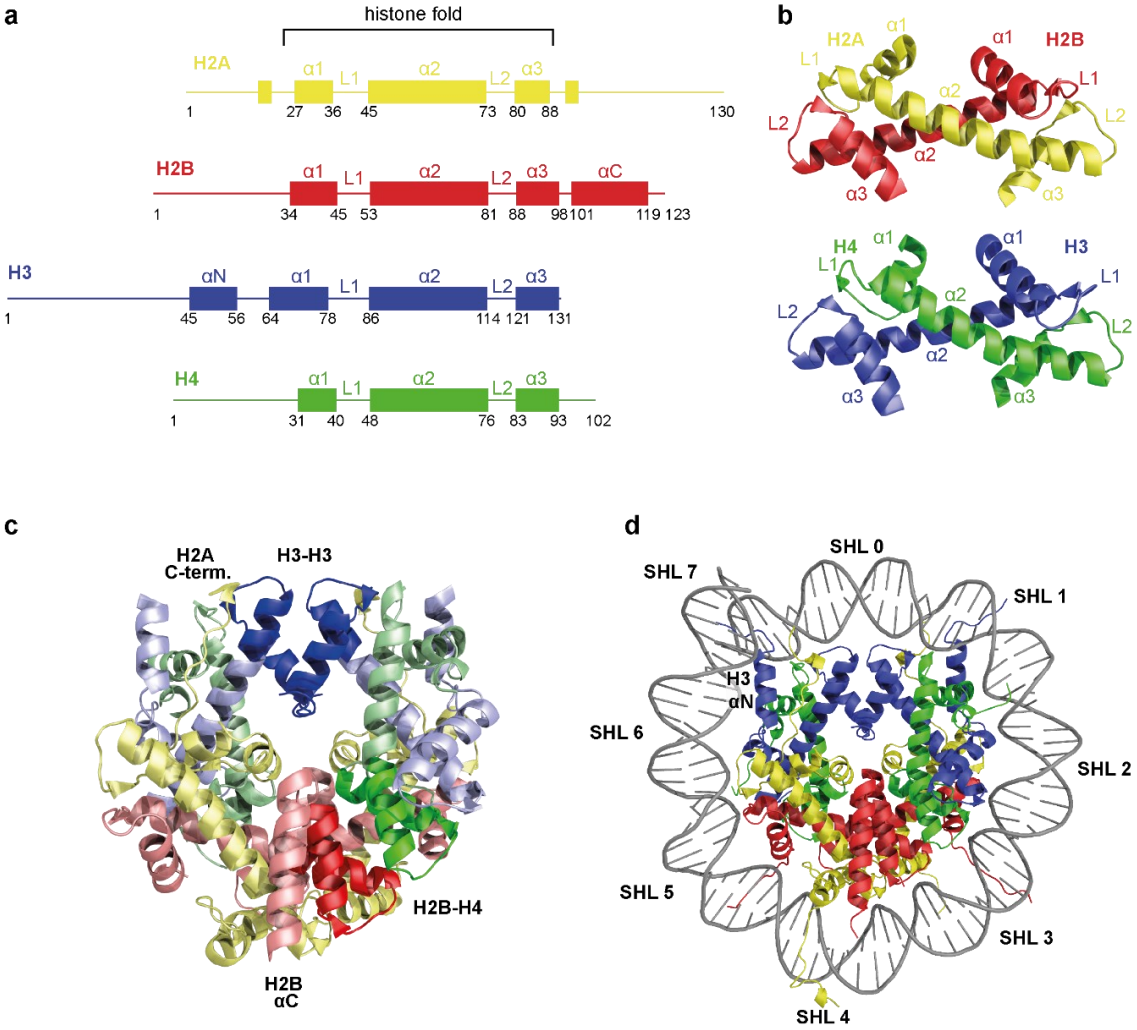

Figure 1: Structure of the nucleosome core particle. a, Domain architecture of core histones. Loops and tails are shown as lines and α-helices as rectangles. **b,** H2A-H2B and H3-H4 histone fold heterodimer handshake motifs. Yellow: H2A; Red: H2B; Blue: H3; Green: H4. **c,** Structure of the histone octamer. Four-helix bundle motifs are highlighted. Histone tails are not shown. **d,** Structure of the nucleosome core particle. Grey: DNA. For simplicity, the second DNA gyre is not shown. Figure adapted from[18] using high-resolution structure[15] (pdb: 1AOI). All figures of 3D models in this thesis were prepared with the PyMOL software (version 2.3)[20].

Around one NCP 145-147 bp of DNA are wrapped in 1.65 turns of a flat, left-handed super helix (Fig. 1d)[15]. Histones and DNA form electrostatic interactions and hydrogen bonds at 14 distinct sites, in each case where a minor groove contacts the octamer (Fig. 1d)[15]. The particle exhibits a twofold symmetry with the symmetry center being formed by one single base pair, the nucleosome dyad[15,21]. By convention, the rotational orientation of the DNA is described relative to the dyad by superhelix locations (SHL)[15]. The dyad is defined as SHL 0 and the location number increases for each successive turn of DNA by ± 1 towards the entry and exit site of the NCP (Fig. 1d)[15]. Thereby 15 superhelix locations ranging from -7 to +7 are defined around the NCP, each where a major groove faces the histone octamer (Fig. 1d)[15,19]. The central ~120 bp of DNA are bound by the histone fold domains[15]. Additionally, about 13 bp at the entry and exit site are organized by the αN helix of H3 (Fig. 1a, d) and these interactions contribute

significantly to the stability of the nucleosome[15,22]. The NCP has a molecular weight of approximately 200 kDa, equally distributed between its protein and DNA content[15]. It possesses a disk-shaped form with a diameter of about 100 Å and a height ranging from 25 Å at the dyad to 60 Å at the H2B αC helices[18]. Its surface is highly complex. Three ridges are formed by the helices H2B α1, H2B αC and H3 α1 together with the H4 tail[18]. The groove between H2B's helices α1 and αC harbors the so-called 'acidic patch' (Fig. 2a; see 2.1.1.2)[18]. Also, a larger depression occurs close to the dyad overlaying the H3-H3 interface[18].
The exact number of base pairs contained in one NCP depends on the DNA sequence. Initial X-ray structures used the human alpha satellite sequence with lengths of 146 bp and 147 bp as a positioning sequence[15,23]. The latter resulted in a higher resolution structure due to reduced disorder[23]. Since the dyad is formed by one base pair, an odd number of base pairs results in a symmetric, better ordered particle in the crystal[23]. The strong positioning Widom 601 sequence[24], however, forms a NCP with only 145 bp[25,26]. This is caused by DNA stretching by one base pair at SHL ±5 compared to the human alpha satellite sequence[18,25,26].

2.1.1.2 The acidic patch

The NCP offers three structurally and chemically distinct binding sites for interaction: the rather unstructured histone tails (see 2.1.1.3), the DNA wrapped around the outside of the histone octamer (see 2.1.1.4) and the central, solvent-exposed disk of the histone octamer[27]. Among the factors characterized, several interact with a specific area on the histone disk[26,28-34], referred to as the acidic patch[35]. This term describes an acidic residue-rich region located in a depression between the distal ends of the helices H2B α1 and H2A α2 as well as the C-terminal helix of H2B (Fig. 1a)[15,27,36]. The cluster of acidic residues results in a negatively charged area on the otherwise positively charged histone octamer surface (Fig. 2b). It comprises the amino acids E56, E61, E64, D90, E91 and E92 of H2A as well as E102 and E110 of H2B[27,36]. While the contributing residues of H2A are located at the bottom of the groove, H2BE102 and E110 project into it (Fig. 2c)[36]. A small ridge divides the acidic patch with H2AE61, D90 and E92 lying in the deeper of two pockets (Fig. 2c)[27]. On top, H2AY50, V54 and Y57 form a hydrophobic pocket, enabling various types of interaction at this site (Fig. 2c)[36]. Of note, the charge of the acidic patch is influenced by H2A variants. While H2A.Z increases its acidity[37], it is decreased by H2ABbd (Barr body deficient)[38].
The acidic patch is important for chromatin organization[36]. It binds to K16 in the H4 tail of neighboring nucleosomes, which drives compaction of the chromatin fiber[15,39]. Modulating this interaction impacts chromatin condensation. While H4K16 acetylation (H4K16ac) inhibits its complete folding, H2A.Z-containing nucleosomal arrays adopt a more compact structure[37,40,41] (discussed in detail in 2.1.2.1). As indicated above, numerous chromatin-associated proteins have been demonstrated to bind to the nucleosome in parts or entirely via the acidic patch. Disruption of these interactions leads to decreased affinity[28-30,32,42,43] and in some cases also to an impaired catalytic action of the bound factor[28,34,44,45]. Some of these factors interact with multiple sites of the nucleosome and they do not share any sequence homology in the acidic-patch-interacting region[27,36]. However, they all contain a critical arginine residue forming polar interactions with H2AE61, D90 and E92, which is therefore termed the arginine anchor motif[27].

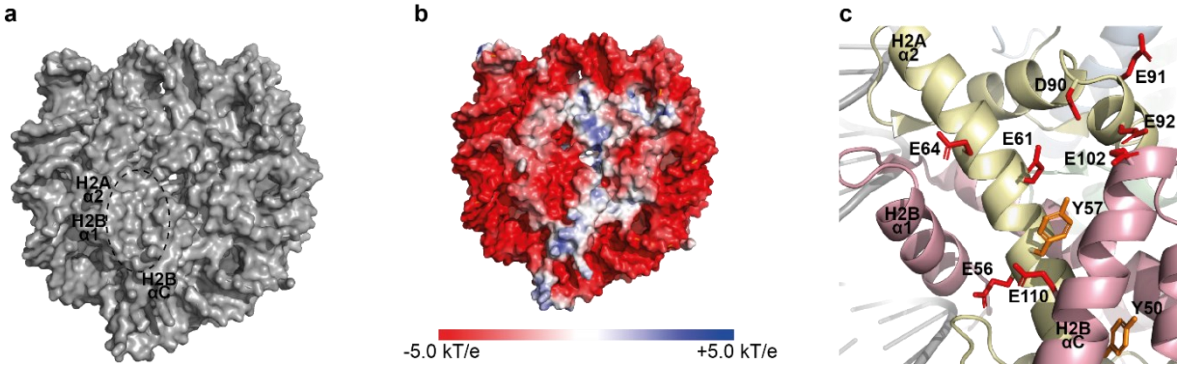

Figure 2: Location and atomic details of the acidic patch. a, Surface representation of the nucleosome core particle. Helices forming ridges are labeled and the location of acidic patch is indicated by a dashed line. **b,** Electrostatic potential of the nucleosome core particle. Potential was calculated using APBS-PDB2PQR[46]. **c,** Close-up view on the acidic patch. Pale yellow: H2A; Pale red: H2B; Grey: DNA. Acidic side chains contributing to acidic patch are shown in red, residues of hydrophobic pocket in orange. Note that H2AV54 is hidden underneath the C-terminal α-helix of H2B. Figure adapted from[27,36] using high-resolution structure[15] (pdb: 1AOI).

2.1.1.3 The histone tails

The eight histone folds, two H2B αC helices and two H3 αN helices form the spool around which DNA is wrapped (Fig. 1c, d)[15]. Beyond this core, each histone is extended at its N-terminus (referred to as N-terminal domain, NTD) while H2A also possesses additional residues at its C-terminus (Fig. 1a)[14]. These extensions are called histone tails and make up 25-30% of the histone mass[47,48]. They are unstructured, more basic than the histone fold and also evolutionarily conserved[16,47]. The tails were initially identified as protease-sensitive regions of the core histones indicating that they are exposed to solvent[49]. They protrude from the nucleosome disk following the minor grooves of the nucleosomal DNA[15,23]. While the tails of H2B and H3 exit between the two DNA gyres, H2A and H4 exit from the top or bottom of the nucleosome disk[15,23]. Histone tails are highly dynamic and interact with the histone spool, nucleosomal DNA, and linker DNA[48,50-52]. Tail interactions stabilize the nucleosome disk and modulate accessibility of the tails[53,54]. Even in condensed nucleosome arrays, histone tails remain dynamic and accessible[55]. Due to their flexible nature, there is little structural knowledge about the histone tails in the context of the entire NCP[47]. Crystal contacts between H4K16 and the acidic patch represent one rare exception (see 2.1.1.2)[15]. However, extensive biochemical work demonstrated the importance of histone tails. They are highly rich in arginine and lysine residues[16]. These can undergo multiple posttranslational modifications (PTMs) especially, but not limited to: acetylation, methylation, phosphorylation, ubiquitylation and ADP-ribosylation[56,57]. A number of factors have been characterized that generate, detect or remove PTMs and are thus categorized as writers, readers or erasers[58]. Histone modifications (also called histone marks) impact nucleosome dynamics as well as manifold chromatin-dependent processes[56,57,59]. A number of amino acids within the histone folds can also be modified in a context-specific manner[59] but the histone tails turned out to be a hot-spot for carrying these epigenetic marks due to their accessibility and number of modifiable residues[56,57].

2.1.1.4 Nucleosome positioning sequences

Early structural studies used nucleosomes from endogenous sources[11,13,60]. In these the NCPs were extracted from chromatin by micrococcal nuclease (MNase) digestion[61,62]. This procedure results in particles containing DNA of mixed sequence and a length of 146 ± 3 bp[11,61]. This inhomogeneity led to disorder in the crystals, which in turn resulted in low resolution structures that did not provide insights on an atomic level[11,13,60]. Highly homogenous, symmetrical phased NCPs turned out to be crucial for high-resolution structure

determination[15,23,63,64]. This limitation could be overcome by modern recombinant DNA technology enabling the production of DNA fragments of defined sequence and length in large quantities[65]. Initially, a sequence from the 5S rRNA gene was used to reconstitute nucleosomes[66]. Later, a fragment of the alpha satellite sequence from the centromere of the human X chromosome was also characterized as a well suited nucleosome positioning sequence[63]. This was used in the first high resolution structure of the NCP and many subsequent studies[15,18]. Progress with nucleosome positioning on DNA fragments longer than 147 bp was made by the discovery of the Widom 601 sequence[24]. This synthetic sequence was found in a SELEX screen and enables the precise positioning of the histone octamer[24]. The tight interaction with the histone octamer is presumably caused by a 10 bp periodicity of TA base steps in the sequence[24]. Structural constraints for DNA are greatest at contact points around the dyad, where minor grooves contact the H3-H4 tetramer (SHL ±0.5, ±1.5, ±2.5; Fig 1d)[67]. It had been suggested earlier that AA, TT, AT and TA steps are favored at these sites[68]. Indeed, crystal structures of NCPs containing the Widom 601 sequence found TA steps at these exact locations[25,67]. It is assumed that the TA step accommodates the conformational challenges best due to its flexibility, resulting in a higher affinity towards the nucleosome[18,67,69]. The Widom 601 sequence is asymmetrical, exhibiting four out of five TA steps at one side of the nucleosome dyad (601L) and only one at the other (601R)[18,24,67]. This suggests different affinities for the two sides and indeed an asymmetry in strength of histone-DNA contacts is observed[70]. Consequently, a palindromic 601L sequence with eight TA steps forms a more stable nucleosome than the palindromic 601R or the Widom 601 sequence[18,67]. The assumption of TA steps at octamer-interacting minor grooves strengthening the interaction is further supported by the fact that in hexasomes, reconstituted with the Widom 601 sequence, 601L is the side to which the remaining H2A-H2B dimer binds[71]. In line with this model, the periodicity of TA base steps also emerges in other strong positioning sequences from the SELEX screen such as the 603 and 605 sequence[24,67]. In any case, the nucleosome dyad is formed by one single base pair, independent of the aforementioned sequences[15,21,25].

2.1.1.5 Linker histones

Individual NCPs are connected by linker DNA, which is often bound to linker histones[18,72]. Multiple H1 variants, including H5, are grouped under this term[73]. Linker histones influence the chromatin structure by modulating the degree of compaction and regulate gene expression[74-76]. One linker histone associates with about 20 bp of linker DNA[6,77]. This gives rise to another defined particle in chromatin organization, called the chromatosome, comprising the histone octamer, one linker histone and ~165 bp of DNA[6,74,78]. Linker histones differ from core histones significantly. They are less conserved in their primary sequence, possess a distinct domain architecture and are presumably of bacterial rather than archaeal origin[73,79,80]. In general, linker histones share a conserved tripartite structure consisting of a flexible N-terminal tail, a central globular domain and a long, basic and intrinsically disordered C-terminal tail[79]. The globular domain interacts with the NCP and linker DNA while the C-terminal tail only binds to linker DNA[79,81-83]. The N-terminal tail in turn, does not show binding affinity to either of them[81]. H1.0 interacts with non-histone proteins, particularly nucleolar

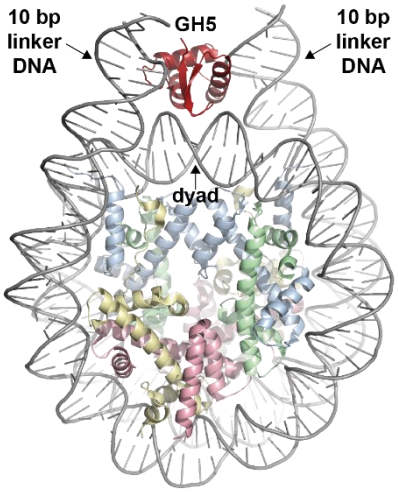

Figure 3: Structure of the chromatosome. Cartoon representation of the high-resolution structure of the chromatosome in the symmetrical binding mode (pdb: 4QLC)[83]. Deep red: globular domain of H5 (GH5); Pale yellow: H2A; Pale red: H2B; pale blue: H3; pale green: H4; Grey: DNA. Figure adapted from[83].

proteins, via all its domains[84]. Exceptions to the tripartite structure occur especially in unicellular eukaryotes[72]. Hho1p from *Saccharomyces cerevisiae*, the only H1-like protein in budding yeast, is one well-studied example[72]. It consists of a short N-terminal tail followed by two globular domains connected by a lysine-rich segment[85]. Similar to core histones, linker-histones can undergo multiple post-translational modifications[86]. The 3D structure of the chromatosome was solved recently by employing a combination of X-ray crystallography and NMR spectroscopy (Fig. 3)[83]. It confirms the symmetric binding model, in which the globular domain of the linker histone interacts with 10 bp of each linker DNA as well as the nucleosome dyad[79,83]. This is supported by earlier computational docking models, which identified three DNA binding domains of the globular domain[87]. However, this study does not exclude asymmetric binding modes in which the globular domain interacts with one linker DNA only without contacts to the NCP[88,89]. It rather suggests that different binding modes impact the higher order chromatin structure differentially[83].

2.1.2 Chromatin folding and architecture

The NCP repeats approximately every 160 – 240 bp across the genome[90]. At low ionic strength, this gives rise to the so-called 'beads on a string' arrangement or 10 nm fiber, an extended nucleosomal array in which the NCPs are the 'beads' connected by linker DNA[9,91,92]. This is also adopted by an *in vitro* reconstituted array of twelve nucleosomes ('208-12 array') under similar experimental conditions[93]. However, to fit into the nucleus, the chromatin fiber has to condense massively[94]. The degree of compaction is illustrated by an early study, which determined a local DNA concentration of 200 $^{mg}/_{mL}$ in eukaryotic nuclei[95]. In the first place, the nucleosomal array folds locally through contacts between neighboring nucleosomes[94]. This is driven by divalent ions and linker histones[83,93]. It further compacts to a fine-tuned arrangement, which is also the result of the action of numerous non-histone proteins[96].

2.1.2.1 Short range nucleosome-nucleosome interactions

Early on, it had been noticed that nucleosomal arrays condense at physiological ion concentration[91,92]. Divalent cations are particularly important for this process[91,92]. They mediate short-range nucleosome-nucleosome interactions[97] resulting in fibers with helical architecture, also referred to as higher-order chromatin structure[92,98,99]. Subsequent studies identified histone tails to also be crucial for this reversible self-association[100]. Structural and biochemical studies showed that divalent cations mediate the interaction between the highly basic H4 tail and the acidic patch of the neighboring nucleosome[15,101]. As observed by crystal contacts, K16 of histone H4 is the main interacting residue with the acidic patch (also see 2.1.1.2)[15,39]. The importance of this polar interaction for chromatin folding is nicely illustrated by two observations made by changing the charge of one binding partner. On the one hand, H4K16ac interferes with fiber compaction, thus representing an important histone modification for controlling chromatin accessibility[40,41]. On the other hand, the more acidic patch of H2A.Z-containing nucleosomes leads to the formation of a more compact chromatin structure[37]. Moreover, structural analyses of the tetranucleosome revealed an interaction of

the C-terminal helices of H2B from adjacent nucleosomes[102,103]. Again, modification of the interacting histone portion affects chromatin compaction, as ubiquitination of H2B αC results in an open and accessible fiber conformation[104].
Thus, the self-association at physiological ion concentration is an intrinsic property of nucleosomal arrays[94]. Linker histones promote this process by stabilizing and further compacting the fiber[99,105]. They stimulate tail-induced chromatin compaction rather than promote folding via an alternative pathway, since the lack of histone tails inhibits fiber formation even in the presence of linker histones[106]. In the condensed chromatin fiber, two left-handed helical stacks are interwound[102,103]. Its repeating unit is the tetranucleosome with asymmetrically bound linker histones directed to the inside[103]. Due to its diameter, it is often referred to as the '30 nm fiber'[99]. It was commonly assumed to be the first level of a hierarchical chromatin folding mechanism[107]. Its highly regular arrangement has been observed *in vitro* for chromatin isolated from endogenous sources as well as recombinantly reconstituted arrays[91,92,103,105]. However, its existence *in vivo* is seriously questioned[108,109]. It could not be detected *in vivo* biochemically and studies using super-resolution microscopy instead suggest that nucleosomes are irregular arranged in heterogeneous clutches[110,111]. One possible explanation for the contradicting observations is the dilution of chromatin *in vitro*, which might restrict nucleosome interactions in *trans*[110,112]. Beyond the controversy about whether or not a 30 nm fiber exists inside eukaryotic nuclei, nucleosome-nucleosome contacts are crucial as a first step in chromatin organization as *in vivo* studies also observe a tri- or tetranucleosome folding motif[110].

2.1.2.2 Chromatin domains

In vitro studies of chromatin fibers have primarily been conducted using electron microscopy, X-ray crystallography and analytical ultracentrifugation[9,91,93,102,103]. To capture chromatin organization *in vivo*, new techniques have been developed in recent years. Chromatin immunoprecipitation (ChIP) enabled the identification and characterization of gene loops and lamina-associated domains (LADs)[113,114]. The family of chromosome conformation capture techniques (3C, 4C, 5C, Hi-C and Micro-C) works independent of nuclear landmarks. Instead, regions in spatial proximity are identified by DNA crosslinking *in vivo*, digestion, re-ligation and subsequent sequencing[115]. Thereby, these methods monitor long-range chromatin interactions and chromosome folding on a genome-wide scale[116]. They led to the discovery of several architectural features, most importantly enhancer-promoter loops, topologically associated domains (TADs) and chromatin compartments[117-121].
The term chromatin loop groups multiple medium- to long-distance interactions in *cis* including, but not limited to, gene loops and enhancer-promoter loops[113,117,122]. They occur in a highly context-specific manner and are frequently mediated by non-histone proteins[122]. They are often anchored at domain boundaries (see below) where they interact with the DNA-binding protein CTCF and appear to be conserved[123].
TADs are a particularly interesting feature. They were identified as segments with pronounced long-range interactions between loci in one domain but reduced contacts to different loci[118,119]. TADs are structurally defined and in mammals several hundred kb in size[118,119]. They constitute functional domains as genes within one TAD can correlate their expression pattern[118]. Most intriguingly, TADs are largely invariant between cell types and even conserved through evolution[118,119]. This suggests that they are fundamental, self-assembling building blocks in higher order chromatin organization and therefore chromosome architecture[124]. Smaller domains are observed in *Saccharomyces cerevisiae* and even bacteria and termed

chromosomally interacting domains (CIDs)[110,125]. Of note, despite being only 2 – 10 kb in size, CIDs of budding yeast comprise a comparable number of genes as mammalian TADs[110].
In mammals, several TADs associate in *cis* and *trans* to chromatin compartments, which are ~5 Mb in size[120]. They occur as more accessible, gene-rich transcriptionally active A compartments or densely packed, gene-poor, transcriptionally repressed B compartments[120]. Therefore, histone marks linked with active transcription are mostly found in A compartments[120]. Sub-types of these compartments were identified subsequently[123]. The compartments alternate along chromosomes and thereby primarily interact with compartments of the same type[120,126,127]. Thus, Hi-C experiments demonstrate that the 3D architecture of chromatin at a given locus depends on the genomic sequence and the local epigenetic states as well as the position on the chromosome[120,126-128]. Unlike TADs, chromatin compartments are tissue specific and correlate with cell specific expression patterns[120]. Moreover, TADs can switch between compartments in a cell-type specific manner[120,129]. This supports the concept of TADs being a fundamental unit of chromatin organization[124].
On a larger scale, single chromosomes occupy discrete territories[130]. While gene-rich chromosomes tend to locate in the center of nuclei, gene-poor chromosomes are primarily found close to the nuclear lamina[122]. Interactions in *trans* are rare but can occur to form large regions of similar transcriptional states[121,122].

2.1.2.3 Euchromatin and heterochromatin

When studying chromatin condensation in 1928, Emil Heitz coined the terms euchromatin and heterochromatin based on chromosomal staining patterns[131]. He defined euchromatin as sections of chromosomes which de-condensate after mitosis while heterochromatin remains densely packed throughout the cell cycle[131,132]. Subsequent studies identified euchromatin as open and flexible, potentially or actively transcribed regions exhibiting high content of RNA polymerase and elevated levels of acetylated histone tails as well as trimethylated H3K4 and H3K36 (H3K4me3, H3K36me3)[133]. Heterochromatin, in contrast, is less dynamic and displays little to no transcriptional activity[134]. Along the chromosome it particularly occurs at telomeres, centromeres and a specific set of genes, presumably involved in developmental processes[135-137]. It can be classified into two sub-categories. While constitutive heterochromatin is consistently formed throughout the cell cycle, facultative heterochromatin specifies locus- and cell-type-specific heterochromatin[134]. The former is enriched in repetitive DNA sequences and methylated H3K9 (H3K9me)[134]. This histone mark serves as a binding platform for heterochromatin protein 1α (HP1α), which compacts the underlying chromatin[138,139]. Facultative heterochromatin is established by Polycomb group (PcG) proteins and particularly rich in di- and trimethylated H3K27 (H3K27me2, H3K27me3)[140]. These modifications are established by the PcG multiprotein complex Polycomb repressive complex 2 (PRC2), which mediates gene silencing in conjunction with PRC1[141].

2.1.2.4 Phase-separation of heterochromatin

Biomolecules in aqueous solution can de-mix at high concentrations to form condensates, which are membraneless functional compartments of enriched multivalent molecules[142,143]. This process is referred to as liquid-liquid phase separation[143]. The formation of condensates enables cells to locally concentrate specific proteins and nucleic acids[142]. This principle was initially demonstrated for P granules in *C. elegans* but has in the meantime been investigated on many more such compartments, such as stress granules, nucleoli and DNA damage repair sites[144-147]. Phase-separation also occurs in constitutive heterochromatin mediating the formation of heterochromatic domains[148,149]. This process is initiated by DNA binding of HP1α or phosphorylation of its N-terminal tail, which thereupon nucleates into liquid droplets[148,149].

The N- and C-terminal portion of HP1α as well as its hinge region contain intrinsically disordered regions (IDRs) and low-complexity sequences, which have been shown to stimulate liquid-liquid demixing[142,149-151]. Phase separation allows HP1α-associated heterochromatin to adopt a range of states of different physical properties[152]. They can be roughly divided in the following three: soluble with dimeric HP1α, liquid droplets containing oligomeric HP1α, and an even denser, gel-like state[148,152]. As these states are associated with increasing compaction, they might represent different levels of transcriptional repression thereby contributing to gene regulation[152]. Also, compartmentalization could regulate processes inside heterochromatin by controlling access to it[149]. Potentially, their formation is controlled by regulating HP1α oligomerization, which is sensitive to PTMs and binding of other factors[148].

2.1.3 Genic nucleosomal arrays

The organization of DNA as the nucleoprotein complex chromatin enables its packing into the eukaryotic nucleus. However, as DNA is compacted by a factor of 10000 and extensively folded, chromatin also constitutes a barrier for accessing the genetic code[153]. At the same time, histones provide a platform to guide enzymes to specific loci by targeted placement of PTMs and histone variants[58,154]. Furthermore, nucleosomes are dynamic as they can slide on DNA and disassemble in a controlled fashion[155,156]. Thus, the access to DNA inside chromatin is controlled by histone modifying enzymes, histone chaperones and chromatin remodellers, thereby regulating DNA-dependent processes[58,155,157]. As these factors all act on single nucleosomes, it is of particular relevance to investigate nucleosomal position, composition and modification on a genome-wide scale. This has become feasible by the family of ChIP-seq and MNase-seq techniques, which combine chromatin immunoprecipitation and / or nucleolytic digest with deep sequencing[158,159].

Transcription and replication of DNA are fundamental biological processes, which both depend on direct access to DNA. They are initiated at promoters and origins of replication, respectively, whose chromatin organization is therefore of special interest[160]. In active states, both are characterized by a central, nucleosome-free or nucleosome-depleted region (NFR / NDR), which is flanked by asymmetric arrays of phased nucleosomes, referred to as genic nucleosomal arrays (Fig. 4)[161,162]. Transcriptionally active gene promoters exhibit an NFR in their core sequence to enable binding of the transcription initiation machinery[163]. It is flanked by the well-positioned -1 and +1 nucleosomes (Fig. 4)[161]. The former is often formed by a "fragile nucleosome", which is more sensitive to MNase digestion[164,165]. Features of the +1 nucleosome are coupled to transcriptional activity of the respective gene. It is particularly precisely positioned and harbors the transcription start site (TSS) in *Saccharomyces cerevisiae*[166,167]. Unlike gene body nucleosomes, it constitutes a major barrier for transcription[168]. However, the incorporation of H2A.Z, predominantly at the promoter-distal side of the +1 nucleosome, promotes the passage of RNA polymerase II (RNAPII) by destabilizing the nucleosome[156,168]. This also directs transcription by introducing an asymmetry in the particle[160]. H2A.Z turnover at the +1 nucleosome depends on proper assembly of the pre-initiation complex (PIC)[169]. In TATA-less promoters, the +1 nucleosome binds to subunits of the PIC and contributes to its positioning relative to the TSS[170]. An upstream shift of the +1 nucleosome leads to decreased transcription rates, possibly by sterically interfering with PIC assembly[171]. In line with this conclusion the +1 nucleosome is the only well-positioned nucleosome of inactive promoters in the human genome, but located 30 bp upstream from its site in active promoters[167]. The promoter-proximal side of the +1 nucleosome of actively transcribed genes is enriched in ubiquitylated H2BK123[156]. Its loss results in accumulation of RNAPII at promoters, indicating that this modification also facilitates

RNAPII penetration into the gene body[172]. Of note, it is located at the H2B αC helix and also inhibits chromatin fiber compaction (see 2.1.2.1)[104]. Thus, the position, composition and PTMs of the +1 nucleosome regulate gene expression. The pattern of regularly spaced and well-positioned nucleosomes continues past the +1 nucleosome but blurs more and more inside the gene body (Fig 4)[161]. The initial and majority of subsequent studies on genic nucleosomal arrays have been conducted in *Saccharomyces cerevisiae*, where the mean internucleosomal distance between the regularly spaced nucleosomes is 165 bp[153,160,161]. However, they have also been observed in *Homo sapiens* and *Drosophila melanogaster*, demonstrating that they are a hallmark feature of active eukaryotic genes[167,173].

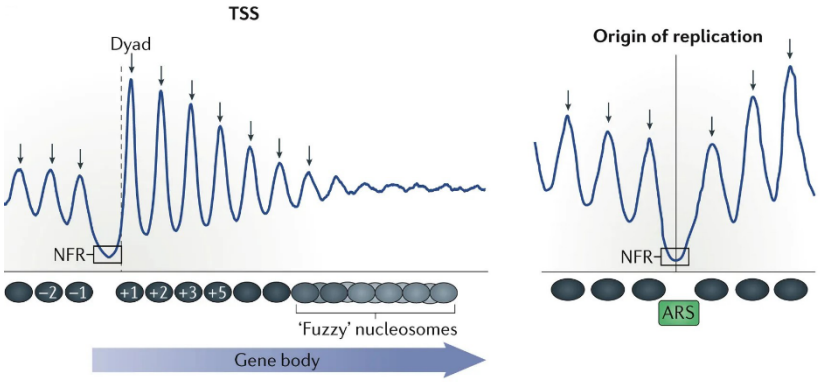

Figure 4: Nucleosome positioning around promoter sites (left) and origins of replication (right). The blue line represents composite occupancy of nucleosomes relative to transcription start site (TSS, left) and autonomously replicating sequence (ARS, right). Peaks and valleys represent high and low nucleosome occupancy, respectively, while peak width indicates relative positioning. Nucleosomes are shown as grey ellipses underneath composite blots. Arrows mark predicted dyad positions. Figure taken from[160].

Eukaryotic DNA replication is initiated at origins of replication (hereafter called origins), which contain binding sites for the origin recognition complex (ORC)[174]. In *Saccharomyces cerevisiae*, origins are defined by autonomously replicating sequences (ARS), which are ~100 bp in size and harbor a 11 bp ORC-binding sequence, the ARS consensus sequence (ACS)[174,175]. ARSs contain three more elements, termed B1-3, which are also required for origin function[175]. The ORC recruits the MCM helicase (mini-chromosome maintenance helicase) and cofactors, which unwind the DNA after cell cycle-dependent activation into the CMG (Cdc45-MCM-GINS) complex[174]. Active, ORC-bound origins exhibit an asymmetrical NFR around the ARS and flanking genic nucleosomal arrays (Fig. 4)[162]. In an *in vitro* reconstituted system, the NFR is more pronounced after ORC-binding indicating that ORC acts as a barrier for nucleosomes[176]. Vice versa, nucleosomes suppress non-specific ORC binding[176]. The -1 and +1 nucleosome are stably positioned and both contain the histone variant H2A.Z[162,177]. They can be positioned by the action of ORC only, but the formation of larger arrays requires additional factors[162]. The genome of *Saccharomyces cerevisiae* contains a considerable number of non-replicative, ORC-free origins that lack the characteristic nucleosome signature and possess a less pronounced NFR[162]. This suggests that DNA replication is regulated by nucleosome positioning[160,162]. Active replication can only occur in the presence of auxiliary factors as chromatin inhibits replisome progression[176]. Intriguingly, the histone chaperone FACT (facilitates chromatin transcription) has recently been identified to be crucial for replication of DNA organized as chromatin[176]. It is not known whether it removes histones ahead of the replication fork, but FACT was shown to deposit H3-H4 tetramers on newly synthesized DNA, presumably in conjunction with another histone chaperone termed Rtt106[178]. Phased nucleosome arrays also occur apart from promoters and origins, where they are formed around DNA sequences acting as barrier elements[179].

That the underlying DNA sequence can contribute to nucleosome positioning is also illustrated by an *in vitro* experiment in which the NFR of yeast promoters is formed by salt gradient dialysis (SGD) of histone octamers and genomic DNA, albeit to a reduced extent[180]. In order to wrap around the disk-shaped histone octamer, DNA needs to bend[15]. Sequences with a 10 bp periodicity of A and / or T (A/T) dinucleotides and G/C dinucleotides running counter phase have been shown to accommodate these torsional demands best (also see 2.1.1.4)[173,177,181,182]. Of note, sequences with periodic AA dinucleotides are modestly enriched in -1 and +1 nucleosomes at promoters of *Saccharomyces cerevisiae*, but without auxiliary factors not sufficient to position nucleosomes[183]. Therefore, DNA shape properties, which can be similar between different DNA sequences, influence nucleosome positioning in presence or absence of additional factors[183]. Consequently, DNA stretches favoring or disfavoring nucleosome formation exist throughout the genome[184]. However, the complex pattern of phased nucleosomes requires the action of numerous *trans*-acting factors, especially chromatin remodellers[179,180,183]. They thereby control DNA-dependent processes and are discussed in the following sections[155].

2.2 Chromatin remodellers

In vitro studies of nucleosome positioning around promoters impressively demonstrate the importance of ATP-hydrolyzing enzymes in chromatin organization[180,183]. These are grouped under the term chromatin remodelling complexes (hereafter termed remodellers), which have not only been shown to be critical for transcription but virtually for all DNA-dependent processes inside eukaryotic nuclei[185]. Nucleosomes can be formed by remodellers by depositing histones on DNA, slid and spaced to control access to DNA or form regulatory arrays, and changed in their composition by incorporation or ejection of histones[183,186-188]. Hence, chromatin dynamics largely depends on the action of remodellers[155].

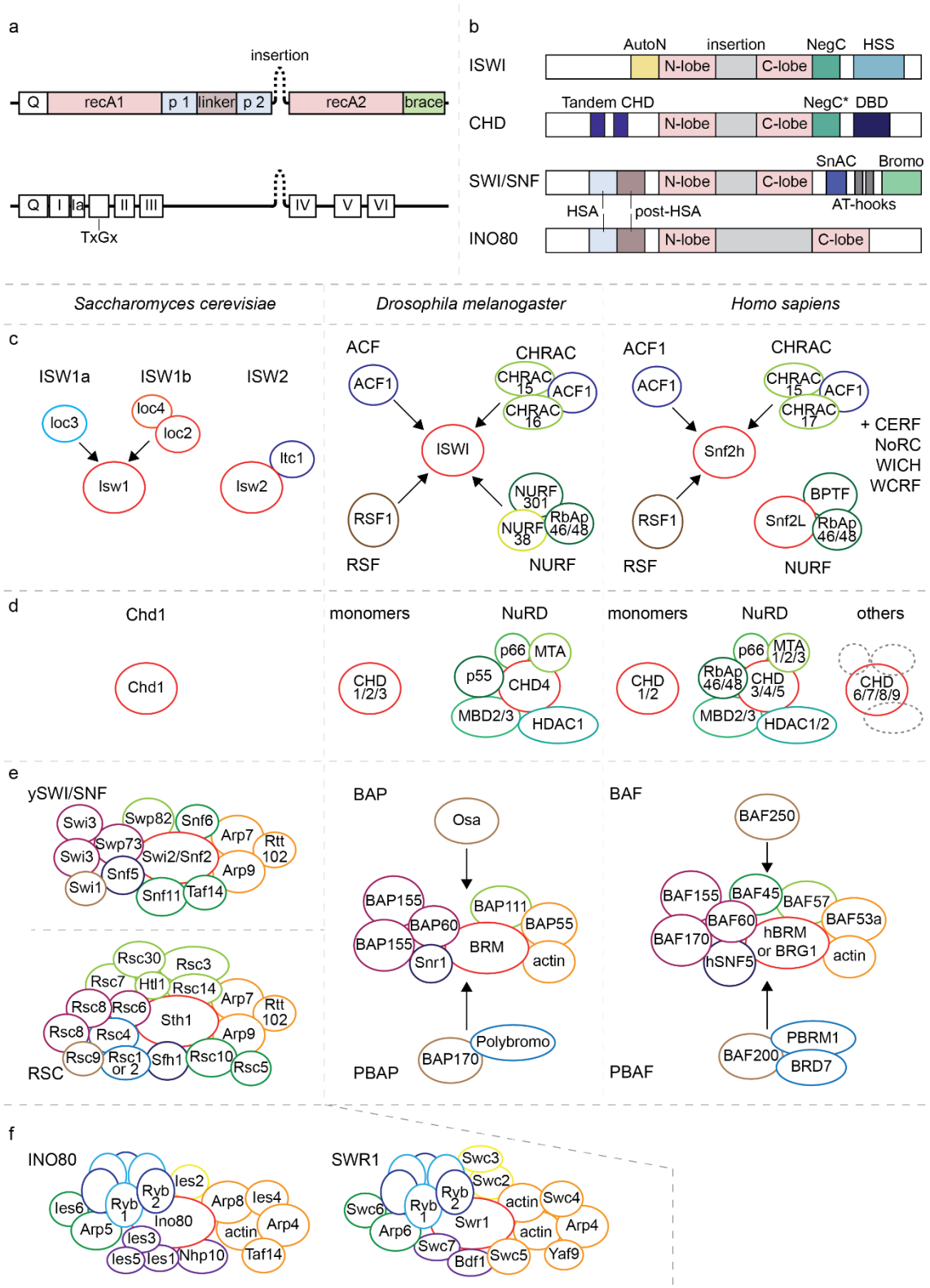

Figure 5: The four families of chromatin remodellers. a, Schematic representation of Snf2-type ATPases. Top: Domain arrangement in Snf2-type ATPases. recA1/2: recA-like domain 1/2; P 1/2: protrusion 1/2. As the length of the insertion varies, it is shown as a dashed line. Bottom: Position of helicase-related motifs in Snf2-type ATPases. Figure adapted from[189]. **b,** Schematic representation of position of conserved domains in ATPases of the four remodeller families. Figure adapted from[155]. **c-f,** Chromatin remodellers in *Saccharomyces cerevisiae* (left panel), *Drosophila melanogaster* (middle panel) and *Homo sapiens* (right panel). **c:** ISWI family, **d:** CHD family, **e:** SWI/SNF family, **f:** INO80 family. ATPase subunits are shown as red ovals. If several complexes are formed based on one ATPase, additional subunits are grouped and labelled with complex name and association to ATPase is indicated by an arrow. Composition of species-specific subunits of metazoan INO80 members is poorly characterized and therefore not shown. Figures adapted from[190-193]. For abbreviations and additional references see main text.

2.2.1 The four families of chromatin remodellers

All remodellers possess an RNA/DNA helicase superfamily 2 (SF2)-type ATPase as a motor domain[189]. More specifically, they can be grouped in the Snf2 family, a subfamily of SF2 (see 2.2.2)[189]. These ATPases consist of two recombination A protein (recA)-like lobes, which are separated by an insertion (Fig. 5a)[194]. Based on the length of this insertion and the presence of unique flanking domains, remodellers can be classified into the following four families: ISWI (imitation switch), CHD (chromodomain helicase DNA-binding), SWI/SNF (switching defective/sucrose non-fermentable) and INO80 (inositol requiring80) (Fig. 5b)[155,185].

2.2.1.1 The ISWI family

The ISWI family is characterized by a short insertion and the small AutoN (autoinhibitory N terminal) and NegC (negative regulator of coupling) domains adjacent to the ATPase lobes as well as the longer, C-terminal HSS (HAND-SANT-SLIDE) domain (Fig. 5b)[195,196]. The latter has been shown biochemically to interact with the H3 tail and linker DNA[195,197]. The ISWI ATPase is intrinsically active and negatively regulated by AutoN and NegC[196]. Upon substrate binding, this effect is overcome mediated by the H4 tail and extranucleosomal DNA[196]. Thus, unlike other remodellers, the ISWI ATPase is efficiently stimulated only by nucleosomes but not free DNA[198].

ISWI remodellers were initially characterized in *Drosophila melanogaster*, where the ATPase assembles with up to three additional factors to form four different complexes: NURF (nucleosome remodelling factor), CHRAC (chromatin accessibility complex), ACF (ATP-utilizing chromatin assembly and remodelling factor) and RSF (remodelling and spacing factor) (Fig. 5c)[190,199]. *Saccharomyces cerevisiae* encodes two versions of the ISWI subunit, Isw1 and Isw2, that form three distinct complexes: ISW1a, ISW1b and ISW2 (Fig. 5c)[200,201]. In *Homo sapiens*, two ISWI-type ATPases also exist, termed Snf2L and Snf2h, which give rise to numerous complexes (Fig. 5c)[190,202]. ISWI complexes can assemble, slide and space nucleosomes[199]. In yeast promoters, ISW2 promotes positioning of the +1 nucleosome while ISW1a generates properly spaced nucleosomal arrays downstream of the +1 nucleosome[183]. These show a nucleosomal repeat length of ~170 bp, which is very similar to the spacing observed *in vivo*[161,183]. ACF, CHRAC and RSF assemble and slide nucleosomes thereby giving rise to nucleosomal arrays[203-205]. However, nucleosome sliding by NURF disrupts this periodicity, illustrating how attendant subunits impact the catalytic action of the same motor[206]. NURF is required for transcription activation[207]. A plant homeodomain (PHD) finger domain in the NURF subunit BPTF (bromodomain and PHD finger transcription factor) specifically interacts with H3K4me3, which is present at TSSs of active genes[208]. This targets NURF to promoters to regulate gene expression[209]. ISWI remodellers also impact higher order chromatin structure. While ACF can move entire chromatosomes within chromatin fibers, the loss of ISWI leads to a reduction of H1-associated chromatin and decondensation of chromosomes[210,211].

2.2.1.2 The CHD family

CHD proteins feature a tandem chromodomain in their N-terminal portion and C-terminal resemble the ISWI family[212]. They possess a NegC-like domain (NegC*) flanking the C-lobe of the ATPase and a DNA-binding domain (DBD) (Fig. 5b)[212,213]. The latter is homologous to the SANT and SLIDE domains from ISWI but lacks the HAND domain[214]. Chromodomains are important for chromatin organization apart from remodellers as they were initially found in the Pc protein and HP1 of *Drosophila melanogaster*[215]. The double chromodomain of human CHD1 binds H3K4me3, an euchromatic hallmark, while the single chromodomains of Pc protein and HP1 differentially read out the heterochromatic histone marks H3K27me3 and

H3K9me3, respectively (also see 2.1.2.3)[216,217]. *Saccharomyces cerevisiae* encodes for one single CHD protein, Chd1, which acts as a single subunit remodeller (Fig. 5d)[212,218,219]. In a cryo-EM study, its chromodomain was shown to bind to nucleosomal DNA at SHL +1[216]. The DBD interacts with DNA at the entry site of the nucleosome, which is detached from the histone octamer[220]. More CHD factors are present in metazoans, as *Drosophila melanogaster* possesses four and mammals nine different CHD proteins (Fig. 5d)[221,222]. These give rise to several complexes but metazoan CHD1 also acts as a monomer[223]. Yet, it catalyzes manifold reactions. It assembles nucleosomes in conjunction with the histone chaperone nucleosome assembly protein-1 (NAP1) and forms regularly spaced nucleosomal arrays in doing so[223]. It stimulates transcription by promoting RNAPII promoter escape and facilitating RNAPII passage through nucleosomes inside the gene body[224]. CHD1 is also involved in nucleosome editing as it contributes to the incorporation of the histone variant H3.3[225]. The later discovered dCHD3 protein from *Drosophila melanogaster* also acts as a single subunit remodeller[226]. Well-studied examples of CHD-containing complexes are the metazoan Nucleosome Remodelling and Deacetlyation (NuRD) complexes, which couple ATP-dependent chromatin remodelling to histone deacetylation thereby contributing to gene silencing[227-229]. In those, one of the CHD proteins 3 - 5 associates with histone deacetylases 1 and / or 2 (HDAC1/2) and further factors, uniquely combining these two enzymatic activities in one complex (Fig. 5d)[227,230-232]. Of note, these CHD proteins also possess an additional double PHD finger N-terminal of the chromodomain[233]. In a recently published cryoEM structure of human CHD4 bound to the nucleosome, the double PHD finger is shown to be located close to the nucleosome dyad[234]. NuRD complexes interact with HP1, emphasizing their role in gene silencing[232]. Acetylation and remodelling activity by NuRD components were also observed separately in *Drosophila melanogaster*[235,236].

2.2.1.3 The SWI/SNF family

Remodellers of the SWI/SNF family form multi-subunit protein complexes in the megadalton range (Fig. 5e)[237]. They slide and eject nucleosomes to control access to chromatin in diverse processes, but do not have a nucleosome editing activity[185]. Their main ATPase is flanked at its N-terminus by a helicase/SANT-associated (HSA) domain, which is coupled to a post-HSA domain (Fig. 5b)[155]. C-terminal, it possesses a Snf2 ATP coupling (SnAC) domain, AT-hooks and a bromodomain (Fig. 5b)[155]. The HSA domain is also present in remodellers of the INO80 family (see 2.2.1.4) and histone acetyltransferase (HAT) complexes[238]. All these complexes contain actin and / or actin-related proteins (ARPs), for which the HSA domain constitutes the primary binding site[238]. The post-HSA domain is not involved in ARP recruitment but is essential for yeast viability and remodeller function *in vivo*[238]. It is a negative regulator of ATPase activity and required for correct nucleosome positioning by the RSC complex (remodels the structure of chromatin; see below)[239]. The SnAC domain positively regulates ATPase activity and couples ATP hydrolysis to nucleosome movement[240,241]. AT-hooks are short DNA-binding motifs, which were first characterized in high-mobility group (HMG)I chromosomal proteins and found to bind the minor groove of AT-rich sequences[242]. They are required for the function of a subset of SWI/SNF remodellers[243]. The bromodomain binds acetylated lysine residues in H3 tails targeting SWI/SNF remodellers to these sites[244].

Two subclasses of SWI/SNF remodellers can be distinguished based on the motor domain and the subunit composition (Fig. 5e)[245]. *Saccharomyces cerevisiae* encodes two SWI/SNF-type ATPases: Swi2/Snf2 and Sth1[246,247]. The former assembles with other factors to the ySWI/SNF complex while the latter gives rise to the even larger and more abundant RSC complexes (Fig. 5e)[245,248]. Two variants of RSC exist, which differ in one subunit[243]. SWI/SNF remodellers

are evolutionary conserved[245]. *Drosophila melanogaster* also possesses two types of SWI/SNF complexes, called BAP (BRM-associated proteins; homologous to ySWI/SNF) and PBAP (Polybromo BAP; homologous to RSC) (Fig. 5e)[249,250]. These, however, share the same catalytic subunit, termed Brahma (BRM)[249-251]. Related complexes are also present in *Homo sapiens* based on the ATPases hBRM (human BRM) and BRG1 (BRM-related gene 1)[245]. HBRM and BRG1 with a specific set of additional subunits can both assemble the BAF (BRG1-associated factors) complex, which is homologous to ySWI/SNF and BAP (Fig. 5e)[245,252]. In turn, BRG1 is the sole catalytic subunit to form PBAF (Polybromo BAF), the homolog of RSC and PBAP (Fig. 5e)[245,253]. However, the situation in mammals appears to be more multifaceted. BAF components were shown to assemble in a combinatorial manner dependent on cell-type and developmental stage specific activities[254]. Humans and mice even possess a third, smaller SWI/SNF complex called GBAF (GLTSCR1 / GLTSCR1L BAF), which carries out cell type-specific functions[255,256]. Moreover, mouse embryonic stem (ES) cells express a specialized BAF complex termed esBAF, which is required for their maintenance and pluripotency[257].
The classification of SWI/SNF complexes in two families is in part based on homology between individual subunits but also on the number of bromodomains present in the complexes[185,245]. YSWI/SNF, BAP and BAF contain one bromodomain in their main ATPase[185]. In turn, RSC, PBAP and PBAF bear multiple bromodomains, which are in RSC distributed over several subunits and in PBAP located on one single protein, termed Polybromo[185]. PBAF comprises two additional subunits with bromodomains, Protein polybromo-1 (PBRM1) and Bromodomain-containing protein 7 (Fig. 5e)[253,258]. Bromodomains interact with H3-acetylated nucleosomes, which impacts location and function of SWI/SNF remodellers[244,259]. It increases affinity of ySWI/SNF and RSC towards nucleosomes and stimulates their remodelling activity[260]. This might partially be caused by structural rearrangement in the complexes, as the nucleosome binding cavity of RSC is opened by an acetylated peptide[261]. HATs introduce these histone marks for instance around DNA double strand breaks (DSBs), where ySWI/SNF binds the modified nucleosomes and promotes phosphorylation of H2A.X, triggering the DSB repair machinery[262]. RSC specifically interacts with acetylated H3K14, a modification found in active gene promoters[263]. This suggests a function of RSC in transcription, which has indeed been observed. It is located at gene promoters and required for normal transcription activity *in vivo*[264,265]. *In vitro*, RSC generates NFRs of physiological width by recognizing the directionality of poly(dA:dT) tracts in promoters[183]. Moreover, bromodomains regulate remodeller activity by intramolecular binding of acetylated residues of SWI/SNF components[263,266].
RSC and ySWI/SNF share only three subunits: Arp7, Arp9 and Rtt102 (repressor of *Ty1* transposition, gene 102) (Fig. 5e)[191]. Arp7 and Arp9 constitute essential building blocks in the complexes and their nucleotide binding and hydrolysis is not required for enzymatic activity of the remodeller[267]. They form a heterodimer, which assembles with Rtt102 and the HSA domain to a distinct module, capable of modulating the activity of the main ATPase[238,267-269]. Intriguingly, minimal complexes of Arp7, Arp9 and Swi2/Snf2 or Sth1 are sufficient to catalyze DNA translocation[270,271]. Metazoan SWI/SNF complexes contain actin and one ARP (*D.m.*: BAP55; *H.s.*: BAF53a)[191].

2.2.1.4 The INO80 family

Like SWI/SNF complexes, INO80 remodellers are multi-subunit protein complexes (Fig. 5f)[188,272-274]. Their main ATPase resembles that of SWI/SNF remodellers as it also bears HSA and post-HSA domain N-terminal of the two ATPase lobes (Fig. 5b)[185]. However, it lacks the C-terminal domains of SWI/SNF-type ATPases[272]. The hallmark feature of INO80 remodellers is the insertion between the two recA-like lobes, which is significantly longer than

in all other remodeller families (Fig. 5b)[185,272]. It comprises ~250 amino acids in *Saccharomyces cerevisiae* and more than 1000 residues in mammals[155]. *Saccharomyces cerevisiae* encodes two INO80-type ATPases, Ino80 (capital letters denote the complex, lowercase letters the catalytic subunit) and Swi2/Snf2-related 1 (Swr1)[188,272,274]. The former was described first and assembles with 14 more subunits to the INO80 complex, the founding member of this remodeller family (Fig. 5f)[273]. Swr1 gives rise to the SWR1 complex, which in total consists of 14 different proteins (Fig. 5f)[188,274].

The complexes share the subunits RuvB-like protein 1 and 2 (Rvb1/2), actin and Arp4 while both possess exclusive components, which are denoted Ino eighty subunit (Ies) 1-5 and SWR1 complex polypeptides (Swc) 2-7 in INO80 and SWR1, respectively (Fig. 5f)[274,275]. The insertions of Ino80 and Swr1 recruits a heterohexameric ring of Rvb1 and Rvb2[276-278]. Their HSA domains bind actin and ARPs similar to the SWI/SNF family[238]. Although homologous to SWI/SNF, it differentially interacts with a distinct set of factors[238]. In INO80, it recruits actin, Arp4 and Arp8 to form the Arp8 module[238]. Ies4 and TBP-associated factor 14 (Taf14) associate with these proteins and are also considered as part of the Arp8 module[276]. SWR1 lacks Arp8 but comprises a second actin molecule[279]. One actin binds to the canonical site in the HSA domain, forming the conserved actin-Arp4 heterodimer[279]. The second actin interacts with the C-terminal part of the HSA domain and / or the N-terminal portion of the post-HSA domain[279]. This approximately corresponds to the interaction site of Arp8 in INO80, which binds to the C-terminal region of the HSA domain[276]. This second actin additionally interacts with Swc5, which in turn binds the C-terminus of Swr1 indicating a looped structure of the Swr1 protein[279]. Moreover, Arp4 interacts with Swc4[280]. Arp4 is an essential protein in *Saccharomyces cerevisiae* and crucial for the activity of both INO80 and SWR1[276,281,282]. Taf14 is not only part of INO80 but also of ySWI/SNF, transcription factor IID (TFIID), TFIIF and NuA3[275,283-285]. In large part, it consists of a Yaf9, ENL, AF9, Taf14, Sas5 (YEATS) domain, which is a specific reader for H3K9 crotonylation[286]. By recognizing this PTM, Taf14 couples gene expression to the fatty acid metabolism[287]. It also binds acetylated H3K9, but at a lower affinity[286,288]. The YEATS domain of human AF9 was shown to preferentially bind crotonyllysine over acetyllysine too[289]. Protein AF-9 homolog (Yaf9) is the homolog of Taf14 in SWR1[290]. Its YEATS domain specifically interacts with acetylated H3K27[291], a histone mark of active enhancer elements[292]. INO80 and SWR1 both contain one ARP outside the module formed around actin and Arp4, which is Arp5 in INO80 and Arp6 in SWR1[188,273,274]. These bind to Rvb1 and Rvb2 giving rise to a core module, which is essential for the catalytic activity of the complexes[275,293,294]. The architecture of INO80 and its components is discussed in detail in 2.2.3.

SWR1 is specialized for editing nucleosomes by exchanging H2A-H2B for H2A.Z-H2B[188,274]. This reaction does not require nucleosome sliding, which has also not been monitored for SWR1[295]. The subunit Swc2 is essential for histone editing as it acts as a chaperone for the H2A.Z/H2B dimer[294,296]. Its specificity for H2A.Z over H2A is in part mediated by the hyperacidic patch of H2A.Z (also see 2.1.1.2)[296]. Additionally, Swr1-Z, a conserved domain within Swr1, binds to H2A.Z at its αC helix and promotes H2A.Z-H2B incorporation[297]. H2A.Z and H3K27ac co-localize at activating gene regulatory elements[298,299]. Thus, it seems likely that the Yaf9 YEATS domain targets SWR1 to active enhancers and promoters where it incorporates H2A.Z (also see 2.1.3)[291]. INO80 has been suggested to catalyze the reverse reaction stimulated by H3K56ac[300-302]. However, this observation is discussed controversially[303].

Unlike SWR1, INO80 is capable of sliding nucleosomes on DNA[273,275]. For this purpose, it requires more than 40 bp of extranucleosomal DNA, indicating that a subset of INO80 subunits binds outside the NCP[304,305]. Indeed, ChIP-exo data of the yeast promoter demonstrate placement of Ies5, non-histone protein (Nhp)10 and Arp8 in the NFR upstream of the +1

nucleosome (also see 2.1.3)[306]. Also, INO80 displays a high binding affinity to free DNA, which stimulates its ATPase activity similar to nucleosomes[275,304]. It is the only remodeller to precisely position -1 and +1 nucleosomes and to create an NFR in yeast promoters without the help of auxiliary factors[183]. This requires an active readout of promoter DNA by INO80, which is potentially accomplished by sensing DNA shape properties[183]. It is capable to space nucleosomes on its own, however not at physiological width [183]. INO80 and SWR1 are bound to more than 90% of all +1 nucleosomes, emphasizing their important functions in organizing the chromatin landscape around yeast promoters[306].

Consequently, INO80 was shown to promote transcription along with its initial characterization[273] and its role in transcription was further characterized more recently. INO80 synergistically acts with the ATM-type kinases Mitosis entry checkpoint protein 1 (Mec1) to evict RNAPII from chromatin under replication stress conditions[307] and targets RNAPII for proteasomal degradation[308]. Furthermore, INO80 coordinates a mechanism to link RNA quality control to transcription in which it co-transcriptionally recruits the RNA surveillance factor Nab2 to chromatin[309]. Intriguingly, this process appears to be linked to a H2A.Z-specific remodelling activity of INO80[309]. Considering the impact of INO80 on genic nucleosomal arrays in *in vitro* experiments and their presence at transcription start sites as well as origins, it is not surprising that several studies find a link between the remodelling activity of INO80 and DNA replication. It was shown to be located at origins to facilitate progression of the replication fork and its recovery in the event of stalling[310-312]. A study on human INO80 characterized its function in more detail by demonstrating that IN80 resolves R-loops (RNA:DNA hybrids), which are major obstacles to replication fork progression[313]. Moreover, INO80 is recruited to DNA damage sites by phosphorylated H2A[314,315]. In this context, Mec1 and Telomere length regulation protein 1 (Tel1) phosphorylate its subunit Ies4, which acts as a checkpoint regulator[316]. INO80 subunits regulate telomere structure and function too[317]. Ies3 particularly contributes to this process by interacting with the telomere protein Est1p[317]. The remodeller is involved in large-scale chromatin organization by controlling the spreading of euchromatin and heterochromatin[318].

The INO80 family of remodellers appears to be the most evolutionary conserved due to a high degree of conservation in the ATPase and the presence of orthologous subunits in many species[319]. However, species-specific subunits and functions beyond the conserved core are scarcely described apart from *Saccharomyces cerevisiae*. INO80 is found in *Drosophila melanogaster* and *Homo sapiens*[320,321]. In mammals, INO80 seems to frequently cooperate with the transcription factor Yin Yang-1 (YY1), which might even be an integral component of the Arp8 module[322-324]. *Drosophila melanogaster* encodes one Swr1-like ATPase, termed domino, of which two splice variants exist[325]. These assemble to complexes with distinct functions[326]. Mammals also possess two SWR1-like complexes; p400 and Snf2-related CREB-binding protein activator protein (SRCAP)[327,328]. While SRCAP exclusively catalyzes H2A.Z incorporation, p400 additionally displays histone acetylation activity and incorporates H3.3 into promoters and enhancers[329].

2.2.2 ATPases of the RNA/DNA helicase superfamily 2

DNA- or RNA-dependent ATP-hydrolyzing enzymes share conserved short ordered helicase-related motifs[330]. Based on sequence homology and spacing of these motifs, the ATPases can be grouped in six superfamilies (SF), with SF1 and SF2 comprising the majority of enzymes[331]. They share the helicase-related motifs I, Ia, II, III, IV, V, VI, TxGx and Q (Fig. 5a)[332-334]. I and II correspond to the Walker A and Walker B sequences, respectively, which are characteristic for ATPases[335]. While the Walker A motif is essential for binding ATP, the Walker B motif is crucial

for binding Mg^{2+} and hence for ATP-hydrolysis[333,336]. The latter is also referred to as the DEA(D/H) box motif of RNA helicases and more general as the DExx box motif[194,337]. SF1- and SF2-type ATPases have a core of two lobes, which are homologous to recA, an enzyme from *Escherichia coli*, which catalyzes homologous pairing and strand exchange of DNA in an ATP-dependent manner (Fig. 5a)[194,338]. These two lobes move relative to each other during ATP-hydrolysis[330].

SF2 can be further classified into several families, one of which is the Snf2 family[189]. It comprises ATPases similar to Swi2/Snf2 (see 2.2.1.3) including all motor domains of remodellers[189]. The spacing between the helicase-related motifs III and IV is elongated in ATPases of the Snf2 family (Fig. 5a)[339]. This area harbors the characteristic insertion, a linker and antiparallel α-helical protrusions of both recA-like folds (Fig. 5a, Fig. 6)[189]. Protrusion 1 is located C-terminal of the N-lobe and protrusion 2 N-terminal of the C-lobe, while the insertion resides between these elements (Fig. 5a, Fig. 6)[189]. The protrusions are separated by a structured linker, which contains a conserved dual arginine morif[189]. The bases of both protrusions and the insertion are conserved within the Snf2 family[189]. A brace element comprising one or two α-helices is located at the very C-terminus of Snf2-type ATPases (Fig. 5a, Fig. 6)[189].

When these proteins were initially categorized, most members with known function were helicases[331]. Helicases unwind and separate DNA or RNA duplex strands in an ATP-dependent manner[340]. In this process, they track along or unwind DNA in steps of 1 bp per cycle of ATP-hydrolysis[340,341]. No enzyme in the Snf2 family displays helicase activity, but several were shown to be DNA translocases including Sth1 and ISWI[342,343]. This holds true for all remodeller ATPases and the translocation reaction provides the underlying force to catalyze nucleosome sliding, repositioning, editing and ejection[155]. Due to the helical path of DNA, it is associated with rotation of the DNA or the enzyme[339]. Analogous to helicases, translocases track along one of the two strands thereby determining directionality[340]. A fundamental step size of 1 bp was identified for the ISWI remodeller too[344].

Recently, the 3D structures of several Snf2-type ATPases from *Saccharomyces cerevisiae* bound to the nucleosome were solved by cryo-EM (Fig. 6)[220,345-347]. The motor domains of Chd1 and Isw1 interact with SHL ±2, while Swi2/Snf2 can bind to both SHL ±2 and SHL ±6 (Fig. 6)[220,345-347]. The recA-like folds bind the minor groove, which is widened from underneath by protrusion 2, with the N-lobe forming secondary DNA contacts to SHL ±6 or SHL ±2 depending on the main interaction site[220,345-347]. The brace elements stabilize the recA-like folds by packing onto them distal to nucleosomal DNA (Fig. 6)[220,345-347]. While Isw1 and Chd1 possess one brace helix, this element forms two helices in the Swi2/Snf2 motor domain[220,345-347]. Compared to the DNA- and nucleosome-free resting state of the ATPase, the two lobes are rotated by 80° relative to each other[345,348]. This arranges the conserved helicase-related motifs to enable nucleotide binding and hydrolysis[345,348]. The binding of the Snf2-type ATPases to nucleosomal DNA introduces a nucleotide state-dependent DNA distortion, which is more pronounced in the tracking strand[346,347]. In the ADP-bound state, a 1 bp bulge is formed, which is delivered to the

exit site of the nucleosome and released upon ATP binding[346,347]. This mechanism might constitute the fundamental reaction of DNA translocation by all Snf2-type ATPases[346,347].

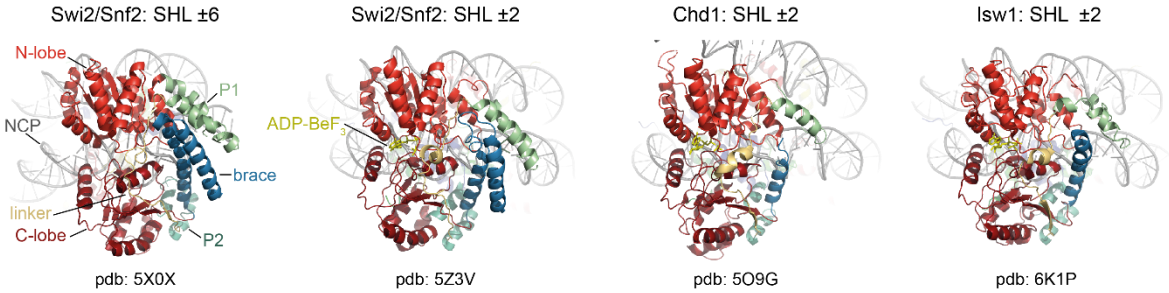

Figure 6: High-resolution structures of isolated Snf2-type ATPases from *Saccharomyces cerevisiae* bound to the nucleosome. ATPases are aligned at their N-lobes and color-coded identically. Light red: N-lobe; Deep red: C-lobe; Light green: Protrusion 1 (P1); Deep green: Protrusion 2 (P2); Sand: linker; Blue: brace helices; Yellow: ADP-BeF_3. All ATPases are in an ATP-bound state including Swi2/Snf2 bound to SHL ±6 although the nucleotide was not built in the active center of this structure. The accession code for each model is indicated under it. Figure created with high-resolution structures published in[220,345-347].

2.2.3 Architecture of the INO80 chromatin remodelling complex

The INO80 remodeller of *Saccharomyces cerevisiae* is composed of 15 different subunits and exhibits a modular architecture (Fig. 7)[275,276]. Ino80 acts as a scaffold on which three different submodules assemble (Fig. 7)[276,349]. These contribute distinctly to the action of INO80[276]. While the core and the Arp8 module are evolutionarily conserved, the Nhp10 module is specific to *Saccharomyces cerevisiae* and dispensable for the sliding reaction catalyzed by INO80 (Fig. 7)[275,276]. The composition of the complex is outlined in 2.2.1.4 and in this paragraph discussed in more detail with an emphasis on the architecture of the complex and of single subunits.

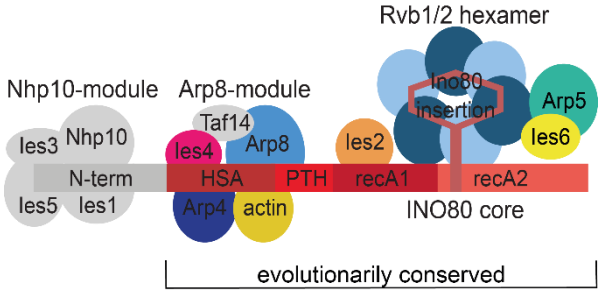

Figure 7: Architecture of the INO80 chromatin remodelling complex of *Saccharomyces cerevisiae*. The three modules of the complex are labelled and subunits for which high-resolution structures are presented in this thesis are colored. Figure based on the cross-linking map published in[276] and designed by Dr. Kilian Knoll and Dr. Sebastian Eustermann.

2.2.3.1 The core module

The core module of INO80 is ~600 kDa in size and formed around a heterohexameric ring of Rvb1 and Rvb2 (Fig. 7)[276-278]. These are closely related AAA+ (ATPases associated with diverse cellular activities) ATPases and integral components of INO80 and SWR1[273,274]. Rvb1/2 are highly conserved and essential proteins impacting transcription, DNA repair, snoRNP assembly, cell differentiation and even cancer metastasis[350]. Their Walker motifs reside in two domains (DI and DIII), which are separated by long insertions (DII) harboring an oligonucleotide-binding (OB) fold (Fig. 8b)[351,352]. Rvb1/2 form a heterohexameric ring of alternating subunits in a 1:1 stoichiometry[352]. In isolation, two Rvb1/2 rings associate with each other to a heterododecamer[352]. In INO80 and SWR1 only one heterohexameric ring is present, which is recruited by the insert domain of Ino80 ($Ino80^{insert}$) or Swr1[276-278,353]. Consequently, peptides of $Ino80^{insert}$ stimulate the ATPase activity of Rvb1/2 by 16-fold[354].

Rvb1/2 are related to the RuvB helicase from *Escherichia coli*, which drives branch migration and resolution of the Holliday junction in complex with RuvA and RuvC[355,356]. Initially, Rvb1/2 were also assumed to exhibit helicase activity but more recent experiments could not reproduce these results[277,357] and instead suggest that Rvb1/2 act as a protein assembly chaperone[354,358]. Their ATPase activity is dispensable for the activity of INO80 and SWR1[353,359]. Rvb1/2 are necessary for recruiting Arp5 and Ies6 to the complex and directly interact with the latter (Fig. 7)[276,293]. The actin fold of Arp5 is preceded by an N-terminal brace and separated by one long insertion, which comprise 51 and 335 residues, respectively in the protein from *Chaetomium thermophilum* (Fig. 8b). Ies6 contains a histidine triad (HIT) zinc finger fold in its C-terminal domain, which has lost the zinc-finger binding cluster. Arp5 is critical for the sliding reaction catalyzed by INO80 *in vitro*[275,276] and important for nucleosome positioning *in vivo*[360]. The Arp5 deletion displays the same phenotype as the Ino80 deletion *in vivo*, demonstrating the importance of this subunit[275]. Intriguingly, deleting Arp5 in *in vitro* experiments leads to a decoupling of sliding and ATPase activity, meaning that the sliding reaction is impaired while robust ATPase activity can be detected[276,278]. Thus, Arp5 is important to transmit ATP hydrolysis by Ino80 to DNA translocation[276,278]. Arp5 and Ies6 form a functional unit as deletion of one subunit results in the loss of both[361]. For this reason, differential effects of these proteins could not be observed. Only recently, recombinant expression protocols for INO80 were described independently by two research groups, one of which is part of this thesis[362]. These enable the use of site-directed mutagenesis to investigate the role of single residues in the catalysis cycle.

The core module also comprises Ies2, which interacts with Rvb1/2 and Ino80 at multiple sites as well as with Ies3 via its N-terminus (Fig. 7)[276]. This N-terminal portion is predicted to be mostly unstructured while the C-terminal part comprises a conserved PAPA-1 (Pim-1-associated protein-1 associated protein-1) domain (Fig. 8b)[276]. For the INO80 complex from *Saccharomyces cerevisiae*, the deletion of Ies2 leads to the loss of Arp5 and Ies6 too[361]. However, this effect was not observed with endogenous and recombinant INO80 from *Homo sapiens*, yet differential roles for Ies2 and Arp5 / Ies6 were suggested[278,349]. This would in principle be in agreement with the cross-linking map of INO80 from *Saccharomyces cerevisiae*, which did not reveal any interactions between Ies2 and Arp5 / Ies6 either[276] but species-specific differences cannot be ruled-out at this point. In the human complex, Ies2 was shown to be a crucial activator for the ATPase activity of INO80 and to be critical for the sliding of mononucleosomes while being dispensable for NCP interaction[278,349]. This led to the suggestion that Ies2 acts as a molecular throttle which clears an auto-inhibited state of the Ino80 ATPase upon NCP binding[278].

ChIP-exo data locates all subunits of the core module at the NCP supporting its crucial impact on the sliding reaction of mononucleosomes suggested by deletion of single subunits[306].

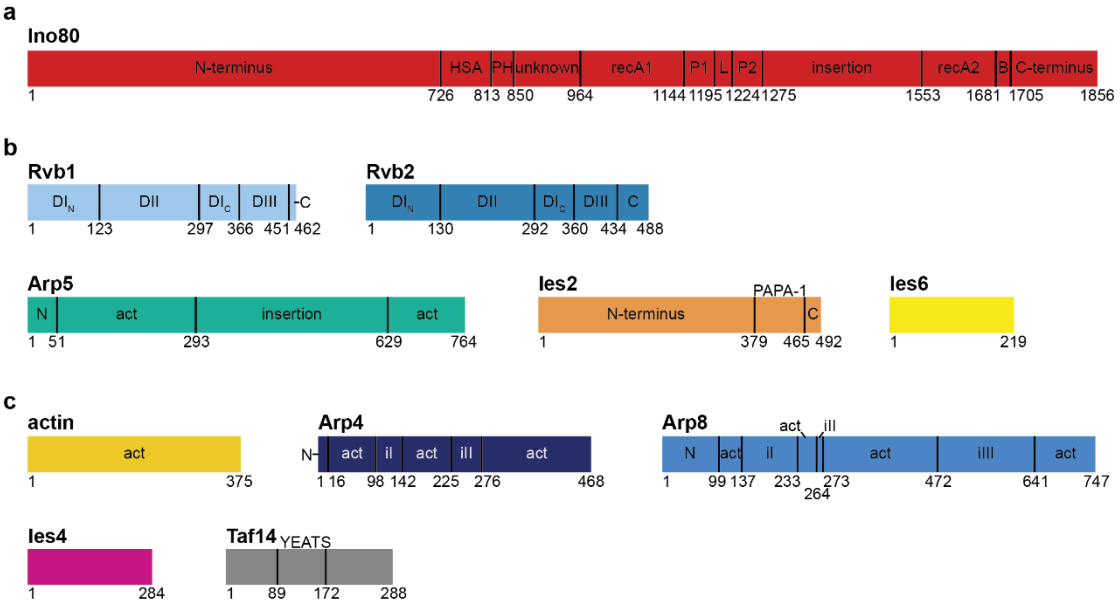

Figure 8: Domain organization of evolutionarily conserved subunits of INO80 from *Chaetomium thermophilum*. a, The Ino80 protein. PH: post-HSA; P1/2: protrusion 1/2; L: linker; B: brace. **b,** Subunits of the core module. DI-III: domains I-III of Rvb proteins; N: N-terminus; C: C-terminus; act: actin-fold. **c,** Subunits of the Arp8 module. iI-III: insertions I-III of Arps. Domain boundaries are indicated below schematic protein representation. Subunits and single domains are shown to scale relative to each other. Figure in parts adapted from[276,352]. For domain abbreviations and detailed references see main text.

2.2.3.2 The Arp8 module

The Arp8 module comprises the three actin-fold proteins actin, Arp4 and Arp8 as well as Ies4 and Taf14, which add up to 240 kDa (Fig. 7)[273,275,276].

Actin is a highly conserved and abundant protein[363]. It displays an U-shaped fold, which can be divided in two lobes and four subdomains (SDs)[364]. Lobe 1 comprises the SDs 1 and 2 and Lobe2 the SDs 3 and 4[364]. Two phosphate-binding loops form a central nucleotide-binding pocket[365]. This architecture is referred to as the actin-fold, which is shared between actin and Arps[366]. These are extended by specific insertions and named according to their decreasing identity and similarity with actin[366]. Monomeric G-actin can polymerize under ATP-hydrolysis to filamentous F-actin[367,368]. These filaments grow at the barbed end (SD1 and SD3) of actin and depolymerizes at its pointed end (SD2 and SD4)[367]. During this process the U-shaped actin undergoes a conformational change from a twisted form of ATP-bound G-actin at the barbed end to a more flat form of ADP-bound F-actin at the pointed end[363]. Although actin filaments were observed in eukaryotic nuclei[369,370], it appears to be solely monomeric as a component of chromatin remodellers[371].

While Arp8 is exclusively found in INO80 (hence the name of the module), the evolutionarily conserved actin-Arp4 dimer is also present in SWR1 and nucleosome acetyltransferase of H4 (NuA4)[188,273,275,372]. RSC and ySWI/SNF contain the structurally related Arp7-Arp9 pair[268,366]. The module is nucleated by the HSA domain of Ino80 (Ino80^{HSA}), located N-terminal of its Snf2-type ATPase (Ino80^{ATPase}) (Fig. 5b, Fig. 7, Fig. 8a; also see 2.2.1.4)[238]. Crystal structures of complexes comprising Swi2/Snf2^{HSA}-Arp7-Arp9-Rtt102 and Swr1^{HSA}-actin-Arp4 reveal that actin-fold proteins bind to the HSA domains via their barbed ends[269,373]. Arp8 is critical for the assembly of the module in INO80 as its deletion results in the loss of the other subunits[275]. Isolated Arp4 and Arp8 display affinity towards the H3-H4 tetramer while an Ino80^{HSA}-actin-Arp4-Arp8 subcomplex binds the NCP[374-376]. More recent biochemical experiments investigated the role of Arps and their binding to the Snf2-type ATPase of RSC[239]. These suggest a regulatory role of Arp7 and Arp9 on the motor domain and demonstrate a direct interaction

with the HSA domain, the post-HSA domain and protrusion 1 but not the NCP[239]. For INO80, these insights are partly lacking but beyond a potential role in *cis*-directed regulation, the Arp8 module is also proposed to bind extranucleosomal DNA[377]. This is in agreement with ChIP-exo data placing Arp8 upstream the +1 nucleosome[306]. The N-terminus of Arp8 from *Saccharomyces cerevisiae* affects the viability of the organism under stress conditions and is important for the sliding reaction catalyzed by INO80[377]. It comprises 197 amino acids in yeast[377] and 99 residues in *Chaetomium thermophilum* (Fig. 8c). In addition, the actin-fold of Arp8 is extended by three insertions of 95, 8 and 168 residues (Fig. 8c). Arp4 possesses a short N-terminal brace and two insertions, which comprise 43 and 50 residues in *Chaetomium thermophilum* (Fig. 8c)[374]. BAF53a is the human homolog of Arp4 and frequently mutated in cancer[378]. Taf14 consists in large parts of a YEATS domain, which is a specific reader for H3 crotonylation (Fig. 8c; see 2.2.1.4)[286]. No similarities to known domains can be found in Ies4, which is phosphorylated by the kinases Mec1 / Tel1 during exposure to DNA-damaging agents[316].

2.2.3.3 The species-specific module

The N-terminus of Ino80 recruits a third, species-specific module, which in *Saccharomyces cerevisiae* comprises Nhp10, Ies1, Ies3 and Ies5 and is therefore also referred to as Nhp10 module (Fig. 7)[276]. This module and the N-terminus of Ino80 are structurally inter-dependent as deletion of Nhp10 results not only in the loss of Ies1, Ies3 and Ies5 but also in a degradation of the Ino80 N-terminus[305]. Early on it was noticed that the module is dispensable for the sliding reaction catalyzed by INO80 but might increase its affinity for free DNA[275]. Moreover, it is important for the recruitment of INO80 to DNA damage sites by interaction with phosphorylated H2AX[314,315]. Nhp10 is a HMG-box protein with two DNA-binding HMG domains followed by an acidic C-terminal tail[379]. One HMG box comprises ~75 residues, which form three α-helices arranged in a L-shaped fold[380]. Box A of Nhp10 is only similar to Box A of HMO1 a highly related protein in *Saccharomyces cerevisiae*[379], which binds and bends DNA[381-383]. Box B of both HMO1 and Nhp10 correspond to Box B of mammalian HMGB proteins[379]. In this class, proteins containing one or multiple HMG boxes are grouped[380]. These preferentially bind the minor groove through the HMG box thereby bending and underwinding DNA[380]. HMGB proteins with tandem HMG boxes generally interact with DNA in a non-sequence specific manner, which holds also true for Nhp10[379,380]. Mediated by Box A, Nhp10 binds sticky and blunt DNA ends, potentially to recruit INO80 to DNA damage sites[314,315,379,383]. Both HMG boxes display a preference for distorted DNA substrates while the acidic tail attenuates DNA binding[383]. This might impact the action of INO80 at stalled replication forks[383]. Ies1, Ies3 and Ies5 do not possess known protein domains and so far, no function could be addresses to these proteins.

The entire Nhp10 module exhibits strong DNA-binding properties on its own and also interacts with the NCP[276]. *In vitro*, it was shown to be important for sensing the length of extranucleosomal DNA, consistent with the DNA-binding properties of Nhp10[305]. If deleted, sliding activity of INO80 on nucleosomes with limiting length of extranucleosomal DNA is increased, which suggests an auto-inhibitory function of the Nhp10 module or the N-terminus of Ino80[305]. This is in line with its previously proposed role in regulating the action of INO80[276,349].

3 Aim of the thesis

The INO80 chromatin remodelling complex converts the energy from ATP hydrolysis into translocation of DNA around the nucleosome[273,275]. This is the fundamental reaction for its action on chromatin[155]. Thus, a detailed understanding of it is indispensable to investigate the role of INO80 in chromatin organization and the regulation of its activity. Despite its importance, this catalytic reaction was not fully understood when the work on this thesis started, although several data suggests that it is conserved among the remodeller families[155].
The mass spectrometry analysis of crosslinked endogenous INO80 from *Saccharomyces cerevisiae* provided fundamental insights into the arrangement of its individual subunits in the protein complex[276]. It revealed that INO80 is organized in three modules and indicated the position of these modules within a low-resolution cryo-EM structure of INO80 in its apo state[276]. Moreover, this study investigated the binding of INO80 to its substrate, the NCP, by describing crosslinks between the subunits of INO80 and the histone proteins[276]. However, due to the limited resolution of the cryo-EM structure and the fact that the NCP is not present in this structure, a detailed analysis of the interaction between INO80 and the NCP remained elusive[276].
Further knowledge of how INO80 engages the NCP was provided by a hydroxyl radical footprinting analysis, which identified SHL -2/-3 and SHL -6 as the main binding sites of INO80 to nucleosomal DNA[302]. Intriguingly, these are the positions to which the isolated Swi2/Snf2 ATPase was also shown to bind[345]. This raises the question whether both positions are occupied by the $Ino80^{ATPase}$. This could either be explained by two distinct conformations of the complex, which engage the NCP in different ways or by the binding of two INO80 complexes to one NCP as suggested by biochemical data[384]. Alternatively, the protection observed by hydroxyl radical footprinting at SHL -2/-3 and SHL -6 can arise from the interaction of two different subunits or modules of INO80 with these sites. In addition, biophysical and biochemical analyses of DNA translocation catalyzed by INO80 indicates a step size of 10 bp or larger[302,305]. This is in contradiction with the fundamental step size of the tracking of Snf2-type ATPases on DNA, which is 1 bp[341]. A smaller step size of 1 – 3 bp was indeed observed for DNA translocation catalyzed by remodellers of the ISWI family[302,344]. Hence, the multi-subunit remodeller INO80 must translocate DNA in a distinct mechanism. Most probably, it transfers nucleosomal DNA in an intermediate state during the translocation reaction before it exits the nucleosome. Why and how this happens cannot be explained with the data, which was available before the work on this thesis started.
This thesis tries to address these open questions by investigating the interaction between INO80 and the nucleosome and thereby the mechanism of DNA translocation. This is primarily done by structural, biochemical and biophysical approaches, in particular cryo-EM[385], which enables the investigation of large and partly flexible biomolecules such as the INO80 complex.

4 Publications

4.1 Structural basis for ATP-dependent chromatin remodelling by the INO80 complex

Eustermann, S.*, Schall, K.*, Kostrewa, D., Lakomek, K., Strauss, M., Moldt, M. and Hopfner, K.P., 2018. Structural basis for ATP-dependent chromatin remodelling by the INO80 complex. *Nature*, *556*(7701), pp.386-390.
*These authors contributed equally

DOI: https://doi.org/10.1038/s41586-018-0029-y
https://www.nature.com/articles/s41586-018-0029-y

Summary

In this publication, we report the high-resolution cryo-EM structure of the core module of INO80 bound to the NCP. It provides novel insights into the interaction between INO80 and the NCP and the arrangement of its subunits allows to propose a mechanism for the catalysis of DNA translocation by INO80. It engages nucleosomal DNA at two main sites by its subunits Ino80^{ATPase} and Arp5 at SHL -6 and SHL -2/3, respectively. This is in accordance with data from hydroxyl radical footprinting. Intriguingly, Ino80^{ATPase} detaches the nucleosomal DNA it interacts with, thereby exhibiting one H2A-H2B dimer. These DNA-binding elements are connected by the Rvb1/2 heterohexameric ring, which does not form contacts to the NCP. It is found in a closed conformation compared to previously determined X-ray structures of isolated Rvb1/2 ring and almost completely encapsulates Ino80^{insert}. Ies2 is anchored in this ring with its C-terminus and binds nucleosomal DNA at SHL +2 and the Ino80^{ATPase} via an element termed 'throttle helix'. Ies6 forms a functional unit with Arp5 as revealed by MS crosslinking and contributes to its interaction with DNA as well as the Rvb1/2 ring. The resolution of the cryo-EM map allows to determine the nucleotide-state of several subunits. Although no nucleotide was added to the sample during purification or grid preparation, all chains of Rvb1 and Rvb2 are bound to ADP while Arp5 is bound to ATP. Ino80^{ATPase} is free of nucleotide. The arrangement of the individual subunits around the NCP reveals that Ino80^{ATPase} is held in a fixed position during the translocation reaction. This enables the transfer of energy derived from ATP hydrolysis into DNA translocation. In analogy to an electrical engine, it can be termed 'motor', while Arp5 and Ies6 act as a 'counter grip' and Rvb1/2 as a 'stator' connecting these two elements. This architecture also explains the large step size of DNA translocation by INO80. Ino80^{ATPase} pumps DNA into the nucleosome against the counter grip. This acts as a roadblock, which DNA cannot pass in the first place. Instead, a DNA strain is generated and only once sufficient force is built up, the counter grip is released and DNA translocation takes place.
Albeit the profound insights into the binding of the core module of INO80 to the NCP, this study could not provide information about the Arp8 module, which is critical for the catalysis of DNA translocation by INO80. Only a low-resolution map could be calculated indicating that the module is located outside the NCP.

Author contribution

I reconstituted and purified nucleosomes from recombinant sources as well as the evolutionarily conserved INO80 complex from *Chaetomium thermophilum* together with Dr. Sebastian Eustermann and Manuela Moldt. I screened and established vitrification conditions of the nucleosome:INO80 complex together with Dr. Sebastian Eustermann.

LETTER

https://doi.org/10.1038/s41586-018-0029-y

Structural basis for ATP-dependent chromatin remodelling by the INO80 complex

Sebastian Eustermann[1,2,5], Kevin Schall[1,2,5], Dirk Kostrewa[1,2], Kristina Lakomek[1,2], Mike Strauss[3], Manuela Moldt[1,2] & Karl-Peter Hopfner[1,2,4]*

In the eukaryotic nucleus, DNA is packaged in the form of nucleosomes, each of which comprises about 147 base pairs of DNA wrapped around a histone protein octamer. The position and histone composition of nucleosomes is governed by ATP-dependent chromatin remodellers[1–3] such as the 15-subunit INO80 complex[4]. INO80 regulates gene expression, DNA repair and replication by sliding nucleosomes, the exchange of histone H2A.Z with H2A, and the positioning of +1 and −1 nucleosomes at promoter DNA[5–8]. The structures and mechanisms of these remodelling reactions are currently unknown. Here we report the cryo-electron microscopy structure of the evolutionarily conserved core of the INO80 complex from the fungus *Chaetomium thermophilum* bound to a nucleosome, at a global resolution of 4.3 Å and with major parts at 3.7 Å. The INO80 core cradles one entire gyre of the nucleosome through multivalent DNA and histone contacts. An Rvb1/Rvb2 AAA$^+$ ATPase heterohexamer is an assembly scaffold for the complex and acts as a 'stator' for the motor and nucleosome-gripping subunits. The Swi2/Snf2 ATPase motor binds to nucleosomal DNA at superhelical location −6, unwraps approximately 15 base pairs, disrupts the H2A–DNA contacts and is poised to pump entry DNA into the nucleosome. Arp5 and Ies6 bind superhelical locations −2 and −3 to act as a counter grip for the motor, on the other side of the H2A–H2B dimer. The Arp5 insertion domain forms a grappler element that binds the nucleosome dyad, connects the Arp5 actin-fold and entry DNA over a distance of about 90 Å and packs against histone H2A–H2B near the 'acidic patch'. Our structure together with biochemical data[8] suggests a unified mechanism for nucleosome sliding and histone editing by INO80. The motor is part of a macromolecular ratchet, persistently pumping entry DNA across the H2A–H2B dimer against the Arp5 grip until a large nucleosome translocation step occurs. The transient exposure of H2A–H2B by motor activity as well as differential recognition of H2A.Z and H2A may regulate histone exchange.

Remodellers are grouped into INO80, SWI/SNF, CHD and ISWI families that collectively shape the nucleosome landscape on chromosomal DNA[7,9]. Although there might be fundamental differences in how remodellers slide, evict and edit nucleosomes[1–3], it has been suggested that a common ATP-dependent DNA translocation of the motor domains underlies these distinct reactions[3]. Recent studies have revealed how the Snf2 motor domain[10] and Chd1 family proteins[11,12] interact with the nucleosome, but there is currently limited understanding of how stepwise DNA translocation results in its various large-scale reconfigurations. INO80 and the related SWR1 complex are large (megadalton) modular complexes[13–15] that carry out intricate editing reactions. SWR1 incorporates H2A.Z[16] whereas INO80 has been shown to exchange H2A.Z with H2A[5,8]. H2A.Z is a H2A variant found at promoter and enhancer elements and has important regulatory functions[17]. INO80 also slides nucleosomes and positions the −1 and +1 nucleosomes of genic arrays that flank nucleosome-depleted promoter regions[6–8]. However, even nucleosome sliding requires extensive inter-subunit coordination[18,19] and a clear mechanistic framework explaining these activities is currently not available. Biochemical evidence indicates that INO80 translocates and loops DNA at the H2A–H2B interface[8], suggesting that sliding and editing may be facets of a common, complex chemo-mechanical reaction.

To provide a structural mechanism for nucleosome recognition and remodelling by INO80, we performed cryo-electron microscopy (cryo-EM) analysis of an evolutionarily conserved, recombinant 11-subunit INO80 complex from *Chaetomium thermophilum* bound to a nucleosome (Fig. 1a–c). Our complex comprises the subunits conserved from yeast to man: the main ATPase Ino80 (INO80 denotes the whole complex; Ino80 refers to the catalytic subunit), actin and actin-related proteins Arp4, Arp5 and Arp8, Ino80 subunits Ies2, Ies4 and Ies6, Taf14 and the AAA$^+$ ATPases Rvb1 and Rvb2. It lacks the evolutionarily less conserved subunits—which, in yeast INO80, are Ies1, Ies3, Ies5 and Nhp10—and the N-terminal part of Ino80 to which these subunits bind. Biochemical analysis shows a stoichiometric complex that stably binds and remodels nucleosomes (Extended Data Fig. 1), consistent with the activities of similar human[14,18] and *Saccharomyces cerevisiae*[13] INO80 complexes. The nucleosome was assembled from human histones H2A, H2B, H3, H4 and a Widom 601 sequence with 50 bp (base pairs) of extranucleosomal DNA that matches the footprint identified for the entire *S. cerevisiae* INO80[8].

Cryo-electron microscopy and single-particle reconstruction resulted in a map with a global resolution of 4.3 Å and did not require crosslinking or the addition of nucleotides (Extended Data Figs. 2, 3 and Extended Data Table 1). The map reveals how a 590-kDa core module of INO80 (denoted INO80^{core}) comprising Ino80, Arp5, Ies6, Ies2 and Rvb1/Rvb2 recognizes and remodels the 200-kDa nucleosome core particle (NCP) (Fig. 1c). Focused refinement resulted in a 3.7 Å map of the Rvb1/Rvb2–Arp5–Ies2–Ies6–Ino80 subcomplex (Extended Data Figs. 2, 3). We built de novo atomic models for the ATP-bound Arp5 actin-fold (denoted Arp5^{core}), Ies2, Ies6 and ADP-bound Rvb1/Rvb2 heterohexamer that incorporated the complete Ino80 ATPase insertion domain (denoted Ino80^{insert}). Pseudo-atomic models for the Ino80 Swi2/Snf2 ATPase domain (termed Ino80^{ATPase}) and the NCP were generated by flexible fitting of crystal structures and homology models (Fig. 1c). DNA visibly protrudes from the NCP and a 20 Å cryo-EM map, obtained from extensive 3D classification, indicates extranucleosomal binding of the 200-kDa Arp8 module (actin, Arp4, Arp8, Taf14 and Ies4) (Fig. 1b), consistent with genome-wide promoter DNA binding of Arp8 proximal to the +1 nucleosome in vivo[20]. However, the Arp8 module proved to be either unstable or too heterogeneous in orientation to yield a high-resolution reconstruction at this stage.

INO80^{core} embraces one entire gyre of the nucleosome and binds in a multivalent fashion to nucleosomal DNA and histones (Fig. 1c). The overall mode of NCP recognition of INO80^{core} closely matches the hydroxyl radical footprints of full *S. cerevisiae* INO80[8]. The two main DNA contacts are to superhelical location (SHL) −6 by the Ino80 ATPase motor[8], and to SHL −2 and SHL −3 by Arp5 and Ies6.

[1]Department of Biochemistry, Ludwig-Maximilians-Universität München, Munich, Germany. [2]Gene Center, Ludwig-Maximilians-Universität München, Munich, Germany. [3]Max Planck Institute of Biochemistry, Martinsried, Germany. [4]Center for Integrated Protein Science, Munich, Germany. [5]These authors contributed equally: Sebastian Eustermann, Kevin Schall. *e-mail: hopfner@genzentrum.lmu.de

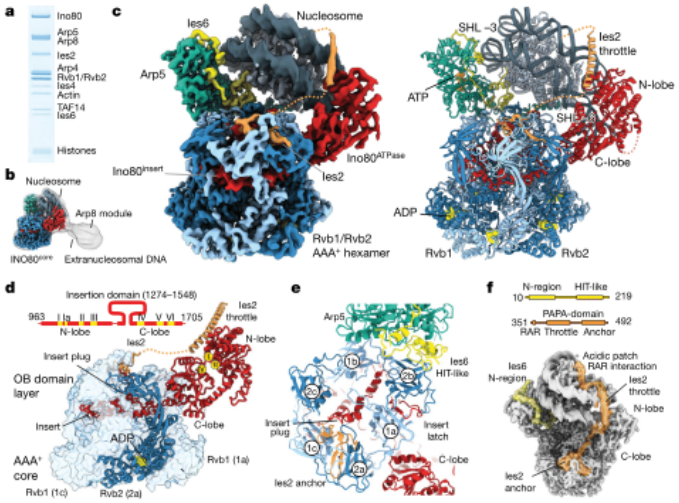

Fig. 1 | Structure of the INO80^{core}–nucleosome complex. a, Gel electrophoresis analysis of the purified recombinant *C. thermophilum* INO80 complex bound to a nucleosome. **b**, Low-resolution cryo-EM map showing extra density for the Arp8 module and extranucleosomal DNA. The high-resolution structure of INO80^{core}, shown in **c** and **d**, is superimposed. **c**, Left, 4.3 Å resolution cryo-EM map reveals the architecture of the nucleosome-remodelling core of INO80. Grey, nucleosome; red, Ino80^{ATPase}; orange, Ies2; green, Arp5; yellow, Ies6; light blue, three Rvb1 subunits; dark blue, three Rvb2 subunits. Right, protein models obtained from interpretation of the cryo-EM map showing how the INO80^{core} binds the NCP. ADP and ATP molecules are indicated. The Rvb1/Rvb2 hexamer is assembled from three Rvb1/Rvb2 pairs (denoted 1a, 1b and 1c, and 2a, 2b and 2c; see **e**) and organizes the nucleosome-binding elements Arp5–Ies6, Ies2 and Ino80^{ATPase}. **d**, Schematic of the Ino80^{ATPase} showing the location of conserved helicase motifs (I–VI) and the insert characteristic of the INO80 family. The insert has a wheel-like structure that binds as a client into the chamber of the three-layered Rvb1/Rvb2 hexamer. One Rvb1/Rvb2 subunit is shown as a ribbon, and the others as transparent surfaces. **e**, Details of the interactions of Arp5–Ies6, Ies2 and Ino80^{ATPase} clients at the OB domain layer of Rvb1/Rvb2. Plug and latch of Ino80^{insert} recruit Ies2 and Arp5–Ies6 clients through direct interactions and/or orienting OB domains. **f**, Ies2 and Ies6 are extended proteins with multiple binding sites that functionally link Rvb1/Rvb2 to the nucleosome via Arp5 and Ino80^{ATPase}, respectively. Of note, Ies2 wraps around the nucleosome and binds the distal acidic patch. The domain architectures are shown above the map.

In addition, we observe contacts of Ino80^{ATPase} and Ies2 to SHL 2, of the 325-amino-acid-long Arp5 insertion domain (termed the grappler) to the dyad, and of the grappler, Ies2 and Ies6 to the histone core (see below). Binding of SHL −6 by the Ino80^{ATPase} motor differs from the SHL + 2-binding of the Chd1[11,12] (Extended Data Fig. 4) and Isw1a remodellers[21], which indicates that these complexes possess distinct remodelling mechanisms. The isolated Snf2 motor bound to SHL + 2 but also to SHL + 6[10]. Therefore, clarification of mechanistic similarities and differences between INO80 and SWI/SNF families require more complete structures of SWI/SNF remodellers.

The Rvb1/Rvb2 AAA$^+$ ATPase is a prominent module of INO80 family remodellers and might act as an assembly chaperone[22]. We previously interpreted a low-resolution negative stain map as harbouring the Rvb1/Rvb2 double-hexamer that forms in solution[13], but our high-resolution structure now shows a single hexamer in nucleosome-bound INO80, consistent with a recently published structure of apo human INO80^{core} [23]. However, with the nucleosome-bound state and the resolution to build atomic models for the clients, we can now reveal how Rvb1/Rvb2 specifically assembles INO80 and that it has a key role in defining the functional arrangement of subunits of INO80 for interaction with the NCP. The C-lobe of Ino80^{ATPase} directly binds Rvb1/Rvb2 and contains the approximately 270 amino acid-long Ino80 insertion domain that adopts a wheel-like structure and sequentially binds to all six Rvb1/Rvb2 protomers in the central cavity (Extended Data Fig. 5). Ino80^{insert} binding induces a marked asymmetry in the oligonucleotide/oligosaccharide-binding (OB) domain ring layer that in turn induces specific recruitment and positioning of Ino80^{ATPase}, Ies2 and Arp5–Ies6 to grab the nucleosome from opposing sides (Fig. 1c).

Ino80^{insert} does not bind to the individual Rvb1/Rvb2 units via a shared sequence or even a common structural fold, but the interactions are governed by different hydrophobic and/or aromatic elements in a manner that resembles how bona fide chaperones may bind partially folded proteins[24]. Comparison with unliganded dodecameric Rvb1/Rvb2[25] reveals client-induced conformational control (Extended Data Fig. 5), consistent with a 16-fold stimulation of the ATP hydrolysis activity of Rvb1/Rvb2 by Ino80 insertion peptides[22]. However, the observed post-hydrolysis ADP state suggests that Rvb1/Rvb2 transforms into a more stable functional scaffold once the correct set of clients is assembled. A 'latch' in Ino80^{insert} binds between OB domains 1a and 2b and generates distinct interaction sites for Arp5 and Ies6 (at OB domains 2a and 2b, respectively). Notably, the C-terminal domain of Ies6 resembles a histidine triad (HIT) zinc finger fold that has lost the zinc-binding cluster, revealing how HIT domains can specifically bind Rvb1/Rvb2 in various complexes[26]. A 'plug' closes the hole in the OB domain layer and directly binds Ies2, which wedges with a β-hairpin between OB domains 2a and 1c (Fig. 1e). Ies2 reaches all the way across from the Rvb1/Rvb2 OB layer via a linker that is flexible but conserved in length, and pins the N-lobe to SHL 2 (Figs. 1f, 2a and Extended Data Fig. 6 b, d). Ies2 wraps around the nucleosome and binds the acidic patch at the distal side of INO80, which links Ino80^{ATPase} to Rvb1/Rvb2 and the nucleosome; this shows how Ies2 acts as a 'throttle' for the remodelling activity of INO80[18].

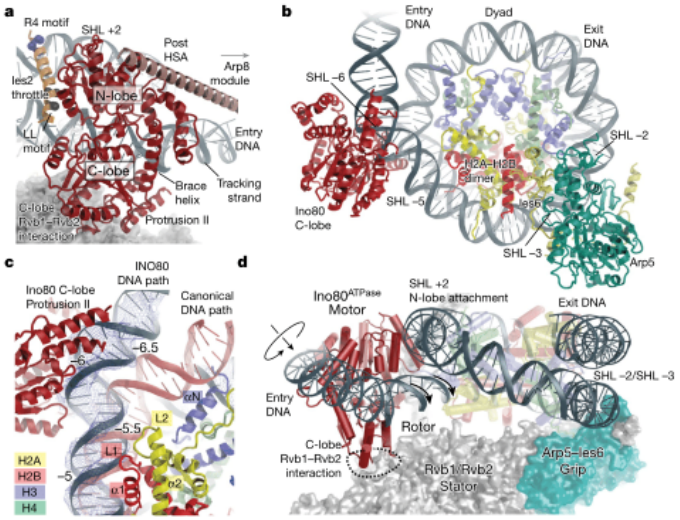

Fig. 2 | Ino80^{ATPase}–nucleosome interaction. a, Details of the Ino80^{ATPase}–Ies2 interaction with annotated tracking-stand and notable conserved Ies2 sequence motifs. The post-helicase-SANT-associated (post-HSA) domain (salmon) is provided as a poly-alanine model (Extended Data Fig. 6). **b**, Ino80^{ATPase} and Arp5 bind to opposing sides of the nucleosome, approximately 90 Å apart (for clarity, Rvb1/Rvb2 is not shown). **c**, The binding of Ino80^{ATPase} to exit DNA (blue with superimposed density) unwraps about 15 bp from the nucleosome, partially exposing H2A at SHL −5.5 and disrupting the H3 interaction at SHL −6.5. The canonical DNA path is shown in red for comparison. The unwrapped DNA is kinked through widening of the minor groove by the C-lobe of Ino80^{ATPase} with its protrusion II element. **d**, Semi-schematic view showing how the Rvb1/Rvb2 hexamer positions the Ino80^{ATPase} motor and Arp5 counter grip on opposite sides of the nucleosome gyre. Rvb1/2 acts as a stator to prevent rotation of the motor with respect to the nucleosome, leading to rotation and translation of entry DNA.

Ino80^{ATPase} is the motor of the remodeller. Conserved Swi2/Snf2 DNA-binding motifs in both the N- and C-lobes engage with double-stranded DNA and the Swi2/Snf2 typical brace helix I reaches across both lobes, stabilizing their mutual orientation (Fig. 2a and Extended Data Fig. 4b). The observed conformation suggests that the motor is poised to bind ATP and to translocate DNA by repetitive cycles of ATP binding and hydrolysis. The binding of Ino80^{ATPase} at SHL −6 unwraps about 15 bp of DNA from the entry site (Fig. 2c). Consequently, DNA contacts to H2A loop 2 (L2) at SHL −5.5 and to H3 helix αN at SHL −6.5 are notably broken, and the H2A–H2B dimer is partially exposed. The full exposure of H2A also requires disruption of the DNA contacts of the loop 1 (L1) and helix α1 of H2A and H2B, which explains why histone exchange additionally requires ATP-driven DNA translocation[8]. The binding of Ino80 ATPase to SHL −6 is accompanied by a widening of the DNA minor groove (Fig. 2c). This finding raises the possibility that the motor domain of INO80 is influenced by DNA shape features, which could be of interest in determining nucleosome positioning at promoter regions[7].

Swi2/Snf2 proteins translocate DNA by minor groove tracking[27,28]. The orientation of the Swi2/Snf2 motor at SHL −6 suggests that Ino80^{ATPase} pumps entry DNA into the nucleosome, consistent with the activity of INO80 to centre nucleosomes (Fig. 2d and Extended Data Fig. 1). An important and poorly understood feature of remodellers is how such stepwise translocation of the motor on DNA leads to large-scale reconfiguration of the nucleosome. Building up force on DNA in a processive manner through multiple consecutive steps requires arresting the motor with respect to the nucleosome. The motor of INO80 is fixed by multiple interactions. Ies2 and a secondary DNA-binding site pin the N-lobe to SHL 2. Importantly, the C-lobe is held in place by Rvb1/Rvb2. Rvb1/Rvb2 therefore acts in conjunction with Arp5–Ies6 as a stator, enabling Ino80^{ATPase} to apply force onto the 'rotor' DNA and to pump DNA into the nucleosome. This provides the means of conducting large-scale reconfigurations through multiple translocation steps.

Here we identify Arp5–Ies6 as a major nucleosome recognition module with multiple DNA and histone contacts with both the Arp5 actin fold and the 325-residue-long insertion domain of Arp5 (Arp5^{insert}) that forms a multi-armed grappler (Fig. 3a, b). The C-terminal HIT fold of Ies6 packs in between Rvb1/Rvb2 OB domain 2b and the histone core H2B αC while the conserved N-region of Ies6 wraps around the Arp5 actin fold at the nucleosome proximal DNA side (Fig. 3c, d). Arp5–Ies6 binds about 7–8 bases at SHL −2 and SHL −3, with both Ies6 and a DNA-binding domain (DBD) of the Arp5 actin fold (termed Arp5^{DBD}) (Fig. 3c). The DNA interaction explains the hydroxyl radical footprints of full *S. cerevisiae* INO80 on nucleosomes that showed increased protection of SHL −2 and SHL −3[8]. Of note, Arp5^{DBD} is conserved from yeast to humans (Fig. 3c), and is the structural equivalent of the 'DNase I binding loop' of actin. Mutating conserved DNA-binding arginines/lysines markedly affected nucleosome sliding under conditions in which INO80 still displayed robust ATPase activity (Fig. 3f and Extended Data Fig. 7). Decoupling of ATPase and sliding recapitulates effects seen with Arp5 deletions[13,29] in *S. cerevisiae* INO80 and human INO180^{core}. We conclude that Arp5–Ies6 couples ATPase activity to nucleosome sliding by gripping DNA and providing an anchor to the histone octamer surface during ratchet translocation steps (see below).

The grappler extends from subdomain 4 of the actin fold of Arp5 and has a multi-armed structure with several notable elements, which we have denoted the 'arm', 'leg', 'foot' and 'bar' (Fig. 3a). Masked 3D classification produced a 4.7 Å map (Fig. 3a) and 4.6 Å map (Extended Data Fig. 6), which together showed that the grappler adopts at least two conformations and enabled us to interpret the topology of its secondary structure with a poly-alanine model. The long N-terminal helix of the Arp5^{insert} forms the bar that, in a closed conformation of the grappler, binds along the nucleosomal dyad and spans between the actin fold of Arp5 and entry DNA at SHL −7.5, over a distance of approximately 90 Å. Importantly, the bar can adopt this binding mode as the entry DNA unwraps from the histone octamer owing to binding of the Ino80

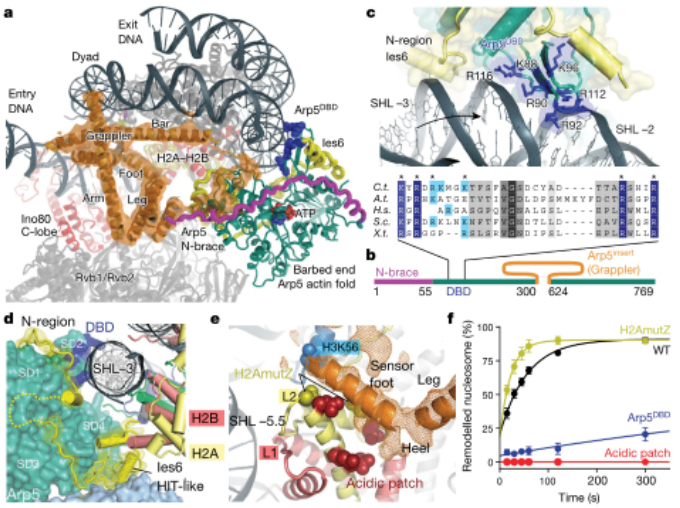

Fig. 3 | Multivalent nucleosome binding by Arp5. a, Map at 4.7 Å resolution showing the Arp5 insertion that forms a multi-armed grappler element (orange), along with the actin fold of Arp5 (green, with blue DBD), the Arp5 N-terminal brace (magenta) and Ies6 (yellow). The grappler has multiple DNA and histone contacts and chemo-mechanically connects Arp5, dyad and H2A–H2B. **b**, Schematic of Arp5 domain structure with green actin-fold and highlighted insertions. **c**, Detailed view of the DNA interactions by Ies6 and DBD of Arp5, along with a multiple sequence alignment showing conservation of DNA-binding arginines/lysines in the DBD. Blue: residues mutated for functional analysis (see **e**). *A.t.*, *Arabidopsis thaliana*; *C.t.*, *C. thermophilum*; *H.s.*, *Homo sapiens*; *S.c.*, *S. cerevisiae*; *X.t.*, *Xenopus tropicalis*. **d**, The C-terminal HIT-like domain of Ies6 binds both H2A (yellow) and Rvb1 (light blue), and the N-terminal region wraps around Arp5^{core}. Actin-fold subdomains SD1–4 are indicated. **e**, Detailed view of the sensor foot and leg of the grappler (orange map and poly-alanine model). The sensor foot binds to the acidic patch of H2A–H2B and to H3 at K56, which suggests it is implicated in controlling histone variant exchange. In **e**, sites mutated (red, acidic patch: E61A, E64A, D72A, D90A; olive, H2A.Z mimic (H2AmutZ): N73L and N89G) for the functional analysis are shown with side chains. **f**, Nucleosome sliding activities of INO80 and histone mutants. H2A.Z-mimicking mutants lead to increased sliding, whereas mutating the H2A acidic patch or Arp5^{DBD} abolishes or strongly reduces sliding under conditions in which INO80 still displays robust ATPase activity. WT, wild-type INO80 with wild-type H2A. Means ± s.d. ($n = 3$) are shown.

ATPase to SHL −6. The arm of the grappler stabilizes the bar at the dyad and connects it to the leg–foot element that packs against the H2A–H2B core at the acidic patch of the histone octamer (Fig. 3e). In an open conformation, the bar is released from the dyad, moves 45° to bind to SHL −1 and blocks the path of the exit DNA (Extended Data Fig. 6). We therefore envision a switch-like behaviour of Arp5 that is sensitive to the path of the entry and exit DNA.

The foot backs H2A opposite L2, as if to stabilize H2A to compensate for the broken DNA contacts that result from the unwrapping of entry DNA. Consequently, the binding of the acidic patch on each side of the nucleosome has an essential role for INO80: the grappler ensures the integrity of the histone octamer where the entry DNA unwraps, and Ies2 binds the acidic patch on the other side of the octamer and acts as a throttle for INO80^{ATPase}. In support of this model, mutating the acidic patch that targets both interactions abrogates nucleosome sliding, although it reduces ATPase rates only moderately (Fig. 3f, Extended Data Fig. 7d, e). Of note, our structure predicts that in a putative dimeric state of INO80[29], Ies2 and Arp5 grappler have to compete for the acidic patches on each side of the histone octamer. This might provide asymmetric control of the two Ino80 ATPases at SHL −6 and SHL + 6 and prevent simultaneous pumping of DNA in opposite directions.

Together with biochemical studies[8], our structure suggests a unified ratchet-like mechanism for how INO80 slides and possibly edits nucleosomes (Fig. 4). We find that INO80^{core} unwraps entry DNA and grips DNA and histones by multivalent interactions. The motor is positioned to pump DNA into the nucleosome against Arp5–Ies6, which could hold onto DNA until a sufficient force is generated by multiple small steps of the motor. Such groove tracking might create a DNA loop between the motor and the Arp5–Ies6 counter grip, persistently disrupting the H2A–H2B DNA interface[8] and thus enabling histone exchange until the amount of DNA pumped propagates across Arp5–Ies6 and the grappler (that is, the ratchet step). As a result, INO80 would move nucleosomes in larger steps (Fig. 4). Step sizes of 10–20 bp

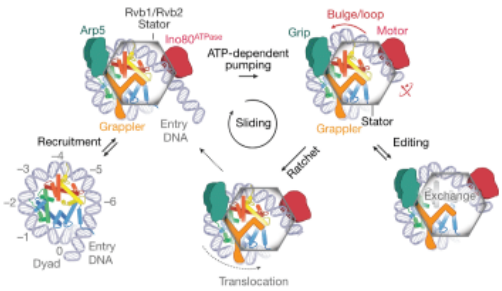

Fig. 4 | Model of INO80 nucleosome remodelling. The unified model integrates our structural data with previous biochemical[8] data. The functional architecture of INO80 with motor, grip and grappler suggests that processive nucleosome sliding proceeds via a ratchet mechanism. Transient generation of loops between the motor and the grip could expose H2A–H2B for editing. Direct binding of H2A–H2B by the grappler sensor-foot could regulate variant- or modification-specific editing.

are indeed observed[8,30]. During loop formation, the grappler ensures structural integrity of the octamer by holding onto H2A–H2B, and our structure suggests that its foot also could function as a sensor during editing. The foot binds to H2A at a site at which H2A differs in some amino acid residues from H2A.Z (Extended Data Fig. 7a). Introducing two H2A.Z-mimicking mutations into H2A at this interface increased sliding velocity (Fig. 3f), consistent with the observed faster sliding of H2A.Z nucleosomes by INO80[8,18]. We observe a direct contact of the 'toe' of the sensor-foot with K56 of histone H3. Although controversial, the acetylation of the K56 of H3 has previously been proposed to promote histone variant exchange by INO80 family remodellers[31] and has a pivotal role in DNA repair and replication as well as in regulating gene expression homeostasis.

In summary, we provide, to our knowledge, the first structural insights into the mechanism by which DNA translocation by a Swi2/Snf2 ATPase of a multisubunit remodeller governs large-scale repositioning and editing reactions on nucleosomes. The motor, stator and multivalent grip of INO80 enable highly processive sliding without release and large-scale reconfigurations such as editing while keeping the remainder of the nucleosome intact. The proposed ratchet mechanism explains DNA loop formation that results in large translocation steps, as well as the means for ATP-dependent H2A.Z → H2A exchange[8]. Thus, our structure visualizes how nucleosome sliding and editing can be achieved by two facets of the same mechano-chemical cycle and how differential regulation might occur. Future studies are needed to address how other modules that are not part of the conserved $INO80^{core}$ function provide an additional layer of regulation (for example, in a promoter-specific manner) and will reveal how the principles discovered for INO80 apply to other remodeller families.

Online content

Any Methods, including any statements of data availability and Nature Research reporting summaries, along with any additional references and Source Data files, are available in the online version of the paper at https://doi.org/10.1038/s41586-018-0029-y.

Received: 18 September 2017; Accepted: 16 February 2018;
Published online: 11 April 2018

1. Bartholomew, B. Regulating the chromatin landscape: structural and mechanistic perspectives. *Annu. Rev. Biochem.* **83**, 671–696 (2014).
2. Narlikar, G. J., Sundaramoorthy, R. & Owen-Hughes, T. Mechanisms and functions of ATP-dependent chromatin-remodeling enzymes. *Cell* **154**, 490–503 (2013).
3. Clapier, C. R., Iwasa, J., Cairns, B. R. & Peterson, C. L. Mechanisms of action and regulation of ATP-dependent chromatin-remodelling complexes. *Nat. Rev. Mol. Cell Biol.* **18**, 407–422 (2017).
4. Shen, X., Mizuguchi, G., Hamiche, A. & Wu, C. A chromatin remodelling complex involved in transcription and DNA processing. *Nature* **406**, 541–544 (2000).
5. Papamichos-Chronakis, M., Watanabe, S., Rando, O. J. & Peterson, C. L. Global regulation of H2A.Z localization by the INO80 chromatin-remodeling enzyme is essential for genome integrity. *Cell* **144**, 200–213 (2011).
6. Udugama, M., Sabri, A. & Bartholomew, B. The INO80 ATP-dependent chromatin remodeling complex is a nucleosome spacing factor. *Mol. Cell. Biol.* **31**, 662–673 (2011).
7. Krietenstein, N. et al. Genomic nucleosome organization reconstituted with pure proteins. *Cell* **167**, 709–72.e712 (2016).
8. Brahma, S. et al. INO80 exchanges H2A.Z for H2A by translocating on DNA proximal to histone dimers. *Nat. Commun.* **8**, 15616 (2017).
9. Jiang, C. & Pugh, B. F. Nucleosome positioning and gene regulation: advances through genomics. *Nat. Rev. Genet.* **10**, 161–172 (2009).
10. Liu, X., Li, M., Xia, X., Li, X. & Chen, Z. Mechanism of chromatin remodelling revealed by the Snf2–nucleosome structure. *Nature* **544**, 440–445 (2017).
11. Sundaramoorthy, R. et al. Structural reorganization of the chromatin remodeling enzyme Chd1 upon engagement with nucleosomes. *eLife* **6**, e22510 (2017).
12. Farnung, L., Vos, S. M., Wigge, C. & Cramer, P. Nucleosome–Chd1 structure and implications for chromatin remodelling. *Nature* **550**, 539–542 (2017).
13. Tosi, A. et al. Structure and subunit topology of the INO80 chromatin remodeler and its nucleosome complex. *Cell* **154**, 1207–1219 (2013).
14. Chen, L. et al. Subunit organization of the human INO80 chromatin remodeling complex: an evolutionarily conserved core complex catalyzes ATP-dependent nucleosome remodeling. *J. Biol. Chem.* **286**, 11283–11289 (2011).
15. Nguyen, V. Q. et al. Molecular architecture of the ATP-dependent chromatin-remodeling complex SWR1. *Cell* **154**, 1220–1231 (2013).
16. Mizuguchi, G. et al. ATP-driven exchange of histone H2AZ variant catalyzed by SWR1 chromatin remodeling complex. *Science* **303**, 343–348 (2004).
17. Albert, I. et al. Translational and rotational settings of H2A.Z nucleosomes across the *Saccharomyces cerevisiae* genome. *Nature* **446**, 572–576 (2007).
18. Willhoft, O., Bythell-Douglas, R., McCormack, E. A. & Wigley, D. B. Synergy and antagonism in regulation of recombinant human INO80 chromatin remodeling complex. *Nucleic Acids Res.* **44**, 8179–8188 (2016).
19. Chen, L., Conaway, R. C. & Conaway, J. W. Multiple modes of regulation of the human Ino80 SNF2 ATPase by subunits of the INO80 chromatin-remodeling complex. *Proc. Natl Acad. Sci. USA* **110**, 20497–20502 (2013).
20. Yen, K., Vinayachandran, V. & Pugh, B. F. SWR-C and INO80 chromatin remodelers recognize nucleosome-free regions near +1 nucleosomes. *Cell* **154**, 1246–1256 (2013).
21. Gangaraju, V. K. & Bartholomew, B. Dependency of ISW1a chromatin remodeling on extranucleosomal DNA. *Mol. Cell. Biol.* **27**, 3217–3225 (2007).
22. Zhou, C. Y. et al. Regulation of Rvb1/Rvb2 by a domain within the INO80 chromatin remodeling complex implicates the yeast Rvbs as protein assembly chaperones. *Cell Reports* **19**, 2033–2044 (2017).
23. Aramayo, R. J. et al. Cryo-EM structures of the human INO80 chromatin-remodeling complex. *Nat. Struct. Mol. Biol.* **25**, 37–44 (2017).
24. Koldewey, P., Horowitz, S. & Bardwell, J. C. A. Chaperone–client interactions: non-specificity engenders multifunctionality. *J. Biol. Chem.* **292**, 12010–12017 (2017).
25. Lakomek, K., Stoehr, G., Tosi, A., Schmailzl, M. & Hopfner, K. P. Structural basis for dodecameric assembly states and conformational plasticity of the full-length AAA+ ATPases Rvb1•Rvb2. *Structure* **23**, 483–495 (2015).
26. Rivera-Calzada, A. et al. The structure of the R2TP complex defines a platform for recruiting diverse client proteins to the HSP90 molecular chaperone system. *Structure* **25**, 1145–1152.e4 (2017).
27. Saha, A., Wittmeyer, J. & Cairns, B. R. Chromatin remodeling by RSC involves ATP-dependent DNA translocation. *Genes Dev.* **16**, 2120–2134 (2002).
28. Dürr, H., Körner, C., Müller, M., Hickmann, V. & Hopfner, K. P. X-ray structures of the *Sulfolobus solfataricus* SWI2/SNF2 ATPase core and its complex with DNA. *Cell* **121**, 363–373 (2005).
29. Willhoft, O. et al. Crosstalk within a functional INO80 complex dimer regulates nucleosome sliding. *eLife* **6**, e25782 (2017).
30. Zhou, C. Y. et al. The yeast INO80 complex operates as a tunable DNA length-sensitive switch to regulate nucleosome sliding. *Mol. Cell* **69**, 677–688. e9 (2018).
31. Watanabe, S., Radman-Livaja, M., Rando, O. J. & Peterson, C. L. A histone acetylation switch regulates H2A.Z deposition by the SWR-C remodeling enzyme. *Science* **340**, 195–199 (2013).

Acknowledgements We thank P. Korber and E. Oberbeckmann for help with biochemical analysis of INO80, E. Hurt for help with *C. thermophilum* genome annotations, O. Berninghausen for help with data collection, and K. Lammens, K. Knoll, R. Byrne, G. Stöhr and G. Witte for discussions and technical help. We thank the LMU Protein Analysis Unit and the MPI of Biochemistry cryo-EM and biophysics core facilities for access and support, and the SuperMUC for computing time. K.-P.H. is supported by the Deutsche Forschungsgemeinschaft (CRC1064, RTG1721), the European Research Council (ERC Advanced Grant ATMMACHINE), the Gottfried-Wilhelm-Leibniz Prize and the Center for Integrated Protein Sciences Munich (CIPSM). S.E. acknowledges an EMBO long-term fellowship and K.S. acknowledges funding by Quantitative Biosciences Munich (QBM).

Reviewer information *Nature* thanks B. Bartholomew, O. Llorca and the other anonymous reviewer(s) for their contribution to the peer review of this work.

Author contributions S.E. prepared cryo-EM samples and performed structure determination. K.S. prepared nucleosomes, performed the biochemical analysis and participated in structure determination. S.E., D.K. and K.-P.H. build atomic models. K.L. characterized INO80 subcomplexes and participated in early stages of the electron microscopy analysis. M.S. operates the MPI Biochemistry cryo-EM facility, helped with electron microscopy data collection and provided general electron microscopy advice. M.M. helped with recombinant protein production. S.E. and K.-P.H. designed the overall study, analysed the results and wrote the paper with contributions from all other authors.

Competing interests The authors declare no competing interests.

Additional information
Extended data is available for this paper at https://doi.org/10.1038/s41586-018-0029-y.
Supplementary information is available for this paper at https://doi.org/10.1038/s41586-018-0029-y.
Reprints and permissions information is available at http://www.nature.com/reprints.
Correspondence and requests for materials should be addressed to K.-P.H.
Publisher's note: Springer Nature remains neutral with regard to jurisdictional claims in published maps and institutional affiliations.

METHODS

No statistical methods were used to predetermine sample size. The experiments were not randomized and investigators were not blinded to allocation during experiments and outcome assessment.

INO80 expression and purification. *C. thermophilum* INO80 subunits were cloned and expressed using the MultiBac technology[32]. Genes coding for Ino80$^{718–1848}$ with a C-terminal 2 × Flag, Taf14 and Ies4 were each cloned in pACEBac1, Rvb2 and actin in pIDC, Ies2 and Arp8 in pIDS and Ies6, Rvb1, Arp5 and Arp4 in pIDK. Resulting gene cassettes coding for Ino80$^{718–1848}$-2 × Flag, Rvb1, Rvb2, Arp5, Ies2 and Ies6 were combined in one bacmid, whereas those coding for Ies4, Taf14, Arp8, actin and Arp4 were combined in a separate bacmid. Recombination steps were carried out in *Escherichia coli* XL1-Blue cells (Stratagene) or pirHC cells (Geneva Biotech) under addition of Cre recombinase (NEB). Baculoviruses were generated in *Spodoptera frugiperda* (SF21) insect cells (IPLB-Sf21AE). *Trichoplusia ni* High Five cells (Invitrogen) were co-infected with 1/100 v/v of each baculovirus. Hi5 and SF9 insect cells were purchased from Invitrogen and used for protein production without further authentication. Cells were cultured for 60 h at 27 °C and collected by centrifugation. For complex purification, cells were disrupted in lysis buffer (30 mM HEPES, pH 7.8, 300 mM NaCl, 10% glycerol, 20 μM $ZnCl_2$, 0.25 mM DTT, 0.28 μg/ml leupeptin, 1.37 μg/ml pepstatin A, 0.17 mg/ml PMSF, 0.33 mg/ml benzamidine) and gently sonified. Raw lysate was cleared by centrifugation at 30500*g* and 4 °C for 30 min. Supernatant was incubated with 4 ml anti-Flag M2 affinity gel (Sigma-Aldrich) for 1 h and washed with 75 ml lysis buffer and 50 ml wash buffer (30 mM HEPES, pH 7.8, 150 mM NaCl, 5% glycerol, 0.5 mM $CaCl_2$, 20 μM $ZnCl_2$, 0.25 mM DTT). The complex was eluted by incubation with 8 ml elution buffer (wash buffer supplemented with 0.2 mg/ml Flag peptide) for 20 min at 4 °C. Next, the sample was loaded onto a Mono Q 5/50 GL column (GE Healthcare) and eluted by a gradient of increasing salt, resulting in a highly pure INO80 sample.

Right-angle light scattering measurement. Molecular weight of apo INO80 was determined by right-angle light scattering. Size-exclusion chromatography (SEC)-coupled static light scattering was performed using an Äkta micro chromatography system equipped with a Superose 6 10/300 Increase column (GE Healthcare) and a right-angle laser static light scattering device and refractive index detector (Malvern/Viscotek). BSA was used to calibrate the system. Evaluation was performed using the OmniSEC software (Malvern/Viscotek).

Purification of mononucleosomes. Canonical human histones and their mutants were purified by a combination of inclusion body purification and ion-exchange chromatography, essentially as previously described[33,34]. In brief, histones were expressed in *E. coli* BL21 (DE3) cells (Novagen) for 2 h after induction at 37 °C. Cells were disrupted under non-denaturing conditions and inclusion bodies were washed with 1% Triton X-100. Inclusion bodies were resuspended in 7 M guanidinium chloride, dialysed in 8 M urea and histones were purified by cation-exchange chromatography. After refolding under low-salt conditions, anion exchange chromatography was performed as a final purification step. Histones were lyophilized for long-time storage. For octamer assembly, single histones were resuspended in 7 M guanidinium chloride, mixed at 1.2-fold excess of H2A and H2B and dialysed against 2 M NaCl for 16 h. Histone octamers were purified by size-exclusion chromatography using a Superdex 200 16/60 column (GE Healthcare) and were stored in 50% glycerol at −20 °C. We used the Widom 601 DNA[35] with 50 or 80 bp extra-nucleosomal DNA in the 0NX orientation[36] for reconstituting mononucleosomes. DNA was amplified by PCR, purified using anion-exchange chromatography and concentrated in vacuum. DNA and histone octamer were mixed at a 1.1-fold excess of DNA at 2 M NaCl and sodium chloride concentration was decreased to 50 mM over 17 h at 4 °C. Finally, nucleosomes were purified by anion-exchange chromatography, dialysed to 50 mM NaCl, concentrated to 1 mg/ml and stored at 4 °C.

Purification and vitrification of the INO80–0N50 complex. INO80 and 0N50 (nucleosome flanked by 0- and 50-base-pair extranucleosomal DNA) nucleosomes were mixed at a ratio of 2:1 and dialysed to binding buffer (20 mM HEPES, pH 8, 60 mM KCl, 0.5% glycerol, 0.25 mM $CaCl_2$, 20 μM $ZnCl_2$, 0.25 mM DTT) for 1 h in Slide-a-lyzer dialysis tubes (Thermo Fisher Scientific). The complex was purified by gel filtration using a Superose 6 3.2/300 column (GE Healthcare) and vitrified at a concentration of 1 mg/ml on Quantifoil R2/1 grids in the presence of 0.05% octyl-β-glucoside using a Leica EM GP (Leica).

Electron microscopy and data collection. The FEI Titan Krios transmission electron microscope was operated at 300 kV using a GIF quantum energy filter (slit width 20 eV) and a Gatan K2 summit direct electron detector. Two datasets of images (dataset I and dataset II) with a defocus ranging from 1.3 to 3.5 μM were collected at a calibrated pixel size of 1.34 Å and 1.06 Å and at a dose rate of 5.63 and 5.96 $e^-/Å^2/s$, respectively. A total dose of 67.5 and 59.6 $e^-/Å^2$ was recorded over 12 and 10 s with a frame rate of 5 and 4 frames stored per second for dataset I and dataset II, respectively. Data acquisition was carried out using SerialEM[37] facilitated by a set of customized scripts that enabled automated execution of low-dose image acquisition, including focus and drift determination as well as beam centring (M.S. et al., manuscript in preparation).

Cryo-EM data processing. Dose-fractionated image stacks were subjected to beam-induced motion correction using MotionCor2[38]. The first and the last frame were discarded and CTF parameters for each sum of remaining frames determined by CTFFIND4[39]. Micrographs that exhibited too much drift, too much contamination or abnormal Fourier patterns were discarded. For dataset I (at 1.34 Å/pixel), 1,282 image stacks were chosen for further processing, and for dataset II (at 1.06 Å/pixel) and 3,932 image stacks were chosen for further processing, carried out using MotionCor2[38]-corrected sums that were filtered according to exposure dose. Particle selection, 2D classification, 3D classification and refinement were performed using RELION[40] version 2.1.1b, unless stated otherwise. All resolutions that we report here were determined by gold standard Fourier shell correlation 0.143 criterion. B-factors were automatically determined within RELION according to a previously published method[41]. Extended Data Fig. 2a, b shows an overview of the cryo-EM processing scheme used for dataset I and dataset II. Two-dimensional class averages (Extended Data Fig. 2d), used as 35 Å low-pass-filtered templates for the initial automated particle picking of dataset I, were calculated from 800 particles that were manually picked from a screening dataset acquired using a FEI Falcon II camera and a FEI Titan Halo transmission electron microscope at 300 kV. Six thousand semi-automatically picked particles from the same dataset were used to generate an 3D ab initio reconstruction in CryoSPARC[42] (Extended Data Fig. 2c), which served as a 40 Å low-pass-filtered reference for the first round of 3D classification in RELION. 2D and 3D classification (3D classification A1 and 3D classification A2, Extended Data Fig. 2a) identified 18,000 particles corresponding to nucleosome-bound INO80^{core} complexes from 295,000 automatically picked particles. Because we refrained from crosslinking to stabilize complexes during sample and grid preparation, we observed a large number of disassembled complexes at vitrified conditions corresponding to free nucleosomes (class 1 of 3D classification A2, Extended Data Fig. 2a) or apo INO80^{core} complex (class 3 of 3D classification A2, Extended Data Fig. 2a). Severe orientational bias of particles in this dataset prevented meaningful refinement of the apo Ino80^{core} complex beyond 8 Å. By contrast, the identified set of 18,000 particles of nucleosome-bound INO80^{core} subjected to RELION refinement and subsequent solvent mask post-processing yielded a cryo-EM map of the nucleosome complex at an overall resolution of 5.8 Å. This map was used as a reference to determine a higher resolution structure using the larger dataset II recorded at higher magnification (1.06 Å/pixel). To improve auto-picking of sparsely populated orientations of the complex, we calculated 2D projections of the experimentally determined 5.8 Å cryo-EM map (Extended Data Fig. 2e). To avoid false positives during particle picking, we applied a 35 Å low-pass filter to the projections before using them as templates and verified the quality of the automated particle picking procedure by visual inspection of the micrographs as well as by diagnostic 2D classifications in RELION. Two hundred and fifty-two thousand particles derived from automated particle picking were subjected to successive rounds of 3D classification (3D classification B1, 3D classification B2 and 3D classification B3, Extended Data Fig. 2b). Notably, an intermediate set of 144,000 particles yielded a cryo-EM map of the INO80^{core} complex at 3.9 Å. Although inspection indicated there was still conformational or compositional heterogeneity within the region of the nucleosome, the particle density and signal-to-noise ratio was sufficiently high to enable movie processing and particle polishing within RELION (using frames 1–30, running averages of 8 frames and a standard deviation of particles of 300 Å). Subsequent refinement of the 'polished' particles yielded a 3.7 Å map that allowed de novo atomic model building and real space refinement of Ies2, Ies6, Arp5, Ino80^{insert} and Arp5 (see below). Three-dimensional classification (3D classification B2) yielded a class of 34,000 nucleosome-bound particles. These particles were subjected to RELION refinement and solvent mask post-processing, yielding a cryo-EM map of the complex at an overall resolution of 4.3 Å (Extended Data Fig. 2f). Finally, two classes showing different conformations of the grappler element were obtained by using a third 3D classification (3D classification B3, Extended Data Fig. 2b) in which the Euler angles derived from the previous refinement were kept fixed and a mask of the respective region of the complex was applied. Local resolution estimation and local resolution filtering was performed as implemented in RELION 2.1.1b.

Model building and refinement. As a first stage we performed rigid-body docking in UCSF Chimera[43] using available crystal structures of *Xenopus laevis* nucleosome with Widom 601 sequence (RCSB Protein Data Bank (PDB) code: 4R8P), crystal structures of *C. thermophilum* Rvb1 and Rvb2 (PDB codes: 4WW4 and 4FM6) and homology models of *C. thermophilum* Arp5^{core} residues 59–755 (excluding insert residues 306–640) as well as *C. thermophilum* Ino80^{ATPase} residues 964–1705 (excluding insert residues 1274–1548). A homology model of the actin fold of Arp5 was built using SWISS-MODEL[44] using ATP-bound actin (PDB code: 1NWK) as a template, while I-TASSER[45] was used to build separate homology models for the N- and C-lobe of Ino80^{ATPase} using multiple high-resolution X-ray structures of related superfamily 2 ATPases as templates. Atomic model building of Ino80 insert (residues 1278–1544), Ies2 (residues 443–478), Ies6 (residues 10–52, 155–213) and

Arp5 (residues 15–107, 111–146, 153–300, 603–769) was performed using the 3.7 Å map of INO80^{core} and a combination of COOT[46] and Moloc[47]. Model building and refinement was performed iteratively using restrained real-space refinement in PHENIX 1.12. We used restraints for secondary structure, side chain rotamers, Ramachandran and Cβ restraints, while we restricted the resolution to 3.7 Å during refinement. In the final macrocycle, grouped B-factor refinement for the main chain and side chain was calculated. Statistics of the final refinement and the obtained structures are reported in Extended Data Table 1. The obtained structures were subsequently used for interpretation and model refinement using the 4.3 Å resolution cryo-EM map of the INO80^{core}–nucleosome complex. To model regions with larger conformational deviations such as the nucleosomal DNA, the Ino80^{ATPase} and regions at the nucleosome interface of INO80^{core} we used a combination of flexible fitting and (re)building using a combination of COOT[46], Moloc[47] and MDFF[48]. This procedure resulted in reasonable refinement of model into the cryo-EM map (Extended Data Fig. 3c). The properties and limitations of the molecular models of the INO80^{core}–NCP complex are summarized in the following. Flexible fitting of nucleosomal DNA accounts for the large conformational change seen in the region between SHL −5.5 and SHL −7. Although additional unambiguous density corresponding to extranucleosomal DNA protrudes from the INO80^{core}–NCP complex, we did not attempt to build DNA beyond SHL −7 at this stage. The histone core required only minor adjustments. However, we do not observe density for H3 tail residues 37–44 at their canonical binding site above SHL 1. We observed instead unassigned density between the foot element of the grappler and the N-terminal H3 helix αN. Because this density can also originate from grappler element of Arp5 (see below), we refrained from building the H3 tail at this stage. Ino80 residues 964–1274 and 1549–1705 were flexibly fitted into the density and readily connected to the refined model of the insert region described above. The topology of the grappler element was unambiguously assigned to the Arp5 insert residues 300–624. However, model building was largely restricted to a poly-alanine model given the limited resolution of this element in the 4.6 Å and 4.7 Å subclasses (Extended Data Fig. 3e). Similarly, we were able to build a poly-alanine model of Ino80 post-HSA residues 820–855 and Ies2 residues 351–443 that includes the throttle helix bound to nucleosomal DNA (Extended Data Fig. 6).

Electrophoretic-mobility shift assays. Electrophoretic-mobility shift assays were used to monitor the interaction between INO80 and 0N50 mononucleosomes. Nucleosomes were labelled at the 5′-end of their extranucleosomal DNA with fluorescein. Nucleosome (15 nM) was incubated with increasing concentrations of INO80 (0, 5, 10, 20 and 40 nM) in electrophoretic mobility shift assay buffer (25 mM HEPES, pH 8, 60 mM KCl, 7% glycerol, 0.25 mM DTT, 2 mM $CaCl_2$) for 20 min on ice. Samples were analysed at 4 °C by native PAGE on a 3–12% acrylamide BIS-Tris gel (Invitrogen) and visualized using the Typhoon imaging system (GE healthcare).

Nucleosome sliding assays. 0N80 (nucleosome flanked by 0- and 80-base-pair extra-nucleosomal DNA) mononucleosomes with 5′-fluorescein-labelled extranucleosomal DNA were used for monitoring the sliding activity of INO80. Nucleosome (150 nM) was incubated with 50 nM INO80 in sliding buffer (25 mM HEPES, pH 8, 60 mM KCl, 7% glycerol, 0.10 mg/ml BSA, 0.25 mM DTT, 2 mM $MgCl_2$) at 25 °C. The reaction was started on addition of 1 mM ATP and stopped at several time points (15, 30, 45, 60, 120, 300, 500 and 1,200 s) by addition of 0.2 mg/ml lambda DNA (NEB). Nucleosome species were separated by native PAGE on a 3–12% acrylamide BIS-Tris gel (Invitrogen) and visualized using the Typhoon imaging system (GE healthcare). ImageJ was used to quantify gel bands and the fraction of remodelled band was plotted against the reaction time. Data describe a saturation curve and were fitted in Prism (GraphPad) using an exponential equation.

ATPase assays. An ATPase assay coupling ATP hydrolysis to NADH oxidation was used to determine the ATPase rate of INO80. INO80 (30 nM) was incubated in assay buffer (25 mM HEPES, pH8, 50 mM KCl, 1 mM DTT, 2 mM $MgCl_2$, 0.1 mg/ml BSA) with 0.5 mM phosphoenolpyruvate, 1 mM ATP, 0.1 mM NADH and 25 U/ml lactate dehydrogenase and pyruvate kinase (Sigma) at 25 °C in a final volume of 50 µl. NADH concentration was monitored fluorescently over 1 h in non-binding black 384-well plates (Greiner Bio-One) using 340 nm for excitation and an emission of 460 nm with a Tecan Infinite M100 (Tecan). Where indicated, ATPase activity was determined in the presence of 150 nM nucleosome. ATP turnover was calculated using maximal initial linear rates, corrected for a buffer blank.

Figure preparation. Figures were prepared with PyMol (The PyMOL Molecular Graphics System, version 1.8 Schrödinger, LLC)), UCSF Chimera[43] and UCSF ChimeraX[49].

Data availability. The electron density reconstruction and final model have been deposited with the Electron Microscopy Data Base under accession codes EMD-4264, EMD-4277, EMD-4278 and EMD-4280, and with the RCSB Protein Data Bank under accession codes 6HFS and 6FML. Uncropped images of the polyacrylamide gels are shown in Supplementary Fig. 1. All other data are available from the corresponding author upon reasonable request.

32. Fitzgerald, D. J. et al. Protein complex expression by using multigene baculoviral vectors. *Nat. Methods* **3**, 1021–1032 (2006).
33. Klinker, H., Haas, C., Harrer, N., Becker, P. B. & Mueller-Planitz, F. Rapid purification of recombinant histones. *PLoS ONE* **9**, e104029 (2014).
34. Dyer, P. N. et al. Reconstitution of nucleosome core particles from recombinant histones and DNA. *Methods Enzymol.* **375**, 23–44 (2004).
35. Lowary, P. T. & Widom, J. New DNA sequence rules for high affinity binding to histone octamer and sequence-directed nucleosome positioning. *J. Mol. Biol.* **276**, 19–42 (1998).
36. Levendosky, R. F., Sabantsev, A., Deindl, S. & Bowman, G. D. The Chd1 chromatin remodeler shifts hexasomes unidirectionally. *eLife* **5**, e21356 (2016).
37. Mastronarde, D. N. Automated electron microscope tomography using robust prediction of specimen movements. *J. Struct. Biol.* **152**, 36–51 (2005).
38. Zheng, S. Q. et al. MotionCor2: anisotropic correction of beam-induced motion for improved cryo-electron microscopy. *Nat. Methods* **14**, 331–332 (2017).
39. Rohou, A. & Grigorieff, N. CTFFIND4: Fast and accurate defocus estimation from electron micrographs. *J. Struct. Biol.* **192**, 216–221 (2015).
40. Scheres, S. H. RELION: implementation of a Bayesian approach to cryo-EM structure determination. *J. Struct. Biol.* **180**, 519–530 (2012).
41. Rosenthal, P. B. & Henderson, R. Optimal determination of particle orientation, absolute hand, and contrast loss in single-particle electron cryomicroscopy. *J. Mol. Biol.* **333**, 721–745 (2003).
42. Punjani, A., Rubinstein, J. L., Fleet, D. J. & Brubaker, M. A. cryoSPARC: algorithms for rapid unsupervised cryo-EM structure determination. *Nat. Methods* **14**, 290–296 (2017).
43. Pettersen, E. F. et al. UCSF Chimera—a visualization system for exploratory research and analysis. *J. Comput. Chem.* **25**, 1605–1612 (2004).
44. Biasini, M. et al. SWISS-MODEL: modelling protein tertiary and quaternary structure using evolutionary information. *Nucleic Acids Res.* **42**, W252–W258 (2014).
45. Yang, J. et al. The I-TASSER suite: protein structure and function prediction. *Nat. Methods* **12**, 7–8 (2015).
46. Emsley, P. & Cowtan, K. Coot: model-building tools for molecular graphics. *Acta Crystallogr. D* **60**, 2126–2132 (2004).
47. Gerber, P. R. & Müller, K. MAB, a generally applicable molecular force field for structure modelling in medicinal chemistry. *J. Comput. Aided Mol. Des.* **9**, 251–268 (1995).
48. Qi, Y. et al. CHARMM-GUI MDFF/xMDFF utilizer for molecular dynamics flexible fitting simulations in various environments. *J. Phys. Chem. B* **121**, 3718–3723 (2017).
49. Goddard, T. D. et al. UCSF ChimeraX: meeting modern challenges in visualization and analysis. *Protein Sci.* **27**, 14–25 (2017).
50. Kucukelbir, A., Sigworth, F. J. & Tagare, H. D. Quantifying the local resolution of cryo-EM density maps. *Nat. Methods* **11**, 63–65 (2014).

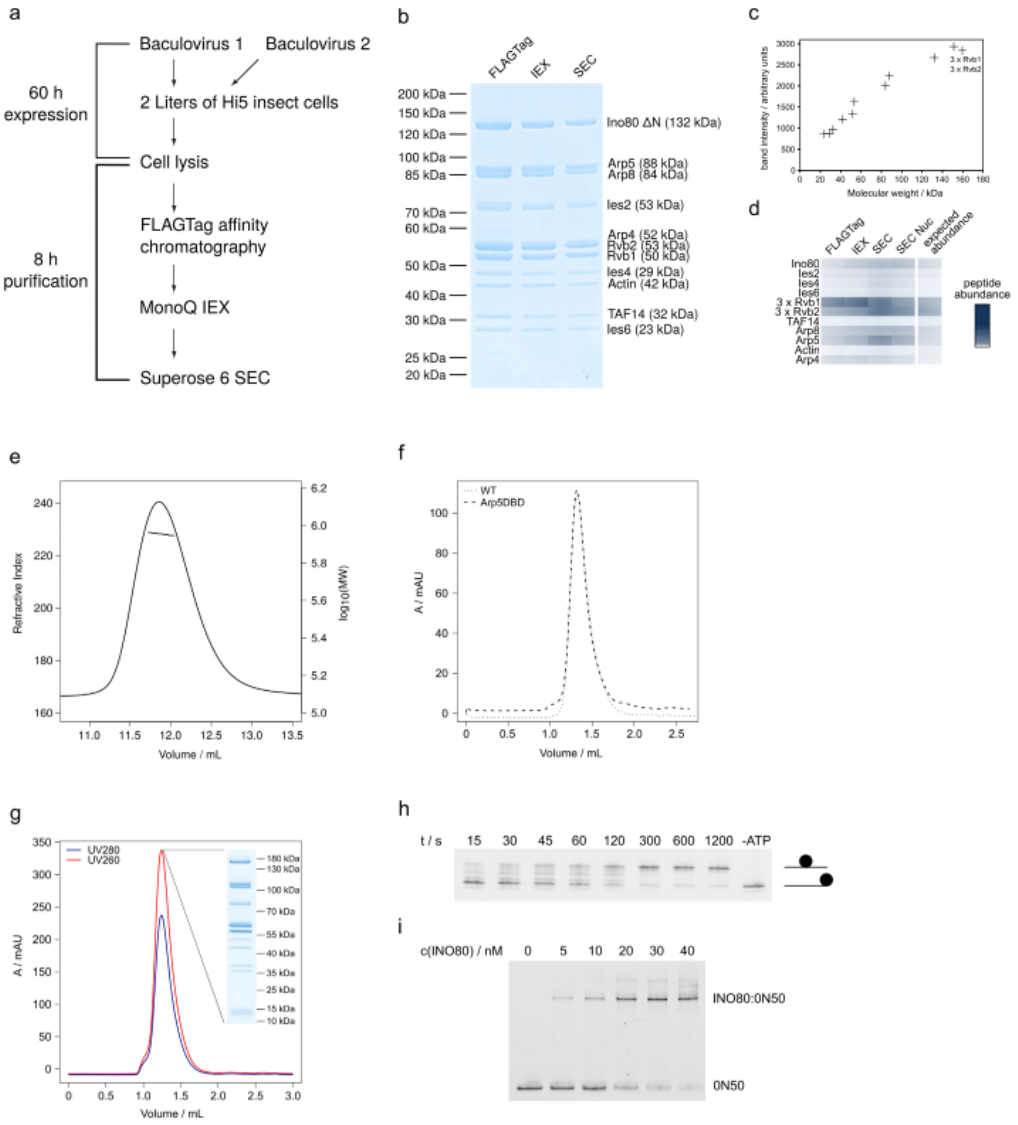

Extended Data Fig. 1 | Purification of apo INO80, INO80–0N50 and sliding activity of INO80. **a**, Schematic of expression and purification of INO80. **b**, SDS–PAGE of INO80 purification steps (stained with SimplyBlue). Protein identity was confirmed by mass spectrometry (data not shown). **c**, Quantification of band intensity from SDS–PAGE (SEC sample) plotted against the molecular weight shows stoichiometric presence of all subunits. **d**, Label-free semi-quantitative mass spectrometry analysis of INO80^{core} complexes after individual purification steps. **e**, Right-angle light scattering measurement of apo INO80. Measured refractive index and calculated logarithmical molecular weight are plotted against the elution volume. The measurement yields a molecular weight of 880 kDa, confirming the integrity and correct stoichiometry of the purified complex. **f**, Comparison of the SEC elution profile of apo INO80 and the Arp5^{DBD} mutant on a Superose 6 3.2/300. **g**, Purification of the INO80–nucleosome complex. SEC elution profile from a Superose 6 3.2/300 is shown together with an analysis of the main peak fraction by SDS–PAGE. **h**, Sliding of end-positioned 0N80 mononucleosomes by INO80. Native PAGE analysis of fluorescein-labelled nucleosome is shown. **i**, Interaction of INO80 and mononucleosome monitored by electrophoretic-mobility shift assay.

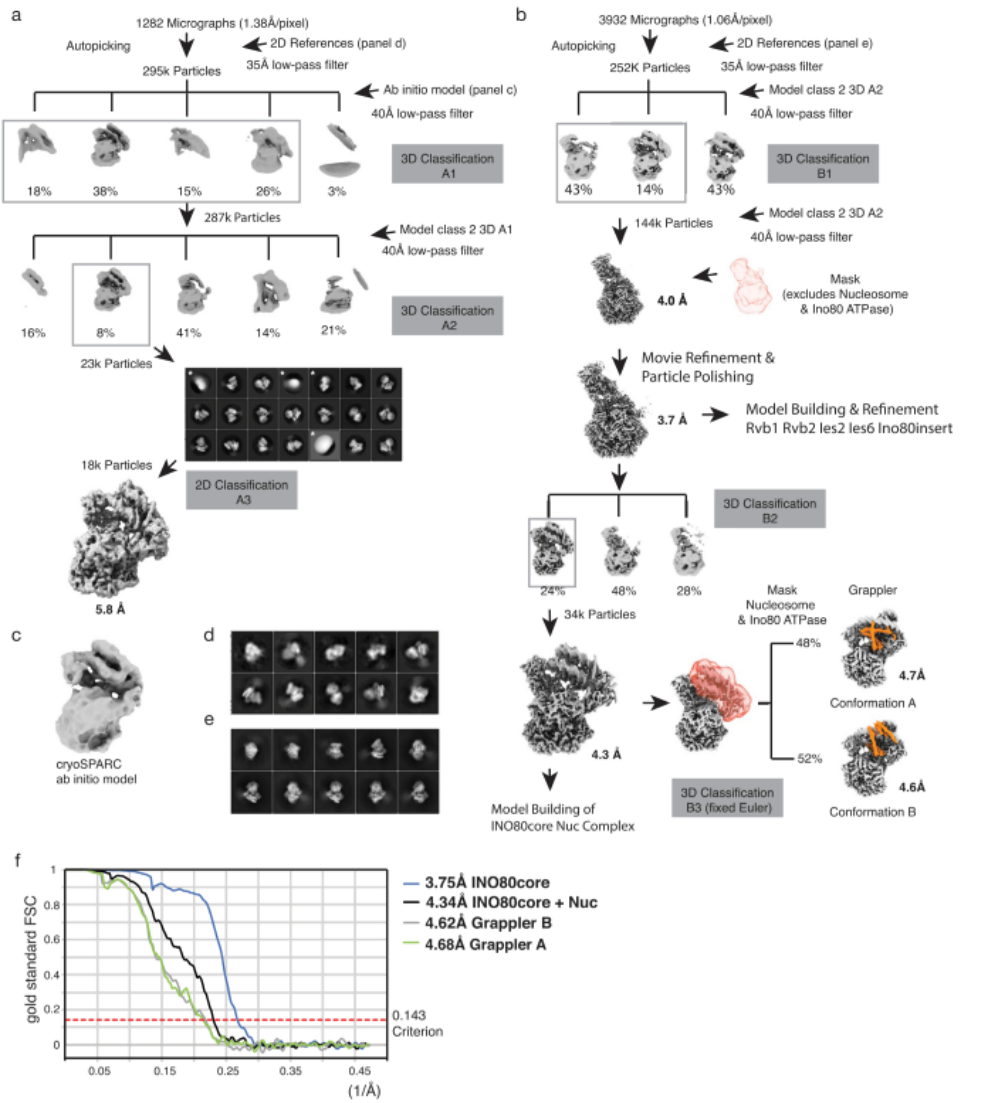

Extended Data Fig. 2 | Cryo-EM data analysis. a, **b**, Schemes of RELION[40] classifications and refinements that were used to obtain cryo-EM reconstructions of the INO80^{core}–NCP complex. **a**, Outline of an initial classification scheme that used a cryoSPARC[42] ab initio 3D reconstruction of the complex as a reference. **b**, Classification scheme that yielded the final cryo-EM reconstructions. In **a** and **b**, boxed 3D classes were selected for further processing as indicated. Two-dimensional classes discarded for further processing are marked with an asterisk. **c**, Ab initio 3D reconstruction by cryoSPARC[42] using 6,000 semi-automatically picked particles **d**, Eight hundred manually picked particles were used to obtain initial 2D classes that were used as references for automated particle picking as indicated in **a**. **e**, Projections of the experimentally determined 5.8 Å cryo-EM reconstructions obtained from the scheme in **a**. These projections were low-pass filtered to 35 Å and used then as templates to improve automated picking of particles corresponding to sparsely populated orientations of the complex (see Methods). The quality of the automated particle picking was verified by visual inspection of micrographs as well as by diagnostic 2D classifications (not shown). Later 3D classifications in the scheme shown in **b** were facilitated by masks and fixed Euler angles from previous refinements as indicated (3D classification B3). **f**, Gold standard Fourier shell correlation curves of final maps (3.75, 4.34, 4.62 and 4.68 Å). The resolutions were determined using the 0.143 Fourier shell correlation criterion as indicated by the dotted line. Extended Data Table 1 summarizes data collection and processing.

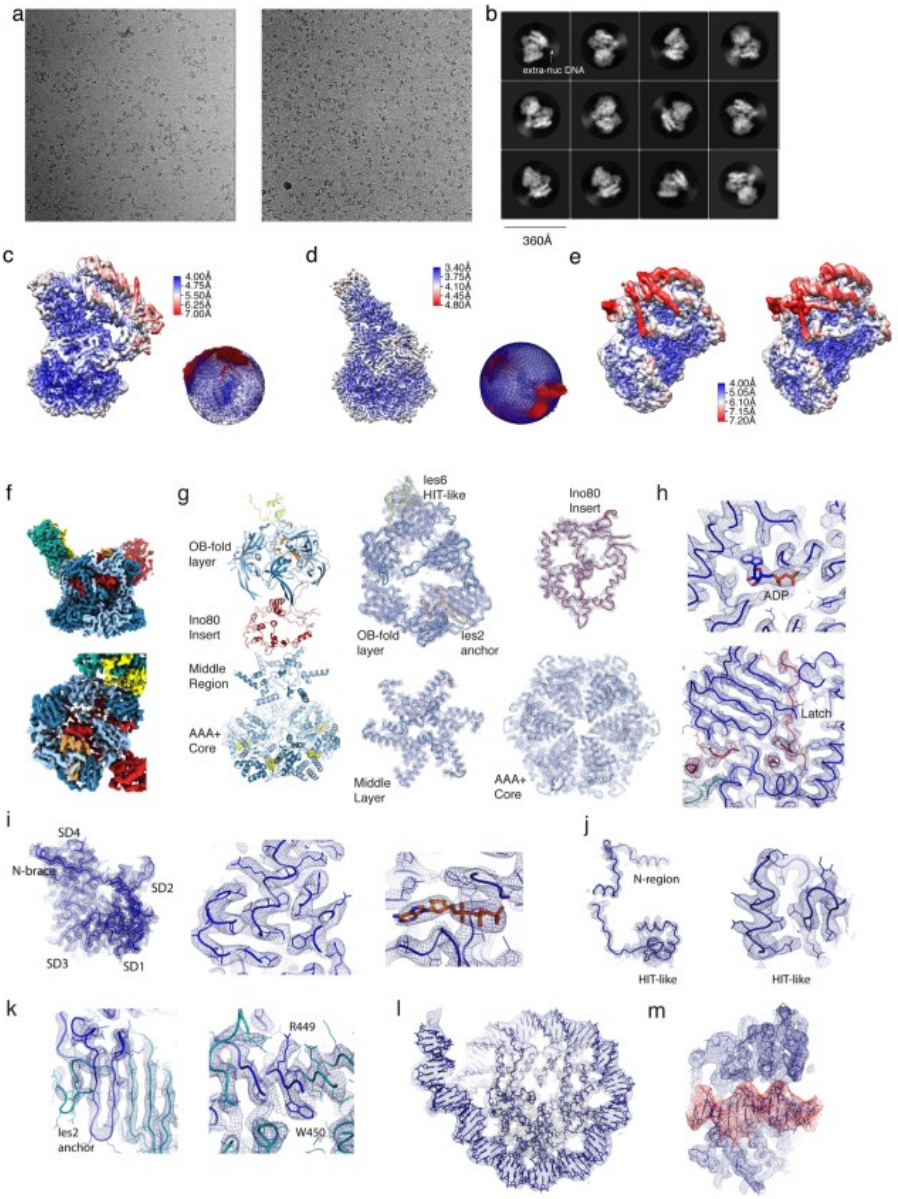

Extended Data Fig. 3 | Cryo-EM data quality. a, Two representative micrographs of the set that was used to determine the structure of the INO80^{core}–NCP complex. **b**, Typical 2D class averages of the INO80^{core}–NCP complex. Note that dynamic extranucleosomal DNA (extra-nuc DNA) visibly protrudes from the well-ordered core complex. **c**–**e**, The final 4.3 Å (**c**, overall), 3.7 Å (**d**, Rvb1/Rvb2–Arp5 mask) and 4.6 Å and 4.7 Å (**e**, grappler conformations A (right) and B (left)) maps were analysed by using ResMap[50]. Local resolution estimates are shown as a colour-coded surface representation along with representations of angular distributions of particles contributing to the 4.3 and 3.7 Å maps. **f**–**m**, Representative examples of cryo-EM map areas used for model building. **f**, The 3.7 Å map using the colour codes of Fig. 1c showing the definition of Rvb1/Rvb2–client interactions. **g**, 'Explosion' figure of the Rvb1/Rvb2 layers, along with corresponding regions of the 3.7 Å map. **h**, Top, details showing a representative ATP/ADP-binding site of Rvb1/Rvb2 with highlighted ADP, and showing the latch of the Ino80^{insert} (red). **i**, Map area at the Arp5^{core} showing the N-terminal brace (left), with representative details of the actin core (middle) and the ATP-binding site (right). **j**, Overview showing Ies6 (left) and details of its HIT-like domain (right). **k**, Map area at the Ies2–Rvb1/Rvb2 interaction (left) with details showing an anchoring tryptophane. **l**, Map area at the NCP. **m**, Map area at the Ino80 motor domain bound to SHL −6 (red).

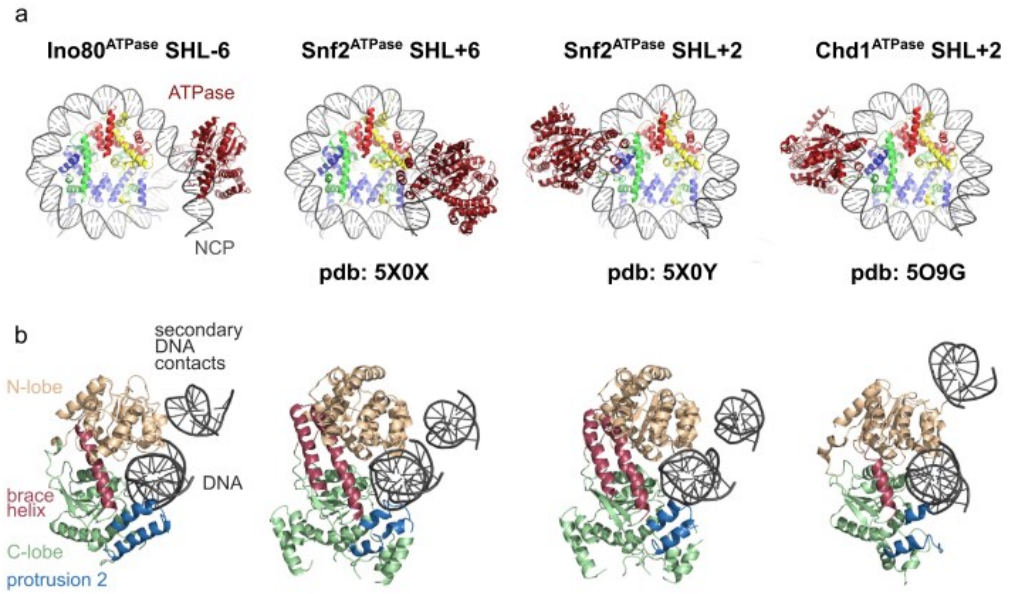

Extended Data Fig. 4 | Comparison of nucleosome-bound Swi2/Snf2-type ATPases. a, Interaction of Ino80^{ATPase} bound to SHL −6 (left, this study), Snf2^{ATPase} bound to SHL + 6 (middle), Snf2^{ATPase} bound to SHL + 2 and Chd1^{ATPase} bound to SHL + 2 (right) with NCPs. **b**, Comparison of domain architectures of the Swi2/Snf2-type ATPases and their interaction with nucleosomal DNA.

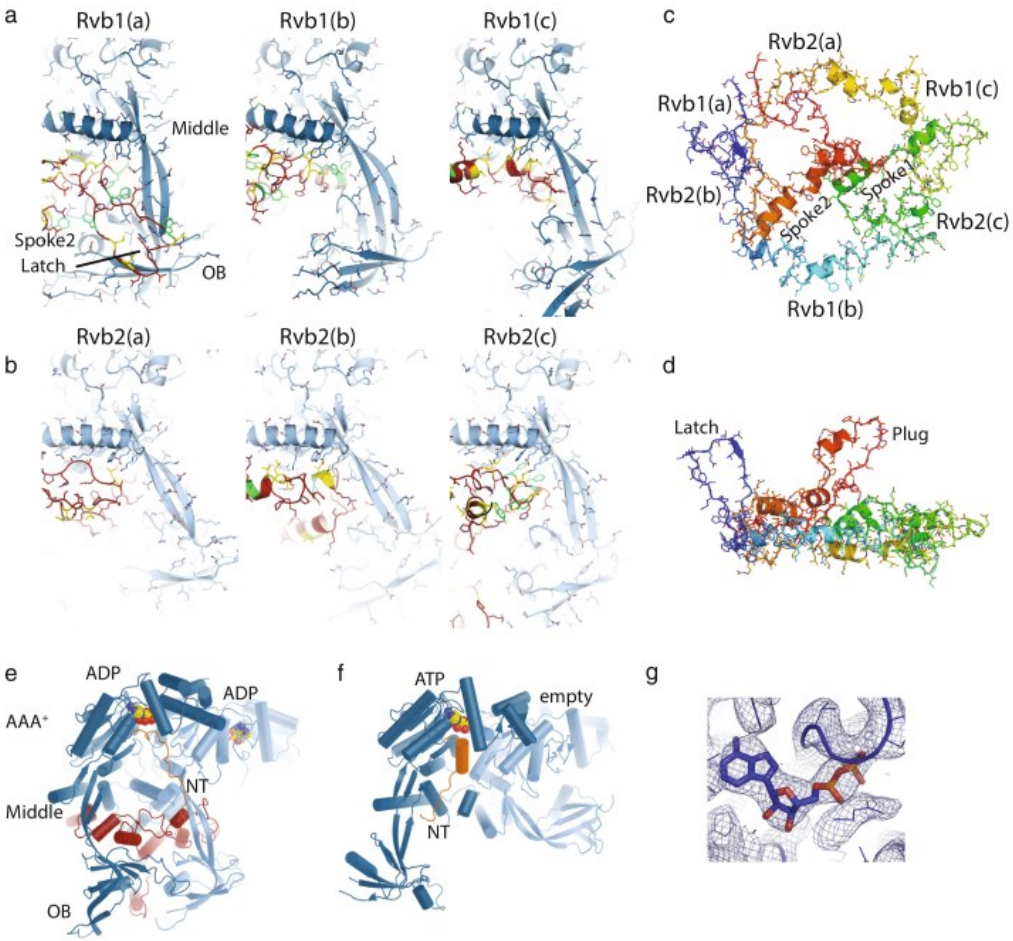

Extended Data Fig. 5 | Details of Rvb1/Rvb2–Ino80^{insert} interactions. **a**, Close-up views of Rvb1 client cavities (blue), bound to the different interaction elements of Ino80^{insert} (red, with yellow hydrophobic and green aromatic side chains). **b**, As in **a** but depicting Rvb2 client cavities. **c**, Ino80^{insert} shown in rainbow colouring from N terminus (red) to C terminus (blue), to highlight the circular fold. Selected elements as well as the positions of the Rvb1/Rvb2 binding partners are annotated. **d**, As in **c** but viewed from the side to highlight the protruding plug and latch elements. **e**, **f**, Rvb1/Rvb2 pair (the pair 1c and 2c from the hexamer in Fig. 1c) bound to Ino80^{insert} (**e**) compared with a Rvb1/Rvb2 pair from the unliganded dodecameric state (**f**) (PDB code: 4WVY). The comparison shows how client binding arranges the AAA$^+$, OB and middle layers and displaces the N-terminal domain of Rvb1 from the client pocket, also seen for human INO80^{core} [23]. Both types of conformational changes have an effect on the ADP-binding site (ADP and ATP represented by colour-coded spheres), which suggests how client interactions are allosterically coupled to the ATPase activity of Rvb1/Rvb2. **g**, Exemplary view of the ADP coordination along with the superimposed map.

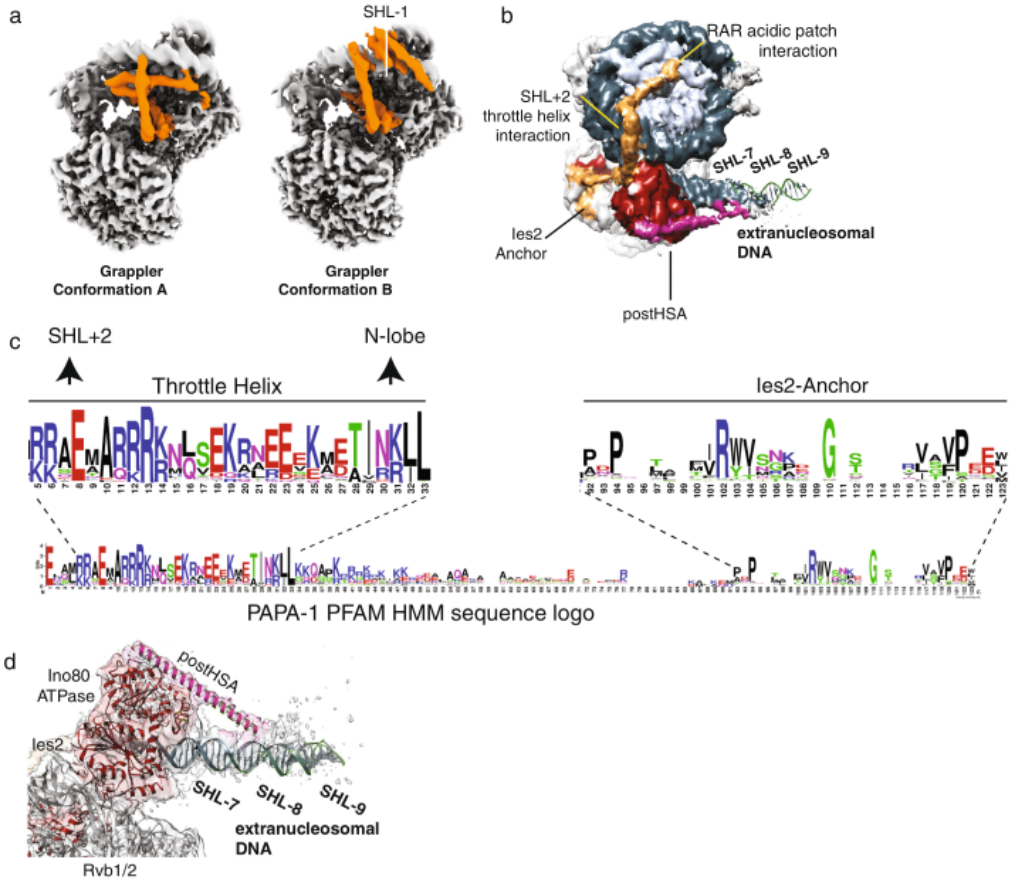

Extended Data Fig. 6 | Two conformations of the grappler element and location of the post-HSA domain. Masked 3D classifications identified two conformations of the grappler element of INO80^{core} and the post-HSA domain of the Ino80^{ATPase}. **a**, Left, grappler conformation A (conformation discussed in this study). Right, open conformation B in which the bar interacts with SHL −1 of the nucleosome. **b**, Subclass showing the post-HSA domain (magenta) at the Ino80^{ATPase} (red). Post-HSA domain protrudes towards extranucleosomal DNA. Ies2 is depicted in orange. **c**, Hidden Markov model (HMM) sequence logo of Ies2, showing high sequence conservation at key Ino80 and Rvb1/Rvb2 interaction sites. **d**, Detailed view of the map around post-HSA domain and extranucleosomal DNA, with superimposed models.

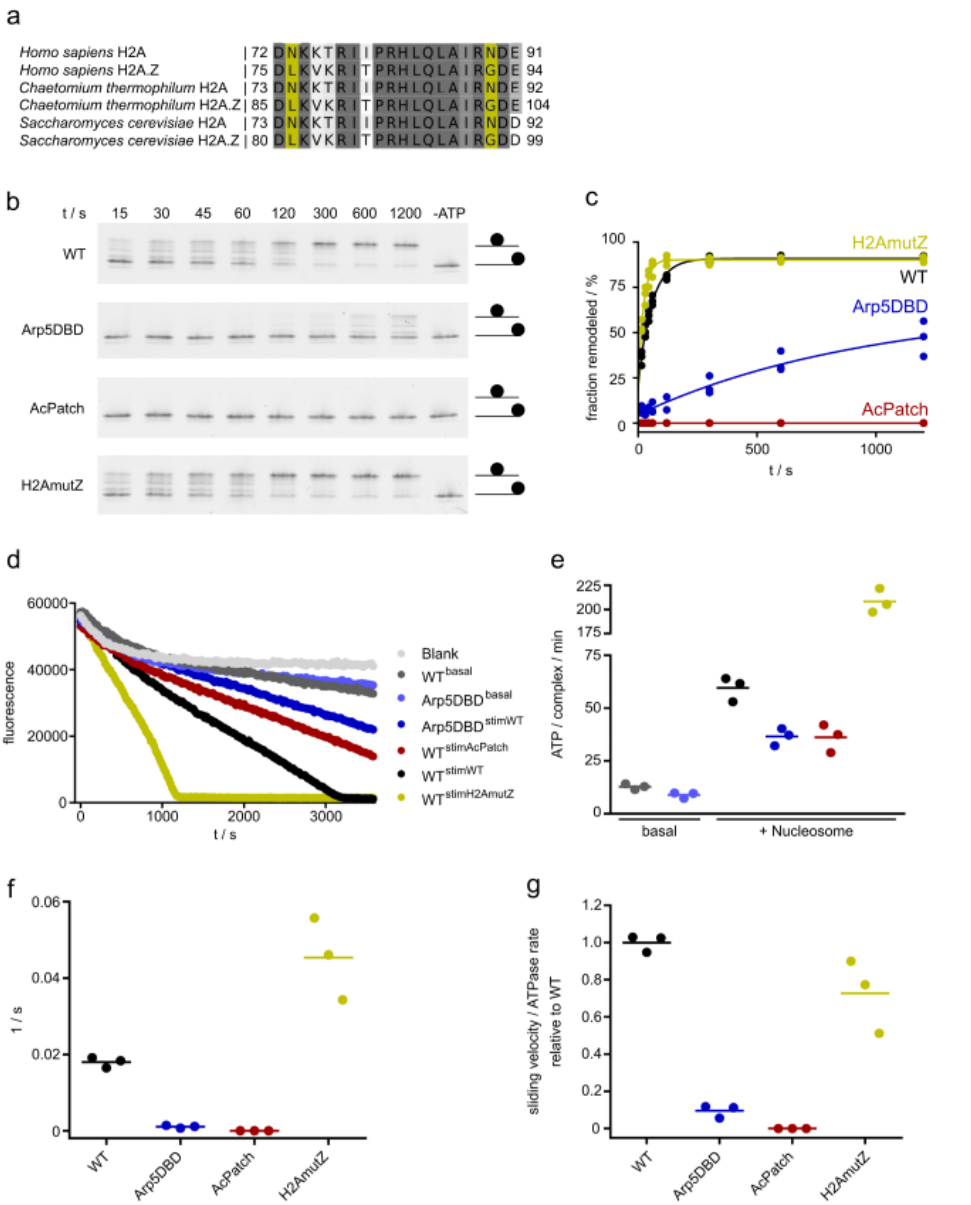

Extended Data Fig. 7 | Analysis of the enzymatic activity of INO80. **a**, Sequence alignment of H2A and H2A.Z. Olive, residues at the interface of H2A with the foot of the grappler differ in a species-conserved fashion from H2A.Z. **b**, Sliding of 0N80 mononucleosomes by INO80 analysed by native PAGE. In the Arp5^{DBD} mutant, K88, R90, R92, K96, R112 and R118 are mutated to alanines. AcPatch (E61A, E64A, D72A and D90A) and H2AmutZ (N73L and N89G) describe mutants of grappler-contacting residues of H2A (see Fig. 3). Individual data points with exponential fit ($n = 3$, technical replicates). **c**, Evaluation of the sliding activity of INO80. Band intensities of remodelled and unremodelled nucleosome species were quantified and the fraction of remodelled nucleosome plotted against time. Data points were fitted using an exponential equation. **d**, Raw data of ATPase assays. Basal ATPase rates were determined for INO80 wild type (WT) and the Arp5^{DBD} mutant, along with nucleosome-stimulated rates. Superscripted text indicates whether a nucleosome was used to stimulate ATPase activity, and if so what type of nucleosome was used. **e**, ATPase rates of INO80 with and without stimulation by nucleosomes. Rates were calculated from the linear area of the raw data and were corrected for a buffer blank (colour code as in **d**). Mean and individual data points ($n = 3$, technical replicates). **f**, Initial sliding rates of INO80 and mutants (colour code as in **c**). Data were derived from exponential fits of individual sliding curves in **c**. Mean and individual data points ($n = 3$, technical replicates). **g**, Quotient of the sliding rate in **f** and ATPase rate in **e** normalized to the wild type. Mean and individual data points ($n = 3$, technical replicates).

Extended Data Table 1 | Cryo-EM data collection, refinement and validation statistics

	#1 INO80core (EMD-4264) (PDB 6FHS)	#2 INO80core+nuc (EMD-4277) (PDB 6FML)	#3 INO80 Grappler A (EMD-4278)	#4 INO80 Grappler B (EMD-4280)
Data collection and processing				
Camera	Gatan K2	Gatan K2	Gatan K2	Gatan K2
Voltage (kV)	300	300	300	300
Electron exposure (e–/Å^2)	59.6	59.6	59.6	59.6
Defocus range (μm)	1.3-3.5	1.3-3.5	1.3-3.5	1.3-3.5
Pixel size (Å)	1.06	1.06	1.06	1.06
Symmetry imposed	C1	C1	C1	C1
Initial particle images (no.)	251692	251692	251692	251692
Final particle images (no.)	144278	33937	16287	17263
Map resolution (Å) 0.143 FSC threshold	3.75	4.34	4.68	4.62
Map sharpening B-factor (Å^2)	-142	-114	-124	-136
Refinement				
Initial model used (PDB code)	models for refinement were built *de novo* or based on 4WW4 (Rvb1/2) and 1NWK (actin)	models for refinement were based on 6FHS (INO80core) and 4R8P (nucleosome)		
Model resolution (Å) 0.5 FSC threshold	3.81	4.47		
Model resolution range (Å)	360.4 - 3.7	360.4 – 4.3		
Map sharpening *B* factor (Å^2)	-142	-114		
Model composition				
Non-hydrogen atoms	27383	43462		
Protein and DNA residues	3510	5114		
Ligands (ADP and ATP)	7	7		
B factors (Å^2)				
Protein and DNA	62.6	112.9		
Ligand	57.8	80.3		
R.m.s. deviations				
Bond lengths (Å)	0.005	0.010		
Bond angles (°)	0.82	1.20		
Validation				
MolProbity score	1.6	1.7		
Clashscore	4.3	4.8		
Poor rotamers (%)	0.0	0.1		
Ramachandran plot				
Favored (%)	93.4	93.3		
Allowed (%)	6.6	6.6		
Disallowed (%)	0.0	0.1		

4.2 The nuclear actin-containing Arp8 module is a linker DNA sensor driving INO80 chromatin remodeling

Knoll, K.R.*, Eustermann, S.*, Niebauer, V., Oberbeckmann, E., Stoehr, G., Schall, K., Tosi, A., Schwarz, M., Buchfellner, A., Korber, P. and Hopfner, K.P., 2018. The nuclear actin-containing Arp8 module is a linker DNA sensor driving INO80 chromatin remodeling. *Nature structural and molecular biology*, *25*(9), pp.823-832.
*These authors contributed equally

DOI: https://doi.org/10.1038/s41594-018-0115-8
https://www.nature.com/articles/s41594-018-0115-8

Summary

This study investigates the impact of the Arp8 module on the catalysis of DNA translocation by INO80. It demonstrates that the Arp8 module indeed binds to extranucleosomal DNA, as suggested by the low-resolution cryo-EM density, and that this interaction is crucial for the catalysis cycle. The 3D structure of actin, Arp4 and Arp8 in complex with $Ino80^{HSA}$ was solved by X-ray crystallography at a resolution of 4.0 Å. It shows that actin is sandwiched between Arp4 and Arp8 and that the HSA domain forms a segmented α-helix, which interacts with the three actin folds via their barbed ends. Actin binds Arp4 in a 'front-to-back' manner, which was also observed in the SWI/SNF Arp module between Arp7 and Ap9. In turn, Arp8 engages actin in a novel 'side-to-back' interaction. The complex was stabilized for crystallization by the addition of the small molecule sea sponge toxin latrunculin A, which binds to actin and inhibits nucleotide exchange of actin. Although no nucleotide was added during sample preparation, Arp4 and actin are both bound to ATP, while Arp8 is found to be in a nucleotide free state. The HSA helix is decorated with conserved, positively charged amino acids, which are exposed to solvent. These residues mediate the interaction between the Arp8 module and extranucleosomal DNA. This is demonstrated by the observation that the Arp8 module binds a nucleosome including extranucleosomal DNA with a higher affinity than the NCP, which depends on these positively charged residues. In the context of the complete remodeller, these residues are essential for the catalysis of DNA translocation and genome-wide nucleosome positioning by INO80. These results explain the crucial role of the Arp8 module for the action of the INO80 remodelling complex. The actin-fold proteins bind and thereby shape the HSA helix in a fashion that it interacts with extranucleosomal DNA. This is presumably essential for the catalysis cycle at that stage at which $Ino80^{ATPase}$ pumps DNA towards Arp5 and Ies6. By holding onto extranucleosomal DNA, the Arp8 module prevents the pumped DNA from flipping back. Instead, a DNA strain is formed between $INO80^{ATPase}$ and Arp5 / Ies6. Once sufficient force is generated, the Arp5 / Ies6 counter grip is released and DNA translocation occurs. In this model, DNA translocation is only possible because the Arp8 module stabilizes the transition state prior to the release of the counter grip.

Author contribution

I reconstituted and purified nucleosomes from recombinant sources with different lengths of extranucleosomal DNA.

nature structural & molecular biology

ARTICLES

https://doi.org/10.1038/s41594-018-0115-8

The nuclear actin-containing Arp8 module is a linker DNA sensor driving INO80 chromatin remodeling

Kilian R. Knoll[1,2,9], Sebastian Eustermann[1,2,9], Vanessa Niebauer[1,2], Elisa Oberbeckmann[3], Gabriele Stoehr[1,2,7], Kevin Schall[1,2], Alessandro Tosi[1,2,8], Marianne Schwarz[1,2,4], Andrea Buchfellner[5], Philipp Korber[3] and Karl-Peter Hopfner[1,2,6]*

Nuclear actin (N-actin) and actin-related proteins (Arps) are critical components of several chromatin modulating complexes, including the chromatin remodeler INO80, but their function is largely elusive. Here, we report the crystal structure of the 180-kDa Arp8 module of *Saccharomyces cerevisiae* INO80 and establish its role in recognition of extranucleosomal linker DNA. Arp8 engages N-actin in a manner distinct from that of other actin-fold proteins and thereby specifies recruitment of the Arp4–N-actin heterodimer to a segmented scaffold of the helicase-SANT-associated (HSA) domain of Ino80. The helical HSA domain spans over 120 Å and provides an extended binding platform for extranucleosomal entry DNA that is required for nucleosome sliding and genome-wide nucleosome positioning. Together with the recent cryo-electron microscopy structure of INO80^{Core}–nucleosome complex, our findings suggest an allosteric mechanism by which INO80 senses 40-bp linker DNA to conduct highly processive chromatin remodeling.

ATP-dependent chromatin remodelers shape the spatial and temporal organization of chromatin and generate hallmark features such as regularly spaced nucleosomal arrays flanking nucleosome-depleted regions at promoters[1,2]. Remodelers are generally grouped into four families, INO80, SWI/SNF, ISWI, and CHD, according to sequence similarities within their common Snf2-type ATPase motor domain. They use ATP-dependent DNA translocation to catalyze different types of large-scale nucleosome remodeling reactions—sliding, eviction/assembly, positioning, and editing (histone exchange)[3,4].

INO80 and SWI/SNF family remodelers are mega-Dalton complexes comprising typically more than 15 different protein subunits[4]. A unifying but poorly understood key feature of these two multisubunit remodeler families is the presence of N-actin and Arps. *Saccharomyces cerevisiae* possesses altogether ten Arps. Arp4–9 localize to the nucleus as integral, functionally important subunits of INO80 and SWI/SNF remodelers and of the histone acetyl transferase NuA4/TIP60[4–8]. Arp4 and N-actin form an evolutionarily conserved pair in all of these enzymes, except yeast SWI/SNF and RSC, where the Arp4–N-actin pair is replaced by the diverged, but structurally related, Arp7–Arp9 pair. Structural studies of Arp4–N-actin or Arp7–Arp9 revealed binding via their barbed ends to a helical helicase-SANT-associated (HSA) domain N-terminal to the Snf2-type ATPase domain of Swr1 and Sth1, respectively[9–11]. N-actin and nuclear Arps play an essential role in cellular stress response as well as during development[12,13], and respective genes, encoding, for example, the human Arp4 homolog BAF53, are frequently mutated in cancer[13,14]. However, the precise molecular mechanism explaining the functional importance of N-actin and nuclear Arps remains still largely elusive.

The INO80 complex is particularly intriguing for studying the functional role of actin-fold proteins in the nucleus[6,15]. In addition to N-actin and Arp4, INO80 contains with Arp5 and Arp8 in total four actin-fold proteins and is conserved in this respect from yeast to man[6,16]. INO80 has pivotal functions in gene regulation, replication, and genome maintenance[16,17], as it slides[15], edits[18], and positions[2,19] nucleosomes including the +1 nucleosome at promoter regions[2]. INO80 has a modular architecture[11,16,20,21]. The Ino80 protein subunit, harboring the Snf2-type ATPase motor, is an assembly platform for the other subunits: its N-terminal region interacts in yeast with the species-specific 'Nhp10 module' (a subcomplex of INO80 subunits Ies1, Ies3, Ies5, and Nhp10), which regulates the switch-like stimulation of INO80's nucleosome sliding efficiency by extranucleosomal DNA >40 bp[22]. The middle region of Ino80 contains the HSA domain (Ino80^{HSA}), which binds the highly conserved 'Arp8 module' composed of N-actin, Arp4, Arp8, Ies4, and Taf14[11,16]. Deletion of Arp8 or the HSA-domain leads to the loss of the whole Arp8 module and results in a remodeling defective INO80 complex[15,16,23]. The C-terminal region of Ino80 forms the equally conserved INO80 core module (INO80^{Core}), containing the Snf2-type ATPase, Ies2, the Arp5–Ies6 complex, and the Rvb1–Rvb2 heterohexameric AAA-type ATPases. The structure and unified mechanism by which INO80^{Core} recognizes and remodels the nucleosome core particle (NCP) has been recently revealed at high resolution by cryo-electron microscopy (cryoEM)[24,25]. We uncovered also that the function of INO80^{Core} as a macromolecular ratchet depends critically on a direct interaction of Arp5 with nucleosomal DNA[24]. It has been proposed that other nuclear Arps could be involved in DNA or nucleosome interactions[23,26,27].

[1]Department of Biochemistry, Ludwig-Maximilians-Universität München, Munich, Germany. [2]Gene Center, Ludwig-Maximilians-Universität München, Munich, Germany. [3]Chair of Molecular Biology, Biomedical Center, Faculty of Medicine, Ludwig-Maximilians-Universität München, Munich, Germany. [4]Institute of Biophysics, Ulm University, Ulm, Germany. [5]ChromoTek GmbH, Planegg, Germany. [6]Center for Integrated Protein Science, Ludwig-Maximilians-Universität München, Munich, Germany. [7]Present address: OmicScouts GmbH, Freising, Germany. [8]Present address: Vossius & Partner, Munich, Germany. [9]These authors contributed equally: K.R. Knoll, S. Eustermann. *e-mail: hopfner@genzentrum.lmu.de

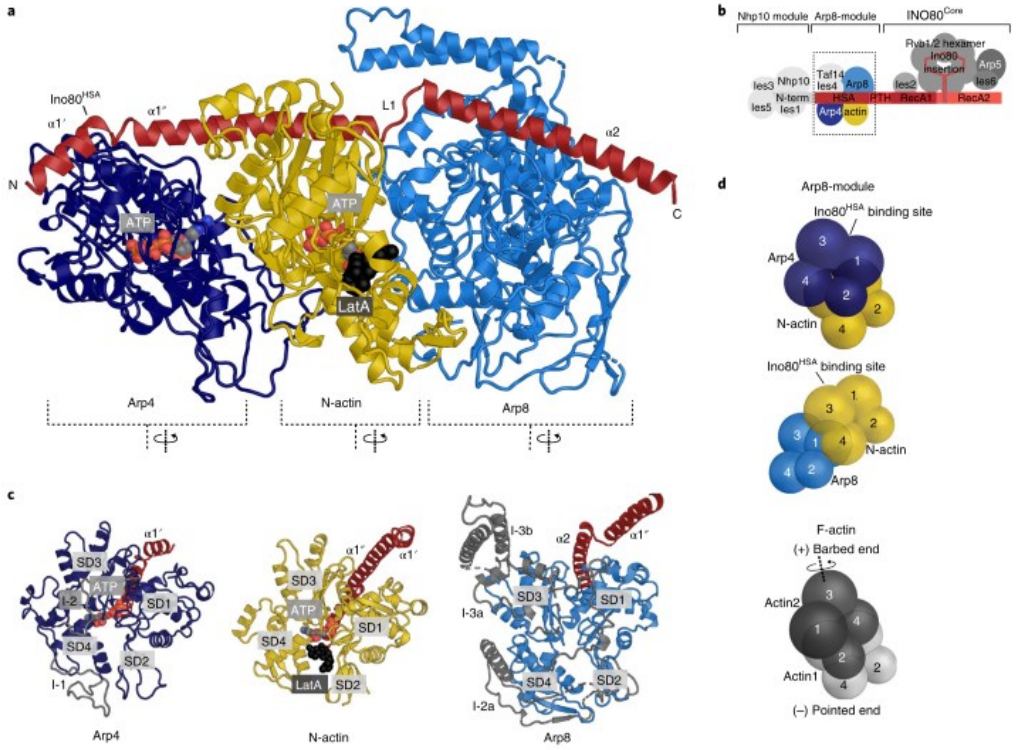

Fig. 1 | Crystal structure of the 180-kDa Ino80^{HSA}-Arp4–N-Actin–Arp8 complex. a, Crystal structure of the INO80 Arp8 module comprising Arp4, N-actin, Arp8, and Ino80^{HSA}. Arp4 and N-actin are ATP-bound (colored spheres), whereas Arp8 is nucleotide-free. LatA (black spheres) is bound next to ATP in the N-actin nucleotide binding cleft. **b**, Schematic overview of the *S. cerevisiae* INO80 complex illustrating its modular architecture. N-term, N-terminal region of the Ino80 polypeptide; HSA, HSA domain of Ino80; PTH, post-HSA domain of Ino80. **c**, Front views of the actin-fold proteins Arp4, N-actin, and Arp8. The Ino80^{HSA} binds to the barbed end of each of the actin folds. Actin fold insertions of Arp4 and Arp8 are shown in gray. **d**, Arrangement of actin-fold proteins. Schematics of actin folds with the individual subdomains shown as spheres. Interaction of Arp4 with N-actin, and N-actin with Arp8 in the Arp8 module is compared with two laterally interacting actin molecules in F-actin.

Indeed, our cryoEM analysis of a fungal INO80 complex, which included all evolutionarily conserved subunits, located the Arp8 module near extranucleosomal entry DNA, but its analysis was, unlike the NCP-INO80^{Core} region of the complex, limited by lower resolution. Until now, high-resolution structural information on the functionally critical architecture of the Arp8 module is missing.

Here, we report the crystal structure of the INO80 Arp8 module and identify it as an allosteric sensor of linker DNA. Strikingly, the Ino80^{HSA} adopts a segmented conformation comprising three helices that bind to the barbed ends of Arp4, N-actin, and Arp8. The Arp8 module binds extranucleosomal DNA, and we identified a conserved positively charged patch on the solvent-accessible site of the Ino80^{HSA} as responsible for DNA binding. Structure-based mutagenesis showed that binding of extranucleosomal, linker DNA by Ino80^{HSA} is critical for INO80 nucleosome sliding, but not for INO80 nucleosome binding and ATP hydrolysis. Thus, linker DNA sensing by the Arp8 module drives remodeling by INO80 via coupling motor activity to nucleosome repositioning.

Results

Crystal structure of the 180-kDa Ino80^{HSA}–Arp4–N-actin–Arp8 complex. To gain molecular and functional insights into the evolutionarily conserved Arp8 module of INO80, we determined its crystal structure (Fig. 1). N-actin, Arp4, Arp8 (residues 255–881, excluding the non-conserved N-terminal region[27]), and Ino80^{HSA} (residues 461–598) from *S. cerevisiae* were produced in insect cells as a stoichiometric 180-kDa complex (Supplementary Fig. 1a). Initial crystallization attempts failed, most probably due to structural flexibility. In a recent study, N-actin adopted a nucleotide-free state[9] bound to Arp4 and Swr1^{HSA}, whereas early biochemical analysis of N-actin in the human BAF complex[28], as well as our own structural analysis using a cameloid nanobody (see below), indicated ATP binding of N-actin. Consequently, we sought to limit the structural heterogeneity of the Arp8 module by using latrunculin A (LatA), a small molecule, sea sponge toxin that inhibits nucleotide exchange of monomeric actin[29]. Addition of LatA yielded crystals of the complex diffracting to 4 Å, and the structure was determined by molecular replacement (see Table 1 for refinement and model statistics).

Table 1 | Data collection and refinement statistics

	NactNB–Arp4–N-actin(ATP) (PDB 5NBM)	NactNB–Arp4–N-actin(apo) (PDB 5NBL)	Ino80^{HSA}–Arp4–N-Actin–Arp8 (PDB 5NBN)
Data collection			
Space group	P 6_5	P 6_5	C 222_1
Cell dimensions			
a, *b*, *c* (Å)	190.58, 190.58, 220.62	191.22, 191.22, 221.97	172.29, 263.91, 241.40
α, β, γ (°)	90.00, 90.00, 120.00	90.00, 90.00, 120.00	90.00, 90.00, 90.00
Resolution (Å)	47.73–3.40 (3.50–3.40)[a]	49.43–2.80 (2.90–2.80)	49.40–4.00 (4.10–4.00)
R_{merge}	0.160 (1.081)	0.146 (1.107)	0.236 (1.336)
$I/\sigma(I)$	12.61 (2.19)	12.08 (2.09)	8.71 (1.87)
$CC_{1/2}$	0.996 (0.719)	0.995 (0.617)	0.996 (0.605)
Completeness (%)	100 (100)	100 (100)	100 (100)
Redundancy	6.5 (6.8)	5.9 (5.4)	9.6 (10.0)
Refinement			
Resolution (Å)	47.73–3.40 (3.50–3.40)	49.43–2.80 (2.90–2.80)	49.40–4.00 (4.10–4.00)
No. reflections	62,264 (6,206)	112,476 (11,263)	46,675 (4,625)
R_{work}/R_{free}	0.152 (0.231)/0.193 (0.281)	0.171 (0.276)/0.204 (0.316)	0.193 (0.254)/0.242 (0.288)
No. atoms			
Protein	13,949	14,000	23,029
Ligand/ion	128[b]	64[c]	186[d]
Water	-	119	-
B factors			
Protein	92.30	58.50	121.87
Ligand/ion	85.97	38.80	101.03
Water	-	48.77	-
R.m.s. deviations			
Bond lengths (Å)	0.004	0.004	0.002
Bond angles (°)	0.66	0.70	0.68

Diffraction data from one NactNB–Arp4–N-actin(ATP), one NactNB–Arp4–N-actin(apo) and one Ino80^{HSA}–Arp4–N-Actin–Arp8 crystal were used to solve the structures. [a]Values in parentheses are for highest-resolution shell. [b]Bound ligands are four ATP and four calcium ions. [c]Bound ligands are two ATP and two calcium ions. [d]Bound ligands are two LatA, four ATP, and four calcium ions.

Figure 1 shows the elongated architecture of the Arp8 module. Ino80^{HSA} forms a markedly segmented α-helix with helical elements α1', α1", and α2, spanning a distance of in total 120 Å (Fig. 1a). All three actin-fold proteins bind via their barbed ends to the different HSA helical elements in a similar and serial fashion, while pointed ends remain accessible (Fig. 1c). From Ino80^{HSA}'s N to C terminus, the order of binding is Arp4 (to α1'), N-actin (to α1"), and Arp8 (to α2). The segmentation of the HSA helix enables N-actin to form multiple contacts to both Arp4 and Arp8. Arp4 engages N-actin in a 'front-to-back' orientation in contrast to the classical fibrous (F) actin 'front to front' interaction[30] (Fig. 1d). However, the staggered packing of their subdomains (SDs) as well as local contacts between Arp4 and N-actin resemble lateral interactions of two F-actin subunits in a filament. In contrast, Arp8 packs against the lateral face of N-actin opposite Arp4 by using a fundamentally different 'side-to-front' type of interaction, unlike any other seen so far between actin-fold proteins. Interestingly, we observed unambiguous density for ATP in the nucleotide binding pocket of Arp4 and N-actin, whereas Arp8 remains nucleotide-free (Supplementary Fig. 1b,c). Constitutive ATP binding by Arp4 is consistent with our previous observations suggesting that Arp4 is catalytically inactive[16]. However, N-actin may still retain its activity as part of chromatin remodelers[28] and was captured here in its ATP state by LatA. Of note, ATP must have been copurified with the complex from the cellular environment, as we did not add any nucleotides and LatA was added after purification.

N-actin and Arp4: a conserved heterodimer in distinct chromatin complexes. Arp4–N-actin within the Arp8 module has an overall configuration similar to Arp4–N-actin bound to Swr1^{HSA} and Arp7–Arp9 bound to Snf2^{HSA}[9,10], suggesting that the Arp4–N-actin heterodimer is a structurally conserved module within the INO80 and SWI/SNF families.

To probe the Arp4–N-actin heterodimer in its native environment, we capitalized on a nanobody (denoted NactNB) that we generated from an alpaca immunized with the endogenous *S. cerevisiae* INO80 complex. Nanobodies emerged as a valuable technology to reveal physiologically important states of cellular key components[31,32]. NactNB is highly selective for the endogenous Arp4–N-actin heterodimer. Affinity enrichment mass spectrometry of yeast whole-cell lysate using NactNB showed all 35 subunits of chromatin-associated yeast complexes containing the Arp4–N-actin heterodimer (INO80, SWR1, and NuA4) (Fig. 2a,b), suggesting that NactNB recognizes a solvent-exposed and conserved feature in all of these complexes. To reveal this binding epitope, we determined crystal structures of the Arp4–N-actin–NactNB ternary complex (Fig. 2c, Supplementary Fig. 2a, and Table 1). NactNB binds into a crevice jointly formed by the pointed ends of the two actin-folds opposite the Ino80^{HSA} binding site (Supplementary Fig. 2b). Satisfyingly, NactNB recognizes the same staggered configuration of N-actin and Arp4, as present in the structure of the Arp8 module (Arp4–N-actin heterodimers align with a backbone r.m.s.d. of 0.68 Å; number of aligned residues

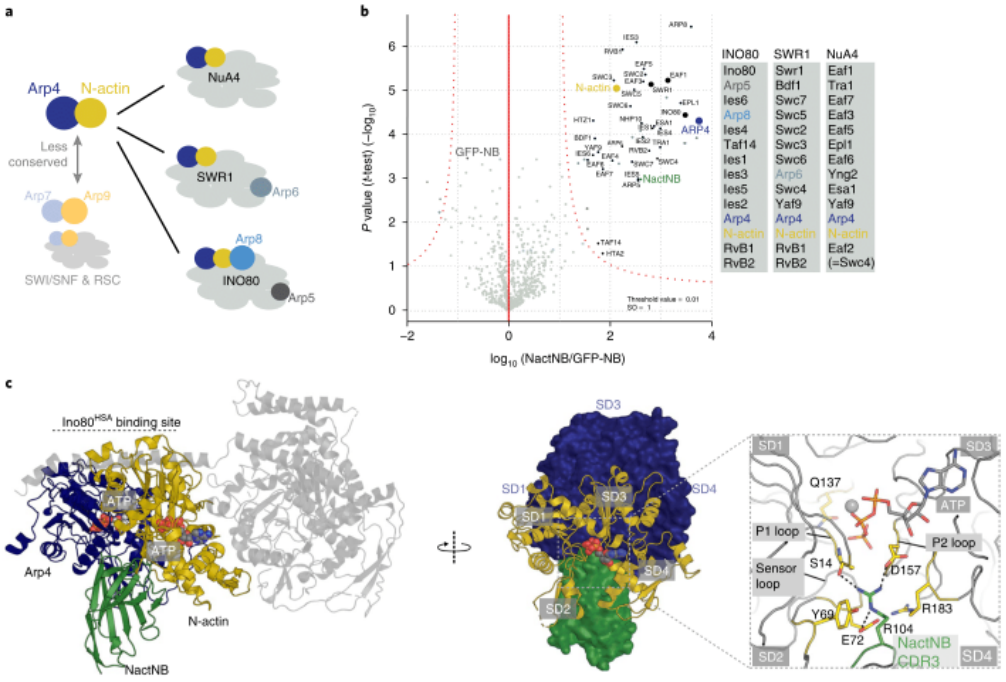

Fig. 2 | The Arp4–N-actin heterodimer is a conserved structural module of chromatin complexes. a, Arp4 and N-actin are conserved core components of all INO80 and SWI/SNF chromatin remodeler families, except for the *S. cerevisiae* SWI/SNF and RSC remodelers, which instead contain the sequence-divergent Arp7 and Arp9 proteins. INO80 and SWR1 contain the additional Arp5, Arp6, and Arp8 subunits. **b**, NactNB captures endogenous Arp4–N-actin heterodimer. Yeast whole-cell extract was subjected to affinity enrichment mass spectrometry experiments using NactNB and a GFP-binding nanobody as a control. Assays were performed in triplicate, and a two-sided and two-sampled *t*-test shows (in a volcano plot representation) significant enrichment of all 34 subunits of INO80, SWR1, and NuA4 complexes (see Methods for details). **c**, Structure of the Arp4–N-actin–NactNB complex in two orientations shown as cartoon and surface representations (left panel: the Arp8 module structure aligned on the Arp4–N-actin dimer is shown in light gray). N-actin and Arp4 are ATP-bound (colored spheres). Boxed 'zoom' image shows that Arg104 of NactNB binds the nucleotide binding cleft of N-actin.

(N_{align}) 753 using Secondary Structure Matching[33] in COOT[34]) and in complex with Swr1^{HSA} (Arp4–N-actin heterodimers align with an r.m.s.d. of 0.96 Å and N_{align} 724). Moreover, residual density in the nucleotide binding pocket in absence of added nucleotide as well as cocrystallization with ATP showed that NactNB recognizes the ATP state of N-actin (Supplementary Fig. 2c–e). NactNB detects the relative orientation of the two N-actin lobes and inserts Arg104 in between SD2 and SD4, where it makes hydrogen bonds to the ATP-bound conformation of Ser14 and Asp157 of the phosphate binding loop P1 and P2, respectively, as well as Glu72 of the ATP sensor loop (Fig. 2c).

Taken together, our data provide direct evidence for a conserved configuration of the Arp4–N-actin heterodimer in the complete endogenous INO80, SWR1, and NuA4 complexes and suggest that N-actin can adopt an ATP-bound state in its native environment, as previously also suggested for the human BAF complex[28]. The conserved nature of the Arp4–N-actin heterodimer may point towards a common, yet so far unknown, functional role of this module in distinct chromatin complexes.

Arp8 recruits Arp4–N-actin to a segmented 'two-plug' scaffold of Ino80^{HSA}. Deletion of Arp8 resulted in partially assembled INO80 lacking also Arp4 and N-actin[15,16]. It rendered yeast cells highly sensitive to metabolic and genotoxic stress[15]. A similar phenotype was observed on partial removal of the Ino80^{HSA} and post-HSA domain (Ino80$^{post\text{-}HSA}$) (residues 531–598)[23]. The structure of the Arp8 module provides a framework for rationalizing the importance of Arp8 and the Ino80^{HSA} for recruitment of the Arp4–N-actin heterodimer to the INO80 complex (Fig. 3a). Arp8 directly engages N-actin through contacts between SD1 and SD2 of Arp8 with SD3 and SD4 of N-actin. In addition, we identify a function for long insertion element I-3a of Arp8. I-3a covers the lateral surface of the Arp8 actin-fold and forms thereby a latch that consolidates the interaction with N-actin. Overall, this bipartite interaction of Arp8 recognizes a 1,392 Å^2 large area of the N-actin lateral face opposite Arp4 and thus specifically helps to recruit and retain the interaction of Arp4–N-actin with Ino80^{HSA}.

Previous models proposed that N-actin and Arps are recruited to chromatin remodelers by a long, continuous HSA helix that provides a binding platform for barbed ends of actin-fold proteins[9,10]. While the general helical structure and serial binding of Arp4 and N-actin barbed ends are consistent with this model, Ino80^{HSA} adopts a distinct segmented structure (Fig. 3b and Supplementary Fig. 3a,b). The N-terminal helix α1 (residues 472–518), bound to the barbed ends of Arp4 and N-actin, has a pronounced kink at position 483–485 that divides it into segments α1' and α1''. The C-terminal

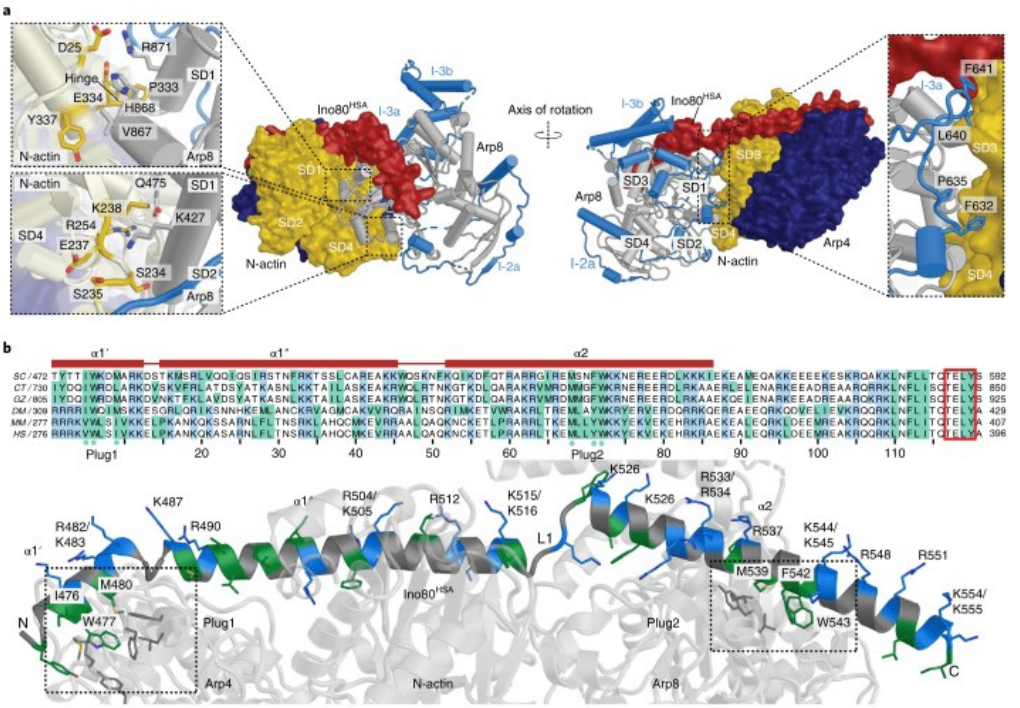

Fig. 3 | Arp8 recruits Arp4–N-actin to a segmented 'two-plug' scaffold of Ino80HSA. a, Cartoon and surface representations of the Arp8 module displaying interaction sites between Arp8 and N-actin. The Arp8 actin core fold is colored in gray and the insertions in blue. Arp8 contacts N-actin SD3 and -4 via its actin core fold, with SD1 and -2 (boxed close-ups in the left panel), and its actin fold insertion 3a (close-up in the right panel). **b**, Sequence alignment of Ino80^{HSA} from different species, with positively charged residues (Arg and Lys) colored in blue and hydrophobic residues (Ile, Leu, Trp, Val, Phe, Tyr, and Met) in green. The region visualized in the crystal structure is indicated by red lines above the sequences. The highly conserved TELY motif is highlighted by a red rectangle. Green dots below the sequences emphasize conserved hydrophobic residues in Plug1 and Plug2 that bind Arp4 and Arp8, respectively. Below, cartoon representation of the Arp8 module. The Ino80^{HSA} domain is shown, with hydrophobic residues colored in green and positively charged residues colored in blue.

helix α2 (residues 522–557) forms the third segment, bound to the barbed end of Arp8. We identified two hydrophobic residue clusters (Plug 1 and Plug 2) that define the register and contain each an anchoring tryptophan residue. A structural shift resulting from segmentation of α1 enables Plug 1 (Ile476, Trp477, and Met480) to insert into a hydrophobic pocket of the barbed end of Arp4 (Fig. 3b and Supplementary Fig. 3c), while well-defined loop L1 in between α1" and α2 shifts α2, enabling insertion of Plug 2 (Met539, Phe542, and Trp543) into a hydrophobic pocket of the barbed end of Arp8. The latter interaction appears to be critical not only for recruitment of Arp8 but also of the Arp4–N-actin dimer. The previously reported partial removal of the Ino80^{HSA} and Ino80$^{post\text{-}HSA}$ includes Plug2 of α2 and leads to loss of the entire Arp8 module in vivo[23], although the Arp4–N-actin binding site of the Ino80^{HSA} is still intact. The distance between the two hydrophobic plugs in conjunction with the asymmetry of Ino80^{HSA} segmentation matches the unique arrangement of actin-folds within the sandwich-like structure of Arp4, N-actin, and Arp8. In addition, loop L1 and the resulting translational and rotational shift of α2 enable formation of the extensive contacts between N-actin and Arp8 that would not be possible for a continuous HSA helix. Thus, our structure shows how Arp8 specifies recruitment of the Arp4–N-actin heterodimer to the segmented, 'two-plug' scaffold of the helical Ino80^{HSA}.

Ino80^{HSA} of the Arp8 module binds extranucleosomal DNA. Our recent cryoEM study of the INO80^{Core}–nucleosome complex revealed density of the Arp8 module adjacent to the well resolved nucleosomal DNA entry site, where the Ino80 Snf2-motor domain pumps DNA into the nucleosome[24] (Fig. 4a). To test for binding of the Arp8 module to nucleosomal and extranucleosomal DNA, we performed electro mobility shift assays (EMSAs) where nucleosomes with (0N80) and without (0N0) 80 bp extranucleosomal DNA on one side compete for binding the Arp8 module (Fig. 4b). In such competition assays, the Arp8 module showed a clear binding preference for the 0N80 over the 0N0 nucleosome, showing that the Arp8 module binds extranucleosomal DNA.

Combination of the INO80^{Core}–nucleosome complex cryoEM structure[24] and the Arp8 module crystal structure leads directly to a structural model of how the Arp8 module might be located at extranucleosomal DNA, as discussed further below. In this

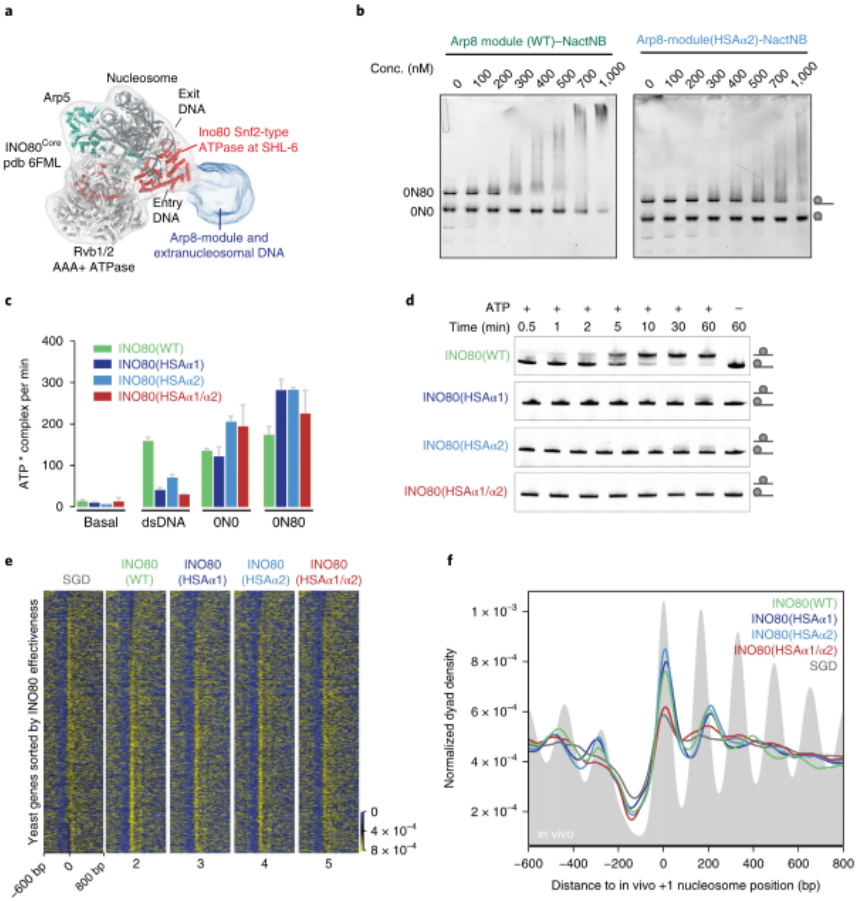

Fig. 4 | Extranucleosomal DNA binding by the Arp8 module is critical for INO80 nucleosome sliding and genome-wide nucleosome positioning. **a**, CryoEM density of the INO80–nucleosome complex[24], with a structural model for Ino80^{Motor}, Ies2, Arp5, Ies6, and the Rvb1–Rvb2 heterohexamer bound to an NCP. Density next to the nucleosomal DNA entry site could be assigned to the Arp8 module (colored in blue). **b**, Competition EMSAs with two nucleosome species (20 nM each; one with (0N80) and one without (0N0) an 80-bp extranucleosomal DNA overhang), showing a clear binding preference of the Arp8 module for 0N80 nucleosomes. Mutation of solvent-exposed basic residues on helix α2 of Ino80^{HSA} (HSAα2) decreases 0N80 binding by the Arp8 module. Assays were performed in triplicate. Conc., molar concentration in nM; WT, wild type. **c**, INO80 (27 nM) ATPase activity, basal or stimulated with 223-bp dsDNA (100 nM), 0N0 (100 nM), and 0N80 (50 nM) nucleosomes. Error bars represent the mean±s.d. from three independent experiments. **d**, Time course of ATP-dependent INO80 nucleosome (0N80) sliding on a single mononucleosome substrate (with 18 nM IN80 and 90 nM 0N80). Reaction educt (end-positioned nucleosome) and product (center-positioned nucleosome) were resolved by NativePAGE. Assays were performed in triplicate. **e**, Genome-wide nucleosome positioning by INO80 (18 nM). Heat map displaying color-coded nucleosome dyad density of YCp50 plasmid library yeast genes aligned on the in vivo-defined +1 nucleosome dyad (0 bp) position, after sequence-intrinsic nucleosome positioning by salt gradient dialysis (SGD), or after additional incubation with indicated wild-type or mutant INO80 complexes. Rows are sorted according to INO80 effectiveness. **f**, Composite plots of heat maps shown in **e**. Grey background displays in vivo nucleosome positioning. Genome-wide nucleosome positioning assays were performed in duplicate. Uncropped gel images are shown in Supplementary Data Set 1.

model, Ino80^{HSA} mediates direct binding of extranucleosomal DNA along the barbed ends of Arp8, N-actin, and Arp4. In isolation, neither actin and Arp4 nor human Arp8 bind double-stranded DNA (dsDNA) with considerable affinity[26], while the Ino80^{HSA} was proposed from sequence analysis to be part of a dsDNA binding domain of Ino80[35]. Having the crystal structure for Ino80^{HSA}, we noticed a set of highly conserved, solvent-accessible lysine and arginine residues that may account for binding of extranucleosomal DNA (Fig. 3b and Supplementary Fig. 4a). To test this hypothesis, we mutated several of these lysine and arginine residues

in the Ino80^{HSA} α2 helix to glutamines (HSAα2). We observed lower expression yields of the mutated minimal Arp8 module, indicating perhaps destabilizing effects of the mutations by lowering the helix propensity of Ino80^{HSA}. However, using complex-stabilizing NactNB for purification provided sufficient quantities of stable material for DNA binding studies (Supplementary Fig. 4b). Fluorescence anisotropy analysis on binding of generic 40 bp dsDNA and competition EMSAs with 0N0 and 0N80 nucleosomes showed that binding of NactNB at the pointed end of N-actin only slightly reduced dsDNA binding (around twofold; Supplementary Fig. 4c,d). So, we used NactNB to rule out that any loss of DNA binding is induced by weakening of the complex. Importantly, the α2 mutations substantially reduced binding of the Arp8 module both to dsDNA (Supplementary Fig. 4c) and nucleosomes (Fig. 4b and Supplementary Fig. 4d). Thus, we conclude that the positively charged HSA domain of Ino80 provides a binding site for extra-nucleosomal DNA.

Arp8 module is important for nucleosome sliding and genome-wide nucleosome positioning. To assess the mechanistic impact of DNA binding by the Arp8 module on nucleosome remodeling by INO80 (Fig. 4), we mutated Ino80^{HSA} in the context of the entire INO80 complex (Supplementary Fig. 4e). Parallel to this study, we established an insect cell co-expression approach for expression and purification of the entire *S. cerevisiae* 15-subunit INO80 complex. Such recombinant INO80 retains the activity of the endogenous complex, but is fully amendable to site-directed mutagenesis (to be published elsewhere by: Krietenstein Nils, Oberbeckmann Elisa, Niebauer Vanessa, Schall Kevin, Schwarz Marianne, Moldt Manuela, Tobias Straub, Korber Philipp, Hopfner Karl-Peter, and Eustermann Sebastian). Using this system, we were able to purify stable INO80 complexes with wild-type-like stoichiometry of all subunits, and also if full-length Ino80 with mutated HSA was co-expressed together with all other 14 subunits of INO80 (Supplementary Fig. 4f). EMSAs with 0N80 nucleosomes showed homogenous complex formation at similar concentrations for wild-type as well as for mutant INO80 (Supplementary Fig. 4g). This was in contrast to the decreased binding affinity of Ino80–HSAα2 in context of the isolated Arp8 module and suggests that binding of the entire complex to nucleosomes is mostly dominated by subunits other than the minimal Arp8 module; for example, subunits of the INO80 core that interact directly with the nucleosome, or other DNA binding subunits such as the Nhp10 module. Of note, Arp8 in the recombinant 15-subunit INO80 complex contains the full N-terminal tail in contrast to the construct used for crystallization. Although the N-terminal region of Arp8 is not well conserved among species, it might additionally contribute to nucleosome interactions, DNA binding, or complex stability.

However, despite retaining high-affinity nucleosome interactions, mutations of the Ino80^{HSA} domain markedly affected dsDNA-stimulated ATPase and ATP-dependent nucleosome sliding activity of INO80. ATP hydrolysis by wild-type INO80 is robustly stimulated on addition of dsDNA or 0N80 nucleosomes (Fig. 4c). Mutations of the helix α1 or α2 of Ino80^{HSA} impaired ATPase stimulation by dsDNA, while the same mutants showed similar or even moderately faster ATP hydrolysis rates than wild-type complex if stimulated by 0N80 nucleosomes. Despite this similar or increased ATP turnover, HSA mutations substantially decreased INO80's activity to slide 0N80 nucleosomes towards the center of a 225-bp DNA substrate (Fig. 4d). Mutations of either helix α1 or α2 reduced nucleosome centering to residual levels, while mutations targeting both helices abrogated this remodeling activity completely.

Given this mechanistic impact on sliding activity in a specialized mononucleosome context, we asked whether Ino80^{HSA} is also more generally important to mobilize and position nucleosomes across the whole yeast genome. To this end, we employed a genome-wide

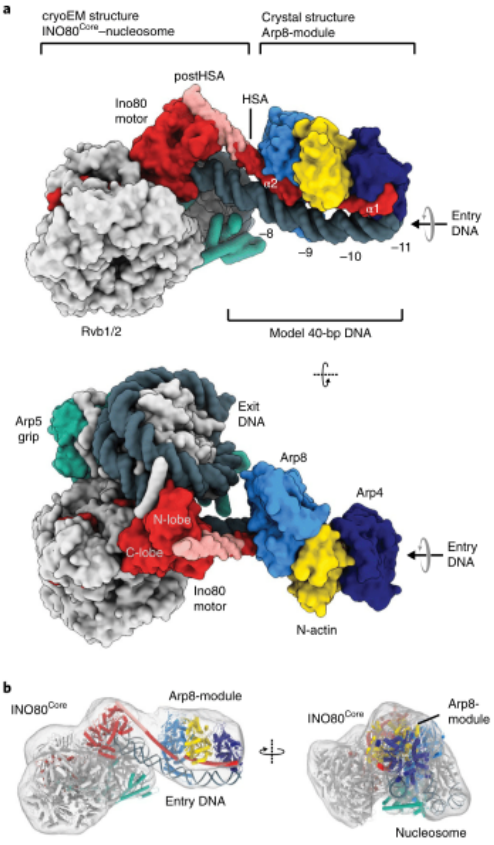

Fig. 5 | Structural model of the INO80$^{Core+Arp}$–nucleosome complex. **a**, Model of the INO80$^{Core+Arp}$–nucleosome complex (shown as surface representation) based on the INO80^{Core}–nucleosome cryoEM structure[24] and the Arp8 module crystal structure (this study). **b**, Previously published cryoEM density map of the INO80$^{Core+Arp}$–nucleosome complex[24] with the model of the INO80$^{Core+Arp}$–nucleosome complex fitted into the density.

reconstitution approach, where it was shown previously that purified INO80 on its own is able to properly position +1 nucleosomes on a genomic plasmid library[2]. A similarly direct analysis of INO80's nucleosome positioning activity would be inherently difficult in vivo, given the complex interplay between different remodeler families as well as other factors such as the transcription and replication machinery[2,36]. Micrococcal nuclease digestion and next generation DNA sequencing (MNase-seq) was used as read out for nucleosome positions across the genomic plasmid library before and after incubation with INO80 and ATP. In contrast to the strongly decreased sliding activity with a mononucleosomal substrate based on the 'Widom 601' sequence (Fig. 4d), INO80 mutations targeting HSA helix α1 or α2 individually did not compromise average patterns of genomic +1 nucleosome positioning (Fig. 4e,f). This finding is intriguing as it suggests that nucleosomes on genomic DNA in plasmids may be a less demanding substrate for translocation and positioning than a 'Widom 601' mononucleosome. This could be,

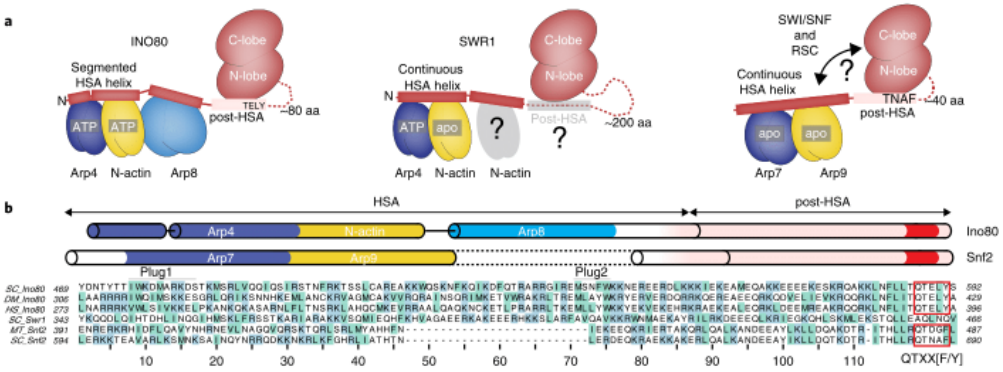

Fig. 6 | Conserved architecture of N-actin-Arp modules in INO80/SWR1 and SWI/SNF family chromatin remodelers. a, Organization of the N-actin-Arp modules in INO80, SWR1, and RSC remodelers with respect to the Snf2-type ATPase. The schematic representation is based on our Ino80$^{Core+Arp}$–nucleosome model (shown in Fig. 5a), the structure-based sequence alignment shown in **b**, and the crystal structures of Arp4–N-actin–Swr1^{HSA} (PDB 5I9E), Arp7–Arp9–Snf2^{HSA} (PDB 4I6M), Arp4–N-actin–Arp8–Ino80^{HSA}, and Snf2 in complex with a nucleosome (PDB 5HZR). Conformation of the respective HSA domains (red) is illustrated by a continuous or segmented helix. The post-HSA of Ino80 and Snf2 (pink) interacts directly with N-lobe of the Snf2-type ATPase (red) and is connected via a linker region (dotted line). The nucleotide state of the actin-fold proteins is indicated according to the respective crystal structure. Interestingly, recent biochemical analysis suggested that the Swr1^{HSA} is bound by Arp4 and two N-actin molecules[49]. Our structure-based alignment shown in **b** reveals that the Arp8 binding site of Ino80^{HSA} corresponds to the second N-actin site in Swr1^{HSA}. aa, amino acids. **b**, Structure-based sequence alignment of the HSA and post-HSA domains of Ino80, Snf2, and Swr1 (basic and hydrophobic residues are highlighted in blue and light green, respectively). Binding sites for Arps and N-actin are conserved between the INO80 and SWI/SNF remodeler families. Our structure-based alignment reveals that the Ino80$^{post-HSA}$ (Q)TELY motif is related to the Snf2$^{post-HSA}$ QTXX[F/Y] motif.

for example, due to the presence of multiple nucleosomes, extranucleosomal DNA on both sides, the absence of DNA ends, or due to lower intrinsic nucleosome stabilities. The former three possibilities seemed unlikely as remodeling an internal nucleosome within an array of 601 sequences separated by 50 bp extranucleosomal DNA[37] was also strongly impaired by mutations targeting either HSA helix individually (Supplementary Fig. 4h,i). Importantly, however, mutation of both HSA helices α1 and α2 at the same time abolished INO80 nucleosome remodeling on all tested substrates including genome-wide nucleosome positioning (Fig. 4d–f and Supplementary Fig. 4i).

Taken together, our biochemical results identify a critical role for binding extranucleosomal DNA by the Arp8 module in coupling the energy derived from ATP hydrolysis to productive nucleosome sliding by INO80. Such chemo-mechanical coupling may be particularly important to mobilize nucleosomes in the context of sequences that strongly bind the histone octamer, such as the 601 sequence. Positioning of +1 nucleosomes guided by promoter sequences is likely to involve also other parts of the INO80 complex, such as the Nhp10 module.

A structural model of the INO80–nucleosome complex including its Arp8 module. Combination of the 4.3-Å cryoEM structure of the *C. thermophilum* INO80^{Core}–nucleosome complex[24] with the 4-Å *S. cerevisiae* crystal structure of the 180-kDa Arp8 module leads directly to a composite model of the evolutionarily conserved INO80$^{Core+Arp}$ complex bound to a nucleosome with a molecular weight of approximately 1 MDa (Fig. 5a). The two structures can be joined in silico by the highly conserved post-HSA and HSA domains of Ino80: helix α2 of the HSA domain crystal structure needs to be extended by only 35 C-terminal residues to include the post-HSA helix that is present in the cryoEM structure[24]. This structural model is consistent with the mapping of INO80 subunits onto nucleosomal substrates in vivo[38], in vitro[39], and with our previous cryoEM data[24] as it places the Arp8 module into the large unassigned density patch (Figs. 4a and 5b) and at the same time maintains a continuous HSA and post-HSA helical structure. In particular, we observed cryoEM density for an extended post-HSA–HSA helix pointing from the N-terminal lobe of the Snf2-type ATPase domain at SHL-6 towards entry DNA at SHL-8[24]. Moreover, the elongated architecture of the Arp8 module accommodates approximately 40 bp extranucleosomal entry DNA and fits thereby into the low-resolution reconstruction obtained for the entire 11-subunit INO80$^{Core+Arp}$–nucleosome complex[24]. The 120-Å HSA domain is positioned along the dsDNA with conserved arginine and lysine residues contacting the phosphate backbone as probed by our biochemical experiments described above. Helix α2 contacts the DNA around SHL-8 while the N-terminal helix α1 reaches SHL-10 to -11. Consequently, Arp8 resides on the extranucleosomal DNA proximal to the Snf2-type ATPase of Ino80, while the Arp4–N-actin heterodimer binds in a distal position. The model is therefore consistent with promoter binding of Arp8 proximal to the +1 nucleosome in vivo[38], as well as cross-linking of Arp4–N-actin heterodimer to extranucleosomal DNA at position −110 nt (SHL-11) in vitro[39]. However, given the flexibility of the Arp8 module in the cryoEM reconstructions, we do not rule out the presence of other conformations and positions of this module during the functional cycle of INO80 in nucleosome remodeling.

Discussion

Here, we provide a structure and function for the enigmatic, evolutionarily conserved actin-fold subunits Arp4, N-actin, and Arp8 in the INO80 chromatin remodeler. We show that the three actin-fold proteins in complex with the Ino80^{HSA} form an extended structural element that recognizes extranucleosomal, linker DNA, a critical feature of INO80 mechanism and function.

INO80 is a highly processive chromatin remodeler[22,40] and we recently proposed a mechanism by which INO80 core subunits

function as a macromolecular ratchet[24]: minor groove tracking by the Ino80 Snf2-type ATPase motor at SHL-6 pumps DNA in multiple 1–2 bp steps against a grip formed by Arp5–Ies6 at SHL-2/-3 until DNA propagates around the histone octamer and translocates nucleosomes by a large step size. Indeed, 10–20 bp translocation steps are observed[22,41], and a kinetic model has been proposed describing the dependency of INO80 on extranucleosomal DNA[22]: the activity of the ATPase motor does not result in efficient DNA translocation unless more than 40 bp of entry DNA are available; the pumped DNA might otherwise collapse backwards[22]. Intriguingly, the footprint of the Arp8 module matches this limiting length of 40 bp DNA (Fig. 5a). If less than 40 bp extranucleosomal, linker DNA are available, pumping an additional 10–20 bp DNA into the nucleosome would substantially shorten the entry DNA beyond this limit; that is, pull away the DNA and thereby abrogate the contacts between DNA and the distal part of the HSA domain, where the Arp4–N-actin heterodimer binds. Consequently, this scenario recapitulates the impact of HSA mutations that also lead to loss of extranucleosomal DNA binding and reduce nucleosome sliding to residual levels, most probably caused by 'back-slippage' of DNA. By combining our structural and biochemical data with previous kinetic insights[22], we thus propose that the Arp8 module within INO80 functions as sensor of extranucleosomal DNA, mechanistically coupling ATP-dependent DNA pumping to processive nucleosome translocation.

Biochemical and genetic evidence for the SWI/SNF chromatin remodeler family suggests that the yeast Arp7–Arp9 module of RSC has a role similar to that proposed here for the Arp8 module of INO80, as it also couples ATP-dependent DNA translocation of the Snf2-type Sth1 motor domain to nucleosome remodeling such as translocation and ejection[42]. It was proposed that the post-HSA domain of Sth1 acts as a 'throttle' controlling ATPase activity[43]. Indeed, our structural study shows that the post-HSA domain interacts with the N-lobe of Ino80[24] in a homologous manner as previously observed for Snf2[43] and Sth1[44]. A structure-based alignment reveals that the highly conserved (Q)TELY motif[6] of the Ino80$^{post\text{-}HSA}$ domain is related to the QTXX[F/Y] motif of Snf2 (Fig. 6a,b), while the interaction with protrusion-I provides, together with brace helix-I, a key allosteric site for controlling DNA groove tracking by the ATPase motor[12,43]. Despite recent progress[10,42,44,45], it is still elusive how the Arp7–Arp9 module of RSC functions at a molecular level. It was suggested that the module folds back onto the Sth1 motor domain acting as 'clutch' to promote nucleosome remodeling. While INO80 might adopt a closed conformation in absence of a nucleosome[46,47], our structural and biochemical data suggest an extended conformation of the Arp8 module which enables extranucleosomal DNA binding. The interplay between the HSA and post-HSA domains may thus link sensing of extranucleosomal DNA to allosteric control of the Snf2-like motor domain of Ino80.

Sensing of linker DNA is a hallmark of chromatin remodelers since it provides mechano-chemical means to conduct higher order remodeling reactions such as spacing and phasing of nucleosomes in genic arrays[6,48]. Future studies will use the mechanistic insights discovered here as a framework to dissect such functions and will show whether they may provide unifying principles for regulation of the INO80 and SWI/SNF families of multi-subunit chromatin remodelers.

Methods

Methods, including statements of data availability and any associated accession codes and references, are available at https://doi.org/10.1038/s41594-018-0115-8.

Received: 24 April 2018; Accepted: 17 July 2018;
Published online: 03 September 2018

References

1. Jiang, C. & Pugh, B. F. Nucleosome positioning and gene regulation: advances through genomics. *Nat. Rev. Genet.* **10**, 161–172 (2009).
2. Krietenstein, N. et al. Genomic nucleosome organization reconstituted with pure proteins. *Cell* **167**, 709–721.e12 (2016).
3. Hopfner, K. P., Gerhold, C. B., Lakomek, K. & Wollmann, P. Swi2/Snf2 remodelers: hybrid views on hybrid molecular machines. *Curr. Opin. Struct. Biol.* **22**, 225–233 (2012).
4. Clapier, C. R., Iwasa, J., Cairns, B. R. & Peterson, C. L. Mechanisms of action and regulation of ATP-dependent chromatin-remodelling complexes. *Nat. Rev. Mol. Cell Biol.* **18**, 407–422 (2017).
5. Dion, V., Shimada, K. & Gasser, S. M. Actin-related proteins in the nucleus: life beyond chromatin remodelers. *Curr. Opin. Cell Biol.* **22**, 383–391 (2010).
6. Shen, X., Mizuguchi, G., Hamiche, A. & Wu, C. A chromatin remodelling complex involved in transcription and DNA processing. *Nature* **406**, 541–544 (2000).
7. Peterson, C. L., Zhao, Y. & Chait, B. T. Subunits of the yeast SWI/SNF complex are members of the actin-related protein (ARP) family. *J. Biol. Chem.* **273**, 23641–23644 (1998).
8. Cairns, B. R., Erdjument-Bromage, H., Tempst, P., Winston, F. & Kornberg, R. D. Two actin-related proteins are shared functional components of the chromatin-remodeling complexes RSC and SWI/SNF. *Mol. Cell* **2**, 639–651 (1998).
9. Cao, T. et al. Crystal structure of a nuclear actin ternary complex. *Proc. Natl Acad. Sci. USA* **113**, 8985–8990 (2016).
10. Schubert, H. L. et al. Structure of an actin-related subcomplex of the SWI/SNF chromatin remodeler. *Proc. Natl Acad. Sci. USA* **110**, 3345–3350 (2013).
11. Szerlong, H. et al. The HSA domain binds nuclear actin-related proteins to regulate chromatin-remodeling ATPases. *Nat. Struct. Mol. Biol.* **15**, 469–476 (2008).
12. Meagher, R. B., Kandasamy, M. K., Smith, A. P. & McKinney, E. C. Nuclear actin-related proteins at the core of epigenetic control. *Plant Signal. Behav.* **5**, 518–522 (2010).
13. Son, E. Y. & Crabtree, G. R. The role of BAF (mSWI/SNF) complexes in mammalian neural development. *Am. J. Med. Genet. C* **166C**, 333–349 (2014).
14. Hodges, C., Kirkland, J.G. & Crabtree, G.R. The many roles of BAF (mSWI/SNF) and PBAF complexes in cancer. *Cold Spring Harb. Perspect. Med.* **6**, (2016).
15. Shen, X., Ranallo, R., Choi, E. & Wu, C. Involvement of actin-related proteins in ATP-dependent chromatin remodeling. *Mol. Cell* **12**, 147–155 (2003).
16. Tosi, A. et al. Structure and subunit topology of the INO80 chromatin remodeler and its nucleosome complex. *Cell* **154**, 1207–1219 (2013).
17. Gerhold, C. B. & Gasser, S. M. INO80 and SWR complexes: relating structure to function in chromatin remodeling. *Trends Cell Biol.* **24**, 619–631 (2014).
18. Papamichos-Chronakis, M., Watanabe, S., Rando, O. J. & Peterson, C. L. Global regulation of H2A.Z localization by the INO80 chromatin-remodeling enzyme is essential for genome integrity. *Cell* **144**, 200–213 (2011).
19. Udugama, M., Sabri, A. & Bartholomew, B. The INO80 ATP-dependent chromatin remodeling complex is a nucleosome spacing factor. *Mol. Cell. Biol.* **31**, 662–673 (2011).
20. Chen, L. et al. Subunit organization of the human INO80 chromatin remodeling complex: an evolutionarily conserved core complex catalyzes ATP-dependent nucleosome remodeling. *J. Biol. Chem.* **286**, 11283–11289 (2011).
21. Jonsson, Z. O., Jha, S., Wohlschlegel, J. A. & Dutta, A. Rvb1p/Rvb2p recruit Arp5p and assemble a functional Ino80 chromatin remodeling complex. *Mol. Cell* **16**, 465–477 (2004).
22. Zhou, C. Y. et al. The yeast INO80 complex operates as a tunable DNA length-sensitive switch to regulate nucleosome sliding. *Mol. Cell* **69**, 677–688.e9 (2018).
23. Kapoor, P., Chen, M., Winkler, D. D., Luger, K. & Shen, X. Evidence for monomeric actin function in INO80 chromatin remodeling. *Nat. Struct. Mol. Biol.* **20**, 426–432 (2013).
24. Eustermann, S. et al. Structural basis for ATP-dependent chromatin remodelling by the INO80 complex. *Nature* **556**, 386–390 (2018).
25. Ayala, R. et al. Structure and regulation of the human INO80–nucleosome complex. *Nature* **556**, 391–395 (2018).
26. Gerhold, C. B. et al. Structure of Actin-related protein 8 and its contribution to nucleosome binding. *Nucleic Acids Res.* **40**, 11036–11046 (2012).
27. Saravanan, M. et al. Interactions between the nucleosome histone core and Arp8 in the INO80 chromatin remodeling complex. *Proc. Natl Acad. Sci. USA* **109**, 20883–20888 (2012).
28. Zhao, K. et al. Rapid and phosphoinositol-dependent binding of the SWI/SNF-like BAF complex to chromatin after T lymphocyte receptor signaling. *Cell* **95**, 625–636 (1998).
29. Dominguez, R. & Holmes, K. C. Actin structure and function. *Annu. Rev. Biophys.* **40**, 169–186 (2011).

30. von der Ecken, J. et al. Structure of the F-actin-tropomyosin complex. *Nature* **519**, 114–117 (2015).
31. Huang, W. et al. Structural insights into micro-opioid receptor activation. *Nature* **524**, 315–321 (2015).
32. Rasmussen, S. G. et al. Crystal structure of the beta2 adrenergic receptor-Gs protein complex. *Nature* **477**, 549–555 (2011).
33. Krissinel, E. & Henrick, K. Secondary-structure matching (SSM), a new tool for fast protein structure alignment in three dimensions. *Acta Crystallogr. D Biol. Crystallogr.* **60**, 2256–2268 (2004).
34. Emsley, P., Lohkamp, B., Scott, W. G. & Cowtan, K. Features and development of Coot. *Acta Crystallogr. D Biol. Crystallogr.* **66**, 486–501 (2010).
35. Bakshi, R., Prakash, T., Dash, D. & Brahmachari, V. In silico characterization of the INO80 subfamily of SWI2/SNF2 chromatin remodeling proteins. *Biochem. Biophys. Res. Commun.* **320**, 197–204 (2004).
36. Yen, K., Vinayachandran, V., Batta, K., Koerber, R. T. & Pugh, B. F. Genome-wide nucleosome specificity and directionality of chromatin remodelers. *Cell* **149**, 1461–1473 (2012).
37. Mueller-Planitz, F., Klinker, H., Ludwigsen, J. & Becker, P. B. The ATPase domain of ISWI is an autonomous nucleosome remodeling machine. *Nat. Struct. Mol. Biol.* **20**, 82–89 (2013).
38. Yen, K., Vinayachandran, V. & Pugh, B. F. SWR-C and INO80 chromatin remodelers recognize nucleosome-free regions near +1 nucleosomes. *Cell* **154**, 1246–1256 (2013).
39. Brahma, S., Ngubo, M., Paul, S., Udugama, M. & Bartholomew, B. The Arp8 and Arp4 module acts as a DNA sensor controlling INO80 chromatin remodeling. *Nat. Commun.* https://doi.org/10.1038/s41467-018-05710-7 (2018).
40. Schwarz, M. et al. Single-molecule nucleosome remodeling by INO80 and effects of histone tails. *FEBS Lett.* **592**, 318–331 (2018).
41. Brahma, S. et al. INO80 exchanges H2A.Z for H2A by translocating on DNA proximal to histone dimers. *Nat. Commun.* **8**, 15616 (2017).
42. Clapier, C. R. et al. Regulation of DNA translocation efficiency within the chromatin remodeler RSC/Sth1 potentiates nucleosome sliding and ejection. *Mol. Cell* **62**, 453–461 (2016).
43. Liu, X., Li, M., Xia, X., Li, X. & Chen, Z. Mechanism of chromatin remodelling revealed by the Snf2-nucleosome structure. *Nature* **544**, 440 (2017).
44. Turegun, B., Baker, R. W., Leschziner, A. E. & Dominguez, R. Actin-related proteins regulate the RSC chromatin remodeler by weakening intramolecular interactions of the Sth1 ATPase. *Commun. Biol.* **1**, 1 (2018).
45. Turegun, B., Kast, D.J. & Dominguez, R. Subunit Rtt102 controls the conformation of the Arp7/9 heterodimer and its interactions with nucleotide and the catalytic subunit of SWI/SNF remodelers. *J. Biol. Chem.* (2013).
46. Aramayo, R. J. et al. Cryo-EM structures of the human INO80 chromatin-remodeling complex. *Nat. Struct. Mol. Biol.* **25**, 37–44 (2018).
47. Watanabe, S. et al. Structural analyses of the chromatin remodelling enzymes INO80-C and SWR-C. *Nat. Commun.* **6**, 7108 (2015).
48. Yamada, K. et al. Structure and mechanism of the chromatin remodelling factor ISW1a. *Nature* **472**, 448–453 (2011).
49. Lin, C.-L. et al. Functional characterization and architecture of recombinant yeast SWR1 histone exchange complex. *Nucleic Acids Res.* **45**, 7249–7260 (2017).

Acknowledgements

We are grateful to M. Moldt for technical support and J. Michaelis, Gregor Witte, Katja Lames, and Robert Byrne for discussion and technical help. We thank the Max-Planck Crystallization Facility (Martinsried, Germany), the staff of the Swiss Light Source (Villingen, Switzerland), and the European-Molecular-Biology-Laboratory/Deutsches-Elektronen-Synchotron (Hamburg, Germany) for support and measurement time. We thank S. Krebs and H. Blum at the Laboratory of Functional Genome Analysis (Gene Center, LMU Munich) for high-throughput sequencing. We thank T. Straub (Bioinformatics Core Unit, Biomedical Center, LMU Munich) for advice on bioinformatics. This work is supported by the Deutsche Forschungsgemeinschaft CRC1064 (to K.-P.H. and P.K.) and the European Research Council (ERC Advanced Grant ATMMACHINE), the Gottfried-Wilhelm-Leibniz Prize, and the Center for Integrated Protein Sciences Munich to K.-P.H. K.R.K. is supported by GRK1721. S.E. acknowledges an EMBO long-term fellowship. V.N., K.S., and M.S. acknowledge funding by Quantitative Biosciences Munich.

Author contributions

K.R.K. and S.E. determined the structures and built atomic models. K.R.K. prepared samples for crystallization and performed biochemical analysis of the Arp8 module. S.E., A.T., M.S., and A.B identified the Arp4–N-actin binding nanobody and performed its initial characterization. K.R.K. and G.S. performed affinity enrichment mass spectrometry analysis. S.E. and K.P.H. devised with a contribution of M.S. preparation and characterization of recombinant INO80 complex. V.N. prepared mutant complexes and performed their biochemical analysis. V.N. and E.O. performed and analyzed genome-wide remodeling assays under supervision by P.K. K.S. prepared nucleosomes. S.E. and K.-P.H. designed the overall study, analyzed the results, and wrote the paper with contributions from K.R.K., V.N., E.O., and P.K.

Competing interests

The authors declare no competing interests.

Additional information

Supplementary information is available for this paper at https://doi.org/10.1038/s41594-018-0115-8.

Reprints and permissions information is available at www.nature.com/reprints.

Correspondence and requests for materials should be addressed to K.-P.H.

Publisher's note: Springer Nature remains neutral with regard to jurisdictional claims in published maps and institutional affiliations.

Methods

Nanobody generation. For generation of the Arp4–N-actin binding nanobody (NactNB), an alpaca was immunized with purified and cross-linked endogenous INO80 complex. INO80 complex for immunization was prepared as earlier described[16]. Alpaca immunization, nanobody library generation, and selection of INO80 binding nanobodies were performed as previously published[28] by ChromoTek GmbH.

Cloning, protein expression, and purification. *Nanobody (NactNB).* The DNA sequence coding NactNB carrying a C-terminal Twin-Strep-Tag was cloned into a pHEN6 vector upstream of the pelB leader sequence[51]. *Escherichia coli* Rosetta (DE3) cells (Merck Millipore) were transformed with the pHEN6–NactNB vector. Freshly transformed cells were cultured at 37 °C in lysogeny broth containing 100 µg ml^{-1} ampicillin. Protein was expressed for 2 h at 22 °C after induction with 0.3 mM isopropyl β-d-1-thiogalactopyranoside at an optical density at 600 nm of 0.6. All protein purification steps were performed at 4 °C. Cells were collected by centrifugation and subsequently incubated for 30 min in lysis buffer (50 mM Tris pH 8.0, 300 mM NaCl, 1× protease inhibitor cocktail (Sigma-Aldrich), 1 mg ml^{-1} lysozyme (Carl Roth), and 12.5 units ml^{-1} benzonase (unit is a measure for the amount of the enzyme and defined by the vendor Sigma-Aldrich)) for periplasmic lysis. The cell debris were separated by centrifugation. NactNB was purified from the soluble extract via the C-terminal Twin-Strep-Tag using Strep-Tactin Sepharose (IBA) in 50 mM Tris pH 8.0 and 300 mM NaCl. NactNB bound to Strep-Tactin Sepharose was stored at 4 °C and used within 2 d for pull-down assays or eluted with buffer containing 2.5 mM d-Desthiobiotin.

Arp4–N-actin–NactNB complex. *S. cerevisiae* genes coding for Arp4, Arp8, actin, Taf14, Ies1, Ies2, Ies3, Ies4, Ies5, and Nhp10 were combined in a single pFBDM vector using the MultiBac system[52]. Integration of genes from the pFBDM vector into the baculoviral genome was performed in DH10MultiBac cells (GenevaBiotech), baculovirus generation in *Spodoptera frugiperda* Sf21 insect cells (IPLB-Sf21AE Invitrogen), and protein co-expression in *Trichoplusia ni* High Five insect cells (BTI-TN-5B1-4 Invitrogen) according to a published protocol[52]. High Five cells were transfected 1/100 (v/v) with baculovirus. Cells were cultured for 60 h at 27 °C until they were collected by centrifugation. Cells were lysed by sonication in 50 mM Tris pH 8, 300 mM NaCl, 5% glycerol, and 1× protease inhibitor cocktail (Sigma-Aldrich). The raw cell lysate was cleared by centrifugation. NactNB-bound Strep-Tactin Sepharose was used to isolate the Arp4–N-actin heterodimer from the soluble cell extract. The Arp4–N-actin–NactNB complex was washed with 50 mM Tris pH 8, 300 mM NaCl, and 5% glycerol and eluted with 50 mM Tris pH 8, 300 mM NaCl, 5% glycerol, and 2.5 mM d-Desthiobiotin. The ternary complex was further purified by ion-exchange chromatography with a HiTrapQ HP column (GE Healthcare; linear gradient 100 mM to 1 M NaCl) and gel filtration with a Superdex 200 column (GE Healthcare) equilibrated with 20 mM HEPES pH 8 and 200 mM NaCl. Pure protein was concentrated to a final concentration of 16–20 mg ml^{-1}, flash frozen in liquid nitrogen, and stored at −80 °C.

Arp8 module. Genes encoding *S. cerevisiae* Arp4 and actin were cloned into one pFBDM vector and those coding for *S. cerevisiae* Arp8 (residues 255–881; the non-conserved N-terminal residues 1–254 were deleted[27]) and Ino80^{HSA} (residues 462–598) carrying a C-terminal StrepTag II were combined on a second pFBDM vector[52]. Baculoviruses for the respective vectors were generated in Sf21 insect cells as described above. For the co-expression of the four proteins, High Five insect cells (BTI-TN-5B1-4 Invitrogen) were co-infected with the two viruses (1/100 (v/v) each), cultivated for 60 h at 27 °C, and collected by centrifugation. High Five cells were lysed by sonication in 20 mM HEPES pH 7.8, 100 mM KCl, 2.5% glycerol, and 1× protease inhibitor cocktail (Sigma-Aldrich). The complex was purified from the cleared cell lysate by affinity chromatography using Strep-Tactin Sepharose (IBA), ion exchange chromatography with a HiTrapQ HP column (GE Healthcare; linear gradient 100–800 mM NaCl), and gel filtration with a Superdex 200 column (GE Healthcare) equilibrated with 20 mM HEPES pH 8, 150 mM KCl, 2.5% glycerol, and 1 mM dithiothreitol. Peak fractions containing homogenous Arp8 module complex were pooled, concentrated, flash frozen, and stored at −80 °C.

For the Arp8 module Ino80–HSAα2 mutant (see Supplementary Table 1 for the mutated sequence range), a single pACE–BacI vector encoding expression cassettes for *S. cerevisiae* Arp4, actin, Arp8 (residues 255–881), and Ino80–HSAα2 (residues 462–598 + C-terminal StrepTag II) was generated by using the latest MultiBac system[24,52]. Generation of the baculovirus, expression in High Five insect cells, and purification of the wild-type and the HSAα2 mutant Arp8 module in complex with NactNB were performed in principle as described above. Prior purification of the respective complex 1 mg of purified NactNB (purification of NactNB is described above) was added directly to 20 ml of cleared insect cell lysate. Further purification followed the procedure described before for the wild-type Arp8 module.

INO80 complex. Purification of recombinant expressed *S. cerevisiae* INO80 complex from insect cells will be published elsewhere (unpublished data by: Krietenstein Nils, Oberbeckmann Elisa, Niebauer Vanessa, Schall Kevin, Schwarz Marianne, Moldt Manuela, Korber Philipp, Hopfner Karl-Peter, and Eustermann Sebastian). Briefly, two Baculoviruses were generated by MultiBac technology[52] using coding sequences for *S. cerevisiae* Ino80(2x Flag), Rvb1, Rvb2, Arp4, Arp5-His, Arp8, Actin, Taf14, Ies1, Ies2, Ies3, Ies4, Ies5, Ies6, and Nhp10 subcloned into pFBDM vectors. For expression, High Five insect cells (BTI-TN-5B1-4 Invitrogen) were co-infected with the two baculoviruses 1/100 (v/v) each. INO80 complex was purified from the insect cells according to a previous published protocol[16] which resulted in a pure and monodisperse sample.

INO80 complex HSA mutants were prepared as described for wild-type INO80. Three Ino80(2x Flag) HSA mutants (HSAα1, HSAα2, or HSAα1/α2) were generated using standard cloning techniques and integrated into above-described Baculovirus using MultiBac technology[52] (mutated residues are shown in Supplementary Fig. 4e and Supplementary Table 1).

Preparation of human mononucleosomes. Canonical human histones were essentially purified as described previously[53].

Briefly, *E. Coli* BL21 (DE3) cells (Novagen) were used to express histones for 2 h at 37 °C. Cells were disrupted using non-denaturing conditions and inclusion bodies were washed using 1% Triton X-100. Guanidinium chloride (7 M) was used for resuspension and inclusion bodies were dialyzed in urea (8 M). Cation exchange chromatography was applied to purify histones. After refolding of histones under low-salt conditions, an anion exchange chromatography step was used as a final purification step. Histones were lyophilized for long-time storage. To assemble histone octamers, single histones were resuspended in 7 M guanidinium chloride, mixed at a 1.2-fold excess of H2A/ H2B, and dialyzed against 2 M NaCl for 16 h. Size exclusion chromatography (Superdex 200 16/600 column; GE Healthcare) was used to purify histone octamers, which were then stored in 50% glycerol at −20 °C. For the purpose of mononucleosome reconstitution we used fluorescein-labeled Widom 601 DNA[54] with 80 bp extranucleosomal DNA in the 0N80 orientation[55] or without extranucleosomal DNA (0N0). After amplification by PCR, the DNA was purified using anion exchange chromatography and concentrated by applying vacuum. Histone octamers and DNA were mixed at 1.1-fold excess of DNA at 2 M NaCl. The sodium chloride concentration was then decreased to a final concentration of 50 mM over 17 h at 4 °C. In a final step, NCPs were purified using anion exchange chromatography. After dialysis to 50 mM NaCl, NCPs were concentrated to 1 mg ml^{-1} and stored at 4 °C.

Crystallization. *Arp4–N-actin–NactNB.* Before crystallization the Arp4–N-actin–NactNB complex (16 mg ml^{-1}) was mixed with subtilisin (1:6,000 (w(protease)/w(complex)) for in-drop proteolysis), 0.2 mM $CaCl_2$, and either 1 mM ATP (buffered at pH 7.5 in 100 mM Tris) for the N-actin ATP-bound structure or with 1 mM ADP (buffered at pH 7.5 in 100 mM Tris) for the nucleotide-free (apo) structure. Crystals were grown by hanging-drop vapor diffusion at 20 °C in 1.4–1.5 M sodium malonate at pH 6.0. The best diffracting crystals were harvested after 4–8 d and cryo-protected with 23% glycerol.

Ino80^{HSA}–Arp4–N-Actin–Arp8. For the crystallization of the Ino80^{HSA}–Arp4–N-Actin–Arp8 complex, protein solution (13 mg ml^{-1}) was mixed with LatA (for the LatA stock solution LatA was dissolved in 100% dimethylsulfoxide to a final concentration of 10 mM) at a molar ratio of 1:1.5 (complex/LatA). Crystals were grown by hanging-drop vapor diffusion at 4 °C against 0.1 M sodium citrate tribasic dihydrate and 18% w/v polyethylene glycol 3,350. The crystals were collected after 30 d and cryo-protected with 20% glycerol.

Data collection and processing, structure determination, and refinement. Diffraction data from all crystals were collected at 100 K with a wavelength of 1.0 Å at the Swiss Light Source beamline X06SA. Data were processed with *XDS*[56] and scaled with *POINTLESS* and *AIMLESS* within the CCP4 suite[57].

Arp4–N-actin–NactNB. The two structures of the Arp4–N-actin–NactNB complex with N-actin ATP bound (Protein Data Bank (PDB) 5NBM) and nucleotide-free (apo) (PDB 5NBL) were determined by molecular replacement with Phaser[58]. For a first model, structures of *S. cerevisiae* actin (PDB 1YAG) and Arp4 (PDB 3QB0) were used as search models following the removal of any nucleotides, water molecules, or metal atoms. A homology model of NactNB was generated using the PHYRE server[59] and the three complementarity-determining region loops were deleted before its use as a search model. Sequential search analyses with two copies of each of the search models for Arp4, actin, and NactNB resulted in a unique solution for two copies of the ternary complex per asymmetric unit. The initial model was used as search model for the analysis of the diffraction data sets from crystals grown in presence of ATP or ADP giving immediately a single solution with two complexes per asymmetric unit for both structures. In crystals grown with ATP, N-actin was clearly ATP bound. In contrast, in crystals grown in presence of ADP, N-actin was nucleotide-free. First models were then improved by iterative rounds of model refinement with *phenix.refine*[60] and manual model building with COOT[54]. Both electron density maps contain density for a peptide of unknown source that we could not assign to any sequence of the expressed proteins. This density was therefore modeled as a poly-UNK (unknown amino acid) peptide. The final model of the N-actin(ATP)–Arp4–NactNB complex (PDB 5NBM) at 3.4 Å resolution has R_{work}/R_{free} values of 15.2%/19.3% and the model of the N-actin(apo)–Arp4–NactNB complex (PDB 5NBL) at 2.8 Å resolution has R_{work}/R_{free} values of 17.1%/20.4% (Table 1).

Ino80^{HSA}–Arp4–N-Actin–Arp8. The Ino80^{HSA}–Arp4–N-Actin–Arp8 structure (PDB 5NBN) was determined by molecular replacement with Phaser[58]. The Arp4–N-actin–NactNB structure (PDB 5NBM) without NactNB and the yeast Arp8CTD structure (PDB 4AM6) were used as search models following the removal of any ligands or waters molecules. A single solution containing two copies of the Arp4–N-actin–Arp8 complex per asymmetric unit was found. Clear difference density for the Ino80^{HSA} domain was visible in the initial map after molecular replacement. The model was improved through iterative rounds of refinement with *phenix.refine*[60], applying secondary structure restraints and NCS restraints, and manual model building with COOT[54]. The Ino80^{HSA} domain was built manually with COOT[54] using B-factor sharpening and feature-enhanced maps[61] (calculated by *phenix.fem*) for model building. Density for bound nucleotides at the canonical nucleotide binding sites of Arp4 and N-actin could be identified as ATP. Building and refinement of ADP into the unbiased density map showed in both cases clear difference density for a missing gamma-phosphate. Subsequent refinement shows similar B-factors for the alpha, beta, and gamma phosphate of each ATP molecule. The final model of the Ino80^{HSA}–Arp4–N-Actin–Arp8 complex at 4.0 Å resolution has R_{work}/R_{free} values of 19.3%/24.2% (Table 1).

Structures were analyzed using COOT[54] and PISA[62]. Superposition of structures was performed by using the Secondary Structure Matching[53] algorithm in COOT[54]. Figures of structures were prepared with PyMOL[63] and ChimeraX[64].

Affinity enrichment mass spectrometry. Yeast with a double FLAG-tagged INO80 (Genotype: MATa INO80-FLAG$_2$ his3Δ200 leu2Δ0 met15Δ0 trp1Δ63 ura3Δ0; kindly provided by X. Shen)[6] were grown for 2 d in YPD medium at 30 °C. Cells were collected by centrifugation. Pellets were re-suspended 5:1 (w(yeast)/w(buffer)) in 20 mM HEPES pH 7.8. The cell suspension was dripped into liquid nitrogen and the frozen cells were lysed using a freezer mill (SPEX SamplePrep). The frozen cell powder was stored at −80 °C until usage.

Frozen yeast cell powder (20 g) was thawed in 20 ml lysis buffer (25 mM HEPES pH 8.0, 500 mM KCl, 10% glycerol, 0.05% NP40, 1 mM EDTA, 4 mM $MgCl_2$, and 1× protease inhibitor cocktail (Sigma-Aldrich)). Chromatin was fragmented with a polytron homogenizer (Kinematica; Fisher Scientific) and by sonication (Branson). The raw cell lysate was cleared by centrifugation and 250 µg ml^{-1} avidin (IBA) was added.

The specific-binder nanobody (NactNB) and the control nanobody (enhancer GFP nanobody; eGFP-NB)[65] both had a C-terminal Twin-Strep-Tag and were expressed and purified as described for above for NactNB. NactNB or eGFP-NB immobilized on Strep-Tactin Sepharose were incubated with equal amounts of cleared yeast cell lysate. Unbound protein was removed by washing with buffer W1 (25 mM HEPES pH 8.0, 500 mM KCl, 10% glycerol, 0.05% NP40, 1 mM EDTA, and 4 mM $MgCl_2$) followed by buffer W2 (25 mM HEPES pH 8.0, 200 mM KCl, 10% glycerol, 1 mM EDTA, and 4 mM $MgCl_2$).

Samples for liquid chromatography-tandem mass spectrometry measurement were in principle prepared as published before[66]. Briefly, equal amounts of the nanobody Strep-Tactin Sepharose beads from each pull-down were incubated in buffer E1 (50 mM Tris-HCl pH 7.5, 2 M urea, 5 µg ml^{-1} trypsin (Promega), and 1 mM dithiothreitol) for 30 min at 30 °C for on-bead digest. Any remaining peptides were eluted from the beads and alkylated with buffer E2 (50 mM Tris-HCl pH 7.5, 2 M urea, 5 mM iodoacetamide). Elution fractions were pooled and incubated in the dark overnight at 32 °C. The digestion was stopped by the addition of 1% trifluoroacetic acid. Samples were loaded on self-made C18 reversed-phase StageTips for purification and enrichment following a standard protocol[67]. Peptides were eluted with 2 × 20 µl buffer B (80% ACN and 0.5% AcOH) and concentrated using a SpeedVac concentrator to a final volume of 5–10 µl. Finally, 2.5 µl buffer A* (2% ACN, 1% TFA) and 2.5 µl buffer A (0.5% AcOH) were added to the sample.

Peptide samples were measured on a liquid chromatography-tandem mass spectrometry system using an ultra-high performance liquid chromatography system (EASY-nLC 1000) coupled to an LTQ Orbitrap Elite (both Thermo Scientific) equipped with a standard nanoelectrospray source. Peptides were loaded onto a 15-cm × 0.050-mm inner diameter reversed phase column packed with 2 µm C18 beads (Acclaim PepMap RSLC analytical column, Thermo Scientific) and subsequently separated using a 90-min gradient of solvent B (98% ACN, 0.1% FA) from 2% to 35% at a flow rate of 250 nl min^{-1}.

*.RAW files from the eGFP-NB (mock) and NactNB triplicate experiments were analyzed together using the MaxQuant software suite (version 1.5.2.18) including the label-free algorithm for label-free quantification intensity calculation[68]. Downstream data analysis was performed in the Perseus environment (version 1.5.0.9.)[69]. Briefly, label-free quantification intensity values were $\log_{10}$ transformed, the data were filtered for at least two valid values in at least one of the two conditions, and missing values were imputed using a normal distribution at the noise level (width: 0.3 s.d. of the data; down shift: 1.8 s.d. of the valid data). To reveal significant outliers, a two-sample *t*-test was performed and data were visualized using an in-house R script.

Fluorescence anisotropy. Arp8 module in solution 40 bp dsDNA binding affinity was measured by fluorescence anisotropy in principle as described before[70].

Equimolar amounts of the two complementary DNA strands (forward 5'–3': fluorescein-CCCTGGCGACTTCGCCTCGTTTTGGCGATTTTCTTAGCAAA TATTCTTTC and reverse 5'–3': GAAAGAATATTTGCTAAGAAAATCGCCA AAACGAGGCGAAGTCGCCAGGG), solved in water, were heated to 95 °C for 10 min and slowly cooled at room temperature to anneal the two DNA strands. Arp8 module was diluted to the respective working concentration and incubated with 20 nM dsDNA on ice for 30 min in 20 mM Tris pH 7.8, 50 mM KCl, and 2.5% glycerol in a total volume of 100 µl. Fluorescence anisotropy was measured in a black flat-bottomed non-binding 96-well plate (Greiner-Bio) on a Tecan Infinite M1000 plate reader (excitation wavelength 470 nM, emission wavelength 520 nM).

Data were analyzed and fitted to a non-linear, non-cooperative 1:1 binding model ($y = Af - (Af - Ab) \times (x/(Kd + x))$; *y* anisotropy; Af anisotropy of free ligand; Ab Anisotropy of bound ligand; Kd dissociation constant; *x* receptor concentration) with the program Prism (GraphPad) to calculate the dissociation constants for the respective complex. Experiments were performed in triplicate.

EMSAs. The Arp8 module binding preference for mononucleosomes with or without extranucleosomal DNA was examined with competition EMSAs.

Increasing amounts of Arp8 module were titrated against a 1:1 mixture of 0N0 and 0N80 (20 nM each) mononucleosomes in 10 mM HEPES pH 8.0, 2 mM $MgCl_2$, 60 mM NaCl, 8% glycerol, and incubated for 20 min on ice. Then, 15 µl of each titration step were loaded on a precast native polyacrylamide gel (NativePAGE Novex 4–16% Bis-Tris Protein Gels; Invitrogen). Arp8 module bound and unbound nucleosomes were resolved by Native-PAGE in 1× NativePAGE Running Buffer (Invitrogen; according to the manufacturer protocol) at 120 V for 120 min at 4 °C. Gels were analyzed on a Typhoon FLA 9000 plate reader (GE Healthcare) with 25 µm pixel size, using FITC fluorescence scan.

To test the binding capability of INO80 to nucleosomes, a titration of the complex was carried out. Increasing amounts of the protein in 25 mM Hepes, pH 8.0, 60 mM KCl, 7% glycerol, and 1 mM $CaCl_2$ were incubated with 20 nM 0N80 nucleosomes for 30 min on ice. INO80 bound and unbound nucleosomes were resolved by NativePAGE (Novex 4–16% Bis-Tris Protein Gels; Invitrogen) and subsequently visualized on a Typhoon FLA 9000 plate reader as described above.

Nucleosome sliding assays. The nucleosome sliding activity of INO80 was monitored on 0N80 mononucleosomes.

INO80 (18 nM) was incubated with 90 nM 0N80 nucleosomes in sliding buffer (25 mM Hepes, pH 8.0, 60 mM KCl, 7% glycerol, 0.10 mg ml^{-1} BSA, 0.25 mM dithiothreitol, 2 mM $MgCl_2$) at 26 °C. The sliding reaction was started by the addition of ATP and $MgCl_2$ (final concentrations: 1 mM ATP and 2 mM $MgCl_2$). At the respective time points (30, 60, 120, 300, 600, 1,800, and 3,600 s), the reaction was stopped by adding lambda DNA (NEB) to a final concentration of 0.2 mg ml^{-1}. NativePAGE (NativePAGE Novex 4–16% Bis-Tris Protein Gels; Invitrogen) was used to separate distinct nucleosome species. Gels were visualized on a Typhoon FLA 9000 plate reader as described above.

ATPase assays. In order to determine the ATPase rate of INO80, we applied an NADH-based ATPase assay in principle as described in[24,71].

Briefly, 27 nM INO80 was incubated in assay buffer (25 mM Hepes, pH 8.0, 50 mM KCl, 5 mM $MgCl_2$, 0.1 mg ml^{-1} BSA) with 0.5 mM phosphoenolpyruvate, 2 mM ATP, 0.2 mM NADH, and 25 units ml^{-1} lactate dehydrogenase/pyruvate kinase (unit is a measure for the amount of the enzymes and defined by the vendor Sigma-Aldrich) in a final volume of 50 µl at 30 °C. The Tecan Infinite M100 (Tecan) was used to monitor the NADH dependent fluorescence signal in non-binding, black, 384-well plates (Greiner) at an excitation wavelength of 340 nm and an emission wavelength of 460 nm over a time course of 40 min. ATPase activity for all samples was determined at conditions of maximum INO80 wild-type ATPase activity. Stimulation was performed with 50 nM 0N80 nucleosome, 100 nM 0N0 nucleosome, or 100 nM 223 bp DNA (DNA template used to reconstitute 0N80 nucleosomes). The final ATP turnover rate was calculated using maximal initial linear rates, which were corrected for a buffer blank.

The genome-wide in vitro reconstitution assay and the restriction enzyme accessibility assay are described in the Supplementary Note.

Reporting Summary. Further information on research design is available in the Nature Research Reporting Summary linked to this article.

Data availability. Coordinates and structure factors have been deposited in the PDB under accession codes 5NBM for the N-actin(ATP)–Arp4–NactNB module, 5NBL for the N-actin(apo)–Arp4–NactNB module, and 5NBN for the Ino80^{HSA}–Arp4–N-actin–Arp8 structures. Data for the genome-wide nucleosome positioning experiments reported in this paper have been deposited in the Gene Expression Omnibus under accession number GSE113401. All other data and materials are available from the corresponding author on reasonable request.

References

50. Rothbauer, U. et al. Targeting and tracing antigens in live cells with fluorescent nanobodies. *Nat. Methods* **3**, 887–889 (2006).
51. Conrath, K. E. et al. Beta-lactamase inhibitors derived from single-domain antibody fragments elicited in the camelidae. *Antimicrob. Agents Chemother.* **45**, 2807–2812 (2001).

52. Trowitzsch, S., Bieniossek, C., Nie, Y., Garzoni, F. & Berger, I. New baculovirus expression tools for recombinant protein complex production. *J. Struct. Biol.* **172**, 45–54 (2010).
53. Dyer, P. N. et al. Reconstitution of nucleosome core particles from recombinant histones and DNA. *Methods Enzymol.* **375**, 23–44 (2004).
54. Lowary, P. T. & Widom, J. New DNA sequence rules for high affinity binding to histone octamer and sequence-directed nucleosome positioning. *J. Mol. Biol.* **276**, 19–42 (1998).
55. Levendosky, R.F., Sabantsev, A., Deindl, S. & Bowman, G.D. The Chd1 chromatin remodeler shifts hexasomes unidirectionally. *eLife* **5** (2016).
56. Kabsch, W. XDS. *Acta Crystallogr. D Biol. Crystallogr.* **66**, 125–132 (2010).
57. Winn, M. D. et al. Overview of the CCP4 suite and current developments. *Acta Crystallogr. D Biol. Crystallogr.* **67**, 235–242 (2011).
58. McCoy, A. J. et al. Phaser crystallographic software. *J. Appl. Crystallogr.* **40**, 658–674 (2007).
59. Kelley, L. A., Mezulis, S., Yates, C. M., Wass, M. N. & Sternberg, M. J. The Phyre2 web portal for protein modeling, prediction and analysis. *Nat. Protoc.* **10**, 845–858 (2015).
60. Adams, P. D. et al. PHENIX: a comprehensive Python-based system for macromolecular structure solution. *Acta Crystallogr. D Biol. Crystallogr.* **66**, 213–221 (2010).
61. Afonine, P. V. et al. FEM: feature-enhanced map. *Acta Crystallogr. D Biol. Crystallogr.* **71**, 646–666 (2015).
62. Krissinel, E. & Henrick, K. Inference of macromolecular assemblies from crystalline state. *J. Mol. Biol.* **372**, 774–797 (2007).
63. *The PyMOL Molecular Graphics System, Version 1.8.* (Schrodinger, LLC, 2015).
64. Goddard, T. D. et al. UCSF ChimeraX: meeting modern challenges in visualization and analysis. *Protein Sci.* **27**, 14–25 (2018).
65. Kirchhofer, A. et al. Modulation of protein properties in living cells using nanobodies. *Nat. Struct. Mol. Biol.* **17**, 133–138 (2010).
66. Keilhauer, E. C., Hein, M. Y. & Mann, M. Accurate protein complex retrieval by affinity enrichment mass spectrometry (AE-MS) rather than affinity purification mass spectrometry (AP-MS). *Mol. Cell. Proteomics* **14**, 120–135 (2015).
67. Rappsilber, J., Mann, M. & Ishihama, Y. Protocol for micro-purification, enrichment, pre-fractionation and storage of peptides for proteomics using StageTips. *Nat. Protoc.* **2**, 1896–1906 (2007).
68. Cox, J. et al. Accurate proteome-wide label-free quantification by delayed normalization and maximal peptide ratio extraction, termed MaxLFQ. *Mol. Cell. Proteomics* **13**, 2513–2526 (2014).
69. Tyanova, S. et al. The Perseus computational platform for comprehensive analysis of (prote)omics data. *Nat. Methods* **13**, 731–740 (2016).
70. Favicchio, R., Dragan, A. I., Kneale, G. G. & Read, C. M. Fluorescence spectroscopy and anisotropy in the analysis of DNA-protein interactions. *Methods Mol. Biol.* **543**, 589–611 (2009).
71. Kiianitsa, K., Solinger, J. A. & Heyer, W.-D. NADH-coupled microplate photometric assay for kinetic studies of ATP-hydrolyzing enzymes with low and high specific activities. *Anal. Biochem.* **321**, 266–271 (2003).

4.3 Single-molecule nucleosome remodeling by INO80 and effects of histone tails

Schwarz, M., Schall, K., Kallis, E., Eustermann, S., Guariento, M., Moldt, M., Hopfner, K.P. and Michaelis, J., 2018. Single-molecule nucleosome remodeling by INO80 and effects of histone tails. *FEBS letters*, *592*(3), pp.318-331.

DOI: 10.1002/1873-3468.12973
https://febs.onlinelibrary.wiley.com/doi/full/10.1002/1873-3468.12973

Summary

This publication explores the effect of histone tails on DNA translocation by INO80. These are flexible and mostly unstructured elements of the core histone proteins and hence challenging to investigate by structural biology. For this reason, singe-molecule nucleosome remodeling FRET was chosen as an alternative method to shed light on the role of histone tails. For this reason, an assay was set up, which reports DNA translocation by a change of FRET efficiency of double labelled nucleosomal DNA. This demonstrates that INO80 processively translocates nucleosomal DNA while maintaining the integrity of the nucleosome. This holds true for wild-type and all tailless nucleosomes. However, the binding of INO80 to all tailless nucleosomes appears to be different than for wild-type nucleosomes. While one relatively defined nucleosome conformation is observed for wild-type nucleosomes, INO80 interaction with all tailless nucleosomes leads to a heterogeneous FRET population demonstrating the presence of several nucleosome conformations. Intriguingly, the binding affinity of INO80 to wild-type and all tailless nucleosomes is comparable, but remodelling is faster for all tailless nucleosomes. Thus, the structurally heterogeneous INO80-bound state of all tailless nucleosomes might represent a lowered energy barrier for the initiation of DNA translocation. In turn, this means that histone tails constitute a barrier for DNA translocation, which needs to be overcome potentially by an additional energy input. Given the profound impact of modifications of histone tails on chromatin organization, it is tempting to speculate that this barrier, and thus chromatin remodelling by INO80, is regulated by PTMs.

Author contribution

I purified the wild-type and all tailless histones from recombinant sources and reconstituted nucleosomes with these. I performed the biochemical analysis of binding and sliding of wild-type and all tailless nucleosomes by INO80.

FEBS Letters

Single-molecule nucleosome remodeling by INO80 and effects of histone tails

Marianne Schwarz[1,2], Kevin Schall[2], Eleni Kallis[1], Sebastian Eustermann[2], Mara Guariento[1], Manuela Moldt[2], Karl-Peter Hopfner[2] and Jens Michaelis[1]

1 Faculty of Natural Sciences, Institute of Biophysics, Ulm University, Germany
2 Gene Center and Department of Biochemistry, Ludwig-Maximilians-University Munich, Munich, Germany

Correspondence
J. Michaelis, Faculty of Natural Sciences, Institute of Biophysics, Ulm University, Albert-Einstein-Allee 11, 89081 Ulm, Germany
Fax: +49 731 50 23059
Tel: +49 731 50 23050
E-mail: jens.michaelis@uni-ulm.de
and
K.-P. Hopfner, Gene Center, Feodor-Lynen-Str. 25, 81377 Munich, Germany
Fax: +49 89 2180 76999
Tel: +49 89 2180 76953
E-mail: hopfner@genzentrum.lmu.de

(Received 15 November 2017, revised 22 December 2017, accepted 29 December 2017, available online 26 January 2018)

doi:10.1002/1873-3468.12973

Edited by Claus Azzalin

Genome maintenance and integrity requires continuous alterations of the compaction state of the chromatin structure. Chromatin remodelers, among others the INO80 complex, help organize chromatin by repositioning, reshaping, or evicting nucleosomes. We report on INO80 nucleosome remodeling, assayed by single-molecule Foerster resonance energy transfer on canonical nucleosomes as well as nucleosomes assembled from tailless histones. Nucleosome repositioning by INO80 is a processively catalyzed reaction. During the initiation of remodeling, probed by the INO80 bound state, the nucleosome reveals structurally heterogeneous states for tailless nucleosomes (in contrast to wild-type nucleosomes). We, therefore, propose an altered energy landscape for the INO80-mediated nucleosome sliding reaction in the absence of histone tails.

Keywords: chromatin remodeling; nucleosome; single-molecule FRET

In eukaryotic cells, DNA is packed into the dense chromatin structure. ATP-dependent chromatin remodelers that are conserved from fungi to mammals [1] balance the tradeoff between the dense packing of DNA and the accessibility of DNA for transcription, DNA damage repair, and DNA replication. They organize chromatin by sliding, repositioning, reshaping, or ejecting nucleosomes [2,3]. These chromatin remodelers with an ATPase domain belonging to the DNA/RNA helicase superfamily 2 (SF2) [4] group into different phylogenetic subfamilies (SWI/SNF, ISWI, CHD, INO80) [1,3,5]. In *Saccharomyces cerevisiae*, different chromatin remodelers are known to have specific and partly redundant functions to establish the position of the +1 nucleosome and to establish well-positioned nucleosome arrays in the gene body [6].

The basic building block of chromatin is the nucleosome core particle (NCP). The NCP contains the histone octamer and 145–147 bp of DNA [7–9]. The histone fold domains of two copies each of histones H2A, H2B, H3, and H4 form the octamer core of the nucleosome, which is wrapped approximately 1.7 times by nucleosomal DNA [8]. This NCP together with linker DNA constitutes the primary substrate for

Abbreviations
at, all tailless; crDNA, competitor DNA; FRET, Foerster Resonance Energy Transfer; PDA, probability distribution analysis; NCP, nucleosome core particle; PIE-MFD, pulsed interleaved excitation combined with multiparameter fluorescence detection; RT, room temperature; SHL, superhelical location; wt, wild-type.

chromatin remodelers. The N-terminal histone tail domains of the four core histones and the C-terminal histone tail of H2A extend beyond the compact NCP structure [8,10].

The stability and plasticity of various nucleosome variants could be an important physicochemical aspect in shaping chromatin and the activity of remodeling processes. While structurally the fold of the histone octamer is well understood, considerably less is known about how histone tails together with numerous functional modifications control the accessibility and stability of nucleosomes [11,12]. For instance, tailless nucleosomes show a decreased stability, in particular attributed to removing stabilizing effects of H2B and H3 tails [13,14]. Direct insight into nucleosome stability comes from single-molecule force spectroscopy experiments [15,16]. In particular, single-molecule methods have been of great interest to delineate altered DNA wrapping dynamics in the absence of histone tails [17] and partial DNA unwrapping for H4 tail acetylation [18]. Along this line, single-molecule Foerster Resonance Energy Transfer (FRET) methods applied on nucleosomes [19] showed altered nucleosome stability due to unspecific histone modifications [20], in the presence of specific globular histone fold acetylation [21,22] or after incorporation of histone variants [23]. Most of these studies probing variations of the histone octamer made use of the SELEX-generated '601 Widom' positioning DNA sequence (601 sequence) [24]. Importantly, also the DNA sequence influences nucleosome stability [20,25]. In particular, in the case of the widely used 601 sequence, it is known that either side of the nucleosome shows differential DNA flexibility [26].

So far, single-molecule nucleosome remodeling FRET studies (that mostly monitor the nucleosome entry and/or exit DNA) probed DNA translocation on canonical nucleosomes by single subunit chromatin remodelers [27], chromatin remodelers comprising a few subunits [28,29], and the multi-subunit RSC remodeler [30]. Interestingly, these and other studies report incremental movement of DNA with 1-2 bp steps [28,30,31] as postulated by structural models [32].

INO80 is a conserved multi-component complex [33], which has been linked to numerous DNA-based metabolic processes, such as transcription regulation [34–37], DNA damage repair [38,39], and DNA replication [40,41]. In yeast, the Ino80-ATPase together with the INO80 subunit 2 (Ies2) form a functional scaffold that assembles three multi-subunit-submodules forming a 19 subunit and > 1 MDa INO80 complex [42,43]. It can robustly slide nucleosomes on DNA *in vitro* [44,45], while its H2A/H2B histone exchange activity is under debate [46–48]. Recently, it has been suggested that both activities can be explained by a unifying mechanism, involving Ino80-ATPase translocation close to the DNA entry site of nucleosomes and thus close to the DNA-H2A/B interface [49]. This interpretation is supported by the observation that in contrast to other remodelers, the INO80 complex does not require octamer flexibility at the H3/H4 protein-protein interface for nucleosome remodeling [50]. However, due to the lack of direct mechanistic studies on nucleosome remodeling at the level of single molecules, such mechanistic hypotheses yet await experimental verification.

Here, we establish single-molecule level binding and sliding assays for INO80 to help decipher its mechanism in sliding and positioning of nucleosomes. We have developed a single-molecule FRET assay that reports on nucleosome sliding by a marked change in FRET efficiency of a double-labeled nucleosome. As a first step, we will focus on the effect of histone tails on nucleosome recognition and sliding by INO80 by comparing results on wild-type and all tailless nucleosomes. When using surface-immobilized nucleosomes, we observe that the INO80 complex repositions both wild-type and all tailless nucleosomes in a processive manner. However, the initial conformation of the nucleosome entry DNA in the presence of INO80 and ADP differs in both cases. We, therefore, propose that the breakage of the histone-DNA contacts near the nucleosome entry site imposes an important regulatory barrier to the initiation of INO80 nucleosome remodeling.

Materials and methods

Protein purification

The DNA sequence of human histone proteins (Table S3) was cloned in individual *pET21a* (Novagen, now Merck, Darmstadt, Germany) vectors and provided by the Längst laboratory (University of Regensburg). Histone proteins were recombinantly expressed in *Escherichia coli* and purified individually, and histone octamers were formed as described in Refs [51] and [52]. The histone octamer refolding product was separated from side products by size exclusion chromatography on a Superdex 200 16/600 (GE Healthcare, Chicago, IL, USA) column in 2 M NaCl, 10 mM Tris pH 7.5, 1 mM EDTA, 5 mM beta-Mercaptoethanol running buffer. Octamer formation was verified on an 18% polyacrylamide SDS gel with Coomassie staining (data not shown).

The *Sc*INO80 complex was recombinantly expressed and purified from insect cells (Eustermann *et al.* to be published elsewhere). The purified INO80 complex was adjusted to

storage buffer conditions, namely final buffer concentrations of 20 mM HEPES pH 8, 350 mM KCl, 25% Glycerol, 0.8 mM DTT, 3.2 mM $MgCl_2$, and stored at −80 °C.

All protein concentrations were estimated from absorbance at 280 nm using extinction coefficients calculated from the sequence with *ProtParam* [53].

Nucleosome assembly

Nucleosomes were assembled from octamers, 601 sequence DNA (Table S2, Doc. S1), and crDNA (Doc. S1) using salt gradient dialysis. The assembly was prepared in 20 mM Tris pH 7.6, 2 M NaCl, 10 mM DTT, and 200 ng·μL^{-1} BSA. For single-molecule applications, 0.38 μM 601 DNA was used, thereof 1/10 labeled 220 bp-601 and 9/10 unlabeled 200 bp-601 derived from *pUC18* digestion. The *pUC18* backbone from the *pUC18::12x200 bp-601* (Doc. S1) digestion was used as crDNA in a mass ratio of 1 : 1 compared to the combined 601 DNA mass. For the establishment of the nucleosome assembly protocol, 0.42 μM of each, 147 bp crDNA and 220 bp 601 DNA, were used. Octamer concentrations were titrated. Each assembly reaction was transferred to a Slide-A-lyzer dialysis chamber (Thermo Fisher, Scientific, Waltham, MA, USA, 7-kDa cutoff). The salt gradient dialysis started in a 300-mL volume of 20 mM Tris pH 7.6, 0.1 mM EDTA, 2 M NaCl, 1 mM DTT buffer; and the NaCl concentration was reduced by adding 20 mM Tris pH 7.6, 0.1 mM EDTA, 50 mM NaCl, 1 mM DTT at 3 mL·min^{-1} up to final 3 L. The products were analyzed on a 0.4 × TBE/6% polyacrylamide gel and imaged on a ChemiDocMP system with the IMAGE LAB software (BioRad Laboratories, Hercules, CA, USA) before and after SybrGold staining. Nucleosomes used in binding assays were additionally purified by anion exchange chromatography (SourceQ). For assessing nucleosome homogeneity, fluorescent bands were analyzed with IMAGEJ [54].

Nucleosome binding and sliding assays

All single-molecule assays were performed in remodeling buffer (25 mM Tris pH 7.6, 4 mM $MgCl_2$, 500 μM DTT, 200 ng·μL^{-1} BSA, 80 mM KCl, 10% Glycerol).

For the sliding assay, 100 nM INO80, 2 mM ATP (Sigma), and the nucleosomes (in the presence of competitor DNA from nucleosome assembly) were used, with a final concentration around 50 nM nucleosomes, thereof 1/10 labeled nucleosomes, and 10 ng·μL^{-1} crDNA. The reaction was incubated for 1 h at 27 °C and stopped by addition of λ-DNA (NEB) to a final concentration of 115 ng·μL^{-1}.

The quenched sample was analyzed by native PAGE (3–12% Bis-Tris; ThermoFisher) and fluorescent samples were imaged on a ChemiDocMP system (BioRad Laboratories).

The binding assays in Fig. 2 were performed in 20 mM HEPES pH 8, 50 mM KCl, 8% Glycerol, 2 mM $CaCl_2$ and 2 mM ADP, analyzed by native PAGE (3–12% Bis-Tris) and visualized using the Typhoon imaging system (GE Healthcare). Gel bands were quantified using IMAGEJ [54].

Total internal reflection fluorescence microscopy (TIRFM)

TIRF microscopy was performed as described in Ref. [55]. Briefly, nucleosomes were diluted in remodeling buffer to a concentration on the order of 10 pM labeled nucleosomes (equivalent to ca. 0.1 nM nucleosomes, <0.05 ng·μL^{-1} crDNA) and loaded to a PEG-coated sample chamber with a syringe pump (PHD2000 Harvard Apparatus) either in the absence or presence of 39 nM INO80 and 2 mM ADP (Calbiochem now Merck). Remodeling was initiated by buffer exchange to 2 mM ATP for 6 min (alternatively by adding 39 nM INO80 and 2 mM ATP in case of Fig. S3). Remodeling was allowed for 25 min at RT. If indicated, the reaction was quenched in the presence of Apyrase (NEB) for 15 min at RT. The nucleosomes were allowed to relax to a new stable position for 10 min at RT after washing the sample chamber with measurement buffer following a modified protocol developed by Blosser *et al.* [29].

The smFRET analysis software was provided by the Lamb Laboratory (LMU Munich) [56]. For calculation of FRET efficiencies, individual γ corrections (accounting for differences in detection efficiencies and quantum yields) and β corrections (accounting for spectral crosstalk) were applied [55] if appropriate, otherwise a mean γ of 0.55 and β of 0.045 were used.

Confocal spectroscopy

For smFRET measurements, nucleosomes were diluted in remodeling buffer to a concentration on the order of 100 pM labeled nucleosomes (equivalent to ca. 1 nM nucleosomes, <0.5 ng·μL^{-1} crDNA). We chased off the INO80 complex from remodeled nucleosomes with competitor DNA for confocal spectroscopy experiments as described in the section Nucleosome binding and sliding assays, which was not useful in TIRF microscopy due to high background. For INO80 bound samples, nucleosomes were incubated with either 39 nM or 156 nM INO80 and 2 mM ADP. The sample was placed on a PEG-coated coverslip into a well formed by Liquid Barrier Marker (Roth).

Freely diffusing fluorescent nucleosomes were recorded at room temperature (RT) on a custom built confocal setup (Doc. S1) using time-correlated single-photon counting and pulsed interleaved excitation combined with multiparameter fluorescence detection (PIE-MFD) [57] similar to Ref. [22,23].

The software for data analysis (PAM – PIE analysis with MATLAB v1.0) was provided by the Lamb Laboratory (LMU Munich) and is available at https://www.gitlab.com/

PAM-PIE/PAM. An all-photon-burst-search was applied to the photon time traces [58], selecting only fluorescent bursts with at least 10 photons in 500 μs and 50 or more photons per burst in total.

Confocal spectroscopy–derived quantitative distance information on dye positions was extracted by probability distribution analysis (PDA) [59] (Doc. S1).

Calculation of dye mean positions

Expected dye mean positions were derived from the 601 nucleosome structure (3LZ0, [60] with a modeled DNA overhang) using the FPS software [61] with a dye linker length of 19 Å (Alexa647) and 15 Å (Tamra6), a dye linker width of 4.5 Å and a dye radius of 6 Å. The isotropic Foerster radius was determined to be 67 Å as described in arXiv:1710.03807v1 [q-bio.QM]. The absorption spectrum of donor only nucleosomes and the emission spectrum of free dye were integrated with the software PhotochemCAD [62] to yield the spectral overlap integral. The donor quantum yield was determined from the universal rate of radiative deexcitation for the donor dye and the fluorescence lifetime of donor-only nucleosomes.

Notably, apparent inter-dye distances are not identical to the distance of dye mean positions. To this end, we converted FRET efficiencies (TIRF data) and inter-dye distances (PDA analysis) to distances of the mean dye positions (Table 1), as described in Ref. [63]. The distance uncertainties (Table 1) are as follows: uncertainty of the apparent inter-dye distance for TIRF data (arXiv:1710.03807v1 [q-bio.QM]); and determination of upper and lower limits for the distance of mean dye positions with respect to the Foerster Radius uncertainty (for confocal data; Doc. S1).

Results

Nucleosome assembly in the presence of competitor DNA yields high sample homogeneity

Mono-nucleosomes consist of DNA and two copies of each individual histone. While *in vivo* histone chaperones help assemble first the H3/4 tetramer and then both H2A/B dimers onto the DNA [64], performing salt gradient nucleosome assembly relies on stoichiometric protein educts [51]. Notably, the observation of subnucleosomal DNA-histone products recently led to the discovery of oriented hexasomes on the 601 sequence [65].

In order to obtain homogenously assembled nucleosomes (7N66, 601 nucleosome with 7 and 66 bp overhang, respectively) and to avoid incomplete assembly side products, we made use of competitor DNA (crDNA) in the salt gradient dialysis assembly reaction (147-bp fragment of a generic DNA sequence from the pUC18 vector [66], Materials and methods). As established for chromatin fiber formation [66], due to its lower affinity for histone octamers, crDNA will form nucleosome core particles only after 601 sequence saturation. We find that 'undersaturated' titration points defined by no visible shift of crDNA as compared with the DNA-only control (e.g. 1.1 : 1 molar ratio of octamer to 601 DNA in Fig. 1A) have a high propensity for an incomplete assembly side product alongside with the completely assembled nucleosome. Presumably, this side product constitutes a hexasome as observed recently [65,67]. In contrast, 'oversaturated' titration points form yet another defined 601 DNA–histone complex with reduced electrophoretic mobility alongside with complete binding of crDNA (e.g., 2.0 : 1 molar ratio of octamer to 601 DNA in Fig. 1A). A possible conformation that can explain the observed reduced mobility is that of an overlapping dinucleosome [68]. At intermediate concentrations, nucleosomes are packed completely and no additional side products are observed (e.g., 1.7 : 1 molar ratio in Fig. 1A). Taken together, nucleosome assembly in the presence of competitor DNA is a convenient tool to assess the 601 DNA saturation of the assembly and to prepare homogenous nucleosome samples.

We extended our protocol using the entire *pUC18* plasmid backbone as crDNA (Fig. 1B). The assembly strategy works equally well for wild-type and all

Table 1. Expected and measured distances of dye mean positions for the LF nucleosome before and after INO80-mediated remodeling. Of note, remodeling was quenched with apyrase in TIRF microscopy and lambda-DNA in confocal spectroscopy measurements.

	Expected distance of mean dye positions			Distance obtained from TIRF microscopy	Distance from PDA analysis of confocal data
Wild-type*(wt)*7N66	76 Å			66 Å ± 8%	66 Å ± 9%
All tailless*(at)*7N66				73 Å ± 8%	74 Å ± 9%
Remodeled(R) *wt*7N66	38 Å (10 bp)	38 Å (20 bp)	36 Å (30 bp)	42 Å ± 10%	n.d.
Remodeled(R) *at*7N66				40 Å ± 11%	n.d.
Quenched R*wt*7N66	38 Å (10 bp)	38 Å (20 bp)	36 Å (30 bp)	42 Å ± 12%	41 Å ± 12%
Quenched R*at*7N66				41 Å ± 11%	42 Å ± 12%

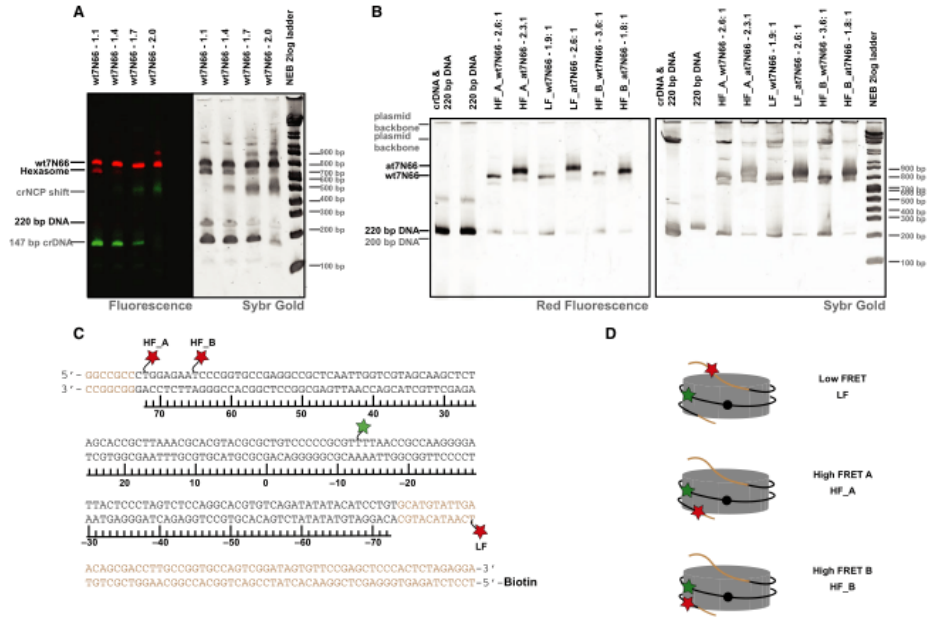

Fig. 1. Homogenous nucleosome sample preparation for single-molecule FRET. (A) Establishment of nucleosome assembly; left: multichannel fluorescence readout for 220 bp 601 DNA (red bands), and for 147 bp crDNA (green bands); right: SybrGold staining of the same gel. Single channel fluorescence readouts in Fig. S1. (B) Overview of the six assembled nucleosome constructs wtHF_A, atHF_A, wtLF, atLF, wtHF_B, atHF_B used for smFRET measurements; left: fluorescence readout for double-labeled 220 bp 601 DNA; right: SybrGold staining of the same gel. (C) 601 sequence [24] for 7N66 nucleosomes with donor (green) and different alternative acceptor (red) label positions, namely HF_A, HF_B, LF (see text). 7-bp and 66-bp linkers are written in brown letters, and the 147-bp nucleosome core DNA in black letters. The 145 bp that form histone–DNA interactions for the 601 sequence [7,95] are underlined with a base-pair-ruler. (D) Description as in (A) depicted in the direction of the dyad (black circle) for the different single-molecule FRET constructs. NCP, nucleosome core particle; wt, wild-type; at, all tailless; crDNA, competitor DNA; molar ratios of octamer:601 DNA are indicated for each lane of the native polyacrylamide gels.

tailless nucleosomes (Fig. S1A,B) and the resulting material (best titration points summarized in Fig. 1B) is highly homogenous. Therefore, it can be used directly without the need of further purification to study nucleosome remodeling at the single-molecule level. Of note, for single-molecule applications, only 1/10 of the nucleosomes (7N66) was packed against labeled 220-bp DNA (fluorescence readouts Fig. 1B, Fig. S1D). As seen in the SybrGold stained gel, 9/10 of nucleosomes are unlabeled and packed to 7N46 particles. The labeled 7N66 mono-nucleosomes used in this single-molecule study are (i) low FRET Fp13(Tamra6)Rm84(Alexa647), abbreviated with 'LF', (ii) high FRET Fp13(Tamra6)Fm72(Alexa647), abbreviated with 'HF_A', and (iii) high FRET Fp13(Tamra6)Fm65(Alexa647), abbreviated with 'HF_B'. The nomenclature directly explains the location of the labels (Fig. 1C), for example, the construct (i) is labeled (on the forward primer, 'F') at a position 13 bp away from the dyad in 3′ direction (plus, 'p') with Tamra 6, and at a position 84 bp away from the dyad in 5′ direction (minus, 'm') with Alexa647 (on the reverse primer, 'R'). Thus, the acceptor label is placed on the entry DNA and the donor label on the opposite side of the nucleosome dyad (near superhelical location SHL-1.5) (Fig. 1D) [69,70].

The INO80 complex binds wild-type and all tailless nucleosomes with equal affinity

In order to determine appropriate conditions for smFRET experiments with very low (ca. 100 pM)

nucleosome concentrations, we next determined INO80 binding conditions for 7N66 nucleosomes (in the absence of competitor DNA) (Fig. 2). We found a regime with < 30% of nucleosomes bound for < 5 nM INO80 and a regime with < 80% bound for < 20 nM INO80. In this intermediate regime, the gel shows different bands, indicative of different complex conformations. For > 40 nM INO80, more than 90% of nucleosomes are bound and only a single band is observed in the gel, that is, the complexes show a uniform conformation. Importantly, the INO80 complex binds wild-type and all tailless 7N66 nucleosomes with equal affinity (Fig. 2, Fig. S2).

The INO80 complex robustly repositions wild-type and all tailless surface tethered nucleosomes while exhibiting marked differences in the bound state

We next tested whether the INO80 complex repositions nucleosomes under smFRET conditions using double-labeled surface-immobilized nucleosomes (Materials and methods). We designed end-positioned nucleosomes (7N66) with an initial FRET efficiency of $E = 48\%$ ($\sigma = 6\%$, Fig. 3A, blue). Assuming that for stable nucleosome states formed either from remodeling intermediates and/or after remodeling, the DNA adopts the canonical path on the octamer core, we postulate the acceptor label on the entry DNA to move into the nucleosome core and the donor label to move from one side of the dyad to the other side of the dyad on the opposite gyre. Therefore, FRET is expected to have increased after remodeling.

When binding INO80 to the wild-type nucleosome in the presence of ADP, the FRET efficiency distribution only changed marginally ($E = 45\%$, $\sigma = 9\%$, Fig. 3B, green). Thus, the INO80 bound state does not substantially alter the apparent distance of the two labels; however, we cannot exclude changes in the nucleosome structure upon INO80 binding, as FRET studies depend on the relative label positions and a particular position could be insensitive to changes in a certain direction [71].

Importantly, upon addition of 2 mM ATP, we observed an increase in FRET efficiency as expected for INO80-mediated nucleosome remodeling ($E = 85\%$, $\sigma = 5\%$, Fig. 3C, red). These data were obtained after incubation with ATP and subsequent relaxation of the remodeled nucleosomes to stable nucleosomal states upon buffer exchange (end-point assay, Materials and methods). Note that remodeling using prebound INO80 complexes was not complete (45% remodeling in Fig. 3C). We attribute this observation to the fact that not all observed nucleosomes had an INO80 complex bound and/or to a small fraction of inactive remodeling complexes. When estimating the expected FRET efficiency for different putative remodeled states (Table 1) of energetically favored positions after 10 bps, 20 bps, or 30 bps [72,73] of remodeling (Materials and methods), we find that the observed FRET efficiency is in a good agreement with any of these possible states.

We used a constant flow of remodeling buffer, to ensure that remodeling of the individual immobilized nucleosomes was driven by a prebound remodeler. Thus, these results proof that the INO80 complex is a processive molecular machine using several ATPase cycles accompanied by incremental translocation steps (Introduction) to reposition nucleosomes while staying engaged to the nucleosome. This result might have been expected since several of the INO80 submodules contribute to nucleosome and/or DNA binding [42,74–76]. We propose that either the ATPase itself acts as a processive translocase, or alternatively the INO80 submodules take turns in tethering the complex to the nucleosome in case the ATPase lets go off its substrate.

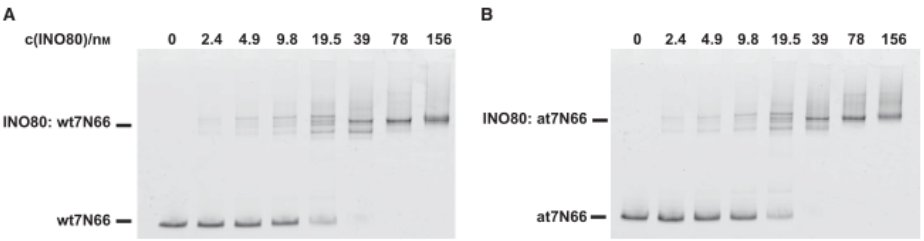

Fig. 2. The INO80 complex binds wild-type and all tailless nucleosomes with equal affinity. (A) INO80 binding to wild-type nucleosomes. (B) INO80 binding to all tailless nucleosomes.

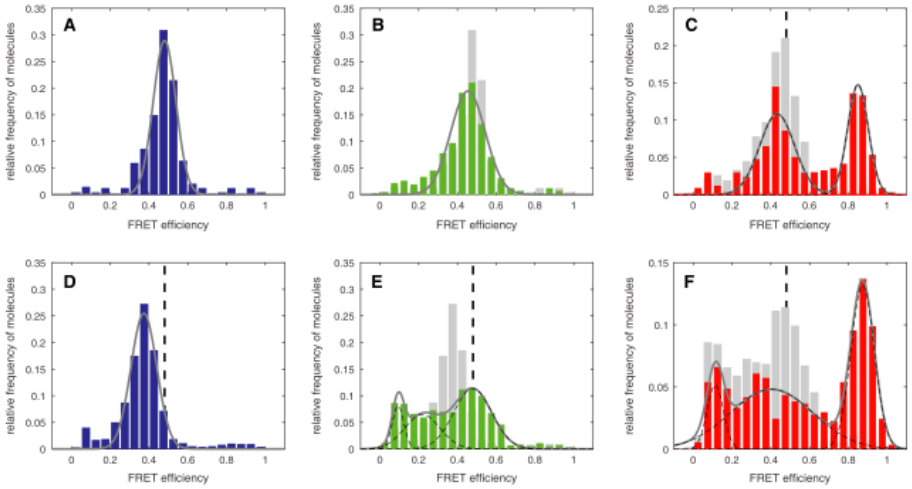

Fig. 3. The INO80 complex remodels nucleosomes in a processive manner for both wild-type and all tailless nucleosomes, but shows marked differences for the respective pre-remodeling bound state. TIRF microscopy data of (A) (blue) wild-type low FRET nucleosome (wtLF). (B) (green) INO80 nucleosome binding in the presence of ADP, compared with wtLF (gray). (C) (red) Processive INO80 nucleosome remodeling upon addition of ATP compared with the bound wtLF (gray). (D) (blue) All tailless low FRET nucleosome (atLF). (E) (green) INO80 nucleosome binding in the presence of ADP, compared with atLF (gray). (F) (red) Processive INO80 nucleosome remodeling upon addition of ATP compared with the bound atLF (gray). Vertical black dashed line at the mean position of wild-type nucleosomes. Fit results in Table S1.

Next, we wanted to test the influence of nucleosome tails on INO80 binding and nucleosome remodeling. Therefore, we repeated the smFRET experiments on immobilized nucleosomes using nucleosomes lacking all histone tails. The all tailless nucleosome showed a somewhat decreased FRET efficiency compared to wild-type nucleosomes ($E = 37\%$, $\sigma = 7\%$, Fig. 3D, blue). Differences in entry DNA coordination for histone tail deletion constructs have been reported previously [13,14,17]. Our observations show that despite a slightly different conformation of the entry DNA and thus lower FRET efficiency for the nucleosome educt, there is a similar FRET efficiency peak width and thus a well-defined DNA conformation of the linker DNA, similar to that observed for wild-type nucleosomes.

In contrast, INO80 binding to all tailless nucleosomes in the presence of ADP led to a significant change in the observed single-molecule FRET distribution (Fig. 3E, green). The resulting histogram can no longer be described using a single Gaussian function; instead, we observe a quasicontinuum of FRET states, which has to be fitted with at least three different Gaussians ($E = 9\%$, 22%, and 48%; $\sigma = 3\%$, 9%, and 10%, respectively, comprising 13%, 30%, and 57% of the data).

We repeated the nucleosome remodeling experiments with the all tailless nucleosomes, resulting in a sharp peak in the observed histogram at high FRET efficiency (Fig. 3F, red, $E = 87\%$, $\sigma = 6\%$). As for wild-type nucleosomes, this peak again arises from processive remodeling of prebound INO80 complexes. Again remodeling is incomplete (39% remodeling in Fig. 3F), and the unremodeled part of the histogram is reminiscent of the heterogeneous bound states in the presence of ADP (gray background histogram). Importantly, > 90% of the observed surface-immobilized all tailless nucleosomes are intact during the course of the experiment.

Given that we tailored experimental conditions for the nucleosome remodeling end-point assay, we observed only a small percentage of dynamically switching fluorescence time trajectories occurring concomitantly with the static molecules presented in Fig. 3 for nucleosomes alone (examples in Fig. S6D,G), nucleosomes in presence of INO80 and ADP (examples in Fig. S6E,F and H,I), or remodeled nucleosomes

(data not shown). However, we observed prolonged real-time smFRET transitions between different states upon addition of INO80 and ATP in the presence of an oxygen scavenging system (exemplary smFRET data shown in Fig. S6B,C). A detailed mechanistic analysis is beyond the scope of this study, as for the label position of our LF construct, discrimination of double-labeled nucleosomes that display previously reported inherent nucleosome dynamics before or after remodeling (such as breathing [77,78], dimer splitting [79], or gapping [80]) from real-time INO80 remodeling is extremely challenging.

Nucleosome integrity is maintained during remodeling and fully consistent with expected remodeled positions

In order to test nucleosome integrity after INO80 remodeling, we used single-molecule FRET confocal spectroscopy (Materials and methods). The above-mentioned labeling scheme for nucleosomes allowed us to make sure that every nucleosome substrate is at the most double labeled, (one acceptor and one donor molecule) in contrast to previous single-molecule FRET studies on chromatin remodelers, which use histone labeling and therefore critically rely on measurements of immobilized complexes to sort out nucleosomes with two donor labeled histones [28–30]. Additionally, the 7N66Fp13(Tamra6)Rm84(Alexa647) construct allows us to clearly discriminate between end-positioned and remodeled nucleosomes without being limited by the dynamic range of FRET. For the educt and remodeled wild-type nucleosomes that show a shift in electrophoretic mobility, the observed FRET efficiency change in the confocal setup is comparable to that obtained using TIRF microscopy (Fig. 4A).

In order to rule out that the observed structural heterogeneity of the INO80 bound states for all tailless nucleosomes (in contrast to a homogenous bound state for wild-type nucleosomes) is caused by interactions with the surface of the flow chamber, to which the nucleosomes are bound, we repeated the experiments

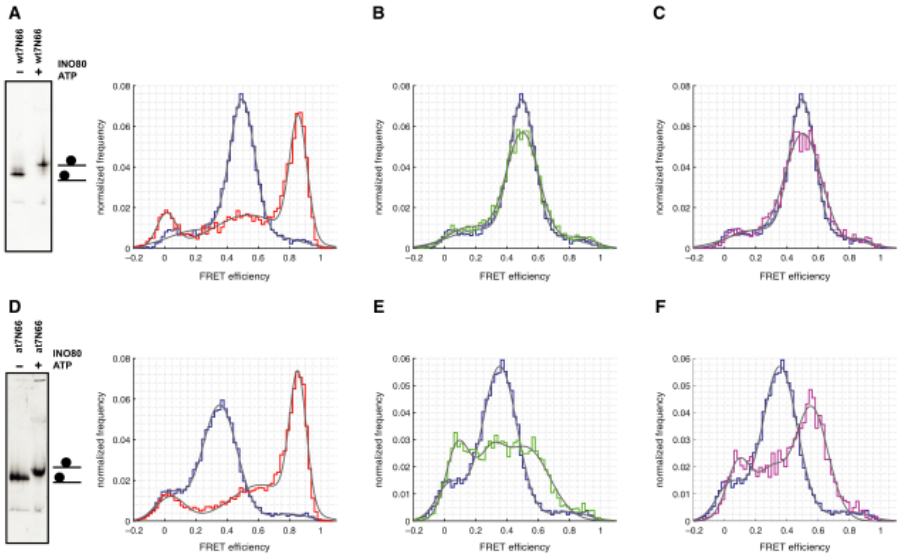

Fig. 4. Nucleosomes remodeled by the INO80 complex can be assigned to FRET efficiencies that are in agreement with biochemical knowledge on repositioned nucleosomes after competing off INO80 with excess DNA. (A) Native PAGE and confocal spectroscopy data of wild-type low FRET nucleosomes (wtLF, educt, blue) compared with repositioned nucleosome (product, red). (B) INO80 (39 nM) bound to wtLF (green), wtLF (blue) as in (A). (C) INO80 (156 nM) bound to wtLF (violet), wtLF (blue) as in (A). (D) Native PAGE and confocal spectroscopy data of all tailless low FRET nucleosomes (atLF, educt, blue) compared with repositioned nucleosome (product, red). (E) INO80 (39 nM) bound to atLF (green), atLF (blue) as in (D). (F) INO80 (156 nM) bound to atLF (violet), atLF (blue) as in (D). Fit results in Table S1. Red fluorescence readout of native PAGE is shown. Green fluorescence readout of the same gels in Fig. S4D,E, respectively.

using nucleosome-ADP-INO80 complexes freely diffusing through the focus of a confocal microscope (Materials and methods). The observed FRET efficiency histograms closely resemble that from the experiment of immobilized complexes (Figs 3B,E and 4B,E), respectively, thus establishing that the observed heterogeneity is a result of INO80 binding to all tailless nucleosomes. We hypothesize that this difference has functional importance (Discussion).

Moreover, the data for remodeled all tailless nucleosomes (Fig. 4D), tested for the new position on the DNA by native PAGE, are in agreement with the data for TIRF microscopy (Fig. 3F). After remodeling, the FRET population for the un-remodeled counterpart for the quenched nucleosomes has disappeared (almost) completely (Fig. 4D), emphasizing that the integrity of the nucleosomes is maintained during remodeling. In contrast to the described experiments (for wild-type and all tailless nucleosomes) using pre-bound INO80 complexes, remodeling is more complete in these experiments (Table S1, Fig. 4A,D, Fig. S4) and is also more complete in similar surface-based experiments (Fig. S3). Presumably, nucleosomes that are processively remodeled are bound by an active remodeler during the incubation period, while in other experimental scenarios, an active remodeling complex can bind to its substrate any point in time.

To quantify the agreement of expected FRET efficiencies with TIRF data and confocal spectroscopy data, we applied PDA to the confocal FRET (Materials and methods, Fig. S5, summarized in Table 1). The consistency of the model with both, confocal and TIRF data, highlights the precision of our study.

Discussion

Here, we report a single-molecule level assay for INO80, based on the relative movement of FRET labels on the nucleosome. We used this assay to address the influence of histone tails on nucleosome recognition and sliding by INO80.

We found that while binding wild-type and all tailless nucleosomes with equal affinity, the bound state of INO80 in the presence of ADP is homogenous for wild-type nucleosomes and heterogeneous for all tailless nucleosomes. When thinking about the mechano-chemical cycle of ATP-dependent nucleosome remodeling by INO80, nucleosome recognition and the bound state are part of the cycle and thus of functional importance. Previously, it had been shown that INO80 remodeling on all tailless nucleosomes is faster than for wild-type nucleosome [45] and that initiation of remodeling is functionally different from the continued remodeling reaction by INO80 [49]. More precisely, nicked nucleosome constructs have been reported to have a considerable effect on initiation of remodeling by INO80, but only have marginal effects on continued remodeling [49]. Based on these results and the data presented here, we conclude that the histone tails are a major regulatory barrier for INO80 nucleosome invasion. We, therefore, propose that for the case of all tailless nucleosomes, the energy landscape has been modified, so that multiple structural states of the nucleosome are populated due to a bound INO80 complex (Fig. 5). Interestingly, INO80 subunits that have been mapped to the periphery of the nucleosome free region like Arp8 and Ies5 [81] also crosslink to histone tails [42], suggesting that histone tail interactions possibly also constrain conformations of the bound INO80.

A consequence of this result is that the structurally heterogeneous INO80 bound state also possesses a lowered energy barrier for initiation of remodeling, thus giving a structural perspective for the previous biochemical results. The INO80 complex is considered to primarily monitor the nucleosome flanking DNA length [45,82] and the observed increase in remodeling

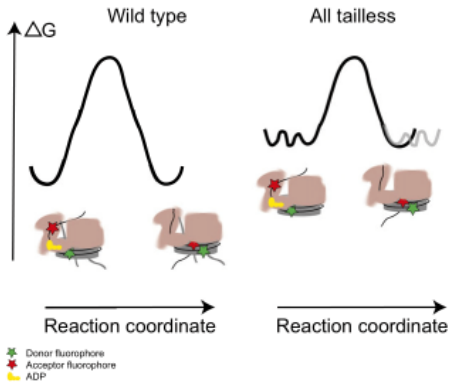

Fig. 5. Model for effect of histone tails on the initiation of INO80 remodeling. While INO80 binds with the same affinity to wild-type and all tailless nucleosomes, single-molecule FRET data show a homogenous bound state for wild-type nucleosomes and a heterogeneous distribution for all tailless nucleosomes. The INO80 complex repositions both, wild-type and all tailless nucleosomes, in a processive manner. We propose that the known faster nucleosome repositioning [45] for all tailless nucleosomes can be explained by the heterogeneity of bound states for the all tailless nucleosomes, which causes a lowered energy barrier (for details see text). For exact FRET label positions, we refer to Fig. 1C,D.

rate in the absence of histone tails is accompanied by an increased ATPase rate [45]. Thus, we assume that studying the INO80 complex activity in the absence of histone tails reports mainly on effects on the active site of the remodeler.

The limited number of available structural [70,83,84] and mechanistic studies on DNA translocation by the ATP-dependent nucleosome remodelers ISWI, Chd1, SWI/SNF, or of histone exchange by SWR1 [73,85–90] revealed a unique ATPase motor position around SHL2/-2. However, the underlying mechanism for INO80 might be different, as the Ino80-ATPase has been mapped near SHL-6 close to the DNA entry site of the nucleosome [49].

Another enzyme that, like the INO80 complex, invades the nucleosome from one side is RNA polymerase (RNAP) [91–93]. In the case of elongating RNAP II, it was shown that RNAP exploits brief nucleosomal fluctuations (partially unwrapped DNA) for transcribing through the nucleosome [93]. For tailless nucleosomes, significantly fewer and shorter pauses of transcription were reported [17,94], specifically at the DNA entry region of the nucleosome [17]. Therefore, the effect of the altered energy landscape for INO80 bound to all tailless nucleosomes likely resembles the situation for RNAP that has to overcome a barrier before passing through the nucleosome. Taken together, this barrier is more rigid in the presence of histone tails. Compared with INO80 remodeling, this notion goes along with the fact that for initiation of remodeling, torsional strain needs to build up [49] and an additional energy input might be required. In the light of our study, this raises the possibility that the reported increase of the rate of INO80-mediated nucleosome movement for histone tail deletion constructs [45] may be due to decreased nucleosome stability. This could lead to an improved accessibility of the ATPase motor to the translocation site or a smaller number of futile ATPase cycles for the all tailless nucleosomes.

Acknowledgements

We thank C. Roecker for discussions and help with Foerster Radius determination. We thank M. Fischer for protocols on single-molecule experiments. We thank D. Lamb (LMU Munich) for smFRET software sharing. We thank G. Laengst (University of Regensburg) for histone expression plasmids and 601 DNA amplification plasmids. MS and KS are supported by a DFG fellowship through the Graduate School of Quantitative Biosciences Munich (QBM). EK is supported by a scholarship for PhD students from the Carl-Zeiss-Stiftung. KPH acknowledges support from SFB1064, the European Research Council Advanced Grant ATMMACHINE and the Center for Integrated Protein Science (CIPSM). SE acknowledges support of a Long-term EMBO fellowship. JM acknowledges support from the ERC starting grant REMODELING and the Deutsche Forschungsgemeinschaft project MI749/4-1.

Author contributions

JM and KPH conceived and supervised the study; MS designed experiments; MS, KS, and MG performed experiments; SE established recombinant INO80; MM and SE purified INO80; MS, KS and EK analyzed data; SE helped with data interpretation; MS and JM wrote the manuscript with input from EK, SE, and KPH.

References

1 Flaus A, Martin DM, Barton GJ and Owen-Hughes T (2006) Identification of multiple distinct Snf2 subfamilies with conserved structural motifs. *Nucleic Acids Res* **34**, 2887–2905.
2 Narlikar GJ, Sundaramoorthy R and Owen-Hughes T (2013) Mechanisms and functions of ATP-dependent chromatin-remodeling enzymes. *Cell* **154**, 490–503.
3 Clapier CR, Iwasa J, Cairns BR and Peterson CL (2017) Mechanisms of action and regulation of ATP-dependent chromatin-remodelling complexes. *Nat Rev Mol Cell Biol* **18**, 407–422.
4 Singleton MR, Dillingham MS and Wigley DB (2007) Structure and mechanism of helicases and nucleic acid translocases. *Annu Rev Biochem* **76**, 23–50.
5 Clapier CR and Cairns BR (2009) The biology of chromatin remodeling complexes. *Annu Rev Biochem* **78**, 273–304.
6 Krietenstein N, Wal M, Watanabe S, Park B, Peterson CL, Pugh BF, Korber P (2016) Genomic nucleosome organization reconstituted with pure proteins. *Cell* **167**, 709–721.e12.
7 Makde RD, England JR, Yennawar HP and Tan S (2010) Structure of RCC1 chromatin factor bound to the nucleosome core particle. *Nature* **467**, 562–566.
8 Luger K (1997) Crystal structure of the nucleosome core particle at 2.8 A resolution. *Nature* **389**, 251–260.
9 Richmond TJ and Davey CA (2003) The structure of DNA in the nucleosome core. *Nature* **423**, 145–150.
10 Davey CA, Sargent DF, Luger K, Maeder AW and Richmond TJ (2002) Solvent mediated interactions in the structure of the nucleosome core particle at 1.9 a resolution. *J Mol Biol* **319**, 1097–1113.

11 Jenuwein T and Allis CD (2001) Translating the histone code. *Science* **293**, 1074–1080.
12 Strahl BD and Allis CD (2000) The language of covalent histone modifications. *Nature* **403**, 41–45.
13 Iwasaki W, Miya Y, Horikoshi N, Osakabe A, Taguchi H, Tachiwana H, Shibata T, Kagawa W and Kurumizaka H (2013) Contribution of histone N-terminal tails to the structure and stability of nucleosomes. *FEBS Open Bio* **3**, 363–369.
14 Ferreira H, Somers J, Webster R, Flaus A and Owen-Hughes T (2007) Histone tails and the H3 alphaN helix regulate nucleosome mobility and stability. *Mol Cell Biol* **27**, 4037–4048.
15 Hall MA, Shundrovsky A, Bai L, Fulbright RM, Lis JT and Wang MD (2009) High-resolution dynamic mapping of histone-DNA interactions in a nucleosome. *Nat Struct Mol Biol* **16**, 124–129.
16 Mihardja S, Spakowitz AJ, Zhang Y and Bustamante C (2006) Effect of force on mononucleosomal dynamics. *Proc Natl Acad Sci U S A* **103**, 15871–15876.
17 Bintu L, Ishibashi T, Dangkulwanich M, Wu YY, Lubkowska L, Kashlev M and Bustamante C (2012) Nucleosomal elements that control the topography of the barrier to transcription. *Cell* **151**, 738–749.
18 Lee JY, Wei S and Lee TH (2011) Effects of histone acetylation by Piccolo NuA4 on the structure of a nucleosome and the interactions between two nucleosomes. *J Biol Chem* **286**, 11099–11109.
19 Buning R and van Noort J (2010) Single-pair FRET experiments on nucleosome conformational dynamics. *Biochimie* **92**, 1729–1740.
20 Gansen A, Tóth K, Schwarz N and Langowski J (2009) Structural variability of nucleosomes detected by single-pair Forster resonance energy transfer: histone acetylation, sequence variation, and salt effects. *J Phys Chem B* **113**, 2604–2613.
21 Neumann H, Hancock SM, Buning R, Routh A, Chapman L, Somers J, Owen-Hughes T, van Noort J, Rhodes D and Chin JW (2009) A method for genetically installing site-specific acetylation in recombinant histones defines the effects of H3 K56 acetylation. *Mol Cell* **36**, 153–163.
22 Di Cerbo V, Mohn F, Ryan DP, Montellier E, Kacem S, Tropberger P, Kallis E, Holzner M, Hoerner L, Feldmann A *et al.* (2014) Acetylation of histone H3 at lysine 64 regulates nucleosome dynamics and facilitates transcription. *Elife* **3**, e01632.
23 Bönisch C, Schneider K, Pünzeler S, Wiedemann SM, Bielmeier C, Bocola M, Eberl HC, Kuegel W, Neumann J, Kremmer E *et al.* (2012) H2A.Z.2.2 is an alternatively spliced histone H2A.Z variant that causes severe nucleosome destabilization. *Nucleic Acids Res* **40**, 5951–5964.
24 Lowary PT and Widom J (1998) New DNA sequence rules for high affinity binding to histone octamer and sequence-directed nucleosome positioning. *J Mol Biol* **276**, 19–42.
25 Tóth K, Böhm V, Sellmann C, Danner M, Hanne J, Berg M, Barz I, Gansen A and Langowski J (2013) Histone- and DNA sequence-dependent stability of nucleosomes studied by single-pair FRET. *Cytometry A* **83**, 839–846.
26 Ngo TT, Zhang Q, Zhou R, Yodh JG and Ha T (2015) Asymmetric unwrapping of nucleosomes under tension directed by DNA local flexibility. *Cell* **160**, 1135–1144.
27 Qiu Y, Levendosky RF, Chakravarthy S, Patel A, Bowman GD and Myong S (2017) The Chd1 chromatin remodeler shifts nucleosomal DNA bidirectionally as a monomer. *Mol Cell* **68**, 76–88.
28 Deindl S, Hwang WL, Hota SK, Blosser TR, Prasad P, Bartholomew B and Zhuang X (2013) ISWI remodelers slide nucleosomes with coordinated multi-base-pair entry steps and single-base-pair exit steps. *Cell* **152**, 442–452.
29 Blosser TR, Yang JG, Stone MD, Narlikar GJ and Zhuang X (2009) Dynamics of nucleosome remodelling by individual ACF complexes. *Nature* **462**, 1022–1027.
30 Harada BT, Hwang WL, Deindl S, Chatterjee N, Bartholomew B and Zhuang X (2016) Stepwise nucleosome translocation by RSC remodeling complexes. *Elife* **5**, e10051.
31 Sirinakis G, Clapier CR, Gao Y, Viswanathan R, Cairns BR and Zhang Y (2011) The RSC chromatin remodelling ATPase translocates DNA with high force and small step size. *EMBO J* **30**, 2364–2372.
32 Hopfner KP and Michaelis J (2007) Mechanisms of nucleic acid translocases: lessons from structural biology and single-molecule biophysics. *Curr Opin Struct Biol* **17**, 87–95.
33 Conaway RC and Conaway JW (2009) The INO80 chromatin remodeling complex in transcription, replication and repair. *Trends Biochem Sci* **34**, 71–77.
34 Lafon A, Taranum S, Pietrocola F, Dingli F, Loew D, Brahma S, Bartholomew B and Papamichos-Chronakis M (2015) INO80 chromatin remodeler facilitates release of RNA polymerase II from chromatin for ubiquitin-mediated proteasomal degradation. *Mol Cell* **60**, 784–796.
35 Poli J, Gerhold CB, Tosi A, Hustedt N, Seeber A, Sack R, Herzog F, Pasero P, Shimada K, Hopfner KP *et al.* (2016) Mec 1, INO80, and the PAF1 complex cooperate to limit transcription replication conflicts through RNAPII removal during replication stress. *Genes Dev* **30**, 337–354.
36 Ebbert R, Birkmann A and Schueller H-J (1999) The product of the SNF2/SWI2 paralogue INO80 of *Saccharomyces cerevisiae* required for efficient expression of various yeast structural genes is part of a high-molecular-weight protein complex. *Mol Microbiol* **32**, 741–751.

37 Neuman SD, Ihry RJ, Gruetzmacher KM and Bashirullah A (2014) INO80-dependent regression of ecdysone-induced transcriptional responses regulates developmental timing in Drosophila. *Dev Biol* **387**, 229–239.
38 Morrison AJ, Highland J, Krogan NJ, Arbel-Eden A, Greenblatt JF, Haber JE and Shen X (2004) INO80 and gamma-H2AX interaction links ATP-dependent chromatin remodeling to DNA damage repair. *Cell* **119**, 767–775.
39 van Attikum H, Fritsch O, Hohn B and Gasser SM (2004) Recruitment of the INO80 complex by H2A phosphorylation links ATP-dependent chromatin remodeling with DNA double-strand break repair. *Cell* **119**, 777–788.
40 Vassileva I, Yanakieva I, Peycheva M, Gospodinov A and Anachkova B (2014) The mammalian INO80 chromatin remodeling complex is required for replication stress recovery. *Nucleic Acids Res* **42**, 9074–9086.
41 Papamichos-Chronakis M and Peterson CL (2008) The Ino80 chromatin-remodeling enzyme regulates replisome function and stability. *Nat Struct Mol Biol* **15**, 338–345.
42 Tosi A, Haas C, Herzog F, Gilmozzi A, Berninghausen O, Ungewickell C, Gerhold CB, Lakomek K, Aebersold R, Beckmann R *et al.* (2013) Structure and subunit topology of the INO80 chromatin remodeler and its nucleosome complex. *Cell* **154**, 1207–1219.
43 Watanabe S, Tan D, Lakshminarasimhan M, Washburn MP, Hong EJ, Walz T and Peterson CL (2015) Structural analyses of the chromatin remodelling enzymes INO80-C and SWR-C. *Nat Commun* **6**, 7108.
44 Shen X, Ranallo R, Choi E and Wu C (2003) Involvement of actin-related proteins in ATP-dependent chromatin remodeling. *Mol Cell* **12**, 147–155.
45 Udugama M, Sabri A and Bartholomew B (2011) The INO80 ATP-dependent chromatin remodeling complex is a nucleosome *spacing factor*. *Mol Cell Biol* **31**, 662–673.
46 Wang F, Ranjan A, Wei D and Wu C (2016) Comment on "A histone acetylation switch regulates H2A.Z deposition by the SWR-C remodeling enzyme". *Science* **353**, 358.
47 Watanabe S and Peterson CL (2016) Response to Comment on "A histone acetylation switch regulates H2A.Z deposition by the SWR-C remodeling enzyme". *Science* **353**, 358.
48 Watanabe S, Radman-Livaja M, Rando OJ and Peterson CL (2013) A histone acetylation switch regulates H2A.Z deposition by the SWR-C remodeling enzyme. *Science* **340**, 195–199.
49 Brahma S, Udugama MI, Kim J, Hada A, Bhardwaj SK, Hailu SG, Lee TH and Bartholomew B (2017) INO80 exchanges H2A.Z for H2A by translocating on DNA proximal to histone dimers. *Nat Commun* **8**, 15616.
50 Sinha KK, Gross JD and Narlikar GJ (2017) Distortion of histone octamer core promotes nucleosome mobilization by a chromatin remodeler. *Science* **355**, eaaa3761.
51 Dyer PN, Edayathumangalam RS, White CL, Bao Y, Chakravarthy S, Muthurajan UM and Luger K (2004) Reconstitution of nucleosome core particles from recombinant histones and DNA. *Methods Enzymol* **375**, 23–44.
52 Klinker H, Haas C, Harrer N, Becker PB and Mueller-Planitz F (2014) Rapid purification of recombinant histones. *PLoS One* **9**, e104029.
53 Gasteiger E, Hoogland C, Gattiker A, Duvaud S, Wilkins MR, Appel RD and Bairoch A (2005) Protein identification and analysis tools on the ExPASy server. In The Proteomics Protocols Handbook (Walker JM, ed.), pp. 571–607. Humana Press, New York, NY.
54 Schneider CA, Rasband WS and Eliceiri KW (2012) NIH Image to ImageJ: 25 years of image analysis. *Nat Methods* **9**, 671–675.
55 Dörfler T, Eilert T, Röcker C, Nagy J and Michaelis J (2017) Structural information from single-molecule FRET experiments using the Fast Nano-Positioning System. *J Vis Exp*, https://doi.org/10.3791/54782
56 Heiss GJ (2011). Single-molecule microscopy study of nano-systems: from synthetic photo-switchable nano-devices to the dynamics of naturally occurring transcription factors. Dissertation, Ludwig-Maximilians-Universität München, München.
57 Kudryavtsev V, Sikor M, Kalinin S, Mokranjac D, Seidel CA and Lamb DC (2012) Combining MFD and PIE for accurate single-pair Forster resonance energy transfer measurements. *ChemPhysChem* **13**, 1060–1078.
58 Nir E, Michalet X, Hamadani KM, Laurence TA, Neuhauser D, Kovchegov Y and Weiss S (2006) Shot-noise limited single-molecule FRET histograms: comparison between theory and experiments. *J Phys Chem B* **110**, 22103–22124.
59 Antonik M, Felekyan S, Gaiduk A and Seidel CA (2006) Separating structural heterogeneities from stochastic variations in fluorescence resonance energy transfer distributions via photon distribution analysis. *J Phys Chem B* **110**, 6970–6978.
60 Vasudevan D, Chua EY and Davey CA (2010) Crystal structures of nucleosome core particles containing the '601' strong positioning sequence. *J Mol Biol* **403**, 1–10.
61 Kalinin S, Peulen T, Sindbert S, Rothwell PJ, Berger S, Restle T, Goody RS, Gohlke H and Seidel CA (2012) A toolkit and benchmark study for FRET-restrained high-precision structural modeling. *Nat Methods* **9**, 1218–1225.

62 Dixon JM, Taniguchi M and Lindsey JS (2005) PhotochemCAD 2: a refined program with accompanying spectral databases for photochemical calculations. *Photochem Photobiol* **81**, 212–213.
63 Eilert T, Beckers M, Drechsler F and Michaelis J (2017) Fast-NPS-A Markov Chain Monte Carlo-based analysis tool to obtain structural information from single-molecule FRET measurements. *Comput Phys Commun* **219**, 377–389.
64 Akey CW and Luger K (2003) Histone chaperones and nucleosome assembly. *Curr Opin Struct Biol* **13**, 6–14.
65 Levendosky RF, Sabantsev A, Deindl S and Bowman GD (2016) The Chd1 chromatin remodeler shifts hexasomes unidirectionally. *Elife* **5**, e21356.
66 Huynh VA, Robinson PJ and Rhodes D (2005) A method for the in vitro reconstitution of a defined "30 nm" chromatin fibre containing stoichiometric amounts of the linker histone. *J Mol Biol* **345**, 957–968.
67 Frouws TD, Barth PD and Richmond TJ (2017) Site-specific disulfide crosslinked nucleosomes with enhanced stability. *J Mol Biol* **430**, 45–57.
68 Kato D, Osakabe A, Arimura Y, Mizukami Y, Horikoshi N, Saikusa K, Akashi S, Nishimura Y, Park SY, Nogami J *et al.* (2017) Crystal structure of the overlapping dinucleosome composed of hexasome and octasome. *Science* **356**, 205–208.
69 Treutlein B. (2012). Mechanisms of eukaryotic gene expression on a single molecule level: from transcription initiation to nucleosome remodeling. Dissertation, Ludwig-Maximilians-Universitaet Muenchen, München.
70 Sundaramoorthy R, Hughes AL, Singh V, Wiechens N, Ryan DP, El-Mkami H, Petoukhov M, Svergun DI, Treutlein B, Quack S *et al.* (2017) Structural reorganization of the chromatin remodeling enzyme Chd1 upon engagement with nucleosomes. *Elife* **6**, e22510.
71 Dimura M, Peulen TO, Hanke CA, Prakash A, Gohlke H and Seidel CA (2016) Quantitative FRET studies and integrative modeling unravel the structure and dynamics of biomolecular systems. *Curr Opin Struct Biol* **40**, 163–185.
72 McGinty RK and Tan S (2015) Nucleosome structure and function. *Chem Rev* **115**, 2255–2273.
73 Schwanbeck R, Xiao H and Wu C (2004) Spatial contacts and nucleosome step movements induced by the NURF chromatin remodeling complex. *J Biol Chem* **279**, 39933–39941.
74 Gerhold CB, Winkler DD, Lakomek K, Seifert FU, Fenn S, Kessler B, Witte G, Luger K and Hopfner KP (2012) Structure of Actin-related protein 8 and its contribution to nucleosome binding. *Nucleic Acids Res* **40**, 11036–11046.
75 Ray S and Grove A (2012) Interaction of *Saccharomyces cerevisiae* HMO2 domains with distorted DNA. *Biochemistry* **51**, 1825–1835.
76 Lakomek K, Stoehr G, Tosi A, Schmailzl M and Hopfner KP (2015) Structural basis for dodecameric assembly states and conformational plasticity of the full-length AAA+ ATPases Rvb1. Rvb2. *Structure* **23**, 483–495.
77 Li G, Levitus M, Bustamante C and Widom J (2005) Rapid spontaneous accessibility of nucleosomal DNA. *Nat Struct Mol Biol* **12**, 46–53.
78 Koopmans WJ, Brehm A, Logie C, Schmidt T and Van Noort J (2007) Single-pair FRET microscopy reveals mononucleosome dynamics. *J Fluoresc* **17**, 785–795.
79 Böhm V, Hieb AR, Andrews AJ, Gansen A, Rocker A, Tóth K, Luger K and Langowski J (2011) Nucleosome accessibility governed by the dimer/tetramer interface. *Nucleic Acids Res* **39**, 3093–3102.
80 Ngo TT and Ha T (2015) Nucleosomes undergo slow spontaneous gaping. *Nucleic Acids Res* **43**, 3964–3971.
81 Yen K, Vinayachandran V and Pugh BF (2013) SWR-C and INO80 chromatin remodelers recognize nucleosome-free regions near +1 nucleosomes. *Cell* **154**, 1246–1256.
82 Willhoft O, McCormack EA, Aramayo RJ, Bythell-Douglas R, Ocloo L, Zhang X and Wigley DB (2017) Crosstalk within a functional INO80 complex dimer regulates nucleosome sliding. *Elife* **6**, e25782. https://doi.org/10.7554/eLife.25782
83 Farnung L, Vos SM, Wigge C and Cramer P (2017) Nucleosome-Chd1 structure and implications for chromatin remodelling. *Nature* **550**, 539.
84 Liu X, Li M, Xia X, Li X and Chen Z (2017) Mechanism of chromatin remodelling revealed by the Snf2-nucleosome structure. *Nature* **544**, 440–445.
85 Zofall M, Persinger J, Kassabov SR and Bartholomew B (2006) Chromatin remodeling by ISW2 and SWI/SNF requires DNA translocation inside the nucleosome. *Nat Struct Mol Biol* **13**, 339–346.
86 Saha A, Wittmeyer J and Cairns BR (2005) Chromatin remodeling through directional DNA translocation from an internal nucleosomal site. *Nat Struct Mol Biol* **12**, 747–755.
87 Nodelman IM, Bleichert F, Patel A, Ren R, Horvath KC, Berger JM and Bowman GD (2017) Interdomain communication of the Chd1 chromatin remodeler across the DNA gyres of the nucleosome. *Mol Cell* **65**, 447–459.
88 Dechassa ML, Hota SK, Sen P, Chatterjee N, Prasad P and Bartholomew B (2012) Disparity in the DNA translocase domains of SWI/SNF and ISW2. *Nucleic Acids Res* **40**, 4412–4421.
89 McKnight JN, Jenkins KR, Nodelman IM, Escobar T and Bowman GD (2011) Extranucleosomal DNA binding directs nucleosome sliding by Chd1. *Mol Cell Biol* **31**, 4746–4759.
90 Ranjan A, Wang F, Mizuguchi G, Wei D, Huang Y and Wu C (2015) H2A histone-fold and DNA elements

in nucleosome activate SWR1-mediated H2A.Z replacement in budding yeast. *Elife* **4**, e06845.
91 Chang HW, Kulaeva OI, Shaytan AK, Kibanov M, Kuznedelov K, Severinov KV, Kirpichnikov MP, Clark DJ and Studitsky VM (2014) Analysis of the mechanism of nucleosome survival during transcription. *Nucleic Acids Res* **42**, 1619–1627.
92 Kulaeva OI, Hsieh FK, Chang HW, Luse DS and Studitsky VM (2013) Mechanism of transcription through a nucleosome by RNA polymerase II. *Biochim Biophys Acta* **1829**, 76–83.
93 Hodges C, Bintu L, Lubkowska L, Kashlev M and Bustamante C (2009) Nucleosomal fluctuations govern the transcription dynamics of RNA polymerase II. *Science* **325**, 626–628.
94 Újvári A, Hsieh FK, Luse SW, Studitsky VM and Luse DS (2008) Histone N-terminal tails interfere with nucleosome traversal by RNA polymerase II. *J Biol Chem* **283**, 32236–32243.
95 Vasudevan D, Chua EYD and Davey CA (2010) Crystal structures of nucleosome core particles containing the '601' strong positioning sequence. *J Mol Biol* **403**, 1–10.

Supporting information

Additional Supporting Information may be found online in the supporting information tab for this article:

Fig. S1. Homogenous nucleosome sample preparation for single-molecule FRET.
Fig. S2. The INO80 complex binds wild-type and all tailless nucleosomes with equal affinity.
Fig. S3. Remodeled TIRF microscopy data after Apyrase quenching compared to unquenched remodeling reactions.
Fig. S4. Nucleosomes remodeled by the INO80 complex are in agreement with biochemical knowledge on repositioned nucleosomes also for high FRET constructs.
Fig. S5. Inter-dye distances for nucleosomes before and after remodeling by the INO80 complex can be extracted by probability distribution analysis.
Fig. S6. Examples for dynamic fluorescence time trajectories and real-time smFRET efficiency changes of double-labeled nucleosomes (wild-type (wt) and all tailless (at) low FRET (LF) construct) for datasets taken in different conditions as indicated.
Doc. S1. Materials and methods.
Table S1. Gaussian distribution fit results for Figures 3, S3 and 4, S4 and Figure S5.
Table S2. Preparative DNA sequences as described in Materials and methods.
Table S3. Histone protein sequences; amino acids comprising the globular regions are highlighted in red.

5 Discussion

The results presented in this thesis reveal how the subunits of INO80 interact with the NCP and catalyze DNA translocation in a coordinated fashion[386,387]. While it was conducted, cryo-EM structures of all four remodeller families in apo[348,388,389] and nucleosome bound states[220,347,353,390-396] were published (Fig. 9). This section compares these structures and discusses their impact on understanding the mechanism by which remodellers catalyze DNA translocation.

5.1 Comparison of cryo-EM structures of the four families of chromatin remodellers

First insights into the mechanism of DNA translocation by Snf2-type ATPases were provided by cryo-EM structures of the ATPase domain of Swi2/Snf2 bound to the nucleosome[345,346]. It interacts with either SHL ±2 or SHL ±6[345] and all chromatin remodelling Snf2-type ATPases characterized to date bind the nucleosome at these locations (Fig. 9)[1]. Histone-DNA contacts are significantly weaker at these points compared to the dyad and the regions between SHL ±3.5 and SHL ±5[70]. Thus binding to these locations potentially facilitates the catalysis of DNA translocation[70]. The interaction of Swi2/Snf2 with nucleosomal DNA distorts primarily the tracking strand by bulging out 1 bp of DNA around its binding site[346]. This leads to a register shift of 1 bp relative to the guide strand, which is slightly relaxed upon ATP binding (see 2.2.2)[346]. As this is similarly observed for the Isw1 ATPase, this mechanism is most probably conserved among chromatin remodelling Snf2-type ATPases and illustrates their fundamental catalyzed reaction, which is the pumping of 1 bp of DNA[155,347]. Two ISWI ATPases have been characterized in complex with the nucleosome so far; Isw1 from *Saccharomyces cerevisiae*[347] and Snf2h from *Homo sapiens* (Fig 9a)[390]. Both bind to SHL -2 and interact with the H4 tail via their C-lobe, which regulates ISWI activity[196,347,390]. Snf2h is reported to change the structure of the histone octamer upon binding, which is proposed to contribute to the translocation reaction[390]. However, this was not observed for Isw1 or for any other remodeller with sliding activity[347]. Hydroxyl radical footprinting of the ISW2-nucleosome complex demonstrates that the remodeller binds entry and extranucleosomal DNA in addition to the interaction of the ATPase domain with SHL -2[397].

The cryo-EM structure of Chd1 provides high resolution information beyond the catalytic domain[220]. Its ATPase domain also interacts with SHL -2 while its double chromodomain contacts SHL -1 (Fig. 9b)[220,396]. The DBD of Chd1, composed of a SANT and SLIDE domain, binds to SHL +5 – SHL +7, where it unravels exit DNA from the histone octamer[220,396]. Single-molecule data suggests that this is dependent on the nucleotide-state of the ATPase[398].

High-resolution information on SWI/SNF and INO80 remodellers increased considerably in the past years. In particular, subunits interacting with the NCP have been identified and visualized for a number of remodellers (Fig. 9c, d)[353,387,389,391-395]. The ATPases of all SWI/SNF remodellers bind to SHL -2 or nearby in an overall similar fashion as remodellers of the ISWI and CHD family (Fig. 9c)[391-394]. Among all remodeller ATPases, Swi2/Snf2 is the only one to form two brace helices in its nucleosome-bound state (see 2.2.2)[345,391]. Different binding sites of the ATPase

[1]As the nucleosome is a symmetric particle, the assignment of a positive or negative sign to a SHL is arbitrary in the first place but becomes important when describing the directed process of DNA translocation. It is differently used in the literature. In this thesis, a negative sign denotes SHLs in the direction of entry DNA and a positive sign SHLs in the direction of exit DNA. Thus, the specified signs might mismatch those given in other publications but is consistent with the numbering in the publications presented in this thesis.

domains are observed in the INO80 family. Swr1^{ATPase} binds to SHL -2 like the ATPases from the other remodeller families[295,353] but Ino80^{ATPase} interacts with SHL -6 (Fig. 9d)[387,395]. Hence it is the only Snf2-type ATPase known to date to contact SHL -6 in the context of a complete remodeller[387,395].

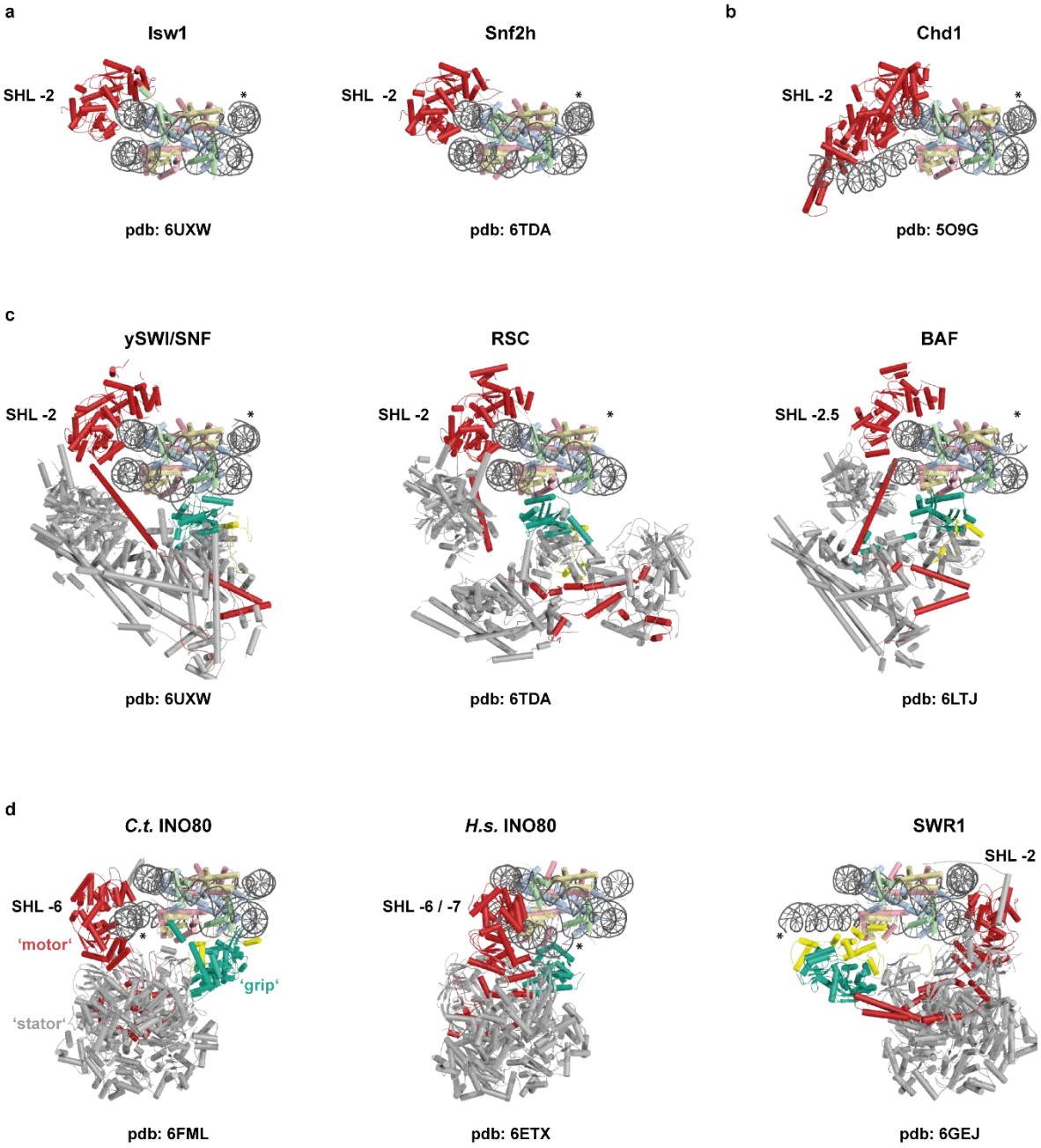

Figure 9: 3D structures of remodellers bound to the nucleosome determined by cryo-EM. a, ISWI family. **b,** CHD family. **c,** SWI/SNF family. **d,** INO80 family. *C.t.*: *Chaetomium thermophilum*; *H.s.*: *Homo sapiens*. Models are aligned on the nucleosome. Asterisk indicates entry DNA. Binding site of each ATPase is indicated as well as pdb code of the models. Deep red: Snf2-type ATPase; Green/Yellow: Potential or characterized counter grips of multi-subunit remodellers; Grey: other subunits; Dark grey: DNA; Light yellow: H2A; Light red: H2B; Light blue: H3; Light green: H4. Figure adapted from[399].

The different position of Ino80^{ATPase} compared to other remodeller ATPases affects the path of DNA translocation. In the INO80 complex, the ATPase interacts with the entry site of the nucleosome and hence pumps extranucleosomal DNA into the NCP (Fig. 10a)[387,395]. All other ATPases are located more centrally at the NCP around SHL -2 (Fig. 9)[220,347,390-394]. Consequently,

they first pull DNA into the NCP and push it across the dyad towards the exit site to translocate DNA (Fig. 10b).

Besides their ATPase domains, all multi-subunit remodellers contact the NCP at a second point[353,387,391-395]. For INO80, this interaction is formed by Arp5 and Ies6 opposite from Ino80^{ATPase} and is essential for the catalysis of DNA translocation[387]. It was termed 'counter grip' in a model, which denotes the ATPase as a motor and Rvb1/2 as a stator connecting motor and counter grip (Fig. 9d, left panel)[387]. This principal arrangement holds also true for human INO80 and SWR1 (Fig. 9d)[353,395]. SWI/SNF remodellers interact with the nucleosome at an additional site as well[391-394]. Different to the INO80 family, this contact is not formed to nucleosomal DNA but to the histone octamer around the acidic patch (Fig. 9c; 2.1.1.2)[391-394]. In ySWI/SNF and RSC, the subunits forming this contact are called arm module[391,392] and in the BAF complex head module, a submodule of the base module[393]. These are all recruited by the pre-HSA domain of SWI/SNF remodellers (Fig. 9c)[391-394]. The pre-HSA domain and associated subunits might thus act as a stator element, similar to the complex of Ino80^{insert} and Rvb1/2 in the INO80 complex (Fig. 9d, left panel)[387]. The function of the counter grip in SWI/SNF remodellers is less well understood, but data from RSC indicates that it might rather be important for nucleosome ejection than sliding[394].

Another feature observed in several cryo-EM structures of NCP-bound remodellers is the detachment of nucleosomal DNA. INO80 and SWR1 unravel DNA at the entry site of the NCP and Chd1 at its exit site (Fig. 9b, d)[220,353,387,395]. To a smaller extent, exit DNA is also detached by ySWI/SNF and RSC[391,392]. This could be a common principle of remodellers to reduce friction by histone-DNA contacts during DNA translocation[353].

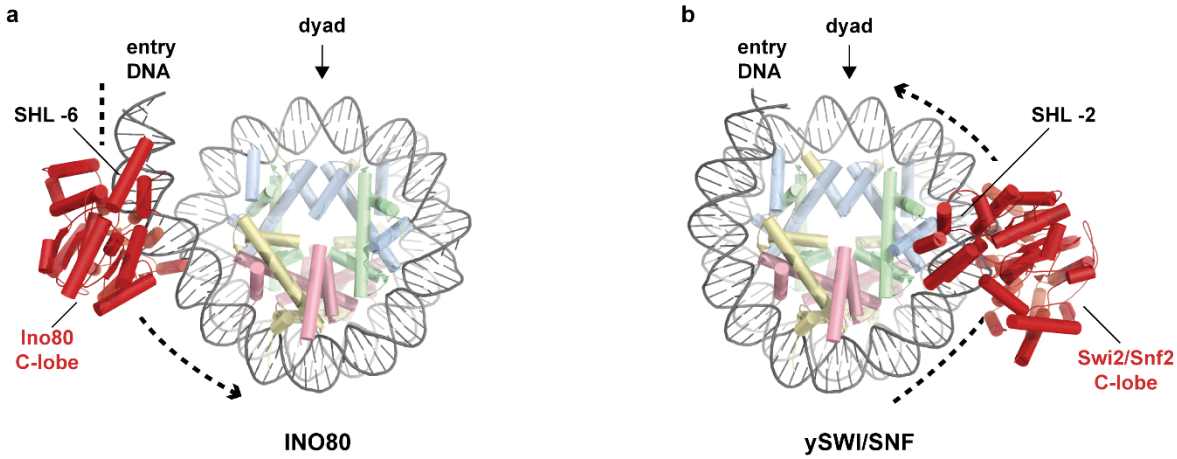

Figure 10: Direction of DNA translocation in INO80 (left) and ySWI/SNF (right). a, The Ino80^{ATPase} binds to SHL -6 and detaches DNA from the histone octamer leading to an exposed H2A-H2B dimer. It pumps extranucleosomal DNA into the nucleosome towards the dyad. pdb code: 6FML[387]. **b,** Swi2/Snf2 as a representative for all Snf2-type ATPases apart from Ino80. It interacts with SHL -2 and introduces a distortion in nucleosomal DNA upstream of its binding site[346]. It pulls DNA into the nucleosome and pumps it across the dyad towards the exit site. pdb code: 6UXW[391]. Path of translocated DNA is indicated by dashed line. Deep red: Snf2-type ATPase; Dark grey: DNA; Light yellow: H2A; Light red: H2B; Light blue: H3; Light green: H4. Figure in parts adapted from[346].

5.2 The architecture of INO80 and SWR1

The SWR1 complex is specialized in nucleosome editing[188,274]. It exchanges H2A-H2B dimers for H2A.Z-H2B dimers in an ATP-dependent manner but does not display nucleosome sliding activity[188]. However, the underlying force for the editing reaction is presumably provided by local and transient DNA translocation[188,400]. The interaction of Swr1^{ATPase} with SHL -2 leads to a mirrored arrangement compared to INO80 (Fig. 9d)[387,395]. Its counter grip is formed by Arp6 and Swc6 and binds to SHL -6, which corresponds to entry DNA (Fig. 9d, Fig. 11b)[353,387,395]. At this site, it detaches DNA from the histone octamer in an overall similar fashion as Ino80^{ATPase}

(Fig. 9d)[353]. But unlike INO80, the main DNA-interacting subunit is not the ARP component (Arp5 in INO80 and Arp6 in SWR1) but Swc6, the SWR1 equivalent of Ies6 (Fig. 11)[353,387]. In INO80 and SWR1, both subunits of the heterodimeric counter grip are anchored in the Rvb1/2 ring by contacts to the OB folds[353,387,395]. Swc6 additionally extends between one Rvb1/2 pair with its N-terminal tail and binds to one H2A chain[353]. Ies6 contacts H2A too, but to a reduced extent[387]. These interactions might contribute to the exchange reactions catalyzed by INO80 and SWR1.

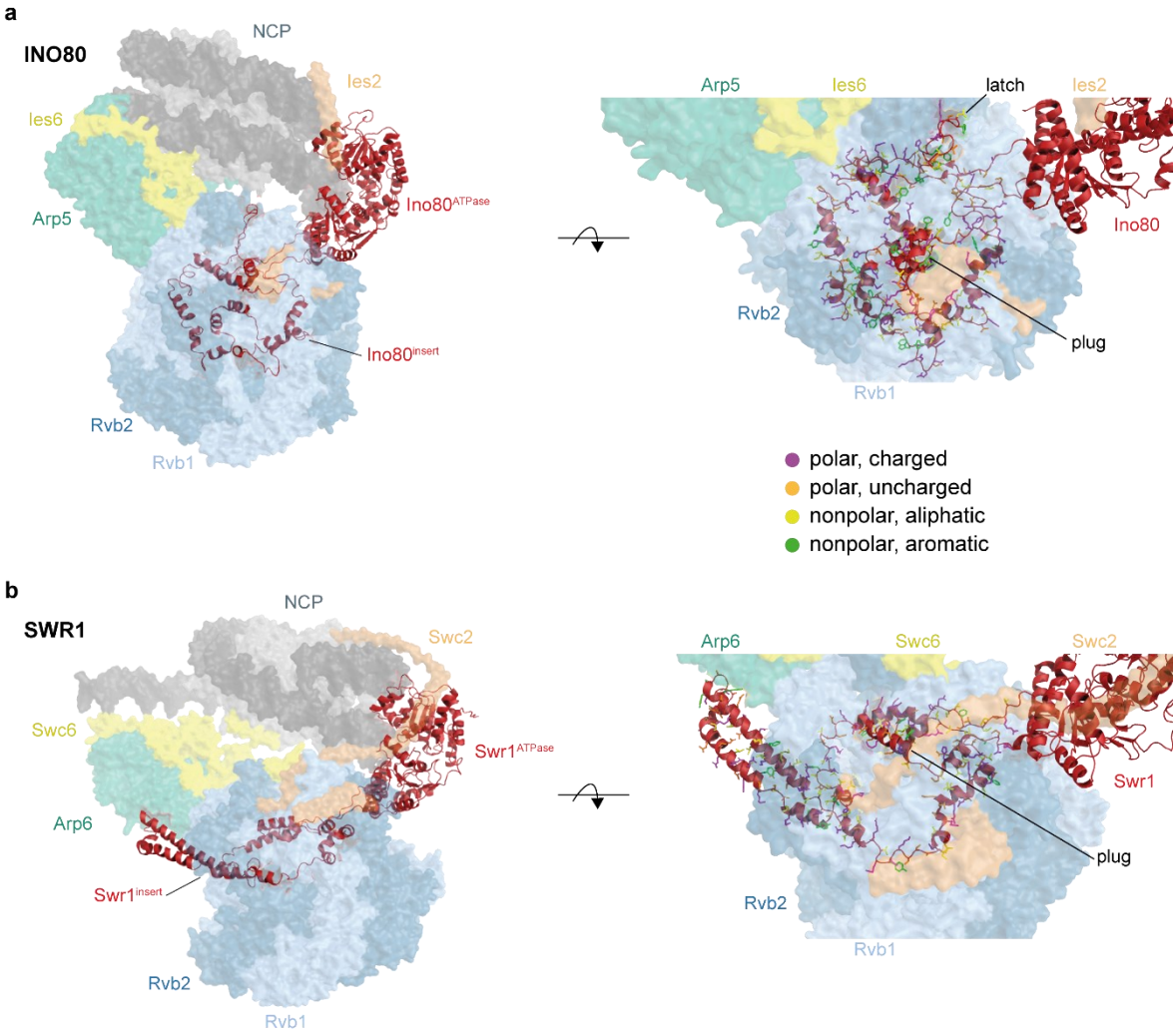

Figure 11: Comparison of the 3D structures of the remodelling complexes INO80 and SWR1. a, Structure of the INO80 complex. Light blue: Rvb1; Deep blue: Rvb2; Green: Arp5; Yellow: Ies6; Red: Ino80; Orange: Ies2; Dark grey: DNA; Grey: histone octamer. pdb code: 6FML[387]. **b,** Structure of the SWR1 complex. Light blue: Rvb1; Deep blue: Rvb2; Green: Arp6; Yellow: Swc6; Red: Swr1; Orange: Swc2; Dark grey: DNA; Grey: histone octamer. pdb code: 6GEJ[353]. Subunits are represented as transparent surface except for Ino80 / Swr1, which are shown as cartoon. Side chains of amino acids of the insert domains of Ino80 and Swr1 are shown as sticks in the right panel and color coded according to their chemical properties (see table in figure). Models of INO80 and SWR1 are aligned on their ATPase domains.

Ies2 in INO80 and Swc2 in SWR1 possess an overall similar 3D structure[353,387]. Both are anchored in the Rvb1/2 ring with their C-terminus, interact with the respective ATPase via an α-helix (termed 'throttle helix' in INO80) and form histone contacts distal to the Rvb1/2 ring including an interaction with the acidic patch (Fig. 11)[353,387]. Swc2 is the subunit with histone chaperone activity in SWR1 and essential for the catalysis of the exchange of H2A for H2A.Z[294,296]. The function of Ies2 is less well understood. It was suggested to clear an auto-inhibitory state of Ino80^{ATPase}, hence its characterization as a molecular throttle[278]. Given the close relationship in structure, it is tempting to speculate that Ies2 might act similarly to Swc2

in the exchange of H2A.Z for H2A catalyzed by INO80. However, whether INO80 can even carry out this reaction is discussed controversially and no activity as a histone chaperone has so far been described for Ies2[300-303]. The N-terminal portion of both proteins is not resolved in the currently published structures, most likely due to intrinsic disorder of these regions[276,353,387]. According to cross-linking data, the N-terminus of Ies2 interacts with the species-specific Nhp10 module[276]. Since this was not included in the samples characterized by cryo-EM so far, no structural insights in this interaction are available[387,395]. Adding the module in future samples might provide a way to stabilize and visualize this part of Ies2 and assign a function to it.

The subunits of Rvb1 and Rvb2 are all found in ADP-bound states in the published cryo-EM structures of INO80 and SWR1[353,387,395]. The heterohexameric ring is in a closed conformation compared to crystal structures of the isolated Rvb1/2 ring, in which the insert domains (DII) are bent outwards relative to the ATPase core (DI + DIII)[352]. As this open arrangement of the isolated Rvb1/2 ring is adopted independent of the nucleotide state, the closure observed in the remodelling complexes is likely to be induced by the interaction with the insert domains of Ino80 and Swr1[352,353,387,395]. This is supported by the observation that peptides of Ino80^{insert} stimulate the ATPase activity of Rvb1/2[354], strongly indicating that ATP hydrolysis by these AAA+ ATPases is important for the biogenesis of remodellers of the INO80 family. This would support the concept of Rvb1/2 acting as assembly chaperones[354]. The insert domains of Ino80 and Swr1 are similar in length but only 15% identical in sequence[401]. This causes differential interactions with the Rvb1/2 ring resulting in distinct 3D structures (Fig. 11)[353,387,388,395]. Both insert domains are planar and adopt a wheel-like structure[353,387,388,395]. Ino80^{insert} resembles a spoked wheel with several connections toward its center while Swr1^{insert} lacks these elements (Fig. 11)[353,387,388,395]. In the INO80 complex, Ino80^{insert} is almost entirely encapsulated by the Rvb1/2 ring and forms a plug and latch, which protrude the ring in the direction of the NCP (Fig. 11a)[387,395]. Swr1^{insert} contains a similar plug helix, but no latch and overall less residues are buried in the Rvb1/2 ring[353]. Instead, two α-helices jut out the ring opposite of Swr1^{ATPase} where they are exposed to solvent and interact with an insertion of Arp6 (Fig. 11b)[353]. The function of this interaction is not known but it might stabilize the more tilted position of Arp6 in SWR1 relative to the Rvb1/2 ring compared to Arp5 in INO80 due to its interaction with unraveled entry DNA.

5.3 The Arp module in INO80 and SWI/SNF remodellers

Remodellers of the SWI/SNF and INO80 family comprise actin and / or ARPs as integral components[188,267,273-275]. These are nucleated by the HSA domain, which precedes the Snf2-type ATPase thereby giving rise to a distinct module within each complex[238]. In SWI/SNF remodellers, this is formed by a heterotrimer of Arp7, Arp9 and Rtt102[238,267-269]. INO80-type remodellers contain a dimer of actin and Arp4, which associates in INO80 with Arp8, Ies4 and Taf14 and in SWR1 with a second actin molecule, Swc4 and Yaf9[275,276,279]. Additionally, both INO80 remodellers comprise another ARP, Arp5 in INO80 and Arp6 in SWR1, which is not part of the Arp module but of the core module[276,279]. The importance of the components of the Arp module was described early on as Arp7 and Arp9 were found to be essential proteins in *Saccharomyces cerevisiae* and Arp8 to be crucial for the activity of INO80[267,275,402]. The Arp module of the RSC remodeller promotes sliding by increasing the coupling of ATP hydrolysis to DNA translocation and is essential for the ejection of nucleosomes[239].

The crystal structure of the isolated Arp module of the SWI/SNF complex reveals that Arp7 and Arp9 bind the HSA domain via their barbed ends and interact with each other in a 'front-to-back' arrangement[269]. This is overall similar to the 'front-to-front' interaction within F-actin

but Arp7 is flipped compared to the second actin molecule in the actin fiber[269]. Rtt102 adopts a highly extended conformation with contacts to Arp7 and Arp9 opposite to the HSA domain thereby stabilizing the module[269]. The architecture observed in the crystal structure matches the conformation of the Arp module in the cryo-EM structure of ySWI/SNF[391]. It bridges the ATPase and the body module, which contacts the histone octamer thereby coupling ATP hydrolysis to DNA translocation (Fig. 9c)[391]. The C-terminal portion of the HSA domain is located close to nucleosomal DNA at SHL +5.5, which is in accordance with its previously reported DNA binding activity (Fig. 12b)[391,403]. Arp7 and Arp9 are positioned opposite the NCP with their pointed ends being exposed to solvent (Fig. 12b)[391]. Previously, biochemical experiments demonstrated that the post-HSA domain interacts with protrusion I thereby regulating the ATPase activity[239,403]. This is confirmed in the cryo-EM structure, in which it binds on top of the N-lobe of Swi2/Snf2[391]. Its connection to the HSA domain is disordered and therefore not resolved in the cryo-EM density (Fig. 12b)[391]. The overall architecture and position of the Arp module is observed likewise in RSC and BAF[392-394].

A first insight into the organization of the Arp module in the INO80 family was provided by a crystal structure of Swr1^{HSA} in complex with actin and Arp4[373]. These also interact in a 'front-to-back' arrangement as previously described for the Arp7-Arp9 dimer while Swr1^{HSA} is bound by their barbed ends too[269,373]. Thus, this type of dimer of actin folds is conserved among the SWI/SNF and INO80 families of remodellers and in the histone acetylase NuA4[386]. The HSA domain of INO80 remodellers is longer than in the SWI/SNF family, providing a binding site for an additional subunit of the Arp module[238]. This is Arp8 in INO80 and a second actin molecule in SWR1[238,276,279]. The Arp modules of INO80 and SWR1 are not resolved in the current cryo-EM structures indicating a high degree of flexibility relative to the core module and the NCP[353,387,395]. For the INO80 complex from *Chaetomium thermophilum*, one sparsely populated 3D class could be identified, which provides density beyond the highly resolved structure of core module and the NCP[387]. This low-resolution map indicates that the Arp8 module interacts with extranucleosomal DNA[387], which is in agreement with ChIP-exo data placing Arp8 outside the +1 nucleosome[306]. However, a detailed interpretation of this interaction was not possible until the crystal structure of the Arp8 module of *Saccharomyces cerevisiae* was solved, which fits well into the additional, low-resolution density[386]. It demonstrates that Arp8 also binds the HSA domain via its barbed end and engages actin opposite of Arp4 in a novel 'side-to-back' interaction[386]. The HSA domain forms a segmented helix and is decorated with lysines and arginines, which mediate the binding to extranucleosomal DNA[386]. DNA crosslinking experiments published in parallel confirm this interaction[377].

Recently, an improved version of the cryo-EM density connecting the core module and the Arp8 module could be determined (unpublished data). It includes Ies4, which binds actin and Arp4 in a similar fashion as Rtt102 interacts with Arp7 and Arp9, indicating a related function of these proteins in stabilizing the Arp modules (Fig. 12). HSA α2 and the post-HSA form a continuous helix connecting the extranucleosomal bound Arp8 module with Ino80^{ATPase} at SHL -6 (Fig. 12a). The post-HSA domain also contacts the N-lobe of INO80^{ATPase}, but is rotated by ~120° compared to ySWI/SNF (Fig. 12a). This leads to a fundamentally different position of the Arp module relative to the ATPase in SWI/SNF remodellers and INO80 (Fig. 12). Taking the Snf2-type ATPases as references, the Arp module of SWI/SNF remodellers follows approximately the path of exit DNA and presumably contributes to its partial detachment from the histone octamer[391-393]. In INO80, the Arp8 module binds extranucleosomal DNA at the NCP's entry site ahead of the ATPase[386]. Point mutations in the HSA domain demonstrate that this interaction is crucial for INO80 to catalyze DNA translocation[386]. One possible explanation

could be, that the Arp8 module prevents DNA, which was pumped into the nucleosome and temporarily resides between Ino80^{ATPase} and Arp5 in an intermediate state, from slipping back[386]. This interpretation is in agreement with the observation that INO80 requires at least 40 bp of extranucleosomal DNA to catalyze DNA translocation[305]. This length exactly matches the footprint of the Arp8 module, thus shortening the extranucleosomal DNA might have the same effect as disrupting Ino80^{HSA}-DNA contacts: the Arp8 module cannot bind extranucleosomal DNA effectively and entry DNA pumped into the NCP by Ino80^{ATPase} slips back instead of being translocated around the NCP[305,386]. Intriguingly, the footprint of the Arp8 module on extranucleosomal DNA module is also similar to the distance between adjacent nucleosomes in genic arrays formed by INO80[183]. Hence, it could be a sensor for the distance to the neighboring nucleosome and thus contribute to space nucleosomes.

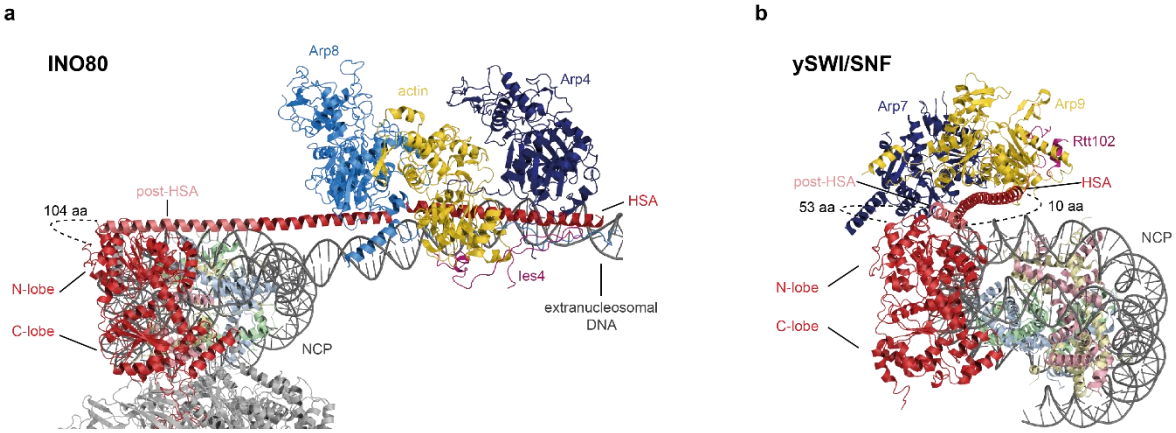

Figure 12: Position of the Arp module in INO80 and ySWI/SNF relative to the Snf2-type ATPase. a, The INO80 complex with the Arp8 module bound to extranucleosomal DNA. The HSA domain of Ino80 is decorated with lysines and arginines, which mediate the interaction with extranucleosomal DNA. Deep red: Ino80 with the post-HSA domain in light red; Light blue: Arp8; Yellow: actin; Dark blue: Arp4; Magenta: Ies4; Grey: DNA and other subunits of the complex; Histones are color-coded as in Fig. 10. **b,** Arp module in the ySWI/SNF complex (pdb: 6UXW)[391]. Deep red: Swi2/Snf2 with the post-HSA domain in light red; Yellow: Arp9; Dark blue: Arp7; Magenta: Rtt102; Grey: DNA; Histones are color-coded as in Fig. 10. Residues, which are not resolved in the structures are indicated by dashed lines. Models are aligned on the N-lobe of their Snf2-type ATPases.

The U-shaped actin adopts two different conformations dependent on its nucleotide state (see 2.2.3.2)[363], which was suggested to allosterically regulate the catalytic action of the BAF complex[404]. For this reason, it was proposed that actin and Arps can act as a conformational switch in remodellers[405], which is why their nucleotide state is of particular interest. Arp4 is bound to ATP-bound in all structures of the actin-Arp4 dimer reported so far[373,386]. However, actin is in a nucleotide-free state in the crystal structure of the actin-Arp4-Swr1^{HSA} construct[373] but bound to ATP in the crystal structure of the Arp8 module of INO80[386]. Of note, for crystallization of the latter no nucleotide was added but the toxin latrunculin A[386], which traps the nucleotide state of actin[405]. In both structures, actin adopts the twisted conformation of ATP-bound G-actin[386]. In the BAF complex, biochemical data suggests that actin is also bound to ATP and might even hydrolyze ATP to some extent[404], while Arp7 and Arp9 are in nucleotide free states in the crystal structure of the Arp module of ySWI/SNF[269]. Furthermore, the nucleotide state of Arp8 differs between the crystalized Arp8 module from *Saccharomyces cerevisiae*[386] and the one determined by cryo-EM from *Chaetomium thermophilum* (unpublished data). Taken together, these results show that actin and Arps can occur nucleotide-free or ATP-bound in the context of different remodellers depending on the experimental conditions. As there are no larger conformational changes associated with these nucleotide states, it is not clear, whether they occur in a context-specific manner thereby regulating the remodeller's activities.

Only a small subset of particles in the cryo-EM data of nucleosome-bound INO80 adopts the conformation described above, in which the Arp8 module binds extranucleosomal DNA[387]. Thus, it is very likely that the module is highly dynamic and can adopt various positions relative the core module on the chromatin template. This is supported by a different position of the Arp8 module observed the cryo-EM structure of INO80 in its apo state, however at limited resolution[388]. The non-conserved residues connecting the post-HSA domain with the N-lobe of Ino80 are not resolved in any of the published cryo-EM structures, presumably because they are disorderd[387,388,395]. This region comprises ~100 amino acids (Fig. 12a)[386] and might contribute to the flexibility of the module by providing a long linker to place the Arp8 module in different positions relative to Ino80^{ATPase}. Different binding configurations of the Arp8 module could also explain the interaction of its isolated components to histones observed earlier. Arp4 was shown to bind H2A[406] while Arp8 shows high affinity towards the H3-H4 tetramer[375,376]. These interactions do not necessarily have to be formed to the same nucleosome the core module binds to but potentially also to an adjacent nucleosome given the extended conformation of the Arp8 module.

5.4 Interaction of chromatin-associated factors with the acidic patch

The NCP offers multiple interaction sites, which differ in their shape and chemical properties[18,27]. Nevertheless, the acidic patch formed by H2A and H2B on the surface of the histone octamer emerged as a hot spot for the binding of chromatin-associated factors (see 2.1.1.2)[27]. INO80 interacts with the acidic patch via the insert domain of Arp5 (Fig. 13a), which is essential for it to catalyze DNA translocation[387,407]. The first factor to be described to bind the acidic patch was a peptide from the Karposi's sarcoma-associated herpesvirus latency-associated nuclear antigen (LANA)[29]. This peptide mediates the attachment of the viral genome to mitotic chromosomes, which is strongly dependent on the interaction of one arginine with the acidic patch (Fig. 13b)[29]. Subsequently, more and more interactions with this area were described structurally and biochemically, among them chromatin-organizing proteins such as regulator of chromosome condensation 1 (RCC1) (Fig. 13c)[26] and the BAH domain of silent information regulator 3 (Sir3) (Fig. 13d)[31]. RCC1 recruits the small GTPase Ran to nucleosomes and activates its GTPase activity[408] while Sir3 contributes to the generation of transcriptionally silenced domains[409]. Although all these enzymes differ fundamentally in their biological action and architecture, they all depend on the interaction with the acidic patch to fulfill their function[26,29,31,387], which holds also true for several other chromatin-associated factors[27,36]. Intriguingly, there is no sequence homology or common structural motif among the acidic patch-interacting protein regions (Fig. 13)[27,36]. Instead, these are highly diverse and specific to each enzyme. However, all interactions depend on one single arginine residue forming electrostatic interactions with the deeper of the two acidic patch pockets, which harbors H2AE61, E64, D90 and E92 (also see 2.1.1.2)[26,27,29,31,36]. This is referred to as the arginine anchor motif[27] and in INO80 formed by R501 of Arp5^{insert} (Fig. 13a, unpublished data). Additional electrostatic interactions are formed by K502, presumably strengthening INO80's binding to the acidic patch (Fig. 13a). This is similarly observed for the Sir3 BAH domain, in which a total of three arginine residues mediate the interaction with the acidic patch (Fig. 13b)[31].

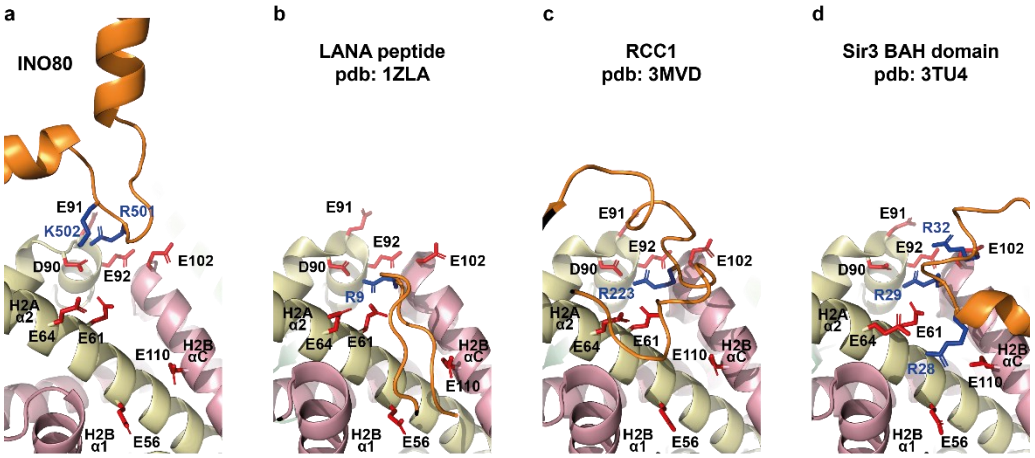

Figure 13: Acidic patch interaction in INO80 and other chromatin-associated factors. a, INO80 interacts with the acidic patch via R501 and K502 of the insert domain of Arp5. **b – d,** Acidic patch interacting regions of other chromatin-associated factors for comparison. **b,** the LANA peptide[29], **c,** RCC1[26], **d,** the BAH domain of Sir3[31]. pdb code of each model is indicated in the figure. Light yellow: H2A; Light red: H2B; Red: Side chains of the residues forming the acidic patch; Orange: acidic patch-interacting region of chromatin-binding proteins; Blue: Basic residues forming electrostatic interactions with the acidic patch.

Interactions with the acidic patch have also been reported for other remodellers, however high-resolution data is lacking for these interactions. In Snf2h, it presumably serves as a landing pad for the auto-inhibitory domains NegC and AutoN (also see 2.2.1.1)[407]. The binding to the acidic patch clears the inhibitory effect of these flanking domains on the ATPase and activates it[407]. RSC binds the acidic patch via the positively charged C-terminal tail of Sfh1 and this interaction is critical for the ejection of nucleosomes from DNA by RSC[394]. These two examples and the observations made for INO80 illustrate that acidic patch is an important binding platform for remodellers. While domains of the catalytic subunit mediate this contact in Snf2h and RSC, it is formed by the non-catalytic subunit Arp5 in INO80[387,394,407]. The multi-subunit remodellers RSC and INO80 show robust ATPase activity when the interaction with the acidic patch is abolished but are severely impaired in their catalytic action[387,394]. In turn, the ATPase activity of Snf2h depends on its binding to the acidic patch[407]. Thus, the acidic patch impacts remodeller activity in an essential yet versatile way.

5.5 Regulation of remodellers by histone tails

The histone tails make up 25 - 30% of the mass of the four core histones but are difficult to visualize by structural methods due to their unordered nature (see 2.1.1.3)[15,47]. This holds also true for most remodellers structures. One exception is the ISWI family. Biochemical approaches identified the H4 tail as a key regulator ISWI activity early on[410]. Along with extranucleosomal DNA, it was found to be essential for ISWI to catalyze DNA translocation by preventing the negative regulation of the domains AutoN and NegC on ATP hydrolysis and the coupling of ATP hydrolysis to DNA translocation, respectively[196]. In the cryo-EM structure of nucleosome-bound Isw1, the H4 tail interacts with the C-lobe including contacts to H4K16[347]. This residue interacts with the acidic patch of the adjacent nucleosome in nucleosomal arrays, compacting the chromatin fiber (see 2.1.1.2)[15,39].

Little is known about the regulation of INO80 by histone tails although they form multiple interactions to subunits of INO80, in particular to the Arp8 module, the Nhp10 module and Ies2[276]. Deletion of the tails of all core histones increases the velocity of DNA translocation around a mononucleosome without affecting the affinity of INO80 towards its substrate[304,411]. Moreover, they are not required for nucleosomes to be positioned around promoter sites by INO80[359]. Single-molecule data suggests that the histone tails are a major regulatory barrier

for INO80 nucleosome invasion[411]. They possibly constrain the conformations of INO80 bound to the NCP thereby increasing the energy barrier to initiating remodelling[411]. This would explain the elevated speed of the sliding reaction observed for nucleosomes lacking the histone tails[304,411]. More recent biochemical experiments indicate that the H3 tail regulates the activity of INO80[395]. The residues 31 – 39 appear to be of particular importance in this process as mimicking acetylation at H3K36 and H3K37 results in an increased sliding velocity and affects the proposed dimerization of INO80 on the nucleosome[384,395]. Although suggested biochemically, this dimer could not be visualized by cryo-EM under various experimental conditions[387,395]. Whether it actually exists inside living cells and how two ATPases would catalyze DNA translocation around the same nucleosome, is currently not understood.

5.6 Mechanism of DNA translocation catalyzed by chromatin remodellers

Before the publication of the cryo-EM structures described above, two main concepts for the mechanism of DNA translocation catalyzed by chromatin remodellers were put forward based on biochemical and biophysical experiments[412]. These are the twist diffusion and loop / bulge propagation model[412].

In the twist diffusion model, 1 bp of DNA is translocated around the nucleosome[413]. Its starting point is a local over- or underwinding of nucleosomal DNA, which results in a twist or untwist (hence the name) to accommodate the gain or loss of a single bp at a given site[412,413]. The twist defect is predicted to be tolerated without destabilizing the entire nucleosome[412]. Translocation occurs, if it is released by being passed on to the next turn of nucleosomal DNA, which is referred to as twist diffusion[413]. In this model the twist defect can be caused by two events: The action of ATP-dependent chromatin remodellers, which pump DNA in steps of 1 bp[412] or torsional oscillations of entry DNA[414]. Hence, it also accounts for the spontaneous motion of nucleosomes on DNA[415]. If the twist is introduced by a remodeller, its diffusion becomes a unidirectional process, in which it circulates around the nucleosome and exits opposite of its site of generation[413]. Other than spontaneous sliding, the directed motion of the twist defect strictly requires a source of energy, which is the hydrolysis of ATP by the Snf2-type ATPase[413]. The twist diffusion model is supported by the observation of a twist of 1 bp in the X-ray structure of the nucleosome reconstituted with the 601 DNA at SHL ±5 compared to the human α-satellite sequence (see 2.1.1.4)[18,25,26]. In addition, it was shown, that remodeller ATPases can introduce superhelicity in linear DNA[416]. Objections to the twist diffusion model arose as it involves a rotation of DNA behind the source of the twist resulting in torsional stress and eventually topological changes of nucleosomal DNA[412,413]. Early biochemical experiments on nucleosome sliding by ISWI could also not confirm the model as it was demonstrated to translocate nicked DNA too[417]. However, it gained new attention by the high-resolution cryo-EM studies of Swi2/Snf2, Isw1 and CHD4 bound to the nucleosome[234,346,347]. In these structures, a distortion[234] or register shift[346,347] of the tracking strand is observed relative to the guide strand.

The loop / bulge propagation model proposes that the remodeller ATPase breaks histone-DNA contacts by pulling (or pushing) entry DNA into the NCP resulting in the formation of a distorted DNA loop[412]. In this concept, the loop stores energy, which is released upon its propagation around the nucleosome resulting in DNA translocation[412]. It was proposed based on experiments using hydroxyl radical footprinting[21], which demonstrate movements of nucleosomes in increments larger than 1 bp[302,418]. Other than the twist diffusion model, this suggests that a larger DNA region is translocated at once[418]. The loop propagation model is supported by the cryo-EM structures of the multi-subunit remodellers, in particular INO80. The existence of the counter grip formed by the actin fold of Arp5 and Ies6 demonstrates how

nucleosomal DNA could be looped when Ino80^{ATPase} pumps DNA in its direction[387]. However, the question remains how this counter grip alternately binds and releases from the NCP to enable formation and propagation of the DNA loop, respectively[412]. Early on, it has been noticed that this is a critical question for this concept and requires coupling of the ATPase activity to the position of non-ATPase subunits[412,418]. The key element for this coupling in INO80 might be the insert domain of Arp5. It physically connects the actin fold of Arp5 (counter grip) as well as the ATPase of Ino80 (motor) and clearly communicates with Ino80^{ATPase} as its differential readout of a histone variant results in an elevated level of ATPase activity[387]. Future studies will show whether this holds true and how this communication works, potentially by snapshots of intermediate translocation steps. Furthermore, these might also answer the question whether the register shift of DNA observed for the isolated ATPase domains is also present in multi-subunit remodellers and how this can be brought in accordance with DNA translocation in increments of 10 – 20 bp by INO80[302,305]. Finally, this will touch on the question why and in which context multi-subunit remodellers are necessary given the manifold actions remodeller ATPases can carry out in small complexes or even as single subunits.

6 Abbreviations

AAA+ ATPases associated with diverse cellular activities
ACF ATP-utilizing chromatin assembly and remodelling factor
ACS ARS consensus sequence
ARP actin-related protein
ARS autonomously replicating sequence
AutoN autoinhibitory N terminal
bp base pair(s)
BAF BRG1-associated factors
BAP BRM-associated proteins
BPTF bromodomain and PHD finger transcription factor
BRD7 Bromodomain-containing protein 7
BRG1 Brahma-related gene 1
BRM Brahma
CHD chromodomain helicase DNA-binding
CHRAC chromatin accessibility complex
ChIP chromatin immunoprecipitation
ChIP-exo chromatin immunoprecipitation followed by 5'-> 3' exonuclease digestion
ChIP-seq chromatin immunoprecipitation followed by deep sequencing
CID chromosomally interacting domain
cryo-EM cryogenic electron microscopy
Da Dalton; unit of mass; 1 Da corresponds to 1 u
DNA deoxyribonucleic acid
DSB double strand break
esBAF embryonic stem cell BAF
FACT facilitates chromatin transcription
GLTSCR1 glioma tumor suppressor candidate region gene 1
GLTSCR1L GLTSCR1-like
HAT histone acetyltransferase
hBRM human Brahma
HDAC histone deacetylase
HIT histidine triad
HMG high-mobility group
HP1 heterochromatin protein 1
HSA helicase/SANT-associated
HSS HAND-SANT-SLIDE
IDR intrinsically disordered region
Ies Ino eighty subunit
INO80 inositol requiring 80
ISWI imitation switch
kb kilo base pairs
LAD lamina-associated domain
LANA latency-associated nuclear antigen
lncRNA long noncoding RNA
Mb mega base pairs
Mec1 Mitosis entry checkpoint protein 1

MNase	micrococcal nuclease
MNase-seq	micrococcal nuclease treatment followed by deep sequencing
NAP1	nucleosome assembly protein-1
NCP	nucleosome core particle
NDR	nucleosome-depleted region
NegC	negative regulator of coupling
NFR	nucleosome-free region
Nhp10	non-histone protein
NTD	N-terminal domain
NuA4	nucleosome acetyltransferase of H4
NURF	nucleosome remodelling factor
NuRD	Nucleosome Remodelling and Deacetlyation
OB	oligonucleotide-binding
ORC	origin recognition complex
PAPA-1	Pim-1-associated protein-1 associated protein-1
PBAP	Polybromo BAP
PcG	Polycomb group
PBRM1	Protein polybromo-1
pdb	protein data bank; refers to the structure's ID in the pdb
PHD	plant homeodomain
PIC	pre-initiation complex
PRC1/2	Polycomb repressive complex 1/2
PTM	posttranslational modification
RCC	regulator of chromosome condensation
recA	recombination protein A
RNA	ribonucleic acid
RNAPII	RNA polymerase II
RSC	remodels the structure of chromatin
RSF	remodelling and spacing factor
Rtt102	repressor of *Ty1* transposition, gene 102
Rvb1/2	RuvB-like protein 1/2
SRCAP	Snf2-related CREB-binding protein activator protein
SD	subdomain
SELEX	Systematic evolution of ligands by exponential enrichment
SGD	salt gradient dialysis
SHL	superhelix location
SIR	silent information regulator
SWI/SNF	switching defective/sucrose non-fermentable
Swr1	Swi2/Snf2-related 1
TAD	topologically associated domain
Taf14	TBP-associated factor 14
Tel1	Telomere length regulation protein 1
TF	transcription factor
wt	wild-type
Yaf9	Protein AF-9 homolog
YEATS	Yaf9, ENL, AF9, TAf14, Sas5

7 References

1 Flemming, W. *Zellsubstanz, kern und zelltheilung*. (Vogel, 1882).

2 Kornberg, R. D. Structure of chromatin. *Annu Rev Biochem* **46**, 931-954, doi:10.1146/annurev.bi.46.070177.004435 (1977).

3 Acharya, S., Hartmann, M. & Erhardt, S. Chromatin-associated noncoding RNAs in development and inheritance. *Wiley Interdiscip Rev RNA* **8**, doi:10.1002/wrna.1435 (2017).

4 Kornberg, R. D. & Thomas, J. O. Chromatin structure; oligomers of the histones. *Science* **184**, 865-868 (1974).

5 Hewish, D. R. & Burgoyne, L. A. Chromatin sub-structure. The digestion of chromatin DNA at regularly spaced sites by a nuclear deoxyribonuclease. *Biochem Biophys Res Commun* **52**, 504-510 (1973).

6 Kornberg, R. D. Chromatin structure: a repeating unit of histones and DNA. *Science* **184**, 868-871 (1974).

7 Sollner-Webb, B. & Felsenfeld, G. A comparison of the digestion of nuclei and chromatin by staphylococcal nuclease. *Biochemistry* **14**, 2915-2920 (1975).

8 Lutter, L. C. Precise location of DNase I cutting sites in the nucleosome core determined by high resolution gel electrophoresis. *Nucleic Acids Res* **6**, 41-56, doi:10.1093/nar/6.1.41 (1979).

9 Olins, A. L. & Olins, D. E. Spheroid chromatin units (v bodies). *Science* **183**, 330-332 (1974).

10 Oudet, P., Gross-Bellard, M. & Chambon, P. Electron microscopic and biochemical evidence that chromatin structure is a repeating unit. *Cell* **4**, 281-300 (1975).

11 Finch, J. T. *et al.* Structure of nucleosome core particles of chromatin. *Nature* **269**, 29-36 (1977).

12 Olins, D. E. & Olins, A. L. Chromatin history: our view from the bridge. *Nat Rev Mol Cell Biol* **4**, 809-814, doi:10.1038/nrm1225 (2003).

13 Richmond, T. J., Finch, J. T., Rushton, B., Rhodes, D. & Klug, A. Structure of the nucleosome core particle at 7 A resolution. *Nature* **311**, 532-537 (1984).

14 Arents, G., Burlingame, R. W., Wang, B. C., Love, W. E. & Moudrianakis, E. N. The nucleosomal core histone octamer at 3.1 A resolution: a tripartite protein assembly and a left-handed superhelix. *Proc Natl Acad Sci U S A* **88**, 10148-10152 (1991).

15 Luger, K., Mader, A. W., Richmond, R. K., Sargent, D. F. & Richmond, T. J. Crystal structure of the nucleosome core particle at 2.8 A resolution. *Nature* **389**, 251-260, doi:10.1038/38444 (1997).

16 Elgin, S. C. & Weintraub, H. Chromosomal proteins and chromatin structure. *Annu Rev Biochem* **44**, 725-774, doi:10.1146/annurev.bi.44.070175.003453 (1975).

17 Smith, E. L., DeLange, R. J. & Bonner, J. Chemistry and biology of the histones. *Physiol Rev* **50**, 159-170, doi:10.1152/physrev.1970.50.2.159 (1970).

18 McGinty, R. K. & Tan, S. Nucleosome structure and function. *Chem Rev* **115**, 2255-2273, doi:10.1021/cr500373h (2015).

19 Zhou, K., Gaullier, G. & Luger, K. Nucleosome structure and dynamics are coming of age. *Nat Struct Mol Biol* **26**, 3-13, doi:10.1038/s41594-018-0166-x (2019).

20 Schrodinger, LLC. *The PyMOL Molecular Graphics System, Version 2.3* (2019).

21 Flaus, A., Luger, K., Tan, S. & Richmond, T. J. Mapping nucleosome position at single base-pair resolution by using site-directed hydroxyl radicals. *Proc Natl Acad Sci U S A* **93**, 1370-1375 (1996).

22 Iwasaki, W. *et al.* Contribution of histone N-terminal tails to the structure and stability of nucleosomes. *FEBS Open Bio* **3**, 363-369, doi:10.1016/j.fob.2013.08.007 (2013).

23 Davey, C. A., Sargent, D. F., Luger, K., Maeder, A. W. & Richmond, T. J. Solvent mediated interactions in the structure of the nucleosome core particle at 1.9 a resolution. *J Mol Biol* **319**, 1097-1113, doi:10.1016/S0022-2836(02)00386-8 (2002).

24 Lowary, P. T. & Widom, J. New DNA sequence rules for high affinity binding to histone octamer and sequence-directed nucleosome positioning. *J Mol Biol* **276**, 19-42, doi:10.1006/jmbi.1997.1494 (1998).
25 Vasudevan, D., Chua, E. Y. D. & Davey, C. A. Crystal structures of nucleosome core particles containing the '601' strong positioning sequence. *J Mol Biol* **403**, 1-10, doi:10.1016/j.jmb.2010.08.039 (2010).
26 Makde, R. D., England, J. R., Yennawar, H. P. & Tan, S. Structure of RCC1 chromatin factor bound to the nucleosome core particle. *Nature* **467**, 562-566, doi:10.1038/nature09321 (2010).
27 McGinty, R. K. & Tan, S. Recognition of the nucleosome by chromatin factors and enzymes. *Curr Opin Struct Biol* **37**, 54-61, doi:10.1016/j.sbi.2015.11.014 (2016).
28 McGinty, R. K., Henrici, R. C. & Tan, S. Crystal structure of the PRC1 ubiquitylation module bound to the nucleosome. *Nature* **514**, 591-596, doi:10.1038/nature13890 (2014).
29 Barbera, A. J. *et al.* The nucleosomal surface as a docking station for Kaposi's sarcoma herpesvirus LANA. *Science* **311**, 856-861, doi:10.1126/science.1120541 (2006).
30 Roussel, L., Erard, M., Cayrol, C. & Girard, J. P. Molecular mimicry between IL-33 and KSHV for attachment to chromatin through the H2A-H2B acidic pocket. *EMBO Rep* **9**, 1006-1012, doi:10.1038/embor.2008.145 (2008).
31 Armache, K. J., Garlick, J. D., Canzio, D., Narlikar, G. J. & Kingston, R. E. Structural basis of silencing: Sir3 BAH domain in complex with a nucleosome at 3.0 A resolution. *Science* **334**, 977-982, doi:10.1126/science.1210915 (2011).
32 Kato, H. *et al.* Architecture of the high mobility group nucleosomal protein 2-nucleosome complex as revealed by methyl-based NMR. *Proc Natl Acad Sci U S A* **108**, 12283-12288, doi:10.1073/pnas.1105848108 (2011).
33 Kato, H. *et al.* A conserved mechanism for centromeric nucleosome recognition by centromere protein CENP-C. *Science* **340**, 1110-1113, doi:10.1126/science.1235532 (2013).
34 Morgan, M. T. *et al.* Structural basis for histone H2B deubiquitination by the SAGA DUB module. *Science* **351**, 725-728, doi:10.1126/science.aac5681 (2016).
35 Clarkson, M. J., Wells, J. R., Gibson, F., Saint, R. & Tremethick, D. J. Regions of variant histone His2AvD required for Drosophila development. *Nature* **399**, 694-697, doi:10.1038/21436 (1999).
36 Kalashnikova, A. A., Porter-Goff, M. E., Muthurajan, U. M., Luger, K. & Hansen, J. C. The role of the nucleosome acidic patch in modulating higher order chromatin structure. *J R Soc Interface* **10**, 20121022, doi:10.1098/rsif.2012.1022 (2013).
37 Fan, J. Y., Rangasamy, D., Luger, K. & Tremethick, D. J. H2A.Z alters the nucleosome surface to promote HP1alpha-mediated chromatin fiber folding. *Mol Cell* **16**, 655-661, doi:10.1016/j.molcel.2004.10.023 (2004).
38 Chadwick, B. P. & Willard, H. F. A novel chromatin protein, distantly related to histone H2A, is largely excluded from the inactive X chromosome. *J Cell Biol* **152**, 375-384, doi:10.1083/jcb.152.2.375 (2001).
39 Yang, D. & Arya, G. Structure and binding of the H4 histone tail and the effects of lysine 16 acetylation. *Phys Chem Chem Phys* **13**, 2911-2921, doi:10.1039/c0cp01487g (2011).
40 Shogren-Knaak, M. *et al.* Histone H4-K16 acetylation controls chromatin structure and protein interactions. *Science* **311**, 844-847, doi:10.1126/science.1124000 (2006).
41 Robinson, P. J. *et al.* 30 nm chromatin fibre decompaction requires both H4-K16 acetylation and linker histone eviction. *J Mol Biol* **381**, 816-825, doi:10.1016/j.jmb.2008.04.050 (2008).
42 England, J. R., Huang, J., Jennings, M. J., Makde, R. D. & Tan, S. RCC1 uses a conformationally diverse loop region to interact with the nucleosome: a model for the RCC1-nucleosome complex. *J Mol Biol* **398**, 518-529, doi:10.1016/j.jmb.2010.03.037 (2010).
43 Ueda, T., Catez, F., Gerlitz, G. & Bustin, M. Delineation of the protein module that anchors HMGN proteins to nucleosomes in the chromatin of living cells. *Mol Cell Biol* **28**, 2872-2883, doi:10.1128/MCB.02181-07 (2008).

44 Stone, E. M., Reifsnyder, C., McVey, M., Gazo, B. & Pillus, L. Two classes of sir3 mutants enhance the sir1 mutant mating defect and abolish telomeric silencing in Saccharomyces cerevisiae. *Genetics* **155**, 509-522 (2000).

45 Norris, A., Bianchet, M. A. & Boeke, J. D. Compensatory interactions between Sir3p and the nucleosomal LRS surface imply their direct interaction. *PLoS Genet* **4**, e1000301, doi:10.1371/journal.pgen.1000301 (2008).

46 Jurrus, E. *et al.* Improvements to the APBS biomolecular solvation software suite. *Protein Sci* **27**, 112-128, doi:10.1002/pro.3280 (2018).

47 Cutter, A. R. & Hayes, J. J. A brief review of nucleosome structure. *FEBS Lett* **589**, 2914-2922, doi:10.1016/j.febslet.2015.05.016 (2015).

48 Lilley, D. M., Howarth, O. W., Clark, V. M., Pardon, J. F. & Richards, B. M. The existence of random coil N-terminal peptides - 'tails' - in native histone complexes. *FEBS Lett* **62**, 7-10, doi:10.1016/0014-5793(76)80004-x (1976).

49 Bohm, L. & Crane-Robinson, C. Proteases as structural probes for chromatin: the domain structure of histones. *Biosci Rep* **4**, 365-386, doi:10.1007/bf01122502 (1984).

50 Walker, I. O. Differential dissociation of histone tails from core chromatin. *Biochemistry* **23**, 5622-5628, doi:10.1021/bi00318a037 (1984).

51 Angelov, D., Vitolo, J. M., Mutskov, V., Dimitrov, S. & Hayes, J. J. Preferential interaction of the core histone tail domains with linker DNA. *Proc Natl Acad Sci U S A* **98**, 6599-6604, doi:10.1073/pnas.121171498 (2001).

52 Wang, X. & Hayes, J. J. Physical methods used to study core histone tail structures and interactions in solution. *Biochem Cell Biol* **84**, 578-588, doi:10.1139/o06-076 (2006).

53 Polach, K. J., Lowary, P. T. & Widom, J. Effects of core histone tail domains on the equilibrium constants for dynamic DNA site accessibility in nucleosomes. *J Mol Biol* **298**, 211-223, doi:10.1006/jmbi.2000.3644 (2000).

54 Widlund, H. R., Vitolo, J. M., Thiriet, C. & Hayes, J. J. DNA sequence-dependent contributions of core histone tails to nucleosome stability: differential effects of acetylation and proteolytic tail removal. *Biochemistry* **39**, 3835-3841, doi:10.1021/bi991957l (2000).

55 Gao, M. *et al.* Histone H3 and H4 N-terminal tails in nucleosome arrays at cellular concentrations probed by magic angle spinning NMR spectroscopy. *J Am Chem Soc* **135**, 15278-15281, doi:10.1021/ja407526s (2013).

56 Kouzarides, T. Chromatin modifications and their function. *Cell* **128**, 693-705, doi:10.1016/j.cell.2007.02.005 (2007).

57 Bowman, G. D. & Poirier, M. G. Post-translational modifications of histones that influence nucleosome dynamics. *Chem Rev* **115**, 2274-2295, doi:10.1021/cr500350x (2015).

58 Strahl, B. D. & Allis, C. D. The language of covalent histone modifications. *Nature* **403**, 41-45, doi:10.1038/47412 (2000).

59 Tessarz, P. & Kouzarides, T. Histone core modifications regulating nucleosome structure and dynamics. *Nat Rev Mol Cell Biol* **15**, 703-708, doi:10.1038/nrm3890 (2014).

60 Finch, J. T. *et al.* X-ray diffraction study of a new crystal form of the nucleosome core showing higher resolution. *J Mol Biol* **145**, 757-769, doi:10.1016/0022-2836(81)90313-2 (1981).

61 Lutter, L. C. Kinetic analysis of deoxyribonuclease I cleavages in the nucleosome core: evidence for a DNA superhelix. *J Mol Biol* **124**, 391-420, doi:10.1016/0022-2836(78)90306-6 (1978).

62 Noll, M. Subunit structure of chromatin. *Nature* **251**, 249-251, doi:10.1038/251249a0 (1974).

63 Harp, J. M. *et al.* Preparative separation of nucleosome core particles containing defined-sequence DNA in multiple translational phases. *Electrophoresis* **16**, 1861-1864 (1995).

64 Harp, J. M. *et al.* X-ray diffraction analysis of crystals containing twofold symmetric nucleosome core particles. *Acta Crystallogr D Biol Crystallogr* **52**, 283-288, doi:10.1107/S0907444995009139 (1996).

65 Sinsheimer, R. L. Recombinant DNA. *Annu Rev Biochem* **46**, 415-438, doi:10.1146/annurev.bi.46.070177.002215 (1977).
66 Simpson, R. T. & Stafford, D. W. Structural features of a phased nucleosome core particle. *Proc Natl Acad Sci U S A* **80**, 51-55, doi:10.1073/pnas.80.1.51 (1983).
67 Chua, E. Y., Vasudevan, D., Davey, G. E., Wu, B. & Davey, C. A. The mechanics behind DNA sequence-dependent properties of the nucleosome. *Nucleic Acids Res* **40**, 6338-6352, doi:10.1093/nar/gks261 (2012).
68 Satchwell, S. C., Drew, H. R. & Travers, A. A. Sequence periodicities in chicken nucleosome core DNA. *J Mol Biol* **191**, 659-675, doi:10.1016/0022-2836(86)90452-3 (1986).
69 Travers, A. A. The structural basis of DNA flexibility. *Philos Trans A Math Phys Eng Sci* **362**, 1423-1438, doi:10.1098/rsta.2004.1390 (2004).
70 Hall, M. A. *et al.* High-resolution dynamic mapping of histone-DNA interactions in a nucleosome. *Nat Struct Mol Biol* **16**, 124-129, doi:10.1038/nsmb.1526 (2009).
71 Levendosky, R. F., Sabantsev, A., Deindl, S. & Bowman, G. D. The Chd1 chromatin remodeler shifts hexasomes unidirectionally. *Elife* **5**, doi:10.7554/eLife.21356 (2016).
72 Cutter, A. R. & Hayes, J. J. Linker histones: novel insights into structure-specific recognition of the nucleosome. *Biochem Cell Biol* **95**, 171-178, doi:10.1139/bcb-2016-0097 (2017).
73 Talbert, P. B. *et al.* A unified phylogeny-based nomenclature for histone variants. *Epigenetics Chromatin* **5**, 7, doi:10.1186/1756-8935-5-7 (2012).
74 Thoma, F. & Koller, T. Influence of histone H1 on chromatin structure. *Cell* **12**, 101-107, doi:10.1016/0092-8674(77)90188-x (1977).
75 Fan, Y. *et al.* Histone H1 depletion in mammals alters global chromatin structure but causes specific changes in gene regulation. *Cell* **123**, 1199-1212, doi:10.1016/j.cell.2005.10.028 (2005).
76 Shen, X. & Gorovsky, M. A. Linker histone H1 regulates specific gene expression but not global transcription in vivo. *Cell* **86**, 475-483, doi:10.1016/s0092-8674(00)80120-8 (1996).
77 Bakayev, V. V., Bakayeva, T. G. & Varshavsky, A. J. Nucleosomes and subnucleosomes: heterogeneity and composition. *Cell* **11**, 619-629, doi:10.1016/0092-8674(77)90079-4 (1977).
78 Simpson, R. T. Structure of the chromatosome, a chromatin particle containing 160 base pairs of DNA and all the histones. *Biochemistry* **17**, 5524-5531, doi:10.1021/bi00618a030 (1978).
79 Allan, J., Hartman, P. G., Crane-Robinson, C. & Aviles, F. X. The structure of histone H1 and its location in chromatin. *Nature* **288**, 675-679, doi:10.1038/288675a0 (1980).
80 Kasinsky, H. E., Lewis, J. D., Dacks, J. B. & Ausio, J. Origin of H1 linker histones. *FASEB J* **15**, 34-42, doi:10.1096/fj.00-0237rev (2001).
81 Singer, D. S. & Singer, M. F. Studies on the interaction of H1 histone with superhelical DNA: characterization of the recognition and binding regions of H1 histones. *Nucleic Acids Res* **3**, 2531-2547, doi:10.1093/nar/3.10.2531 (1976).
82 Zhou, B. R. *et al.* Structural insights into the histone H1-nucleosome complex. *Proc Natl Acad Sci U S A* **110**, 19390-19395, doi:10.1073/pnas.1314905110 (2013).
83 Zhou, B. R. *et al.* Structural Mechanisms of Nucleosome Recognition by Linker Histones. *Mol Cell* **59**, 628-638, doi:10.1016/j.molcel.2015.06.025 (2015).
84 Kalashnikova, A. A. *et al.* Linker histone H1.0 interacts with an extensive network of proteins found in the nucleolus. *Nucleic Acids Res* **41**, 4026-4035, doi:10.1093/nar/gkt104 (2013).
85 Landsman, D. Histone H1 in Saccharomyces cerevisiae: a double mystery solved? *Trends Biochem Sci* **21**, 287-288 (1996).
86 Harshman, S. W., Young, N. L., Parthun, M. R. & Freitas, M. A. H1 histones: current perspectives and challenges. *Nucleic Acids Res* **41**, 9593-9609, doi:10.1093/nar/gkt700 (2013).
87 Fan, L. & Roberts, V. A. Complex of linker histone H5 with the nucleosome and its implications for chromatin packing. *Proc Natl Acad Sci U S A* **103**, 8384-8389, doi:10.1073/pnas.0508951103 (2006).

88 An, W., Leuba, S. H., van Holde, K. & Zlatanova, J. Linker histone protects linker DNA on only one side of the core particle and in a sequence-dependent manner. *Proc Natl Acad Sci U S A* **95**, 3396-3401, doi:10.1073/pnas.95.7.3396 (1998).
89 Zhou, Y. B., Gerchman, S. E., Ramakrishnan, V., Travers, A. & Muyldermans, S. Position and orientation of the globular domain of linker histone H5 on the nucleosome. *Nature* **395**, 402-405, doi:10.1038/26521 (1998).
90 McGhee, J. D. & Felsenfeld, G. Nucleosome structure. *Annu Rev Biochem* **49**, 1115-1156, doi:10.1146/annurev.bi.49.070180.005343 (1980).
91 Woodcock, C. L., Safer, J. P. & Stanchfield, J. E. Structural repeating units in chromatin. I. Evidence for their general occurrence. *Exp Cell Res* **97**, 101-110 (1976).
92 Thoma, F., Koller, T. & Klug, A. Involvement of histone H1 in the organization of the nucleosome and of the salt-dependent superstructures of chromatin. *J Cell Biol* **83**, 403-427, doi:10.1083/jcb.83.2.403 (1979).
93 Hansen, J. C., Ausio, J., Stanik, V. H. & van Holde, K. E. Homogeneous reconstituted oligonucleosomes, evidence for salt-dependent folding in the absence of histone H1. *Biochemistry* **28**, 9129-9136, doi:10.1021/bi00449a026 (1989).
94 Horn, P. J. & Peterson, C. L. Molecular biology. Chromatin higher order folding--wrapping up transcription. *Science* **297**, 1824-1827, doi:10.1126/science.1074200 (2002).
95 Olins, D. E. & Olins, A. L. Physical studies of isolated eucaryotic nuclei. *J Cell Biol* **53**, 715-736, doi:10.1083/jcb.53.3.715 (1972).
96 Dekker, J. & Mirny, L. The 3D Genome as Moderator of Chromosomal Communication. *Cell* **164**, 1110-1121, doi:10.1016/j.cell.2016.02.007 (2016).
97 Korolev, N. *et al.* The effect of salt on oligocation-induced chromatin condensation. *Biochem Biophys Res Commun* **418**, 205-210, doi:10.1016/j.bbrc.2011.12.112 (2012).
98 Hansen, J. C. Conformational dynamics of the chromatin fiber in solution: determinants, mechanisms, and functions. *Annu Rev Biophys Biomol Struct* **31**, 361-392, doi:10.1146/annurev.biophys.31.101101.140858 (2002).
99 Finch, J. T. & Klug, A. Solenoidal model for superstructure in chromatin. *Proc Natl Acad Sci U S A* **73**, 1897-1901, doi:10.1073/pnas.73.6.1897 (1976).
100 Schwarz, P. M., Felthauser, A., Fletcher, T. M. & Hansen, J. C. Reversible oligonucleosome self-association: dependence on divalent cations and core histone tail domains. *Biochemistry* **35**, 4009-4015, doi:10.1021/bi9525684 (1996).
101 Dorigo, B., Schalch, T., Bystricky, K. & Richmond, T. J. Chromatin fiber folding: requirement for the histone H4 N-terminal tail. *J Mol Biol* **327**, 85-96, doi:10.1016/s0022-2836(03)00025-1 (2003).
102 Schalch, T., Duda, S., Sargent, D. F. & Richmond, T. J. X-ray structure of a tetranucleosome and its implications for the chromatin fibre. *Nature* **436**, 138-141, doi:10.1038/nature03686 (2005).
103 Song, F. *et al.* Cryo-EM study of the chromatin fiber reveals a double helix twisted by tetranucleosomal units. *Science* **344**, 376-380, doi:10.1126/science.1251413 (2014).
104 Fierz, B. *et al.* Histone H2B ubiquitylation disrupts local and higher-order chromatin compaction. *Nat Chem Biol* **7**, 113-119, doi:10.1038/nchembio.501 (2011).
105 Carruthers, L. M., Bednar, J., Woodcock, C. L. & Hansen, J. C. Linker histones stabilize the intrinsic salt-dependent folding of nucleosomal arrays: mechanistic ramifications for higher-order chromatin folding. *Biochemistry* **37**, 14776-14787, doi:10.1021/bi981684e (1998).
106 Carruthers, L. M. & Hansen, J. C. The core histone N termini function independently of linker histones during chromatin condensation. *J Biol Chem* **275**, 37285-37290, doi:10.1074/jbc.M006801200 (2000).
107 Travers, A. Structural biology. The 30-nm fiber redux. *Science* **344**, 370-372, doi:10.1126/science.1253852 (2014).
108 Fussner, E., Ching, R. W. & Bazett-Jones, D. P. Living without 30nm chromatin fibers. *Trends Biochem Sci* **36**, 1-6, doi:10.1016/j.tibs.2010.09.002 (2011).

109 Maeshima, K., Imai, R., Tamura, S. & Nozaki, T. Chromatin as dynamic 10-nm fibers. *Chromosoma* **123**, 225-237, doi:10.1007/s00412-014-0460-2 (2014).
110 Hsieh, T. H. *et al.* Mapping Nucleosome Resolution Chromosome Folding in Yeast by Micro-C. *Cell* **162**, 108-119, doi:10.1016/j.cell.2015.05.048 (2015).
111 Ricci, M. A., Manzo, C., Garcia-Parajo, M. F., Lakadamyali, M. & Cosma, M. P. Chromatin fibers are formed by heterogeneous groups of nucleosomes in vivo. *Cell* **160**, 1145-1158, doi:10.1016/j.cell.2015.01.054 (2015).
112 Nishino, Y. *et al.* Human mitotic chromosomes consist predominantly of irregularly folded nucleosome fibres without a 30-nm chromatin structure. *EMBO J* **31**, 1644-1653, doi:10.1038/emboj.2012.35 (2012).
113 O'Sullivan, J. M. *et al.* Gene loops juxtapose promoters and terminators in yeast. *Nat Genet* **36**, 1014-1018, doi:10.1038/ng1411 (2004).
114 Pickersgill, H. *et al.* Characterization of the Drosophila melanogaster genome at the nuclear lamina. *Nat Genet* **38**, 1005-1014, doi:10.1038/ng1852 (2006).
115 van Steensel, B. & Dekker, J. Genomics tools for unraveling chromosome architecture. *Nat Biotechnol* **28**, 1089-1095, doi:10.1038/nbt.1680 (2010).
116 Dekker, J., Marti-Renom, M. A. & Mirny, L. A. Exploring the three-dimensional organization of genomes: interpreting chromatin interaction data. *Nat Rev Genet* **14**, 390-403, doi:10.1038/nrg3454 (2013).
117 Sanyal, A., Lajoie, B. R., Jain, G. & Dekker, J. The long-range interaction landscape of gene promoters. *Nature* **489**, 109-113, doi:10.1038/nature11279 (2012).
118 Nora, E. P. *et al.* Spatial partitioning of the regulatory landscape of the X-inactivation centre. *Nature* **485**, 381-385, doi:10.1038/nature11049 (2012).
119 Dixon, J. R. *et al.* Topological domains in mammalian genomes identified by analysis of chromatin interactions. *Nature* **485**, 376-380, doi:10.1038/nature11082 (2012).
120 Lieberman-Aiden, E. *et al.* Comprehensive mapping of long-range interactions reveals folding principles of the human genome. *Science* **326**, 289-293, doi:10.1126/science.1181369 (2009).
121 Grob, S., Schmid, M. W. & Grossniklaus, U. Hi-C analysis in Arabidopsis identifies the KNOT, a structure with similarities to the flamenco locus of Drosophila. *Mol Cell* **55**, 678-693, doi:10.1016/j.molcel.2014.07.009 (2014).
122 Bonev, B. & Cavalli, G. Organization and function of the 3D genome. *Nat Rev Genet* **17**, 772, doi:10.1038/nrg.2016.147 (2016).
123 Rao, S. S. *et al.* A 3D map of the human genome at kilobase resolution reveals principles of chromatin looping. *Cell* **159**, 1665-1680, doi:10.1016/j.cell.2014.11.021 (2014).
124 Gibcus, J. H. & Dekker, J. The hierarchy of the 3D genome. *Mol Cell* **49**, 773-782, doi:10.1016/j.molcel.2013.02.011 (2013).
125 Le, T. B., Imakaev, M. V., Mirny, L. A. & Laub, M. T. High-resolution mapping of the spatial organization of a bacterial chromosome. *Science* **342**, 731-734, doi:10.1126/science.1242059 (2013).
126 Imakaev, M. *et al.* Iterative correction of Hi-C data reveals hallmarks of chromosome organization. *Nat Methods* **9**, 999-1003, doi:10.1038/nmeth.2148 (2012).
127 Zhang, Y. *et al.* Spatial organization of the mouse genome and its role in recurrent chromosomal translocations. *Cell* **148**, 908-921, doi:10.1016/j.cell.2012.02.002 (2012).
128 Kalhor, R., Tjong, H., Jayathilaka, N., Alber, F. & Chen, L. Genome architectures revealed by tethered chromosome conformation capture and population-based modeling. *Nat Biotechnol* **30**, 90-98, doi:10.1038/nbt.2057 (2011).
129 Dixon, J. R. *et al.* Chromatin architecture reorganization during stem cell differentiation. *Nature* **518**, 331-336, doi:10.1038/nature14222 (2015).
130 Cremer, T. & Cremer, C. Chromosome territories, nuclear architecture and gene regulation in mammalian cells. *Nat Rev Genet* **2**, 292-301, doi:10.1038/35066075 (2001).
131 Heitz, E. *Das heterochromatin der moose*. (Bornträger, 1928).

132 Straub, T. Heterochromatin dynamics. *PLoS Biol* **1**, E14, doi:10.1371/journal.pbio.0000014 (2003).
133 Ahringer, J. & Gasser, S. M. Repressive Chromatin in Caenorhabditis elegans: Establishment, Composition, and Function. *Genetics* **208**, 491-511, doi:10.1534/genetics.117.300386 (2018).
134 Allshire, R. C. & Madhani, H. D. Ten principles of heterochromatin formation and function. *Nat Rev Mol Cell Biol* **19**, 229-244, doi:10.1038/nrm.2017.119 (2018).
135 Misteli, T. The long reach of telomeres. *Genes Dev* **28**, 2445-2446, doi:10.1101/gad.254573.114 (2014).
136 Pidoux, A. L. & Allshire, R. C. The role of heterochromatin in centromere function. *Philos Trans R Soc Lond B Biol Sci* **360**, 569-579, doi:10.1098/rstb.2004.1611 (2005).
137 Politz, J. C., Scalzo, D. & Groudine, M. Something silent this way forms: the functional organization of the repressive nuclear compartment. *Annu Rev Cell Dev Biol* **29**, 241-270, doi:10.1146/annurev-cellbio-101512-122317 (2013).
138 Eissenberg, J. C. & Elgin, S. C. The HP1 protein family: getting a grip on chromatin. *Curr Opin Genet Dev* **10**, 204-210, doi:10.1016/s0959-437x(00)00058-7 (2000).
139 Lachner, M., O'Carroll, D., Rea, S., Mechtler, K. & Jenuwein, T. Methylation of histone H3 lysine 9 creates a binding site for HP1 proteins. *Nature* **410**, 116-120, doi:10.1038/35065132 (2001).
140 Heard, E. Delving into the diversity of facultative heterochromatin: the epigenetics of the inactive X chromosome. *Curr Opin Genet Dev* **15**, 482-489, doi:10.1016/j.gde.2005.08.009 (2005).
141 Cao, R. *et al.* Role of histone H3 lysine 27 methylation in Polycomb-group silencing. *Science* **298**, 1039-1043, doi:10.1126/science.1076997 (2002).
142 Banani, S. F., Lee, H. O., Hyman, A. A. & Rosen, M. K. Biomolecular condensates: organizers of cellular biochemistry. *Nat Rev Mol Cell Biol* **18**, 285-298, doi:10.1038/nrm.2017.7 (2017).
143 Narlikar, G. J. Phase-separation in chromatin organization. *J Biosci* **45** (2020).
144 Brangwynne, C. P. *et al.* Germline P granules are liquid droplets that localize by controlled dissolution/condensation. *Science* **324**, 1729-1732, doi:10.1126/science.1172046 (2009).
145 Patel, A. *et al.* A Liquid-to-Solid Phase Transition of the ALS Protein FUS Accelerated by Disease Mutation. *Cell* **162**, 1066-1077, doi:10.1016/j.cell.2015.07.047 (2015).
146 Brangwynne, C. P., Mitchison, T. J. & Hyman, A. A. Active liquid-like behavior of nucleoli determines their size and shape in Xenopus laevis oocytes. *Proc Natl Acad Sci U S A* **108**, 4334-4339, doi:10.1073/pnas.1017150108 (2011).
147 Altmeyer, M. *et al.* Liquid demixing of intrinsically disordered proteins is seeded by poly(ADP-ribose). *Nat Commun* **6**, 8088, doi:10.1038/ncomms9088 (2015).
148 Larson, A. G. *et al.* Liquid droplet formation by HP1alpha suggests a role for phase separation in heterochromatin. *Nature* **547**, 236-240, doi:10.1038/nature22822 (2017).
149 Strom, A. R. *et al.* Phase separation drives heterochromatin domain formation. *Nature* **547**, 241-245, doi:10.1038/nature22989 (2017).
150 Kato, M. *et al.* Cell-free formation of RNA granules: low complexity sequence domains form dynamic fibers within hydrogels. *Cell* **149**, 753-767, doi:10.1016/j.cell.2012.04.017 (2012).
151 Velez, G. *et al.* Evidence supporting a critical contribution of intrinsically disordered regions to the biochemical behavior of full-length human HP1gamma. *J Mol Model* **22**, 12, doi:10.1007/s00894-015-2874-z (2016).
152 Larson, A. G. & Narlikar, G. J. The Role of Phase Separation in Heterochromatin Formation, Function, and Regulation. *Biochemistry* **57**, 2540-2548, doi:10.1021/acs.biochem.8b00401 (2018).
153 Jiang, C. & Pugh, B. F. Nucleosome positioning and gene regulation: advances through genomics. *Nat Rev Genet* **10**, 161-172, doi:10.1038/nrg2522 (2009).
154 Talbert, P. B. & Henikoff, S. Histone variants on the move: substrates for chromatin dynamics. *Nat Rev Mol Cell Biol* **18**, 115-126, doi:10.1038/nrm.2016.148 (2017).

155 Clapier, C. R., Iwasa, J., Cairns, B. R. & Peterson, C. L. Mechanisms of action and regulation of ATP-dependent chromatin-remodelling complexes. *Nat Rev Mol Cell Biol* **18**, 407-422, doi:10.1038/nrm.2017.26 (2017).
156 Rhee, H. S., Bataille, A. R., Zhang, L. & Pugh, B. F. Subnucleosomal structures and nucleosome asymmetry across a genome. *Cell* **159**, 1377-1388, doi:10.1016/j.cell.2014.10.054 (2014).
157 Gurard-Levin, Z. A., Quivy, J. P. & Almouzni, G. Histone chaperones: assisting histone traffic and nucleosome dynamics. *Annu Rev Biochem* **83**, 487-517, doi:10.1146/annurev-biochem-060713-035536 (2014).
158 Barski, A. *et al.* High-resolution profiling of histone methylations in the human genome. *Cell* **129**, 823-837, doi:10.1016/j.cell.2007.05.009 (2007).
159 Rhee, H. S. & Pugh, B. F. Comprehensive genome-wide protein-DNA interactions detected at single-nucleotide resolution. *Cell* **147**, 1408-1419, doi:10.1016/j.cell.2011.11.013 (2011).
160 Lai, W. K. M. & Pugh, B. F. Understanding nucleosome dynamics and their links to gene expression and DNA replication. *Nat Rev Mol Cell Biol* **18**, 548-562, doi:10.1038/nrm.2017.47 (2017).
161 Yuan, G. C. *et al.* Genome-scale identification of nucleosome positions in S. cerevisiae. *Science* **309**, 626-630, doi:10.1126/science.1112178 (2005).
162 Eaton, M. L., Galani, K., Kang, S., Bell, S. P. & MacAlpine, D. M. Conserved nucleosome positioning defines replication origins. *Genes Dev* **24**, 748-753, doi:10.1101/gad.1913210 (2010).
163 Lee, C. K., Shibata, Y., Rao, B., Strahl, B. D. & Lieb, J. D. Evidence for nucleosome depletion at active regulatory regions genome-wide. *Nat Genet* **36**, 900-905, doi:10.1038/ng1400 (2004).
164 Xi, Y., Yao, J., Chen, R., Li, W. & He, X. Nucleosome fragility reveals novel functional states of chromatin and poises genes for activation. *Genome Res* **21**, 718-724, doi:10.1101/gr.117101.110 (2011).
165 Kubik, S. *et al.* Nucleosome Stability Distinguishes Two Different Promoter Types at All Protein-Coding Genes in Yeast. *Mol Cell* **60**, 422-434, doi:10.1016/j.molcel.2015.10.002 (2015).
166 Mavrich, T. N. *et al.* A barrier nucleosome model for statistical positioning of nucleosomes throughout the yeast genome. *Genome Res* **18**, 1073-1083, doi:10.1101/gr.078261.108 (2008).
167 Schones, D. E. *et al.* Dynamic regulation of nucleosome positioning in the human genome. *Cell* **132**, 887-898, doi:10.1016/j.cell.2008.02.022 (2008).
168 Weber, C. M., Ramachandran, S. & Henikoff, S. Nucleosomes are context-specific, H2A.Z-modulated barriers to RNA polymerase. *Mol Cell* **53**, 819-830, doi:10.1016/j.molcel.2014.02.014 (2014).
169 Tramantano, M. *et al.* Constitutive turnover of histone H2A.Z at yeast promoters requires the preinitiation complex. *Elife* **5**, doi:10.7554/eLife.14243 (2016).
170 Rhee, H. S. & Pugh, B. F. Genome-wide structure and organization of eukaryotic pre-initiation complexes. *Nature* **483**, 295-301, doi:10.1038/nature10799 (2012).
171 Reja, R., Vinayachandran, V., Ghosh, S. & Pugh, B. F. Molecular mechanisms of ribosomal protein gene coregulation. *Genes Dev* **29**, 1942-1954, doi:10.1101/gad.268896.115 (2015).
172 Batta, K., Zhang, Z., Yen, K., Goffman, D. B. & Pugh, B. F. Genome-wide function of H2B ubiquitylation in promoter and genic regions. *Genes Dev* **25**, 2254-2265, doi:10.1101/gad.177238.111 (2011).
173 Mavrich, T. N. *et al.* Nucleosome organization in the Drosophila genome. *Nature* **453**, 358-362, doi:10.1038/nature06929 (2008).
174 Sclafani, R. A. & Holzen, T. M. Cell cycle regulation of DNA replication. *Annu Rev Genet* **41**, 237-280, doi:10.1146/annurev.genet.41.110306.130308 (2007).
175 Marahrens, Y. & Stillman, B. A yeast chromosomal origin of DNA replication defined by multiple functional elements. *Science* **255**, 817-823, doi:10.1126/science.1536007 (1992).

176 Kurat, C. F., Yeeles, J. T. P., Patel, H., Early, A. & Diffley, J. F. X. Chromatin Controls DNA Replication Origin Selection, Lagging-Strand Synthesis, and Replication Fork Rates. *Mol Cell* **65**, 117-130, doi:10.1016/j.molcel.2016.11.016 (2017).
177 Albert, I. *et al.* Translational and rotational settings of H2A.Z nucleosomes across the Saccharomyces cerevisiae genome. *Nature* **446**, 572-576, doi:10.1038/nature05632 (2007).
178 Yang, J. *et al.* The Histone Chaperone FACT Contributes to DNA Replication-Coupled Nucleosome Assembly. *Cell Rep* **16**, 3414, doi:10.1016/j.celrep.2016.08.070 (2016).
179 Baldi, S. *et al.* Genome-wide Rules of Nucleosome Phasing in Drosophila. *Mol Cell* **72**, 661-672 e664, doi:10.1016/j.molcel.2018.09.032 (2018).
180 Zhang, Z. *et al.* A packing mechanism for nucleosome organization reconstituted across a eukaryotic genome. *Science* **332**, 977-980, doi:10.1126/science.1200508 (2011).
181 Segal, E. *et al.* A genomic code for nucleosome positioning. *Nature* **442**, 772-778, doi:10.1038/nature04979 (2006).
182 Ioshikhes, I. P., Albert, I., Zanton, S. J. & Pugh, B. F. Nucleosome positions predicted through comparative genomics. *Nat Genet* **38**, 1210-1215, doi:10.1038/ng1878 (2006).
183 Krietenstein, N. *et al.* Genomic Nucleosome Organization Reconstituted with Pure Proteins. *Cell* **167**, 709-721 e712, doi:10.1016/j.cell.2016.09.045 (2016).
184 Rando, O. J. & Ahmad, K. Rules and regulation in the primary structure of chromatin. *Curr Opin Cell Biol* **19**, 250-256, doi:10.1016/j.ceb.2007.04.006 (2007).
185 Clapier, C. R. & Cairns, B. R. The biology of chromatin remodeling complexes. *Annu Rev Biochem* **78**, 273-304, doi:10.1146/annurev.biochem.77.062706.153223 (2009).
186 Torigoe, S. E., Urwin, D. L., Ishii, H., Smith, D. E. & Kadonaga, J. T. Identification of a rapidly formed nonnucleosomal histone-DNA intermediate that is converted into chromatin by ACF. *Mol Cell* **43**, 638-648, doi:10.1016/j.molcel.2011.07.017 (2011).
187 Langst, G., Bonte, E. J., Corona, D. F. & Becker, P. B. Nucleosome movement by CHRAC and ISWI without disruption or trans-displacement of the histone octamer. *Cell* **97**, 843-852, doi:10.1016/s0092-8674(00)80797-7 (1999).
188 Mizuguchi, G. *et al.* ATP-driven exchange of histone H2AZ variant catalyzed by SWR1 chromatin remodeling complex. *Science* **303**, 343-348, doi:10.1126/science.1090701 (2004).
189 Flaus, A., Martin, D. M., Barton, G. J. & Owen-Hughes, T. Identification of multiple distinct Snf2 subfamilies with conserved structural motifs. *Nucleic Acids Res* **34**, 2887-2905, doi:10.1093/nar/gkl295 (2006).
190 Yadon, A. N. & Tsukiyama, T. SnapShot: Chromatin remodeling: ISWI. *Cell* **144**, 453-453 e451, doi:10.1016/j.cell.2011.01.019 (2011).
191 Kasten, M. M., Clapier, C. R. & Cairns, B. R. SnapShot: Chromatin remodeling: SWI/SNF. *Cell* **144**, 310 e311, doi:10.1016/j.cell.2011.01.007 (2011).
192 Bao, Y. & Shen, X. SnapShot: Chromatin remodeling: INO80 and SWR1. *Cell* **144**, 158-158 e152, doi:10.1016/j.cell.2010.12.024 (2011).
193 Sims, J. K. & Wade, P. A. SnapShot: Chromatin remodeling: CHD. *Cell* **144**, 626-626 e621, doi:10.1016/j.cell.2011.02.019 (2011).
194 Subramanya, H. S., Bird, L. E., Brannigan, J. A. & Wigley, D. B. Crystal structure of a DExx box DNA helicase. *Nature* **384**, 379-383, doi:10.1038/384379a0 (1996).
195 Grune, T. *et al.* Crystal structure and functional analysis of a nucleosome recognition module of the remodeling factor ISWI. *Mol Cell* **12**, 449-460, doi:10.1016/s1097-2765(03)00273-9 (2003).
196 Clapier, C. R. & Cairns, B. R. Regulation of ISWI involves inhibitory modules antagonized by nucleosomal epitopes. *Nature* **492**, 280-284, doi:10.1038/nature11625 (2012).
197 Dang, W. & Bartholomew, B. Domain architecture of the catalytic subunit in the ISW2-nucleosome complex. *Mol Cell Biol* **27**, 8306-8317, doi:10.1128/MCB.01351-07 (2007).
198 Corona, D. F. *et al.* ISWI is an ATP-dependent nucleosome remodeling factor. *Mol Cell* **3**, 239-245, doi:10.1016/s1097-2765(00)80314-7 (1999).

199 Langst, G. & Becker, P. B. Nucleosome mobilization and positioning by ISWI-containing chromatin-remodeling factors. *J Cell Sci* **114**, 2561-2568 (2001).
200 Tsukiyama, T., Palmer, J., Landel, C. C., Shiloach, J. & Wu, C. Characterization of the imitation switch subfamily of ATP-dependent chromatin-remodeling factors in Saccharomyces cerevisiae. *Genes Dev* **13**, 686-697, doi:10.1101/gad.13.6.686 (1999).
201 Vary, J. C., Jr. *et al.* Yeast Isw1p forms two separable complexes in vivo. *Mol Cell Biol* **23**, 80-91, doi:10.1128/mcb.23.1.80-91.2003 (2003).
202 Aihara, T. *et al.* Cloning and mapping of SMARCA5 encoding hSNF2H, a novel human homologue of Drosophila ISWI. *Cytogenet Cell Genet* **81**, 191-193, doi:10.1159/000015027 (1998).
203 Ito, T., Bulger, M., Pazin, M. J., Kobayashi, R. & Kadonaga, J. T. ACF, an ISWI-containing and ATP-utilizing chromatin assembly and remodeling factor. *Cell* **90**, 145-155, doi:10.1016/s0092-8674(00)80321-9 (1997).
204 Varga-Weisz, P. D. *et al.* Chromatin-remodelling factor CHRAC contains the ATPases ISWI and topoisomerase II. *Nature* **388**, 598-602, doi:10.1038/41587 (1997).
205 Hanai, K., Furuhashi, H., Yamamoto, T., Akasaka, K. & Hirose, S. RSF governs silent chromatin formation via histone H2Av replacement. *PLoS Genet* **4**, e1000011, doi:10.1371/journal.pgen.1000011 (2008).
206 Tsukiyama, T. & Wu, C. Purification and properties of an ATP-dependent nucleosome remodeling factor. *Cell* **83**, 1011-1020, doi:10.1016/0092-8674(95)90216-3 (1995).
207 Badenhorst, P., Voas, M., Rebay, I. & Wu, C. Biological functions of the ISWI chromatin remodeling complex NURF. *Genes Dev* **16**, 3186-3198, doi:10.1101/gad.1032202 (2002).
208 Wysocka, J. *et al.* A PHD finger of NURF couples histone H3 lysine 4 trimethylation with chromatin remodelling. *Nature* **442**, 86-90, doi:10.1038/nature04815 (2006).
209 Kwon, S. Y. *et al.* The nucleosome remodeling factor (NURF) regulates genes involved in Drosophila innate immunity. *Dev Biol* **316**, 538-547, doi:10.1016/j.ydbio.2008.01.033 (2008).
210 Maier, V. K., Chioda, M., Rhodes, D. & Becker, P. B. ACF catalyses chromatosome movements in chromatin fibres. *EMBO J* **27**, 817-826, doi:10.1038/sj.emboj.7601902 (2008).
211 Corona, D. F. *et al.* ISWI regulates higher-order chromatin structure and histone H1 assembly in vivo. *PLoS Biol* **5**, e232, doi:10.1371/journal.pbio.0050232 (2007).
212 Woodage, T., Basrai, M. A., Baxevanis, A. D., Hieter, P. & Collins, F. S. Characterization of the CHD family of proteins. *Proc Natl Acad Sci U S A* **94**, 11472-11477, doi:10.1073/pnas.94.21.11472 (1997).
213 Hauk, G., McKnight, J. N., Nodelman, I. M. & Bowman, G. D. The chromodomains of the Chd1 chromatin remodeler regulate DNA access to the ATPase motor. *Mol Cell* **39**, 711-723, doi:10.1016/j.molcel.2010.08.012 (2010).
214 Ryan, D. P., Sundaramoorthy, R., Martin, D., Singh, V. & Owen-Hughes, T. The DNA-binding domain of the Chd1 chromatin-remodelling enzyme contains SANT and SLIDE domains. *EMBO J* **30**, 2596-2609, doi:10.1038/emboj.2011.166 (2011).
215 Paro, R. & Hogness, D. S. The Polycomb protein shares a homologous domain with a heterochromatin-associated protein of Drosophila. *Proc Natl Acad Sci U S A* **88**, 263-267, doi:10.1073/pnas.88.1.263 (1991).
216 Flanagan, J. F. *et al.* Double chromodomains cooperate to recognize the methylated histone H3 tail. *Nature* **438**, 1181-1185, doi:10.1038/nature04290 (2005).
217 Fischle, W. *et al.* Molecular basis for the discrimination of repressive methyl-lysine marks in histone H3 by Polycomb and HP1 chromodomains. *Genes Dev* **17**, 1870-1881, doi:10.1101/gad.1110503 (2003).
218 Tran, H. G., Steger, D. J., Iyer, V. R. & Johnson, A. D. The chromo domain protein chd1p from budding yeast is an ATP-dependent chromatin-modifying factor. *EMBO J* **19**, 2323-2331, doi:10.1093/emboj/19.10.2323 (2000).

219 Qiu, Y. *et al.* The Chd1 Chromatin Remodeler Shifts Nucleosomal DNA Bidirectionally as a Monomer. *Mol Cell* **68**, 76-88 e76, doi:10.1016/j.molcel.2017.08.018 (2017).
220 Farnung, L., Vos, S. M., Wigge, C. & Cramer, P. Nucleosome-Chd1 structure and implications for chromatin remodelling. *Nature* **550**, 539-542, doi:10.1038/nature24046 (2017).
221 Bouazoune, K. & Brehm, A. ATP-dependent chromatin remodeling complexes in Drosophila. *Chromosome Res* **14**, 433-449, doi:10.1007/s10577-006-1067-0 (2006).
222 Marfella, C. G. & Imbalzano, A. N. The Chd family of chromatin remodelers. *Mutat Res* **618**, 30-40, doi:10.1016/j.mrfmmm.2006.07.012 (2007).
223 Lusser, A., Urwin, D. L. & Kadonaga, J. T. Distinct activities of CHD1 and ACF in ATP-dependent chromatin assembly. *Nat Struct Mol Biol* **12**, 160-166, doi:10.1038/nsmb884 (2005).
224 Skene, P. J., Hernandez, A. E., Groudine, M. & Henikoff, S. The nucleosomal barrier to promoter escape by RNA polymerase II is overcome by the chromatin remodeler Chd1. *Elife* **3**, e02042, doi:10.7554/eLife.02042 (2014).
225 Konev, A. Y. *et al.* CHD1 motor protein is required for deposition of histone variant H3.3 into chromatin in vivo. *Science* **317**, 1087-1090, doi:10.1126/science.1145339 (2007).
226 Murawska, M. *et al.* dCHD3, a novel ATP-dependent chromatin remodeler associated with sites of active transcription. *Mol Cell Biol* **28**, 2745-2757, doi:10.1128/MCB.01839-07 (2008).
227 Tong, J. K., Hassig, C. A., Schnitzler, G. R., Kingston, R. E. & Schreiber, S. L. Chromatin deacetylation by an ATP-dependent nucleosome remodelling complex. *Nature* **395**, 917-921, doi:10.1038/27699 (1998).
228 Xue, Y. *et al.* NURD, a novel complex with both ATP-dependent chromatin-remodeling and histone deacetylase activities. *Mol Cell* **2**, 851-861, doi:10.1016/s1097-2765(00)80299-3 (1998).
229 Denslow, S. A. & Wade, P. A. The human Mi-2/NuRD complex and gene regulation. *Oncogene* **26**, 5433-5438, doi:10.1038/sj.onc.1210611 (2007).
230 Taunton, J., Hassig, C. A. & Schreiber, S. L. A mammalian histone deacetylase related to the yeast transcriptional regulator Rpd3p. *Science* **272**, 408-411, doi:10.1126/science.272.5260.408 (1996).
231 Kolla, V. *et al.* The tumour suppressor CHD5 forms a NuRD-type chromatin remodelling complex. *Biochem J* **468**, 345-352, doi:10.1042/BJ20150030 (2015).
232 Hoffmeister, H. *et al.* CHD3 and CHD4 form distinct NuRD complexes with different yet overlapping functionality. *Nucleic Acids Res* **45**, 10534-10554, doi:10.1093/nar/gkx711 (2017).
233 Bracken, A. P., Brien, G. L. & Verrijzer, C. P. Dangerous liaisons: interplay between SWI/SNF, NuRD, and Polycomb in chromatin regulation and cancer. *Genes Dev* **33**, 936-959, doi:10.1101/gad.326066.119 (2019).
234 Farnung, L., Ochmann, M. & Cramer, P. Nucleosome-CHD4 chromatin remodeler structure maps human disease mutations. *Elife* **9**, doi:10.7554/eLife.56178 (2020).
235 Kunert, N. *et al.* dMec: a novel Mi-2 chromatin remodelling complex involved in transcriptional repression. *EMBO J* **28**, 533-544, doi:10.1038/emboj.2009.3 (2009).
236 Zhang, W. *et al.* The Nucleosome Remodeling and Deacetylase Complex NuRD Is Built from Preformed Catalytically Active Sub-modules. *J Mol Biol* **428**, 2931-2942, doi:10.1016/j.jmb.2016.04.025 (2016).
237 Cote, J., Quinn, J., Workman, J. L. & Peterson, C. L. Stimulation of GAL4 derivative binding to nucleosomal DNA by the yeast SWI/SNF complex. *Science* **265**, 53-60, doi:10.1126/science.8016655 (1994).
238 Szerlong, H. *et al.* The HSA domain binds nuclear actin-related proteins to regulate chromatin-remodeling ATPases. *Nat Struct Mol Biol* **15**, 469-476, doi:10.1038/nsmb.1403 (2008).

239 Clapier, C. R. *et al.* Regulation of DNA Translocation Efficiency within the Chromatin Remodeler RSC/Sth1 Potentiates Nucleosome Sliding and Ejection. *Mol Cell* **62**, 453-461, doi:10.1016/j.molcel.2016.03.032 (2016).
240 Sen, P., Ghosh, S., Pugh, B. F. & Bartholomew, B. A new, highly conserved domain in Swi2/Snf2 is required for SWI/SNF remodeling. *Nucleic Acids Res* **39**, 9155-9166, doi:10.1093/nar/gkr622 (2011).
241 Sen, P. *et al.* The SnAC domain of SWI/SNF is a histone anchor required for remodeling. *Mol Cell Biol* **33**, 360-370, doi:10.1128/MCB.00922-12 (2013).
242 Reeves, R. & Nissen, M. S. The A.T-DNA-binding domain of mammalian high mobility group I chromosomal proteins. A novel peptide motif for recognizing DNA structure. *J Biol Chem* **265**, 8573-8582 (1990).
243 Cairns, B. R. *et al.* Two functionally distinct forms of the RSC nucleosome-remodeling complex, containing essential AT hook, BAH, and bromodomains. *Mol Cell* **4**, 715-723, doi:10.1016/s1097-2765(00)80382-2 (1999).
244 Hassan, A. H. *et al.* Function and selectivity of bromodomains in anchoring chromatin-modifying complexes to promoter nucleosomes. *Cell* **111**, 369-379, doi:10.1016/s0092-8674(02)01005-x (2002).
245 Mohrmann, L. & Verrijzer, C. P. Composition and functional specificity of SWI2/SNF2 class chromatin remodeling complexes. *Biochim Biophys Acta* **1681**, 59-73, doi:10.1016/j.bbaexp.2004.10.005 (2005).
246 Laurent, B. C., Yang, X. & Carlson, M. An essential Saccharomyces cerevisiae gene homologous to SNF2 encodes a helicase-related protein in a new family. *Mol Cell Biol* **12**, 1893-1902, doi:10.1128/mcb.12.4.1893 (1992).
247 Du, J., Nasir, I., Benton, B. K., Kladde, M. P. & Laurent, B. C. Sth1p, a Saccharomyces cerevisiae Snf2p/Swi2p homolog, is an essential ATPase in RSC and differs from Snf/Swi in its interactions with histones and chromatin-associated proteins. *Genetics* **150**, 987-1005 (1998).
248 Cairns, B. R. *et al.* RSC, an essential, abundant chromatin-remodeling complex. *Cell* **87**, 1249-1260, doi:10.1016/s0092-8674(00)81820-6 (1996).
249 Papoulas, O. *et al.* The Drosophila trithorax group proteins BRM, ASH1 and ASH2 are subunits of distinct protein complexes. *Development* **125**, 3955-3966 (1998).
250 Mohrmann, L. *et al.* Differential targeting of two distinct SWI/SNF-related Drosophila chromatin-remodeling complexes. *Mol Cell Biol* **24**, 3077-3088, doi:10.1128/mcb.24.8.3077-3088.2004 (2004).
251 Tamkun, J. W. *et al.* brahma: a regulator of Drosophila homeotic genes structurally related to the yeast transcriptional activator SNF2/SWI2. *Cell* **68**, 561-572, doi:10.1016/0092-8674(92)90191-e (1992).
252 Wang, W. *et al.* Purification and biochemical heterogeneity of the mammalian SWI-SNF complex. *EMBO J* **15**, 5370-5382 (1996).
253 Xue, Y. *et al.* The human SWI/SNF-B chromatin-remodeling complex is related to yeast rsc and localizes at kinetochores of mitotic chromosomes. *Proc Natl Acad Sci U S A* **97**, 13015-13020, doi:10.1073/pnas.240208597 (2000).
254 Ho, L. & Crabtree, G. R. Chromatin remodelling during development. *Nature* **463**, 474-484, doi:10.1038/nature08911 (2010).
255 Alpsoy, A. & Dykhuizen, E. C. Glioma tumor suppressor candidate region gene 1 (GLTSCR1) and its paralog GLTSCR1-like form SWI/SNF chromatin remodeling subcomplexes. *J Biol Chem* **293**, 3892-3903, doi:10.1074/jbc.RA117.001065 (2018).
256 Gatchalian, J. *et al.* A non-canonical BRD9-containing BAF chromatin remodeling complex regulates naive pluripotency in mouse embryonic stem cells. *Nat Commun* **9**, 5139, doi:10.1038/s41467-018-07528-9 (2018).
257 Ho, L. *et al.* An embryonic stem cell chromatin remodeling complex, esBAF, is essential for embryonic stem cell self-renewal and pluripotency. *Proc Natl Acad Sci U S A* **106**, 5181-5186, doi:10.1073/pnas.0812889106 (2009).

258 Kaeser, M. D., Aslanian, A., Dong, M. Q., Yates, J. R., 3rd & Emerson, B. M. BRD7, a novel PBAF-specific SWI/SNF subunit, is required for target gene activation and repression in embryonic stem cells. *J Biol Chem* **283**, 32254-32263, doi:10.1074/jbc.M806061200 (2008).
259 Ferreira, H., Flaus, A. & Owen-Hughes, T. Histone modifications influence the action of Snf2 family remodelling enzymes by different mechanisms. *J Mol Biol* **374**, 563-579, doi:10.1016/j.jmb.2007.09.059 (2007).
260 Chatterjee, N. *et al.* Histone H3 tail acetylation modulates ATP-dependent remodeling through multiple mechanisms. *Nucleic Acids Res* **39**, 8378-8391, doi:10.1093/nar/gkr535 (2011).
261 Skiniotis, G., Moazed, D. & Walz, T. Acetylated histone tail peptides induce structural rearrangements in the RSC chromatin remodeling complex. *J Biol Chem* **282**, 20804-20808, doi:10.1074/jbc.C700081200 (2007).
262 Bennett, G. & Peterson, C. L. SWI/SNF recruitment to a DNA double-strand break by the NuA4 and Gcn5 histone acetyltransferases. *DNA Repair (Amst)* **30**, 38-45, doi:10.1016/j.dnarep.2015.03.006 (2015).
263 VanDemark, A. P. *et al.* Autoregulation of the rsc4 tandem bromodomain by gcn5 acetylation. *Mol Cell* **27**, 817-828, doi:10.1016/j.molcel.2007.08.018 (2007).
264 Ng, H. H., Robert, F., Young, R. A. & Struhl, K. Genome-wide location and regulated recruitment of the RSC nucleosome-remodeling complex. *Genes Dev* **16**, 806-819, doi:10.1101/gad.978902 (2002).
265 Parnell, T. J., Huff, J. T. & Cairns, B. R. RSC regulates nucleosome positioning at Pol II genes and density at Pol III genes. *EMBO J* **27**, 100-110, doi:10.1038/sj.emboj.7601946 (2008).
266 Kim, J. H., Saraf, A., Florens, L., Washburn, M. & Workman, J. L. Gcn5 regulates the dissociation of SWI/SNF from chromatin by acetylation of Swi2/Snf2. *Genes Dev* **24**, 2766-2771, doi:10.1101/gad.1979710 (2010).
267 Cairns, B. R., Erdjument-Bromage, H., Tempst, P., Winston, F. & Kornberg, R. D. Two actin-related proteins are shared functional components of the chromatin-remodeling complexes RSC and SWI/SNF. *Mol Cell* **2**, 639-651, doi:10.1016/s1097-2765(00)80162-8 (1998).
268 Szerlong, H., Saha, A. & Cairns, B. R. The nuclear actin-related proteins Arp7 and Arp9: a dimeric module that cooperates with architectural proteins for chromatin remodeling. *EMBO J* **22**, 3175-3187, doi:10.1093/emboj/cdg296 (2003).
269 Schubert, H. L. *et al.* Structure of an actin-related subcomplex of the SWI/SNF chromatin remodeler. *Proc Natl Acad Sci U S A* **110**, 3345-3350, doi:10.1073/pnas.1215379110 (2013).
270 Yang, X., Zaurin, R., Beato, M. & Peterson, C. L. Swi3p controls SWI/SNF assembly and ATP-dependent H2A-H2B displacement. *Nat Struct Mol Biol* **14**, 540-547, doi:10.1038/nsmb1238 (2007).
271 Sirinakis, G. *et al.* The RSC chromatin remodelling ATPase translocates DNA with high force and small step size. *EMBO J* **30**, 2364-2372, doi:10.1038/emboj.2011.141 (2011).
272 Ebbert, R., Birkmann, A. & Schuller, H. J. The product of the SNF2/SWI2 paralogue INO80 of Saccharomyces cerevisiae required for efficient expression of various yeast structural genes is part of a high-molecular-weight protein complex. *Mol Microbiol* **32**, 741-751, doi:10.1046/j.1365-2958.1999.01390.x (1999).
273 Shen, X., Mizuguchi, G., Hamiche, A. & Wu, C. A chromatin remodelling complex involved in transcription and DNA processing. *Nature* **406**, 541-544, doi:10.1038/35020123 (2000).
274 Krogan, N. J. *et al.* A Snf2 family ATPase complex required for recruitment of the histone H2A variant Htz1. *Mol Cell* **12**, 1565-1576, doi:10.1016/s1097-2765(03)00497-0 (2003).
275 Shen, X., Ranallo, R., Choi, E. & Wu, C. Involvement of actin-related proteins in ATP-dependent chromatin remodeling. *Mol Cell* **12**, 147-155, doi:10.1016/s1097-2765(03)00264-8 (2003).
276 Tosi, A. *et al.* Structure and subunit topology of the INO80 chromatin remodeler and its nucleosome complex. *Cell* **154**, 1207-1219, doi:10.1016/j.cell.2013.08.016 (2013).

277 Watanabe, S. *et al.* Structural analyses of the chromatin remodelling enzymes INO80-C and SWR-C. *Nat Commun* **6**, 7108, doi:10.1038/ncomms8108 (2015).
278 Willhoft, O., Bythell-Douglas, R., McCormack, E. A. & Wigley, D. B. Synergy and antagonism in regulation of recombinant human INO80 chromatin remodeling complex. *Nucleic Acids Res* **44**, 8179-8188, doi:10.1093/nar/gkw509 (2016).
279 Lin, C. L. *et al.* Functional characterization and architecture of recombinant yeast SWR1 histone exchange complex. *Nucleic Acids Res* **45**, 7249-7260, doi:10.1093/nar/gkx414 (2017).
280 Nguyen, V. Q. *et al.* Molecular architecture of the ATP-dependent chromatin-remodeling complex SWR1. *Cell* **154**, 1220-1231, doi:10.1016/j.cell.2013.08.018 (2013).
281 Harata, M., Karwan, A. & Wintersberger, U. An essential gene of Saccharomyces cerevisiae coding for an actin-related protein. *Proc Natl Acad Sci U S A* **91**, 8258-8262, doi:10.1073/pnas.91.17.8258 (1994).
282 Wu, W. H. *et al.* N terminus of Swr1 binds to histone H2AZ and provides a platform for subunit assembly in the chromatin remodeling complex. *J Biol Chem* **284**, 6200-6207, doi:10.1074/jbc.M808830200 (2009).
283 Cairns, B. R., Henry, N. L. & Kornberg, R. D. TFG/TAF30/ANC1, a component of the yeast SWI/SNF complex that is similar to the leukemogenic proteins ENL and AF-9. *Mol Cell Biol* **16**, 3308-3316, doi:10.1128/mcb.16.7.3308 (1996).
284 Henry, N. L. *et al.* TFIIF-TAF-RNA polymerase II connection. *Genes Dev* **8**, 2868-2878, doi:10.1101/gad.8.23.2868 (1994).
285 John, S. *et al.* The something about silencing protein, Sas3, is the catalytic subunit of NuA3, a yTAF(II)30-containing HAT complex that interacts with the Spt16 subunit of the yeast CP (Cdc68/Pob3)-FACT complex. *Genes Dev* **14**, 1196-1208 (2000).
286 Andrews, F. H. *et al.* The Taf14 YEATS domain is a reader of histone crotonylation. *Nat Chem Biol* **12**, 396-398, doi:10.1038/nchembio.2065 (2016).
287 Gowans, G. J. *et al.* Recognition of Histone Crotonylation by Taf14 Links Metabolic State to Gene Expression. *Mol Cell* **76**, 909-921 e903, doi:10.1016/j.molcel.2019.09.029 (2019).
288 Shanle, E. K. *et al.* Association of Taf14 with acetylated histone H3 directs gene transcription and the DNA damage response. *Genes Dev* **29**, 1795-1800, doi:10.1101/gad.269977.115 (2015).
289 Li, Y. *et al.* Molecular Coupling of Histone Crotonylation and Active Transcription by AF9 YEATS Domain. *Mol Cell* **62**, 181-193, doi:10.1016/j.molcel.2016.03.028 (2016).
290 Zhang, H. *et al.* The Yaf9 component of the SWR1 and NuA4 complexes is required for proper gene expression, histone H4 acetylation, and Htz1 replacement near telomeres. *Mol Cell Biol* **24**, 9424-9436, doi:10.1128/MCB.24.21.9424-9436.2004 (2004).
291 Klein, B. J. *et al.* Yaf9 subunit of the NuA4 and SWR1 complexes targets histone H3K27ac through its YEATS domain. *Nucleic Acids Res* **46**, 421-430, doi:10.1093/nar/gkx1151 (2018).
292 Creyghton, M. P. *et al.* Histone H3K27ac separates active from poised enhancers and predicts developmental state. *Proc Natl Acad Sci U S A* **107**, 21931-21936, doi:10.1073/pnas.1016071107 (2010).
293 Jonsson, Z. O., Jha, S., Wohlschlegel, J. A. & Dutta, A. Rvb1p/Rvb2p recruit Arp5p and assemble a functional Ino80 chromatin remodeling complex. *Mol Cell* **16**, 465-477, doi:10.1016/j.molcel.2004.09.033 (2004).
294 Wu, W. H. *et al.* Swc2 is a widely conserved H2AZ-binding module essential for ATP-dependent histone exchange. *Nat Struct Mol Biol* **12**, 1064-1071, doi:10.1038/nsmb1023 (2005).
295 Ranjan, A. *et al.* H2A histone-fold and DNA elements in nucleosome activate SWR1-mediated H2A.Z replacement in budding yeast. *Elife* **4**, e06845, doi:10.7554/eLife.06845 (2015).
296 Liang, X. *et al.* Structural basis of H2A.Z recognition by SRCAP chromatin-remodeling subunit YL1. *Nat Struct Mol Biol* **23**, 317-323, doi:10.1038/nsmb.3190 (2016).

297 Hong, J. *et al.* The catalytic subunit of the SWR1 remodeler is a histone chaperone for the H2A.Z-H2B dimer. *Mol Cell* **53**, 498-505, doi:10.1016/j.molcel.2014.01.010 (2014).
298 Calo, E. & Wysocka, J. Modification of enhancer chromatin: what, how, and why? *Mol Cell* **49**, 825-837, doi:10.1016/j.molcel.2013.01.038 (2013).
299 de Dieuleveult, M. *et al.* Genome-wide nucleosome specificity and function of chromatin remodellers in ES cells. *Nature* **530**, 113-116, doi:10.1038/nature16505 (2016).
300 Papamichos-Chronakis, M., Watanabe, S., Rando, O. J. & Peterson, C. L. Global regulation of H2A.Z localization by the INO80 chromatin-remodeling enzyme is essential for genome integrity. *Cell* **144**, 200-213, doi:10.1016/j.cell.2010.12.021 (2011).
301 Watanabe, S., Radman-Livaja, M., Rando, O. J. & Peterson, C. L. A histone acetylation switch regulates H2A.Z deposition by the SWR-C remodeling enzyme. *Science* **340**, 195-199, doi:10.1126/science.1229758 (2013).
302 Brahma, S. *et al.* INO80 exchanges H2A.Z for H2A by translocating on DNA proximal to histone dimers. *Nat Commun* **8**, 15616, doi:10.1038/ncomms15616 (2017).
303 Wang, F., Ranjan, A., Wei, D. & Wu, C. Comment on "A histone acetylation switch regulates H2A.Z deposition by the SWR-C remodeling enzyme". *Science* **353**, 358, doi:10.1126/science.aad5921 (2016).
304 Udugama, M., Sabri, A. & Bartholomew, B. The INO80 ATP-dependent chromatin remodeling complex is a nucleosome spacing factor. *Mol Cell Biol* **31**, 662-673, doi:10.1128/MCB.01035-10 (2011).
305 Zhou, C. Y. *et al.* The Yeast INO80 Complex Operates as a Tunable DNA Length-Sensitive Switch to Regulate Nucleosome Sliding. *Mol Cell* **69**, 677-688 e679, doi:10.1016/j.molcel.2018.01.028 (2018).
306 Yen, K., Vinayachandran, V. & Pugh, B. F. SWR-C and INO80 chromatin remodelers recognize nucleosome-free regions near +1 nucleosomes. *Cell* **154**, 1246-1256, doi:10.1016/j.cell.2013.08.043 (2013).
307 Poli, J. *et al.* Mec1, INO80, and the PAF1 complex cooperate to limit transcription replication conflicts through RNAPII removal during replication stress. *Genes Dev* **30**, 337-354, doi:10.1101/gad.273813.115 (2016).
308 Lafon, A. *et al.* INO80 Chromatin Remodeler Facilitates Release of RNA Polymerase II from Chromatin for Ubiquitin-Mediated Proteasomal Degradation. *Mol Cell* **60**, 784-796, doi:10.1016/j.molcel.2015.10.028 (2015).
309 Luzzi, S. *et al.* The INO80 remodeler couples premature termination of mRNA synthesis with transcription elongation. *bioRxiv* (2020).
310 Vincent, J. A., Kwong, T. J. & Tsukiyama, T. ATP-dependent chromatin remodeling shapes the DNA replication landscape. *Nat Struct Mol Biol* **15**, 477-484, doi:10.1038/nsmb.1419 (2008).
311 Papamichos-Chronakis, M. & Peterson, C. L. The Ino80 chromatin-remodeling enzyme regulates replisome function and stability. *Nat Struct Mol Biol* **15**, 338-345, doi:10.1038/nsmb.1413 (2008).
312 Shimada, K. *et al.* Ino80 chromatin remodeling complex promotes recovery of stalled replication forks. *Curr Biol* **18**, 566-575, doi:10.1016/j.cub.2008.03.049 (2008).
313 Prendergast, L. *et al.* Resolution of R-loops by INO80 promotes DNA replication and maintains cancer cell proliferation and viability. *Nat Commun* **11**, 4534, doi:10.1038/s41467-020-18306-x (2020).
314 Morrison, A. J. *et al.* INO80 and gamma-H2AX interaction links ATP-dependent chromatin remodeling to DNA damage repair. *Cell* **119**, 767-775, doi:10.1016/j.cell.2004.11.037 (2004).
315 van Attikum, H., Fritsch, O., Hohn, B. & Gasser, S. M. Recruitment of the INO80 complex by H2A phosphorylation links ATP-dependent chromatin remodeling with DNA double-strand break repair. *Cell* **119**, 777-788, doi:10.1016/j.cell.2004.11.033 (2004).

316 Morrison, A. J. *et al.* Mec1/Tel1 phosphorylation of the INO80 chromatin remodeling complex influences DNA damage checkpoint responses. *Cell* **130**, 499-511, doi:10.1016/j.cell.2007.06.010 (2007).
317 Yu, E. Y. *et al.* Regulation of telomere structure and functions by subunits of the INO80 chromatin remodeling complex. *Mol Cell Biol* **27**, 5639-5649, doi:10.1128/MCB.00418-07 (2007).
318 Xue, Y. *et al.* The Ino80 complex prevents invasion of euchromatin into silent chromatin. *Genes Dev* **29**, 350-355, doi:10.1101/gad.256255.114 (2015).
319 Morrison, A. J. & Shen, X. Chromatin remodelling beyond transcription: the INO80 and SWR1 complexes. *Nat Rev Mol Cell Biol* **10**, 373-384, doi:10.1038/nrm2693 (2009).
320 Klymenko, T. *et al.* A Polycomb group protein complex with sequence-specific DNA-binding and selective methyl-lysine-binding activities. *Genes Dev* **20**, 1110-1122, doi:10.1101/gad.377406 (2006).
321 Jin, J. *et al.* A mammalian chromatin remodeling complex with similarities to the yeast INO80 complex. *J Biol Chem* **280**, 41207-41212, doi:10.1074/jbc.M509128200 (2005).
322 Cai, Y. *et al.* YY1 functions with INO80 to activate transcription. *Nat Struct Mol Biol* **14**, 872-874, doi:10.1038/nsmb1276 (2007).
323 Wu, S. *et al.* A YY1-INO80 complex regulates genomic stability through homologous recombination-based repair. *Nat Struct Mol Biol* **14**, 1165-1172, doi:10.1038/nsmb1332 (2007).
324 Chen, L. *et al.* Subunit organization of the human INO80 chromatin remodeling complex: an evolutionarily conserved core complex catalyzes ATP-dependent nucleosome remodeling. *J Biol Chem* **286**, 11283-11289, doi:10.1074/jbc.M111.222505 (2011).
325 Ruhf, M. L. *et al.* The domino gene of Drosophila encodes novel members of the SWI2/SNF2 family of DNA-dependent ATPases, which contribute to the silencing of homeotic genes. *Development* **128**, 1429-1441 (2001).
326 Borner, K. & Becker, P. B. Splice variants of the SWR1-type nucleosome remodeling factor Domino have distinct functions during Drosophila melanogaster oogenesis. *Development* **143**, 3154-3167, doi:10.1242/dev.139634 (2016).
327 Fuchs, M. *et al.* The p400 complex is an essential E1A transformation target. *Cell* **106**, 297-307, doi:10.1016/s0092-8674(01)00450-0 (2001).
328 Ruhl, D. D. *et al.* Purification of a human SRCAP complex that remodels chromatin by incorporating the histone variant H2A.Z into nucleosomes. *Biochemistry* **45**, 5671-5677, doi:10.1021/bi060043d (2006).
329 Pradhan, S. K. *et al.* EP400 Deposits H3.3 into Promoters and Enhancers during Gene Activation. *Mol Cell* **61**, 27-38, doi:10.1016/j.molcel.2015.10.039 (2016).
330 Singleton, M. R. & Wigley, D. B. Modularity and specialization in superfamily 1 and 2 helicases. *J Bacteriol* **184**, 1819-1826, doi:10.1128/jb.184.7.1819-1826.2002 (2002).
331 Gorbalenya, A. E. & Koonin, E. V. Helicases: amino acid sequence comparisons and structure-function relationships. *Current opinion in structural biology* **3**, 419-429 (1993).
332 Gorbalenya, A. E., Koonin, E. V., Donchenko, A. P. & Blinov, V. M. A novel superfamily of nucleoside triphosphate-binding motif containing proteins which are probably involved in duplex unwinding in DNA and RNA replication and recombination. *FEBS Lett* **235**, 16-24, doi:10.1016/0014-5793(88)81226-2 (1988).
333 Pause, A. & Sonenberg, N. Mutational analysis of a DEAD box RNA helicase: the mammalian translation initiation factor eIF-4A. *EMBO J* **11**, 2643-2654 (1992).
334 Tanner, N. K., Cordin, O., Banroques, J., Doere, M. & Linder, P. The Q motif: a newly identified motif in DEAD box helicases may regulate ATP binding and hydrolysis. *Mol Cell* **11**, 127-138, doi:10.1016/s1097-2765(03)00006-6 (2003).
335 Walker, J. E., Saraste, M., Runswick, M. J. & Gay, N. J. Distantly related sequences in the alpha- and beta-subunits of ATP synthase, myosin, kinases and other ATP-requiring enzymes and a common nucleotide binding fold. *EMBO J* **1**, 945-951 (1982).

336 Brosh, R. M., Jr. & Matson, S. W. Mutations in motif II of Escherichia coli DNA helicase II render the enzyme nonfunctional in both mismatch repair and excision repair with differential effects on the unwinding reaction. *J Bacteriol* **177**, 5612-5621, doi:10.1128/jb.177.19.5612-5621.1995 (1995).
337 Schmid, S. R. & Linder, P. D-E-A-D protein family of putative RNA helicases. *Mol Microbiol* **6**, 283-291, doi:10.1111/j.1365-2958.1992.tb01470.x (1992).
338 Cox, M. M. Why does RecA protein hydrolyse ATP? *Trends Biochem Sci* **19**, 217-222, doi:10.1016/0968-0004(94)90025-6 (1994).
339 Durr, H., Flaus, A., Owen-Hughes, T. & Hopfner, K. P. Snf2 family ATPases and DExx box helicases: differences and unifying concepts from high-resolution crystal structures. *Nucleic Acids Res* **34**, 4160-4167, doi:10.1093/nar/gkl540 (2006).
340 Singleton, M. R., Dillingham, M. S. & Wigley, D. B. Structure and mechanism of helicases and nucleic acid translocases. *Annu Rev Biochem* **76**, 23-50, doi:10.1146/annurev.biochem.76.052305.115300 (2007).
341 Gu, M. & Rice, C. M. Three conformational snapshots of the hepatitis C virus NS3 helicase reveal a ratchet translocation mechanism. *Proc Natl Acad Sci U S A* **107**, 521-528, doi:10.1073/pnas.0913380107 (2010).
342 Saha, A., Wittmeyer, J. & Cairns, B. R. Chromatin remodeling by RSC involves ATP-dependent DNA translocation. *Genes Dev* **16**, 2120-2134, doi:10.1101/gad.995002 (2002).
343 Whitehouse, I., Stockdale, C., Flaus, A., Szczelkun, M. D. & Owen-Hughes, T. Evidence for DNA translocation by the ISWI chromatin-remodeling enzyme. *Mol Cell Biol* **23**, 1935-1945, doi:10.1128/mcb.23.6.1935-1945.2003 (2003).
344 Deindl, S. *et al.* ISWI remodelers slide nucleosomes with coordinated multi-base-pair entry steps and single-base-pair exit steps. *Cell* **152**, 442-452, doi:10.1016/j.cell.2012.12.040 (2013).
345 Liu, X., Li, M., Xia, X., Li, X. & Chen, Z. Mechanism of chromatin remodelling revealed by the Snf2-nucleosome structure. *Nature* **544**, 440-445, doi:10.1038/nature22036 (2017).
346 Li, M. *et al.* Mechanism of DNA translocation underlying chromatin remodelling by Snf2. *Nature* **567**, 409-413, doi:10.1038/s41586-019-1029-2 (2019).
347 Yan, L., Wu, H., Li, X., Gao, N. & Chen, Z. Structures of the ISWI-nucleosome complex reveal a conserved mechanism of chromatin remodeling. *Nat Struct Mol Biol* **26**, 258-266, doi:10.1038/s41594-019-0199-9 (2019).
348 Xia, X., Liu, X., Li, T., Fang, X. & Chen, Z. Structure of chromatin remodeler Swi2/Snf2 in the resting state. *Nat Struct Mol Biol* **23**, 722-729, doi:10.1038/nsmb.3259 (2016).
349 Chen, L., Conaway, R. C. & Conaway, J. W. Multiple modes of regulation of the human Ino80 SNF2 ATPase by subunits of the INO80 chromatin-remodeling complex. *Proc Natl Acad Sci U S A* **110**, 20497-20502, doi:10.1073/pnas.1317092110 (2013).
350 Matias, P. M. *et al.* The AAA+ proteins Pontin and Reptin enter adult age: from understanding their basic biology to the identification of selective inhibitors. *Front Mol Biosci* **2**, 17, doi:10.3389/fmolb.2015.00017 (2015).
351 Jha, S. & Dutta, A. RVB1/RVB2: running rings around molecular biology. *Mol Cell* **34**, 521-533, doi:10.1016/j.molcel.2009.05.016 (2009).
352 Lakomek, K., Stoehr, G., Tosi, A., Schmailzl, M. & Hopfner, K. P. Structural basis for dodecameric assembly states and conformational plasticity of the full-length AAA+ ATPases Rvb1 . Rvb2. *Structure* **23**, 483-495, doi:10.1016/j.str.2014.12.015 (2015).
353 Willhoft, O. *et al.* Structure and dynamics of the yeast SWR1-nucleosome complex. *Science* **362**, doi:10.1126/science.aat7716 (2018).
354 Zhou, C. Y. *et al.* Regulation of Rvb1/Rvb2 by a Domain within the INO80 Chromatin Remodeling Complex Implicates the Yeast Rvbs as Protein Assembly Chaperones. *Cell Rep* **19**, 2033-2044, doi:10.1016/j.celrep.2017.05.029 (2017).
355 Tsaneva, I. R., Muller, B. & West, S. C. RuvA and RuvB proteins of Escherichia coli exhibit DNA helicase activity in vitro. *Proc Natl Acad Sci U S A* **90**, 1315-1319, doi:10.1073/pnas.90.4.1315 (1993).

356 Davies, A. A. & West, S. C. Formation of RuvABC-Holliday junction complexes in vitro. *Curr Biol* **8**, 725-727, doi:10.1016/s0960-9822(98)70282-9 (1998).
357 Gribun, A., Cheung, K. L., Huen, J., Ortega, J. & Houry, W. A. Yeast Rvb1 and Rvb2 are ATP-dependent DNA helicases that form a heterohexameric complex. *J Mol Biol* **376**, 1320-1333, doi:10.1016/j.jmb.2007.12.049 (2008).
358 Nano, N. & Houry, W. A. Chaperone-like activity of the AAA+ proteins Rvb1 and Rvb2 in the assembly of various complexes. *Philos Trans R Soc Lond B Biol Sci* **368**, 20110399, doi:10.1098/rstb.2011.0399 (2013).
359 Oberbeckmann, E. *et al. Genome information processing by the INO80 chromatin remodeler positions nucleosomes* (2020).
360 Yen, K., Vinayachandran, V., Batta, K., Koerber, R. T. & Pugh, B. F. Genome-wide nucleosome specificity and directionality of chromatin remodelers. *Cell* **149**, 1461-1473, doi:10.1016/j.cell.2012.04.036 (2012).
361 Yao, W. *et al.* Assembly of the Arp5 (Actin-related Protein) Subunit Involved in Distinct INO80 Chromatin Remodeling Activities. *J Biol Chem* **290**, 25700-25709, doi:10.1074/jbc.M115.674887 (2015).
362 Rees, D. M., Willhoft, O., Lin, C. L., Bythell-Douglas, R. & Wigley, D. B. Production and Assay of Recombinant Multisubunit Chromatin Remodeling Complexes. *Methods Enzymol* **592**, 27-47, doi:10.1016/bs.mie.2017.03.015 (2017).
363 Dominguez, R. & Holmes, K. C. Actin structure and function. *Annu Rev Biophys* **40**, 169-186, doi:10.1146/annurev-biophys-042910-155359 (2011).
364 Kabsch, W., Mannherz, H. G., Suck, D., Pai, E. F. & Holmes, K. C. Atomic structure of the actin:DNase I complex. *Nature* **347**, 37-44, doi:10.1038/347037a0 (1990).
365 Kudryashov, D. S. & Reisler, E. ATP and ADP actin states. *Biopolymers* **99**, 245-256, doi:10.1002/bip.22155 (2013).
366 Dion, V., Shimada, K. & Gasser, S. M. Actin-related proteins in the nucleus: life beyond chromatin remodelers. *Curr Opin Cell Biol* **22**, 383-391, doi:10.1016/j.ceb.2010.02.006 (2010).
367 Carlier, M. F. & Shekhar, S. Global treadmilling coordinates actin turnover and controls the size of actin networks. *Nat Rev Mol Cell Biol* **18**, 389-401, doi:10.1038/nrm.2016.172 (2017).
368 Merino, F. *et al.* Structural transitions of F-actin upon ATP hydrolysis at near-atomic resolution revealed by cryo-EM. *Nat Struct Mol Biol* **25**, 528-537, doi:10.1038/s41594-018-0074-0 (2018).
369 Caridi, C. P. *et al.* Nuclear F-actin and myosins drive relocalization of heterochromatic breaks. *Nature* **559**, 54-60, doi:10.1038/s41586-018-0242-8 (2018).
370 Schrank, B. R. *et al.* Nuclear ARP2/3 drives DNA break clustering for homology-directed repair. *Nature* **559**, 61-66, doi:10.1038/s41586-018-0237-5 (2018).
371 Kapoor, P., Chen, M., Winkler, D. D., Luger, K. & Shen, X. Evidence for monomeric actin function in INO80 chromatin remodeling. *Nat Struct Mol Biol* **20**, 426-432, doi:10.1038/nsmb.2529 (2013).
372 Galarneau, L. *et al.* Multiple links between the NuA4 histone acetyltransferase complex and epigenetic control of transcription. *Mol Cell* **5**, 927-937, doi:10.1016/s1097-2765(00)80258-0 (2000).
373 Cao, T. *et al.* Crystal structure of a nuclear actin ternary complex. *Proc Natl Acad Sci U S A* **113**, 8985-8990, doi:10.1073/pnas.1602818113 (2016).
374 Fenn, S. *et al.* Structural biochemistry of nuclear actin-related proteins 4 and 8 reveals their interaction with actin. *EMBO J* **30**, 2153-2166, doi:10.1038/emboj.2011.118 (2011).
375 Gerhold, C. B. *et al.* Structure of Actin-related protein 8 and its contribution to nucleosome binding. *Nucleic Acids Res* **40**, 11036-11046, doi:10.1093/nar/gks842 (2012).
376 Saravanan, M. *et al.* Interactions between the nucleosome histone core and Arp8 in the INO80 chromatin remodeling complex. *Proc Natl Acad Sci U S A* **109**, 20883-20888, doi:10.1073/pnas.1214735109 (2012).

377 Brahma, S., Ngubo, M., Paul, S., Udugama, M. & Bartholomew, B. The Arp8 and Arp4 module acts as a DNA sensor controlling INO80 chromatin remodeling. *Nat Commun* **9**, 3309, doi:10.1038/s41467-018-05710-7 (2018).
378 Hodges, C., Kirkland, J. G. & Crabtree, G. R. The Many Roles of BAF (mSWI/SNF) and PBAF Complexes in Cancer. *Cold Spring Harb Perspect Med* **6**, doi:10.1101/cshperspect.a026930 (2016).
379 Ray, S. & Grove, A. The yeast high mobility group protein HMO2, a subunit of the chromatin-remodeling complex INO80, binds DNA ends. *Nucleic Acids Res* **37**, 6389-6399, doi:10.1093/nar/gkp695 (2009).
380 Malarkey, C. S. & Churchill, M. E. The high mobility group box: the ultimate utility player of a cell. *Trends Biochem Sci* **37**, 553-562, doi:10.1016/j.tibs.2012.09.003 (2012).
381 Kamau, E., Bauerle, K. T. & Grove, A. The Saccharomyces cerevisiae high mobility group box protein HMO1 contains two functional DNA binding domains. *J Biol Chem* **279**, 55234-55240, doi:10.1074/jbc.M409459200 (2004).
382 Bauerle, K. T., Kamau, E. & Grove, A. Interactions between N- and C-terminal domains of the Saccharomyces cerevisiae high-mobility group protein HMO1 are required for DNA bending. *Biochemistry* **45**, 3635-3645, doi:10.1021/bi0522798 (2006).
383 Ray, S. & Grove, A. Interaction of Saccharomyces cerevisiae HMO2 domains with distorted DNA. *Biochemistry* **51**, 1825-1835, doi:10.1021/bi201700h (2012).
384 Willhoft, O. *et al.* Crosstalk within a functional INO80 complex dimer regulates nucleosome sliding. *Elife* **6**, doi:10.7554/eLife.25782 (2017).
385 Kuhlbrandt, W. Biochemistry. The resolution revolution. *Science* **343**, 1443-1444, doi:10.1126/science.1251652 (2014).
386 Knoll, K. R. *et al.* The nuclear actin-containing Arp8 module is a linker DNA sensor driving INO80 chromatin remodeling. *Nat Struct Mol Biol* **25**, 823-832, doi:10.1038/s41594-018-0115-8 (2018).
387 Eustermann, S. *et al.* Structural basis for ATP-dependent chromatin remodelling by the INO80 complex. *Nature* **556**, 386-390, doi:10.1038/s41586-018-0029-y (2018).
388 Aramayo, R. J. *et al.* Cryo-EM structures of the human INO80 chromatin-remodeling complex. *Nat Struct Mol Biol* **25**, 37-44, doi:10.1038/s41594-017-0003-7 (2018).
389 Patel, A. B. *et al.* Architecture of the chromatin remodeler RSC and insights into its nucleosome engagement. *Elife* **8**, doi:10.7554/eLife.54449 (2019).
390 Armache, J. P. *et al.* Cryo-EM structures of remodeler-nucleosome intermediates suggest allosteric control through the nucleosome. *Elife* **8**, doi:10.7554/eLife.46057 (2019).
391 Han, Y., Reyes, A. A., Malik, S. & He, Y. Cryo-EM structure of SWI/SNF complex bound to a nucleosome. *Nature* **579**, 452-455, doi:10.1038/s41586-020-2087-1 (2020).
392 Wagner, F. R. *et al.* Structure of SWI/SNF chromatin remodeller RSC bound to a nucleosome. *Nature*, 1-4 (2020).
393 He, S. *et al.* Structure of nucleosome-bound human BAF complex. *Science* **367**, 875-881, doi:10.1126/science.aaz9761 (2020).
394 Ye, Y. *et al.* Structure of the RSC complex bound to the nucleosome. *Science* **366**, 838-843, doi:10.1126/science.aay0033 (2019).
395 Ayala, R. *et al.* Structure and regulation of the human INO80-nucleosome complex. *Nature* **556**, 391-395, doi:10.1038/s41586-018-0021-6 (2018).
396 Sundaramoorthy, R. *et al.* Structure of the chromatin remodelling enzyme Chd1 bound to a ubiquitinylated nucleosome. *Elife* **7**, doi:10.7554/eLife.35720 (2018).
397 Kagalwala, M. N., Glaus, B. J., Dang, W., Zofall, M. & Bartholomew, B. Topography of the ISW2-nucleosome complex: insights into nucleosome spacing and chromatin remodeling. *EMBO J* **23**, 2092-2104, doi:10.1038/sj.emboj.7600220 (2004).
398 Sundaramoorthy, R. *et al.* Structural reorganization of the chromatin remodeling enzyme Chd1 upon engagement with nucleosomes. *Elife* **6**, doi:10.7554/eLife.22510 (2017).

399 Jungblut, A., Hopfner, K. P. & Eustermann, S. Megadalton chromatin remodelers: common principles for versatile functions. *Curr Opin Struct Biol* **64**, 134-144, doi:10.1016/j.sbi.2020.06.024 (2020).
400 Singh, R. K. *et al.* Transient Kinetic Analysis of SWR1C-Catalyzed H2A.Z Deposition Unravels the Impact of Nucleosome Dynamics and the Asymmetry of Histone Exchange. *Cell Rep* **27**, 374-386 e374, doi:10.1016/j.celrep.2019.03.035 (2019).
401 Willhoft, O. & Wigley, D. B. INO80 and SWR1 complexes: the non-identical twins of chromatin remodelling. *Curr Opin Struct Biol* **61**, 50-58, doi:10.1016/j.sbi.2019.09.002 (2020).
402 Peterson, C. L., Zhao, Y. & Chait, B. T. Subunits of the yeast SWI/SNF complex are members of the actin-related protein (ARP) family. *J Biol Chem* **273**, 23641-23644, doi:10.1074/jbc.273.37.23641 (1998).
403 Turegun, B., Baker, R. W., Leschziner, A. E. & Dominguez, R. Actin-related proteins regulate the RSC chromatin remodeler by weakening intramolecular interactions of the Sth1 ATPase. *Commun Biol* **1**, 1, doi:10.1038/s42003-017-0002-6 (2018).
404 Zhao, K. *et al.* Rapid and phosphoinositol-dependent binding of the SWI/SNF-like BAF complex to chromatin after T lymphocyte receptor signaling. *Cell* **95**, 625-636, doi:10.1016/s0092-8674(00)81633-5 (1998).
405 Yarmola, E. G., Somasundaram, T., Boring, T. A., Spector, I. & Bubb, M. R. Actin-latrunculin A structure and function. Differential modulation of actin-binding protein function by latrunculin A. *J Biol Chem* **275**, 28120-28127, doi:10.1074/jbc.M004253200 (2000).
406 Harata, M. *et al.* The nuclear actin-related protein of Saccharomyces cerevisiae, Act3p/Arp4, interacts with core histones. *Mol Biol Cell* **10**, 2595-2605, doi:10.1091/mbc.10.8.2595 (1999).
407 Gamarra, N., Johnson, S. L., Trnka, M. J., Burlingame, A. L. & Narlikar, G. J. The nucleosomal acidic patch relieves auto-inhibition by the ISWI remodeler SNF2h. *Elife* **7**, doi:10.7554/eLife.35322 (2018).
408 Clarke, P. R. & Zhang, C. Spatial and temporal coordination of mitosis by Ran GTPase. *Nat Rev Mol Cell Biol* **9**, 464-477, doi:10.1038/nrm2410 (2008).
409 Rusche, L. N., Kirchmaier, A. L. & Rine, J. The establishment, inheritance, and function of silenced chromatin in Saccharomyces cerevisiae. *Annu Rev Biochem* **72**, 481-516, doi:10.1146/annurev.biochem.72.121801.161547 (2003).
410 Clapier, C. R., Langst, G., Corona, D. F., Becker, P. B. & Nightingale, K. P. Critical role for the histone H4 N terminus in nucleosome remodeling by ISWI. *Mol Cell Biol* **21**, 875-883, doi:10.1128/MCB.21.3.875-883.2001 (2001).
411 Schwarz, M. *et al.* Single-molecule nucleosome remodeling by INO80 and effects of histone tails. *FEBS Lett* **592**, 318-331, doi:10.1002/1873-3468.12973 (2018).
412 Bowman, G. D. Mechanisms of ATP-dependent nucleosome sliding. *Curr Opin Struct Biol* **20**, 73-81, doi:10.1016/j.sbi.2009.12.002 (2010).
413 van Holde, K. & Yager, T. Models for chromatin remodeling: a critical comparison. *Biochem Cell Biol* **81**, 169-172, doi:10.1139/o03-038 (2003).
414 Van Holde, K. & Yager, T. D. in *Structure and Function of the Genetic Apparatus* 35-53 (Springer, 1985).
415 Beard, P. Mobility of histones on the chromosome of simian virus 40. *Cell* **15**, 955-967, doi:10.1016/0092-8674(78)90279-9 (1978).
416 Havas, K. *et al.* Generation of superhelical torsion by ATP-dependent chromatin remodeling activities. *Cell* **103**, 1133-1142, doi:10.1016/s0092-8674(00)00215-4 (2000).
417 Langst, G. & Becker, P. B. ISWI induces nucleosome sliding on nicked DNA. *Mol Cell* **8**, 1085-1092, doi:10.1016/s1097-2765(01)00397-5 (2001).
418 Zofall, M., Persinger, J., Kassabov, S. R. & Bartholomew, B. Chromatin remodeling by ISW2 and SWI/SNF requires DNA translocation inside the nucleosome. *Nat Struct Mol Biol* **13**, 339-346, doi:10.1038/nsmb1071 (2006).

8 Acknowledgements

I would like to thank Prof. Dr. Karl-Peter Hopfner for the chance to conduct this thesis in his research group. I never took this for granted and am very grateful for his advise and supervision.
I would like to thank Dr. Sebastian Eustermann with whom I worked on the structural characterization of INO80. His enthusiasm and persistence drove the project and his profound knowledge about chromatin has always been inspiring and admirable.
I would like to thank Manuela Moldt for her expertise and effort, which has been critical for the work on recombinant INO80.
I would like to thank Dr. Kilian Knoll and Dr. Robert Byrne for proofreading this thesis and for countless scientific and non-scientific discussion, which shaped my understanding of science and the world.
I would like to thank all other members of the INO80 subgroup for their help and support throughout the years, in particular Dr. Kristina Lakomek, Dr. Gabriele Stoehr, Dr. Stephan Woike, Franziska Kunert and Dr. Vanessa Niebauer.
I would like to thank our collaboration partner, in particular PD Dr. Philipp Korber together with Dr. Elisa Oberbeckmann and Dr. Nils Krietenstein from the Biomedical Center of the LMU Munich and Prof. Dr. Jens Michaelis together with Dr. Marianne Schwarz from the University of Ulm. The work with you has always been stimulating and exciting and provided views form different angels on the scientific projects. Especially, I would like to thank Prof. Dr. Jens Michaelis for his support during the 'Machines On Genes' conference in Snow mass Villiage.
I would like to thank all other members of the Hopfner lab for their help and a positive working atmosphere and in particular Dr. Katja Lammens and Dr. Gregor Witte for their technical support. I would also like to thank Dr. Mike Strauss for his support with cryo-EM during early stages of this project.
I would like to thank the graduate school QBM for their financial and scientific support.
I would like to thank my second reviewer PD Dr. Philipp Korber and the co-reviewers Prof. Dr. Roland Beckmann, Prof. Dr. Julian Stingele, Prof. Dr. Klaus Förstermann and PD. Dr. Dietmar Martin for reviewing this thesis.
Finally, I would like to thank my family, Sandra and Oskar, for their patience, support and love during all the ups and downs. The work on this thesis has been extremely challenging and I never could have finished it without you.